Vibro-acoustics substructuring : Combining simulations and experimental identification of subdomains for low frequency vehicle acoustics

Matthieu Grialou

N° d'ordre NNT : 2018LYSEI109

THESE de DOCTORAT DE L'UNIVERSITE DE LYON

Opérée au sein de
l'INSA de Lyon

Ecole Doctorale N° 162
Mécanique – Energétique – Génie civil – Acoustique
Spécialité de doctorat : Acoustique

Soutenue publiquement le 04/12/2018, par :
Matthieu Grialou

Vibro-acoustics Substructuring:

Combining simulations and experimental identification of subdomains for low frequency vehicle acoustics

Devant le jury composé de :

Thomas Jean-Hugh	Professeur des Universités	Le Mans Université	Président
Leclaire Philippe	Professeur des Universités	Université de Bourgogne	Rapporteur
Rakotonarivo Sandrine	Maître de Conférences	Aix Marseille Université	Examinatrice
Guyader Jean-Louis	Professeurs des Universités	INSA Lyon	Directeur de thèse
Totaro Nicolas	Maître de Conférences HDR	INSA Lyon	co Directeur de thèse
Bocquillet Arnaud	Docteur	BMW Group	Invité

Département FEDORA – INSA Lyon - Ecoles Doctorales – Quinquennal 2016-2020

SIGLE	ECOLE DOCTORALE	NOM ET COORDONNEES DU RESPONSABLE
CHIMIE	**CHIMIE DE LYON** http://www.edchimie-lyon.fr Sec. : Renée EL MELHEM Bât. Blaise PASCAL, 3e étage secretariat@edchimie-lyon.fr INSA : R. GOURDON	M. Stéphane DANIELE Institut de recherches sur la catalyse et l'environnement de Lyon IRCELYON-UMR 5256 Équipe CDFA 2 Avenue Albert EINSTEIN 69 626 Villeurbanne CEDEX directeur@edchimie-lyon.fr
E.E.A.	**ÉLECTRONIQUE, ÉLECTROTECHNIQUE, AUTOMATIQUE** http://edeea.ec-lyon.fr Sec. : M.C. HAVGOUDOUKIAN ecole-doctorale.eea@ec-lyon.fr	M. Gérard SCORLETTI École Centrale de Lyon 36 Avenue Guy DE COLLONGUE 69 134 Écully Tél : 04.72.18.60.97 Fax 04.78.43.37.17 gerard.scorletti@ec-lyon.fr
E2M2	**ÉVOLUTION, ÉCOSYSTÈME, MICROBIOLOGIE, MODÉLISATION** http://e2m2.universite-lyon.fr Sec. : Sylvie ROBERJOT Bât. Atrium, UCB Lyon 1 Tél : 04.72.44.83.62 INSA : H. CHARLES secretariat.e2m2@univ-lyon1.fr	M. Philippe NORMAND UMR 5557 Lab. d'Ecologie Microbienne Université Claude Bernard Lyon 1 Bâtiment Mendel 43, boulevard du 11 Novembre 1918 69 622 Villeurbanne CEDEX philippe.normand@univ-lyon1.fr
EDISS	**INTERDISCIPLINAIRE SCIENCES-SANTÉ** http://www.ediss-lyon.fr Sec. : Sylvie ROBERJOT Bât. Atrium, UCB Lyon 1 Tél : 04.72.44.83.62 INSA : M. LAGARDE secretariat.ediss@univ-lyon1.fr	Mme Emmanuelle CANET-SOULAS INSERM U1060, CarMeN lab, Univ. Lyon 1 Bâtiment IMBL 11 Avenue Jean CAPELLE INSA de Lyon 69 621 Villeurbanne Tél : 04.72.68.49.09 Fax : 04.72.68.49.16 emmanuelle.canet@univ-lyon1.fr
INFOMATHS	**INFORMATIQUE ET MATHÉMATIQUES** http://edinfomaths.universite-lyon.fr Sec. : Renée EL MELHEM Bât. Blaise PASCAL, 3e étage Tél : 04.72.43.80.46 Fax : 04.72.43.16.87 infomaths@univ-lyon1.fr	M. Luca ZAMBONI Bât. Braconnier 43 Boulevard du 11 novembre 1918 69 622 Villeurbanne CEDEX Tél : 04.26.23.45.52 zamboni@maths.univ-lyon1.fr
Matériaux	**MATÉRIAUX DE LYON** http://ed34.universite-lyon.fr Sec. : Marion COMBE Tél : 04.72.43.71.70 Fax : 04.72.43.87.12 Bât. Direction ed.materiaux@insa-lyon.fr	M. Jean-Yves BUFFIÈRE INSA de Lyon MATEIS - Bât. Saint-Exupéry 7 Avenue Jean CAPELLE 69 621 Villeurbanne CEDEX Tél : 04.72.43.71.70 Fax : 04.72.43.85.28 jean-yves.buffiere@insa-lyon.fr
MEGA	**MÉCANIQUE, ÉNERGÉTIQUE, GÉNIE CIVIL, ACOUSTIQUE** http://edmega.universite-lyon.fr Sec. : Marion COMBE Tél : 04.72.43.71.70 Fax : 04.72.43.87.12 Bât. Direction mega@insa-lyon.fr	M. Jocelyn BONJOUR INSA de Lyon Laboratoire CETHIL Bâtiment Sadi-Carnot 9, rue de la Physique 69 621 Villeurbanne CEDEX jocelyn.bonjour@insa-lyon.fr
ScSo	**ScSo*** http://ed483.univ-lyon2.fr Sec. : Viviane POLSINELLI Brigitte DUBOIS INSA : J.Y. TOUSSAINT Tél : 04.78.69.72.76 viviane.polsinelli@univ-lyon2.fr	M. Christian MONTES Université Lyon 2 86 Rue Pasteur 69 365 Lyon CEDEX 07 christian.montes@univ-lyon2.fr

*ScSo : Histoire, Géographie, Aménagement, Urbanisme, Archéologie, Science politique, Sociologie, Anthropologie

Abstract

During the development process of a vehicle, the area of expertise of noise vibration and harshness—known as NVH—appears in various contexts. The spectrum of activities starts from the confrontation of inconvenient noises up to the sound design of the vehicle acoustical character. Exhaust noise has a significant impact on acoustic comfort and has to correspond to the typical sound related to the brand.

The driver and passenger's perception of the exhaust sound can be optimized by means of two levers: acoustical exhaust strength and sound isolation. The first lever consists in working on the side of the exhaust system itself. The second consists in working on the structure, and the sound isolation package of the full vehicle. The present study concerns solely the second lever: "*Description and quantification of the sound transmission from the exhaust outlet into the interior of a vehicle*". Physically the noise propagation from the exhaust pipe to the cabin consists of three steps:

> *Exterior*. Propagation of sound waves surrounding the outer skin of the structure of the vehicle. Conversion into vibrations.
> *Structure*. Transmission of the vibrations from the external skin to the inner skin.
> *Interior*. Acoustic radiation of the inner skin inside the cabin to the passengers.

The Patch Transfer Functions method, which is based on the framework of dynamic substructuring, allows considering this complex problem as the interaction of easier subsystems. The vibro-acoustics behavior of each subsystem can be estimated independently with various methods: finite element method, boundary element method, experimental testing etc. Once the acoustical response of each isolated subsystem has been determined, the whole system can be assembled mathematically. The mathematical model offers several advantages in terms of *physical understanding*, *target setting*, *modification prediction*, and *optimization*.

However, this method relies on the prior knowledge of the inherent vibro-acoustical impedance of each uncoupled subsystem—in the form of a condensed impedance matrix. This inherent property is often computed by numerical methods. Nevertheless, in many industrial applications, some subsystems are so complex (as encountered in a "trimmed structure") that numerical methods commonly deliver unsatisfactory results. In this case the acoustical impedances can be obtained using experimental characterization. Unfortunately, in practical industrial situations, it is often impossible to characterize a standalone subsystem independently from others and measurements can only be carried out on a full scale system. Therefore, some subsystems cannot be characterized independently and mandatorily remain coupled with other ones.

The work presented in this dissertation addresses the problem "*Characterization of Patch Transfer Functions of a subsystem by means of measurement on a coupled system*". The proposed method relies on a specific *set of experiments* on the fully coupled system. This *set of experiments* allows the identification of the researched information—condensed impedance matrix—by means of an inverse method.

This work proposes an alternative to the well-known Tikhonov regularization. In the present approach, some variations are voluntary added to a *set of experiments*, each one results in a different identification of the impedance matrix, but still contains a partial physical signification. Among all identified impedance matrices—one per *set of experiments*—some statistical indicator allows to recover the underlying physical reality.

It will be shown on an experimental setup that the *median* of this set of impedance matrices converges towards the researched physical impedance matrix.

Résumé

Tout au long du développement d'un véhicule, l'expertise dans le domaine de l'acoustique et des vibrations se manifeste de plusieurs façons. Les activités vont de la résolution d'un problème particulier au design de la signature acoustique du véhicule. Par exemple, la sonorité de l'échappement a un rôle significatif sur le confort acoustique des occupants, ainsi que sur le caractère du véhicule.

La perception de la sonorité de l'échappement à l'intérieur du véhicule peut être ajustée par deux leviers : l'amplitude de la source et l'isolation acoustique du véhicule. Pour actionner le premier levier il faut travailler sur le système d'échappement lui-même. Le second levier consiste à travailler sur la structure du véhicule et sur son insonorisation. L'étude proposée porte uniquement sur le second levier : « *Description et quantification de la transmission du son entre la bouche d'échappement et l'intérieur du véhicule* ». Physiquement la transmission sonore entre l'échappement et l'intérieur du véhicule s'effectue en trois étapes :

> *Extérieur*. Propagation des ondes sonores de la canule à la surface extérieure du véhicule et conversion en énergie vibratoire.
> *Structure*. Le bruit structurel se propage de la peau extérieure du véhicule à l'habillage intérieur.
> *Intérieur*. La surface intérieure du véhicule rayonne de l'énergie dans l'air à l'intérieur.

La méthode de sous structuration de domaine, Patch Transfer Functions permet de décrire un système complexe basé sur l'interaction entre ses sous-systèmes. Le comportement vibro-acoustique de chaque sous-système peut être étudié par n'importe quelle méthode appropriée : méthode des éléments finis ; méthode des éléments finis de frontière ; tests etc. Lorsque tous les systèmes isolés sont connus, la réponse du système complet peut être obtenue mathématiquement. Le modèle mathématique a plusieurs avantages. En plus d'améliorer la compréhension physique des phénomènes, il permet de créer des objectifs à l'échelle des sous-systèmes. Enfin il permet de prédire l'impact d'une modification d'un sous-système sur le système complet, et donne ainsi une possibilité d'optimisation.

La méthode fonctionne sur la base d'une matrice d'impédance condensée. Cette caractéristique intrinsèque au sous-système est souvent calculée par une méthode de simulation. Cependant, pour un système complexe, comme un véhicule complet, les résultats sont souvent trop écartés de la réalité. Dans ce cas une caractérisation expérimentale est envisageable. Hélas, il est souvent impossible de mesurer un sous-système de façon isolée. Ainsi, la contrainte est de caractériser un tel sous-système alors même qu'il reste couplé à un ou plusieurs autres sous-systèmes.

Le travail présenté dans cette étude porte sur la problématique « *Caractérisation expérimentale d'un sous-système par des mesures sur un système couplé* ». La méthode proposée repose sur une configuration expérimentale constituée d'un *ensemble d'expériences*, et d'une méthode inverse.

Cette étude propose une alternative aux méthodes conventionnelles de régularisation. Dans l'approche proposée, des variations sont volontairement ajoutées aux expériences à réaliser. Il en résulte plusieurs matrices d'impédance. Chacune contient une part de sens physique. Une méthode statistique permet de retrouver la signification physique partiellement contenue dans chacune de ces matrices—une par *ensemble d'expériences*.

L'indicateur *médiane*, donne de bons résultats confirmés par une vérification expérimentale.

“But why, some say, the moon? Why choose this as our goal? And they may well ask why climb the highest mountain? Why, 35 years ago, fly the Atlantic? Why does Rice play Texas?”

John Fitzgerald Kennedy (1917–1963) in “Address at Rice University in Houston on the Nation's Space Effort”, 1962 [1].

Acknowledgement

"We choose to go to the moon. We choose to go to the moon in this decade and do the other things, not because they are easy, but because they are hard, because that goal will serve to organize and measure the best of our energies and skills, because that challenge is one that we are willing to accept, one we are unwilling to postpone, and one we intend to win, and the others, too."

These are the words U.S. President John F. Kennedy, used on September 12, 1962 in his historical speech "Address at Rice University in Houston on the Nation's Space Effort" [1]. Does my journey toward the PhD bear the comparison with one of the most substantial projects undertaken by the humanity? From the perspective of scope, performance, cost—or almost any other perspective—it absolutely does not! But from the perspective of the core values exposed in this historical speech, it definitively endures the comparison.

As a young engineer working at BMW on structural dynamics, when I heard from Dr. Arnaud Bocquillet that his department was looking for a PhD student to work on the—unsolved—problem of "Vibro-acoustic transfer path analysis from exhaust sound to the interior of a vehicle", I immediately realized that it was a hard challenge. A few months later, I chose to embark in this PhD and realized that it was not one challenge, but two challenges! The first challenge was to work on the industrial problem in order to earn value for the BMW Group—a problem, a solution. The second challenge was to work in a way to earn value for science—extending the state of the art. Combining these two—almost incompatible—challenges were not straightforward, yet necessary.

Thankfully Dr. Arnaud Bocquillet, Dr. Nicolas Totaro; Prof. Dr. Jean-Louis Guyader, and I have found a way to combine the two challenges in one challenge. In other words, it was suddenly possible to work on the industrial problem in a way that extends the current state of the art. The solution was not ours to see, but it was absolutely ours to create, to make slightly different than anything we have known before.

The path in the field of research was not a straightforward journey toward our goal. I have been a beginner again, less sure about everything. In the end, it happens to be one of the most creative periods of my life. I am absolutely sure none of this would have happened without the people I have been working with—and the people who have been supporting the project.

First of all I would like to thank the executive and chief executive of the BMW Group who support the project—Dr. Martin Wechs; Dr. Peter Kalinke; Dr. Martin Grabenstein; Dr. Mihiar Ayoubi and Dr. Martin Kaufmann. You share the core values of the BMW Group: responsibility, appreciation, trust, and openness. It has contributed to create a *"sheer working pleasure"*.

Most of all, I thank Dr. Arnaud Bocquillet for being such a committed project leader. In the field of research and development, the expression "God is in the detail" often appears in its pessimistic formulation "The devil is in the detail". When we happened to get to close from this "devil", his outstanding physical and mathematical understanding was our secret weapon.

My co-promotor Dr. Nicolas Totaro and my promotor Prof. Dr. Jean-Louis Guyader shares the largest contribution to our goal achievement. Their eminent technical knowledge, experience, and know-how combined with human skills have been keys success factors. In

the summer 2016, faced to repetitive and major numerical problems, I had almost lost faith and decided to try an alternative method. When I informed you three weeks later, you clearly and strongly disagreed with my idea—not because it was not a good one, but because it was not the moment. It was awful tasting medicine, but the patient needed it. After a few days without results, the reason of the numerical problem becomes clear and we entered into the most successful period of the projects.

My mentor Dr. Florian Preuß has provided me countless clear and efficient strategical tips. Your external vision, combined with a high capacity to understand things and people, has helped me a lot. Despite your position in the top level of management, you have invested a great amount of energy to help me—and others. Many thanks.

I would also like to thank the Msc. Students I had the opportunity working with: Mr. Nicolas Izac, Ms. Eloise Wladyszewski, and Mr. Hai Nguyen. Your contribution has been really important to keep the project moving forward from the industrial perspective.

Finally, I am really appreciative the support of my family, friends, including colleague in Munich and in Lyon, and of course my partner. You were all necessary to maintain a good work-life balance—which happened to be critical to maintain an adequate level of creativity.

On July 20, 1969 Neil Armstrong stepped onto the lunar surface and fulfilled a national goal proposed by U.S. President John F. Kennedy, with an historical metaphor: *"That's one small step for [a] man, one giant leap for mankind."*

In the sense that a journey through a PhD is before anything else a personal challenge, Neil Armstrong's metaphor could be reformulated as following:

"That's one giant leap for [a] man, one small step for mankind."

Matthieu Grialou

Toulouse, June 2017

Contents

Abstract **5**

Résumé **7**

Acknowledgement **11**

Contents **13**

Nomenclature **15**

1 General introduction **17**

1.1 Research context 17

1.2 Trends & challenges 18

1.3 Exhaust sound transmission 20

1.4 State of the Art 26

1.5 Dissertation contribution 34

2 Coupling of vibro-acoustical subsystems **37**

2.1 Introduction 37

2.2 Acoustical cavities 38

2.3 Numerical simulation 47

2.4 Formulation for a vehicle 55

2.5 Summary 62

3 Decoupling & Experimental characterization **63**

3.1 Introduction 63

3.2 Theoretical background 65

3.3 Numerical experiment 68

3.4 Results of the numerical experiment 72

3.5 Summary 80

4 Limits of the method **81**

4.1 Introduction 81

4.2 Metrics for results quality 82

4.3 Reference analysis in depth 83

4.4 Instability due to the choice of set of experiments 89

4.5 Instability to measurement noise 95
4.6 Summary 101
5 Advanced strategies 103
5.1 Introduction 103
5.2 Statistical identification 104
5.3 Statistical stability: set of experiments 107
5.4 Statistical stability: addition of noise 118
5.5 Summary 123
6 Experimental validation 125
6.1 Introduction 125
6.2 Problem statement 126
6.3 Experimental setup 127
6.4 Statistical identification 129
6.5 Summary 131
7 Conclusions 133
7.1 Summary 133
7.2 Recommendation 135
7.3 Résumé étendu en français 136
References 143

Nomenclature

Abbreviations

BMW: Bayerische Motoren Werke

PTF: Patch Transfer Functions

SEA: Statistical Energy Analysis

SmEdA: Statistical modal Energy distribution Analysis

FEM: Finite Element Method

BEM: Boundary Element Method

Complex algebra

In this dissertation harmonic quantities—e.g. an acoustical pressure $p(t)$ —are mathematically represented using complex algebra—e.g. $p(t) = p(\omega)e^{+i\omega t}$. This representation relies on two *arbitrary*[1] conventions:

> *Physical result* p(t). Is the real part of the complex quantity—i.e. $\Re\left(p(\omega)e^{+i\omega t}\right)$.
> *Rotation direction*. Counterclockwise—i.e. $e^{+i\omega t}$.

While the first convention is almost universal, the second varies from reference to reference. If in some reference the rotation direction happens to be clockwise—i.e. $e^{-i\omega t}$— all sign of i in all equations should be changed to $-i$.

Blue paragraph

The *blue paragraphs* are not strictly necessary to the comprehension of the *core message* of this dissertation. On the opposite they represents in some measure a kind of embellishment. The following content will be found along the dissertation: Physical interpretation, definition, practical consideration, precision, vulgarization, personal experience, and even some anecdotes.

[1] A convention is per definition an arbitrary choice and has no influence on the physical result. The only thing is to be consistent with this choice.

1 General introduction

"The vast stretches of the unknown and the unanswered and the unfinished still far out-strip our collective comprehension."

John Fitzgerald Kennedy (1917–1963) in "Address at Rice University in Houston on the Nation's Space Effort", 1962 [1].

Chapter contents:

1.1 Research context **17**

1.2 Trends & challenges **18**

1.2.1 Exhaust sound in the interior of a vehicle 18

1.2.2 Challenge of acoustic performance 19

1.3 Exhaust sound transmission **20**

1.3.1 Measure 21

1.3.2 Physical description 22

1.3.3 Industrial functional specifications 25

1.4 State of the Art **26**

1.4.1 Substructuring of a complex system 26

1.4.2 Characterization of a subsystem 32

1.5 Dissertation contribution **34**

1.1 Research context

This study has been financed by the BMW Group and it has been realized within a collaboration with the "Laboratoire Vibrations Acoustique" of the INSA Lyon. It concerns the physical description of the sound transmission from the exhaust outlet into the interior of a vehicle. More specifically, the low frequency acoustical phenomenon "booming noise". The human perception of this phenomenon stands in the overlapping of hearing and feeling—e.g. loud music with a lot of "bass" or blast of air caused by a thunderclap. Whether this physical phenomenon is for good or ill depends on the vehicle's character and the occupants' expectations—e.g. comfortable ride or feedback of a powerful acceleration.

In every instance, it must be understood, the control lever should be identified and their effect might be predicted. However, NVH engineers are not, for now, able to design the acoustic perception of a vehicle and the "booming noise" is most of the time a non-desirable effect due to a complex combination of coupled vibro-acoustic systems. The customer's experience of the car should be devaluated when such a "booming noise" appears in a top-level automotive. When it appears on a prototype, a correcting solution has to be found without degrading the other performances of the car. Unfortunately, the

complexity of the structure makes the understanding of the phenomenon difficult and therefore the choice of a solution as well.

The present work has been initiated in the field of this kind of engineering problem. The transition from the industrial problem to the scientific problem of this thesis has been an integral part of the study.

1.2 Trends & challenges

During the development process of a vehicle, the area of expertise of noise vibration and harshness—known as NVH—appears in various contexts. The spectrum of activities starts from the confrontation of inconvenient noises up to the sound design of the vehicle acoustical character. Despite the fact that almost all components and subsystems are contributing to the NVH property of the full vehicle, nearly none of them does it as its first purpose [2]. Achieving some satisfactory NVH performances is still a challenging work considering the decrease of the total weight of the vehicle and the number of noisy components that the engine noise does not mask anymore in a modern vehicle [3].

1.2.1 Exhaust sound in the interior of a vehicle

Exhaust sound has a significant impact on the acoustic comfort and defines the acoustic signature profile of the car brand. The driver and/or passenger's perception of the exhaust sound is determined by the source, the transmission, and the receptor himself. This description is depicted in Figure 1.1.

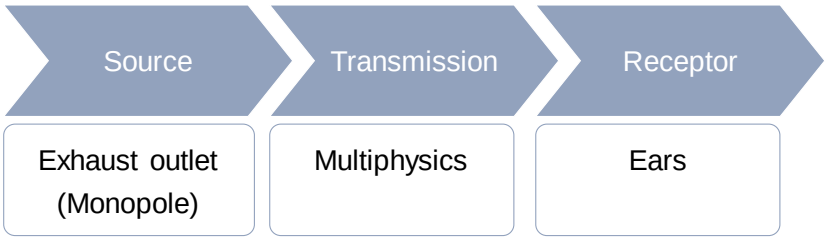

Figure 1.1: Factors of driver and/or passenger's perception of exhaust sound: source, transmission, and receptor. The source is approximated as a point source.

As the automotive manufacturer does not have any control over the receptor (driver's ears), the exhaust sound perception can be optimized only through source or transmission adjustment. The receptor itself is not considered in this study. Yet, according to H. Fastl, the psychoacoustics[2] is an important aspect of acoustics [4].

Physically, the sound pressure at the driver and passenger's ears can be described in the frequency range with a complex spectrum $P(L,\omega)$. The sound pressure P is physically expressed in Pascal [Pa]. The point L represents the position of a listening point and ω represents the angular frequency in $[\mathrm{rad.s^{-1}}]$. This notation stresses the fact that the pressure in the interior of a vehicle is a function of at least two parameters: the position and the frequency. Finally, the sound pressure spectrum $P(L,\omega)$ is represented with complex algebra—phase and amplitude. Mathematically, the sound pressure at a given listing position L and at a given frequency ω is a complex function $P(L,\omega)$: $(\mathbb{R}^3,\mathbb{R}) \mapsto \mathbb{C}$.

The mathematical counterpart of the Figure 1.1 is given by Eq. (1.1):

[2] As a serious *anecdote*, it appears that even the color of a vehicle has an influence on loudness judgment [102].

$$P(L,\omega) = H(L,S,\omega).Q(\omega) \tag{1.1}$$

where $Q(\omega)\colon \mathbb{R} \mapsto \mathbb{C}$ represents the source strength of unit $[\mathrm{m}^3.\mathrm{s}^{-2}]$ given in the form of a complex spectrum. S stands for the position of the monopole source—i.e. the exhaust outlet for example. The complex function $H(L,S,\omega)\colon (\mathbb{R}^3,\mathbb{R}^3,\mathbb{R}) \mapsto \mathbb{C}$ is the transfer function from the geometrical source position S to the listening point L. This function is also described as a complex frequency spectrum of unit $[\mathrm{Pa}/(\mathrm{m}^3.\mathrm{s}^{-2})]$.

If the vehicle exhaust system consists of several exhaust outlets, denoted with the subscript o, the total sound pressure at a given listening position is calculated using the superposition principle—valid for linear acoustics. In other words, the sound pressure is the sum of the strength of each exhaust outlet $Q_o(\omega)$ weighted with a specific transfer function $H_o(L,S,\omega)$. In this case, Eq. (1.1) becomes Eq. (1.2):

$$P(L,\omega) = \sum_o H_o(L,S_o,\omega).Q_o(\omega) \tag{1.2}$$

Eq. (1.1) or Eq. (1.2) makes it clear that for a given exhaust outlet position S, the sound level in the interior of the vehicle can be optimized by working on the source strength $Q(\omega)$, the transfer function $H(L,S,\omega)$, or both.

The following subsection presents briefly the industrial challenge of exhaust sound in a vehicle from both perspectives—i.e. source and transmission.

1.2.2 Challenge of acoustic performance

Target for the exhaust sound

From a theoretical point of view, the sound from the exhaust outlet in a vehicle, at a specific listening position, is predictable if the source strength $Q(\omega)$ and the transfer function $H(L,S,\omega)$ are known.

As the source strength at the exhaust outlet $Q(\omega)$ has a leading contribution for the external noise—which is subject to strict regulation—much more effort has been done to simulate and control it. On the opposite, the transfer function $H(L,S,\omega)$ is "just" a matter of comfort, and has not been subject to a comparable effort.

In this way, the present strategy to control the exhaust sound level in the interior of a vehicle consists of considering the transfer function $H(L,S,\omega)$ as a given measured parameter and adjusting the strength of the exhaust outlet sound $Q(\omega)$ in consequence.

This strategy presents the inconvenience to take advantage of only one of two optimization parameters—i.e. $Q(\omega)$. Technically, the adjustment of the exhaust outlet sound is done with optimization of the power strain. The exhaust system itself is one of the most efficient and controlled levers. Yet, the acoustic optimization might result in conflicts with some other important functions or constraints—e.g. energy efficiency, weight, cost, reliability, assembly, commonality, available space …

The current study intends to move forward in the direction of the comprehension and the optimization of the transfer function $H(L,S,\omega)$. This supplementary degree of optimization would allow the full vehicle concept to be closer to a global optimum.

Structure and power train

The current trend of lightweight construction combined with engine downsizing adds more difficulties in the development process. Indeed, the reduction of the number of

cylinders intensifies the excitation and the lightweight structure has an increased tendency to vibrate. A schematic representation of this context is depicted in Figure 1.2. On the one hand, the trend of downsizing, low end torque and downspeeding tends to increase the source strength q(ω) and to shift its spectrum to a lower frequency range (right side of the figure). On the other hand, the sound insulation of the vehicle tends to decrease due to the lightweight design (left side of the figure). As a result, the worst combination of low insolation and high source strength could occur more frequently. It might result in an exhaust inferred booming noise (bottom of the figure).

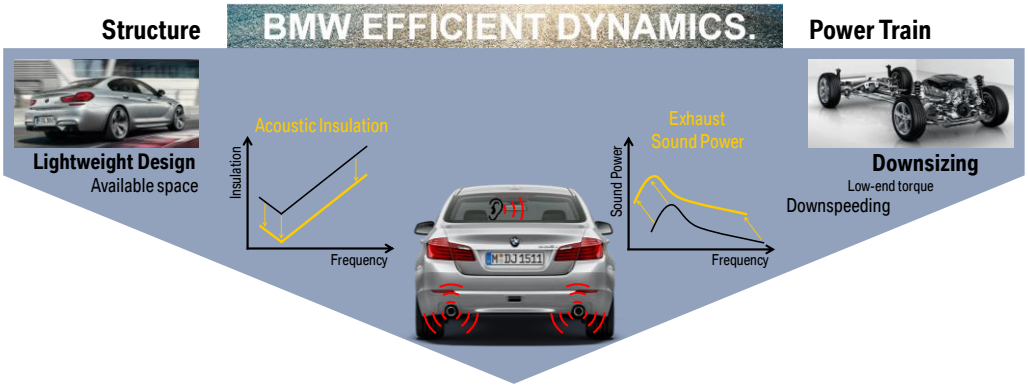

Figure 1.2: Schematic representation on how the BMW EfficientDynamics strategy leads to new challenges for the acoustic performance.

In other words, without additional effort, the current trend tends to deteriorate both factors involved for the exhaust sound level in a vehicle. Indeed, the exhaust sound strength $Q(\omega)$ at the outlet tends to increase and the transfer function $H(L,S,\omega)$ tends to be physically more favorable to the sound transmission.

Consequently, the demands for a descriptive and predictive method have grown. It is not anymore a question of finding a global optimum, but a necessity to achieve the same acoustical quality for the new vehicles within the presence of new, non-acoustically driven constraints.

All of this justifies the effort which is done for the description, the prediction, and the optimization of the vibro-acoustical transfer function from the exhaust outlet to the interior of a vehicle.

1.3 Exhaust sound transmission

> *"The discussion of any problem in science or engineering has two aspects: the physical side, the statement of the facts of the case in everyday language and of the results in a manner that can be checked by experiment; and the mathematical side, the working out of the intermediate steps by means of the symbolized logic of calculus. These two aspect are equally important and are used side by side in every problem, one checking the other. ... The stating of the problem to be solved is not always the easiest part of an investigation. One must decide which properties of the system to be studied are important and which can be neglected, what facts must be given in a quantitative manner and what others need only a qualitative statement."*

This quotation is to be found in the introduction of the book “Theoretical Acoustics” of P.M. Morse and K. Uno Ingard [5]. This section intends to cover solely the first aspect of the discussion.

The importance of the right hypothesis

The fundamentals of sound and vibration have promised hardship to preeminent scientists such as Lord Rayleigh, Hermann von Helmholtz, Sir Isaac Newton, Marquis Pierre-Simon de Laplace, Leonhard Euler, and others.

The “error” Newton did in the calculation of the speed of sound is an edifying anecdote. He considered the “wrong” hypothesis that the thermodynamic effect of an elementary volume of air would be in the field of acoustics well described with an isothermal compression. It has led to a wrong estimation of the celerity of sound propagation. Laplace found that the adiabatic hypothesis was more adequate with the experimentally measured celerity of sound.

1.3.1 Measure

The exhaust outlet is idealized as a monopole point source of given strength. The transfer from this monopole point source to the passengers’ ears is described as a transfer function with the unit $[\mathrm{Pa}/(\mathrm{m}^3.\mathrm{s}^{-2})]$. A practical, though non-rigorous, approach is to represent this transfer function as a sound insulation curve. When the monopole source is active (Figure 1.3), the sound pressure is measured simultaneously inside and outside of the vehicle with microphones. A sound insulation curve is represented in 3rd octave as the difference in dB between the sound pressure close to the monopole point source (reference microphone) and the sound pressure inside the vehicle (listening point).

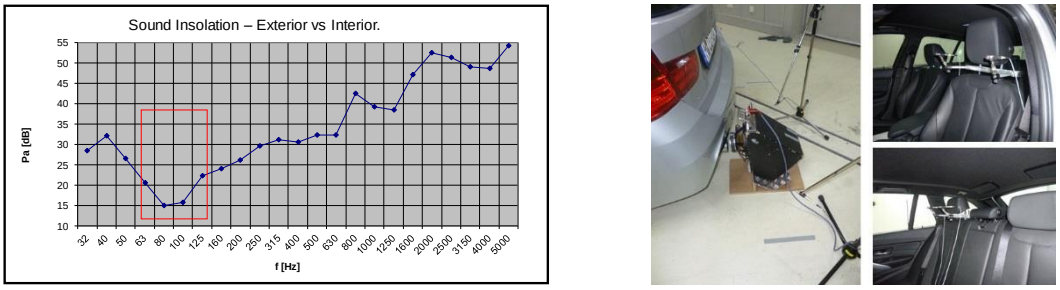

(a) (b)

Figure 1.3: (a): Sound insulation in 3rd octave representation. A minimum is observed in low frequency range—marked with the red rectangle. This critical insulation could result in exhaust-inferred booming; (b): Measurement setup showing the external acoustic source and the microphones’ positions inside the car.

The curve of the sound insulation of a vehicle typically shows a minimum in the low frequency range. Depending on the vehicle’s architecture, this minimum could be observed in a frequency range from 30 Hz up to 140 Hz. At this frequency, the sound isolation is critical and might result in exhaust-inferred booming noise.

To certainly outline the problem of a low sound isolation, the descriptive method of the sound transmission from the exhaust to the interior of a vehicle should work at least within a frequency range starting from 20 Hz and ending up at 250 Hz.

Another determining information, is that the relationship between the *cause* and the *effect*—i.e. *source* strength and *pressure* at a given position—is linear. Therefore, the full study and this dissertation in particular, is realized within the framework of *linear acoustics*.

1.3.2 Physical description

Observability and Predictability

The easiness of the measure of the sound transmission from the exhaust outlet to the interior of a vehicle does not imply that the result is easy to interpret nor to predict. It is quite the opposite from a physical point of view. For a given phenomenon, there is no direct link between observability and predictability.

Observations

When the exhaust outlet, or a monopole source, radiates sound in the exterior of a vehicle, it results in an acoustical pressure in the interior of the vehicle. This trivial[3] observation proves that the sound can be transmitted from the exterior to the interior of a vehicle. In short, four facts are observed and depicted in Figure 1.4:

External radiation of sound. The source, exhaust outlet or loudspeaker, radiates sound Figure 1.4 (a).
Scattering of sound. A sound field is present at the exterior of the vehicle Figure 1.4 (b).
Vibrations. The structure of the vehicle is vibrating Figure 1.4 (c).
Internal radiation of sound. There is a sound field in the interior of the vehicle Figure 1.4 (d).

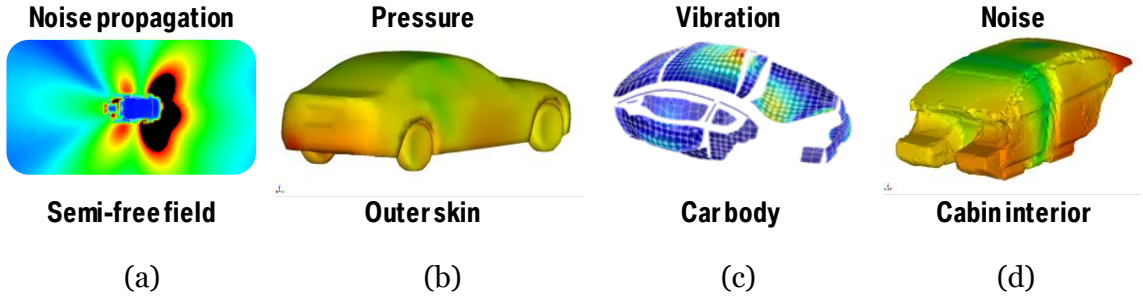

Figure 1.4: State of the facts observed while an acoustical source like an exhaust outlet is placed in the exterior of a vehicle. From the left to the right: Radiation of sound (illustrated here by an acoustical simulation). The sound waves are reflected on the ground and on the complex external vehicle geometry. It results in a complex scattering effects; An acoustical load is present on the vehicle outer skin (illustrated here by an acoustical simulation); The car body vibrates (illustrated here by measurement of vibration of a vehicle under an acoustical excitation); A sound field is present in the interior of the vehicle (illustrated here by a simulation).

Weak coupling vision

Before going any further, the graphic and typographical conventions for the representation of the coupling of two domains are presented in Table 1.1:

[3] This would not be the case if the vehicle was totally closed and infinitively stiff.

Table 1.1: Typographical and graphical convention for the representation of different kinds of coupling. D_1 and D_2 represents any arbitrary domain. In this dissertation, the frequent occurrences are $fluid|fluid$ and $fluid|structure$.

Phenomenon	Typography	Graphical
Unspecified coupling	$D_1 \vert D_2$	—
Weak coupling	$D_1 \rightarrow D_2$	Arrow mapping D_1 to D_2
Strong coupling	$D_1 \leftrightarrow D_2$	Arrow mapping D_1 to D_2 and vice versa

The discussion starts from the radiated sound from the source as depicted in Figure 1.5.

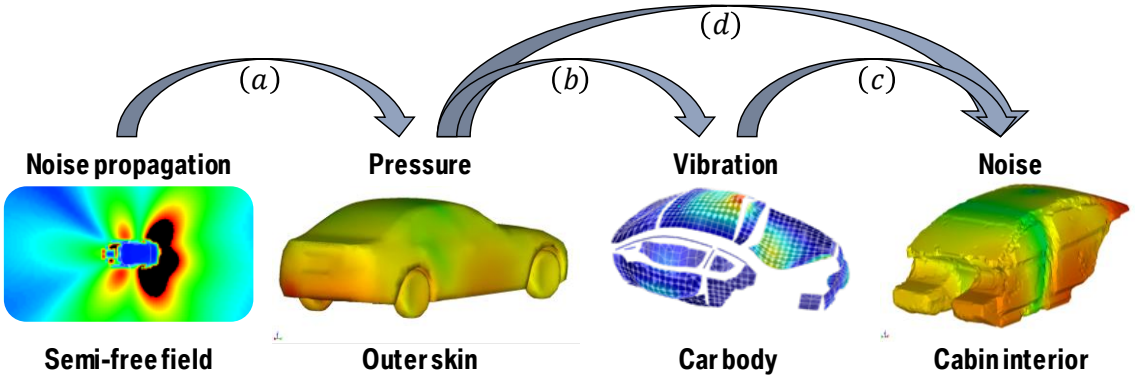

Figure 1.5: Physical description of the sound propagation from the exhaust outlet to the interior of a vehicle within the hypothesis of weak coupling. (a): Sound waves are generated by the source results in a complex sound pressure repartition on the outer skin of the vehicle; (b): Under this dynamic acoustical load on the outer skin, the light vehicle structure vibrates; (c): The inner skin radiates sound in the interior of the vehicle; (d) if the vehicle presents an aperture—e.g. open window, a leakage, or even an opened cabriolet—some energy can be transferred from the exterior to the interior directly—i.e. without the intermediary of structural vibration.

As many physical phenomena are involved for the sound transmission from the exhaust to the interior of a vehicle, its description is not easy. Even though this description sounds complex, this vision relies on two fundamental simplifications:

> *Weak external coupling*. The sound field resulting from the vibration of the structure—i.e. structure acting as a secondary source—is neglected compared to the sound field created by the primary source. In other words, the external coupling $air|structure$ is considered solely in the direction $air \rightarrow structure$, as depicted by the one direction arrow (b) in Figure 1.5.
> *Weak internal coupling*. The sound pressure in the interior of the vehicle does not have any retroaction on the structure. It means that the internal coupling $structure|air$ is considered solely in the direction $structure \rightarrow air$, as depicted by the one direction arrow (c) in Figure 1.5.

From a formal sense, none of these two hypotheses is strictly valid, but they are often conducing to satisfying results. Actually, the second hypothesis is the basis of the field of acoustics *radiation of sound*. Many industrial structures are relatively stiff—i.e. high local impedance in comparison to the impedance of the air—such as, the resulting acoustical load does not impact the vibration state of the structure at all. In other words, the hypothesis is that a structural vibration results in a sound field in the air (c), but that a sound field in the volume results in a neglected structural vibration.

Strong coupling vision

The weak coupling approach is frequently used in acoustic radiation and is a commonly accepted hypothesis. Nevertheless, in the case of exhaust-inferred booming noise, the industrial experience shows that this bidirectional coupling cannot be neglected. This observation pointed out two additional couplings that represent the retroaction of the fluid and structure:

> *Internal coupling*. The arrow (c) describing the direct coupling $structure \rightarrow fluid$ might be crossed in the reverse direction $structure \leftarrow fluid$. This reverse coupling is depicted with arrow (c').
> *External coupling*. The arrow (b) describing the coupling $fluid \rightarrow structure$ might be travelled in the reverse direction $fluid \leftarrow structure$ depicted by arrow (b').

Even though, the strong coupling vision complicates drastically the physical and mathematical representation, the graphical representation is solely enriched by two arrows (b') and (c'). The strongly coupled vision is depicted in Figure 1.6.

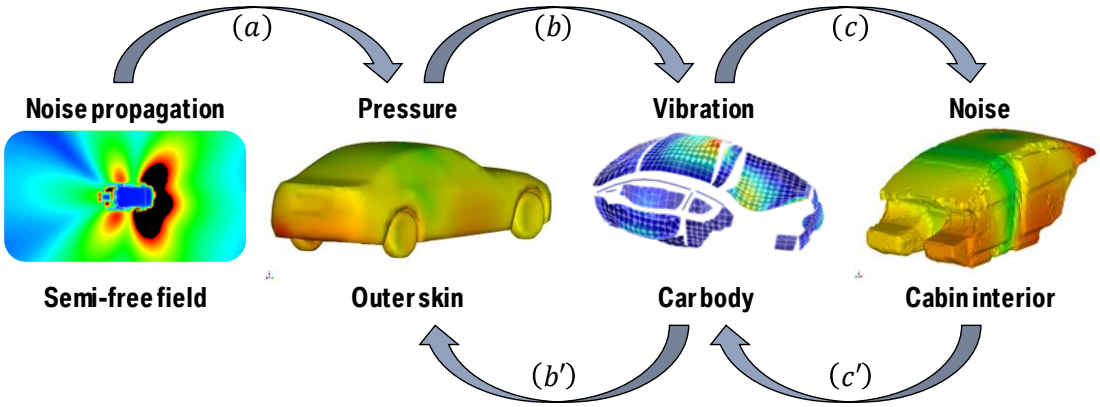

Figure 1.6: Physical description of the sound propagation from the exhaust outlet to the interior of a vehicle within the hypothesis of full coupling. (a): Sound waves are generated by the source it results in a complex sound pressure repartition on the outer skin of the vehicle; (b): Under this dynamic acoustical load on the outer skin, the light vehicle structure vibrates. (c): The inner skin radiates sound in the interior of the vehicle; (c'): The sound field in the interior of the vehicle retroact on the state of vibration of the structure; (b'): The vibrating structure radiates sound in the exterior. The external sound field becomes the superposition of the direct effect of the sound scattering on a rigid structure and the sound radiated by the structure.

As illustrated in Figure 1.6, the coupling between the structure and the fluid should be considered as a mutual coupling. The full coupling of the internal fluid and the structure means that the vibration has an influence on the acoustic pressure, and that this acoustic pressure retroacts on the structural vibration. The method to be developed must be able to handle this large complication.

The necessity to use experimental data

The complexity of a fully trimmed vehicle—i.e. a complete vehicle without any simplification—is still too complex to be tackled by a numerical model. Such a model should be representative of every single complexity—e.g. geometrical, physical, or coupling properties. In addition, even if a model existed for each subsystem or coupling, the question of assumptions and estimation of parameters would still remain an inextricable issue. The numerical simulation of the full trimmed vehicle is not currently possible, but NVH engineers face some immediate undesirable phenomena that can degrade the quality perceived by the customers. The booming noise is, among others, such an acoustical

problem which is extremely complicated to simulate. However, this kind of problem has to be understood and solutions have to be found—the solution can be a minor design change.

Anecdote of the warning triangle:

The example of a problematic booming noise on one of the BMW vehicles, is perfectly illustrative. Some engineers have found on the test rig that removing the *lightweight* warning triangle fixed in the trunk would have solved the problem. Removing the warning triangle was not an option; nevertheless, the problem was solved by removing a *superfluous* screw. Any automotive constructor has hundreds of such anecdotes.

Despite the fact that more and more attention is carried out for the numerical simulation, the simulation might still not be able to catch this kind of detail. This observation is the consequence of deliberate strategical choices. From a practical point of view, it would be possible to design a vehicle, within the constraints, to be able to simulate everything within an acceptable precision. This strategy is followed in critical fields, such as space science or nuclear science, where tests in real conditions are extremely limited. Nevertheless, this strategy leads to dismiss some technically interesting solutions in favor of other perspectives—e.g. mass production, cost, design, performance, tight development cycle, as well as others. For all these reasons, the development in the automotive industry still relies on tests.

1.3.3 Industrial functional specifications

Up to this section, the industrial context has been presented and a qualitative physical description of the sound transmission from the exhaust outlet to the interior of a vehicle has been addressed. This section presents the resulting industrial functional specifications. The principal function of the method to be developed is:

> *Description and quantification of the sound transmission from the exhaust outlet into the interior of a vehicle.*

The following constraint functions have to be considered:

> *Low frequency range*. Starting from the threshold of hearing 20 Hz and up to 250 Hz.
> *Strong coupling*. The lightweight vehicle structure is fully coupled with the air.
> *Opened system*. The vehicle might present leakage or openings.
> *Experimental data*. Some information might be acquired with experimental method only on available prototypes.

The experiment allows to consider the following hypothesis:

> *Linear acoustics*. The linearity of the phenomenon has been validated.

The next section presents the current state of the art method that might be able to satisfy these industrial functional specifications.

Low frequency range

The term “low frequency” does not match a predetermined absolute frequency range and it might be confusing. The physical phenomena that occur for objects of different sizes are similar, but with a frequency shift. In this extend, there is a link between the object’s size and the “low frequency” range. For a large object the words “low frequency” match to some

Hz (typically 10-50Hz); while for a small object the words “low frequency” match to a much higher frequency (typically thousands of Hz).

From the perspective of a structural borne noise, the low frequencies are corresponding to the range in which the modal density is low. In this case, the structural waves are strongly reflected on the boundary of the system and there is almost no propagation phenomenon. All vibrations are really global—e.g. opposite to locally reacting material. It means that a single force can excite the whole structure.

1.4 State of the Art

The state of the art presented in this section addresses two goals with the following perspectives:

Industrial. Which scientific methods—framework of methods—might address or at least partially address the industrial specifications listed in Sec. 1.4.1.
Academical. Identification of the current state of the art of the method being selected in order to justify that the work exposed in this dissertation extends the current state of the art—Sec. 1.5.

Considering the severe industrial functional specification of the method to be developed, the framework of substructuring method is deemed to be appropriate. Indeed, these methods allow to create a *model of a complex system*—Sec. 1.4.1—based on the *model* of each of its subsystems—Sec. 1.4.2.

1.4.1 Substructuring of a complex system

> *“Music, poetry, and programming, all three as symbolic constructs of the human brain, are found to be naturally structured into hierarchies that have many different nested levels. Sound (phonemes) form small meaningful units (morphemes) which in turn form words; words group into phrases, which group into sentences; sentences make paragraphs, and these are organized into higher levels of meanings. Notes form musical phrases, which form themes, counterpoints, harmonies, etc.; which form movements, which form concertos, symphonies, and so on. The structure in programs is equally hierarchical, if not so universally recognized.” [6].*

The word “substructuring” refers in the field of mechanics to a piecewise description of a “structure”. If the model being created intends to represent dynamic properties of this structure, it is part of the framework of “dynamic substructuring”. According to M. V. van der Seijs, a substructuring approach assumes that the dynamic interaction between the subsystems takes place at a limited set of interfaces [7].

D. de Klerk has listed [8] four advantages of a component wise vision over a global method where the full system is handled at once:

Handling of large structure. Handling a large and complex system as a whole might be problematic—e.g. size of the numerical model and the experimental facilities.
Effect of a subsystem. Identification and optimization of a local problem. Elimination of non-relevant subsystems on the assembled system.
Hybrid model. Subsystem might be modeled separately by the best appropriated method.

Organization. Sharing and combining substructures from different actors.

In the following, three classes of methods are addressed.

Impedance and Mobility

The concept of electrical impedance has been introduced in 1884 by Heaviside [9]. In the late 19th, the research in the field of electrical network has been increased by the needs of the commercial development of the telegraph and the telephone. The concept of electrical impedance combined with other practical tools—e.g. theorems of Kirchhoff, Thévenin, Norton—has allowed a systematic depiction of complex electrical networks. Progressively it has been possible to describe an electrical network as several "subsystems" interacting together with physical quantities *current* and *voltage*—i.e. "*through*" and "*across*".

According to the review paper of Gardonio [10], Webster has been the first to propose the use of the concept of electrical impedance for the needs of mechanics [11]. Nevertheless, the analogy between electrical and mechanical systems has not been straightforward. On the opposite, many years of controversy have been necessary. The first analogy proposed by Webster—subsequently called *direct analogy*—is based on the following consideration:

> *Force* [N]. "cause" of the motion, equivalent to the electromotive force "across" [V].
> *Velocity* $[\mathrm{m.s^{-1}}]$. "effect" of the force, equivalent to the current "through" [A].
> *Impedance* $[\mathrm{N/(m.s^{-1})}]$. Defined as the ratio Force/Velocity.

Unfortunately, the direct analogy proposed by Webster has suffered many limitations and even some incoherencies. Firestone has proposed in 1933 "A new analogy between mechanical and electronical systems" [12]. The so-called inverse analogy is founded on:

> *Force* [N]. Equivalent to the current "through" [A].
> *Velocity* $[\mathrm{m.s^{-1}}]$. "effect" of the force, equivalent to the current "across" [V].
> *Bar Impedance*[4] subsequently called *Mobility* $[\mathrm{m.s^{-1}/N}]$. Defined as the ratio Velocity/Force.

Le Corbeiller had sided in "Duality in Mechanics" with the mobility analogy vision proposed by Firestone [13]. Despite a somewhat less intuitive depiction of a mechanical system (electrical node does not match a mechanical node; electrical mesh does not match a mechanical loop) the vision of Firestone is conform to the principle of duality[5]. This conformity allows overcoming all difficulties encountered with the impedance vision.

The inverse analogy proposed by Firestone is still in use today. In its paper "Twixt Earth and Sky with Rod and Tube; the Mobility and Classical Impedance Analogies" [12], Firestone proposes a set of tools allowing the depiction of a complex mechanical network with both, the classical analogy—i.e. direct analogy—and the inverse analogy—i.e. mobility.

---

[4] Firestone if arrived first would have called *impedance* the ratio Velocity/Force and not the ratio Force/Velocity as done by Webster. In [12] he has proposed to use the word *bar impedance* instead. The intention was that the prefix *bar* would dismiss with time after the adoption of his vision. And so, the world *impedance* would have been redefined has Velocity/Force. Even if Firestone vision's has been more and more adopted, the definition of mechanical *impedance* proposed by Webster [11] has not been changed. Actually, the word *mobility* has been adopted instead. As a result, a *mechanical mobility* is in some measure the pendant of an *electrical impedance*.

[5] The duality in mechanics is an important concept with major consequences. One of which is the principle of reciprocity. The application of the principle of reciprocity in vibro-acoustics is exposed by Fahy in [96].

As the adoption of the *mobility* instead of *impedance* has been a long controversy, O'Hara has summarized the major differences in [14]. He wrote in the conclusion: "*Mobilities describe invariant characteristics of the whole structure, impedance generally concern themselves only with segments. Impedance are dependent upon the number of observation points considered and, consequently, do not possess invariant characteristics*".

Principle of sufficient reason: "Cause", "Effect", philosophy [6] and metaphysics.

The difficulty of the adoption of the *mobility*—indirect analogy—vision in comparison to the *impedance*—direct analogy is probably rather a philosophical consideration. In the 17th the "principle of sufficient reason" developed by Leibniz had created a deep metaphysical sense of "cause" and "effect". Le Corbeiller wrote a philosophical aside [13]: "*The reader may wonder how it is possible to derive the dynamical behavior of a system from kinematic equations. This question arises because we are accustomed in dynamics to a mistaken emphasis on forces, traceable to a metaphysical attitude current in Newton's times. From this emphasis on force considered as the "cause" of motion, there followed in electricity an emphasis on electromotive force considered as the "cause" of the current flow. To one without such preconceptions, it should be clear that in Ohm's law* $E = IR$*, as well as in Newton's law* $f = ma$*, the general gas law* $PV = nRT$*, or any natural law whatsoever, there is no cause and no effect, there are only variable physical quantities permanently connected by a mathematical equation. For instance, whenever any two of the quantities* E, I, R *are known at any time* t *Ohm's law allows us to find the third one; if* I *and* R *happen to be known, it would make little sense to call them the "cause" of* E*, and call* E *their "effect" "*.

The need of considering systems with multiple inputs and multiple outputs has been addressed by Rubin in "Transmission matrices for vibration and their relation to admittance and impedance" [15]. Each subsystem is characterized with impedance or mobility matrices. In a further development he addressed in "Mechanical Immittance- and Transmission-Matrix Concepts" [16] the operations necessary to assemble subsystems together.

The impedance/mobility framework is still an open area of research. Nowadays, the efforts are mainly concentrated on two aspects: the characterization of a subsystem by means of inverse method such as exposed by Höller in [17] on the one hand, the consideration of complex interfaces—i.e. line or surface instead of points—on the other hand. As an example of the research of Meyer exposed in "prediction of the vibroacoustic behavior of a submerged shell with non-axisymmetric internal substructures by a condensed transfer function method" proposes a method to address line interfaces [18].

Kim suggest "a compact matrix formulation using the impedance and mobility approach for the analysis of structural-acoustics systems" [19]. This work has extended the application of the mobility method to vibro-acoustical system—i.e. system with a structure and a fluid. The Patch Transfer Functions method has also been developed with the intention to address the field of vibro-acoustics.

[6] From the side of history, philosophy and sociology of the scientific knowledge, the philosopher T. S. Kuhn has set a milestone with his work and among other the book "The Structure of Scientific Revolutions" [94].

Patch Transfer Functions method (PTF)

Entering the 21st century, the *mobility* method has been adapted for the needs of acoustics and vibro-acoustics. The main challenge was the consideration of continuous interfaces—as often encountered in acoustics and vibro-acoustics. Both visions, *impedance* and *mobility*, have been addressed.

Cacciolati initiated first a *mobility* approach for acoustic problem: "acoustic mobility for vibroacoustic prediction" [20]. The continuous coupling interface is discretized in elementary surfaces called patches. The term "*patch-mobility method*" was born. The method relies on the characterization of each uncoupled subsystem—by means of either numerical, analytical or measurement method. Once a database of *mobilities*—stored in matrices—is complete, the framework of the mobility method allows to calculate the response of the coupled system.

After the resolution of some numerical complications, such as the inversion of *ill-conditioned matrices*, many applications have been proposed. Chazot has addressed the problem of "prediction of transmission loss of double panels with a patch-mobility method" [21]. After some additions, this work has been published under the title: "transmission loss of double panels filled with porogranular materials" [22]. A year later, Guyader added the consideration of stiffeners: "transmission loss prediction of double panels filled with porous materials and mechanical stiffeners" [23].

In opposition to Cacciolati who sided in 2000 with the *mobility* approach [20], Maxit sided with the *impedance* approach. As a result, he presented in 2002 a similar approach for acoustical system: "airborne noise prediction using patch acoustic impedance" [24]. The term "*patch-impedance*" was born. The name of the method has been subsequently changed to "Patch Transfer Functions" (PTF). The paper of Ouisse: "Patch Transfer Functions as a Tool to Couple Linear Acoustic Problems" is a milestone in the development of this method [25]. Indeed this papers addresses, the theoretical framework of the method, a numerical validation—covering the convergence of the method and other numerical considerations—and concludes with a successful application on an automotive.

By using the vibro-acoustics substructuring method Patch Transfer Functions, a coupled system can be considered as several subsystems connected through elementary surfaces called patches. In terms of methodology, the large and complex problem can be broken down into simpler sub-problems. Various methods can then be applied on these patches to calculate the vibro-acoustical behavior of each subsystem. Upon the attainment of these individual vibro-acoustical responses, the acoustical response of the fully coupled system can be predicted by reassembling the subsystems using continuity relations. One example of a hybrid PTF model is found in "a Combined Computational-Experimental Approach for Modelling of Coupled Vibro-Acoustic Problems" experimented by Rejlek [26].

If the controversy of the 20th century "*impedance*" versus "*mobility*" had slowly turned in the advantage of the "*mobility*", the opposite has happened in the field of acoustics. Starting at the beginning of the 21st century both alternatives "*patch-mobility method*" versus "*patch-impedance method*" has been developed simultaneously. Nevertheless, in this case the approach in terms of "*impedance*" has been found numerically more stable than the "*mobility*" one. As a result the Patch Transfer Function (PTF) has been further developed.

As the method has gained more and more interest in the last two decades, several studies have been published. Motivated by industrial needs—automotive pass-by noise—Totaro has proposed an "Extension of the Patch Transfer Functions method (PTF method) to high

frequency domain (sub-cavities decomposition)" [27]. In this study, the division of a large size cavity, into smaller sub-cavities, allows to reduce the total number of modes that must be computed Figure 1.7.

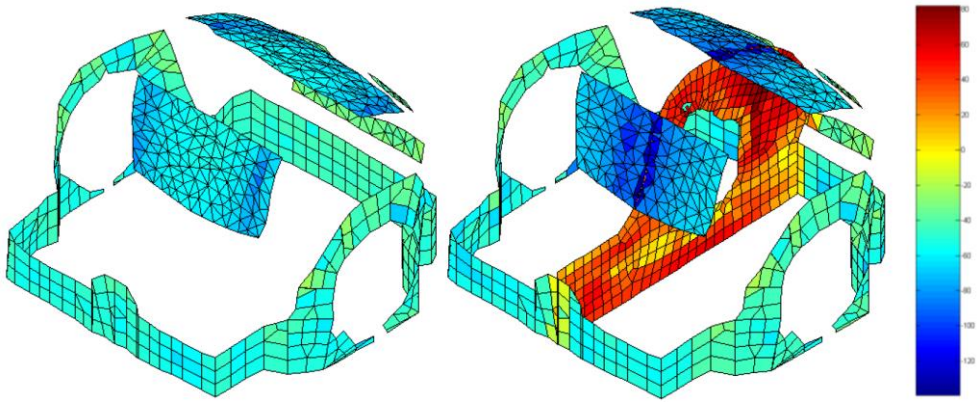

Figure 1.7: Patch Transfer Functions method model of an engine compartment. Coupling velocities at 200 Hz. Left: 1 cavity; Right: 2 sub-cavities. The model with 2 sub-cavities allows to decrease the computational cost (less modes)—or to extend the upper frequency for the same computational cost. This figure is found in [27].

After many applications for airborne noise configuration, the Patch Transfer Functions method has been applied to underwater structures such as encountered for submarines [28]. Considering the FEM computation of Patch Transfer Functions for the coupling in heavy fluid, Aucejo encountered convergence issues. As a result, he proposed the article "convergence acceleration using the residual shape technique when solving structure–acoustic coupling with the Patch Transfer Functions method" [29]. Maxit has continued to improve this technique resulting in: "improving the Patch Transfer Function Approach for Fluid-Structure Modelling in Heavy Fluid" [30].

As acoustical material are of great use for acoustics, some studies have covered this aspect. Maxit has investigated the "modeling of micro-perforated panels in a complex vibro-acoustic environment using patch transfer function approach" [31]. Veronesi has proposed "Patch Transfer Function Approach for Analysis of Coupled Vibro-Acoustic Problems Involving Porous Materials" [32]. Based on an extension of this work, Albert has proposed the "Prediction of the vibro-acoustic response of a structure-liner-fluid system based on a patch transfer function approach and direct experimental subsystem characterisation" [33].

The creation of a Patch Transfer Functions model allows a correct physical description of a problem of acoustics or vibro-acoustics. As the model is extremely small—i.e. matrices involved in the PTF calculation are much smaller than the one involved in a FEM or BEM calculation—it allows running optimization algorithms. In "efficient positioning of absorbing material in complex systems by using the Patch Transfer Function method", Totaro has illustrated one application of acoustical optimization [34].

Statistical energy analysis (SEA)

The Statistical Energy Analysis (SEA) has been developed in the sixties. Based on the generalization of power balance between coupled oscillators, this method estimates the energy exchanges between weakly coupled subsystems. The extreme simplicity of the system of equations to be solved is due to the use of random variables and random excitations and relies on several constraining assumptions that are mostly valid at high frequency. Conversely, in this frequency range, the Finite Element methods are facing

some difficulties related to the size of the model (the number of degrees of freedom increases with frequency) and to high variabilities of the structures in high frequency.

Le Bot [35] considers SEA as the pendant of thermodynamics in the field of sound and vibration. The fundamental of SEA is the "*coupling power proportionality*". It states that two subsystems are exchanging a power proportionally to the difference of "*vibrational temperature*". The factor of proportionality is called "*coupling loss factor*". Working with scalars instead of displacements and velocities has several advantages. Nevertheless, this approximation relies on several hypotheses partially reviewed by T. Lafont [36]: Random forces such as rain-on-the-roof; diffuse field; energy equipartition; conservative, weak and direct coupling; light damping.

As the SEA method is based on power transfer between subsystems, it is part of the framework of substructuring. The drawback is that the substructure must be defined respecting the hypotheses of SEA. In this case, the weak coupling hypothesis is the most important one and often the most difficult to guarantee. J.-L. Guyader [37] and N. Totaro [38] tackle this problem by introducing an automatic partitioning technique analyzing energy transfer function with a clustering algorithm. An index—MIR for Mutual Inertia Ratio—allows to check the validity of the proposed structural partitioning. A low value indicates a weak coupling and supports the usage of the SEA method.

The substructuring with SEA has been applied to many industrial structures. N. Totaro has applied it to the case of a high-speed train TGV-Duplex [39]. M. Kassem has proposed an application in the field of automotive "Structural partitioning of complex structures in the medium-frequency range. An application to an automotive vehicle" [40]. For structure of growing complexity, a judicious partitioning might be time consuming. In this context, C. Díaz-Cereceda has proposed an "Automatic subsystem identification in statistical energy analysis" [41]. Some other applications are found in the field of complex acoustical network such as proposed by A. Bocquillet in [42].

SEA hypotheses are generally met in the high frequency range. The frequency gap between low frequency addressed by FE methods and the high frequency solved by SEA is still an open topic in the field of sound and vibration.

Statistical modal Energy distribution Analysis (SmEdA)

The Statistical modal Energy distribution Analysis (SmEdA) first proposed by L. Maxit is an extension of SEA with the relaxation of the hypothesis of equipartition of modal energies [43]. The relaxation of this hypothesis allows to tackle the problem of strong coupling, low modal density and localized force. As a result, this method is well suited for the mid frequency range.

The method relies on the calculation of the coupling loss factors between the modes of the uncoupled subsystems by means of Finite Element Method calculations applied on uncoupled subsystems. The theory is presented in "Estimation of SEA coupling loss factors using a dual formulation and FEM modal information, Part I: Theory" [44]. This paper is completed with a numerical validation [45]. Further developments are presented in "Extension of SEA model to subsystems with non-uniform modal energy distribution" [46]. The method is validated on a laboratory setup and on some parts of vehicles (truck cabin, car firewall, side glazing of a car excited by a Turbulent Boundary Layer, etc…).

N. Totaro [47] has demonstrated in "SEA Coupling Loss Factors of Complex Vibro-Acoustic Systems" that SmEdA can be applied on a structure-to-cavity coupling and has shown an application on a complex automotive system.

Finally, H. D. Hwang has introduced the possibility of local distribution of dissipative treatment in "SmEdA vibro-acoustic modelling in the mid-frequency range including the effect of dissipative treatments" [48] [49].

1.4.2 Characterization of a subsystem

Characterization by means of numerical modelling

The physical domain is generally described with local fundamental principles of mechanics: law of conservation of mass and Newton's second law $\vec{F} = m\vec{a}$. These local principles are often represented with differential equations such as the equation of Navier-Stokes [50]. For an acoustical medium it results to the Helmholtz's equation [51]. In order to fully describe the system some information about the boundary such as imposed stresses or displacement are necessary [52].

Solving this set of differential equations—i.e. local and boundary conditions—might be done analytically for simple academical cases. For more complex systems, many numerical methods are able to find an approached solution. The Finite Element Method (FEM) and the Boundary Element Method (BEM) are among the most common in the field of vibro-acoustics [53].

FEM

> *"The limitations of the human mind are such that it cannot grasp the behaviour of its complex surroundings and creations in one operation. Thus the process of subdividing all systems into their individual components or 'elements', whose behaviour is readily understood, and then rebuilding the original system from such components to study its behaviour is a natural way in which the engineer, the scientist, or even the economist proceeds." [54].*

The Finite Element Method (FEM) is a versatile numerical method to solve problems described by means of partial differential equations. The partial differential equations are representing a local problem of equilibrium, written with a variational formulation [55]. The latter are written in terms of interpolation functions, describing a relation between the nodes of an element. An element is defined by a set of nodes and an interpolation function. The mesh is a set of elements.

Finally, the set of partial differential equations to be solved turns into the resolution of a linear set of equations. The latter is written with matrices as proposed in Eq. 1.3 for the case of NVH:

$$[K + i\omega D - \omega^2 M]\{X\} = \{F\} \tag{1.3}$$

The stiffness matrix K, the damping matrix D and the mass matrix M are representing inherent properties of the system. The vectors $\{X\}$ and $\{F\}$ are describing the response of the system. Vector $\{X\}$ represents the response at each node in terms—displacement or pressure. Vector $\{F\}$ represent the effort applied to the nodes.

Eq. 1.3 might be solved directly or using a modal basis. If all modes are considered this approach does not result in an additional approximation. Nevertheless, considering all modes would not bring any computational cost reduction. The interest of the modal synthesis is that the solution up to a given frequency is well approximated with a reduced number of modes.

The description of a system with its eigenmodes allows to bridge the gap between simulation and experiment. Indeed the mathematical model can be found by means of experiments. The book “Modal Testing: Theory, Practice and Application” written by Ewins is considered as the reference in modal testing [56]. The comparison of numerical simulation and testing allows updating the numerical model to fit the physical reality—e.g. many hypotheses such as the value of damping are generally not known *a priori*. Many commercial solutions have been developed, reaching a broad number of users. For the need of the *non-specialist* users, Avitabile has proposed a rigorous vulgarization of the method in “experimental Modal Analysis (A Simple Non-Mathematical Presentation)” [57].

Another approach to gain more confidence in numerical model is “toward simulation-based design” [58]. In this paper, Shephard addresses the problem of coupling the computer-aided design, with computer-aided engineering. According to the author, the simulation should rather be considered through the full development cycle than as a validation test at the end of the process. This consideration should promote design decision making according to the criterion of the ability to simulate it.

BEM

The Boundary Element Method (BEM) is in some measure the pendant of the Finite Element Method (FEM) for infinite system. The method relies on a numerical resolution of the partial differential equations representing a local behavior. The differential equations are formulated within the framework of the acoustical integral formulation [59].

A BEM method can also be used for a non-infinite cavity. The advantages is that the BEM approach relies on a surface mesh while the FEM approach relies on a volume mesh [60]. Despite that, the calculation of the Green’s function in a closed cavity might result in many numerical difficulties. Many commercial tools include advanced methods to overcome these difficulties. As a result, in the field of acoustics both approaches are valid [61].

Characterization by means of experiment

For some subsystems, an experimental characterization is preferred over numerical modeling. This choice might be motivated by several factors but generally, it is motivated by a compromise in terms of quality, cost and schedule. The framework of dynamic substructuring allows assembling subsystems characterized by means of different methods. In this case, the word “*hybrid model*” is used. More information are available in “Advancements in hybrid dynamic models combining experimental and finite element substructures” [62].

In the framework of sound and vibration, a complex problem is often partitioned in an active and a passive part [63]. Both parts of the system—active/passive—have to be characterized in order to describe the later assembled system. The vibration of the active part are generally too complex to be modeled or measured directly. As a result, many methods for source characterization have been developed.

A. T. Moorhouse has addressed the characterization of both airborne and structure borne source. In “Characterisation of an airborne sound source for use in a virtual acoustic prototype” [64], he has characterized an electrical motor. A simple model—line of four monopoles—combined with measurements in a free field environment and an inverse method allows to find the strength of each supposed source. From the side of structure borne source he has proposed “In situ measurement of the blocked force of structure-borne

sound sources" [65]. The proposed method relies on an inverse method. The method has practical advantages, such as no need of a blocked force test rig.

Many characterization methods are based on an inverse formulation. In this case, accurate measurements are mandatory and, among other, the position of the sensors is of key importance. M. W. F. Wernsen has proposed in "An indicator sensor criterion for in-situ characterisation of source vibrations" [66]. This paper is focused on the identification of in situ blocked force of an active component. It is found that indicator sensors should be placed close to the force intended to be identified.

Several inverse formulations of the Patch Transfer Functions method have been proposed for the need of characterization of acoustical sources. G. Pavic proposes the "Air-borne sound source characterization by patch impedance coupling approach" [67]. Other alternatives are found in the PhD thesis of M. Aucejo [68] and D. Vigoureux [69].

In her PhD thesis "Characterisation of Air-borne Sound Sources using Surface Coupling Techniques" L. Du addresses among other a particular system characterization [70]. Indeed in the proposed method, the source is placed in a source space coupled with a receiver space. For the needs of the method, the receiver space is described with Patch Transfer Functions—i.e. blocked pressure. The database of Patch Transfer Functions method is measured directly with a special experimental setup. In this extend, the continuous virtual interface is physically discretized in mobile pistons—pendant of patches. Each piston can be activated separately, or blocked. This setup is the first attempt to measure directly Patch Transfer Functions for an acoustical cavity.

G. Veronesi has also proposed a direct approach in his PhD thesis "A novel PTF-based experimental characterisation for poro-elastic liners: Method and sampling criterion" [71]. In the direct approach the Patches, of the Patch Transfer Functions method, are also physically materialized by rigid pistons. Yet the originality of his work relies in the proposition of an inverse method. In this case the blocking conditions are not satisfied at the interface during the test. Yet a special experimental setup combined to an inverse method allows to determine indirectly this blocked pressure.

A slightly comparable method, but not in the framework of the Patch Transfer Functions method, is proposed by S. Rakotonarivo in [72]. The method intends the characterization of the impedance matrix of a complex system by means of experiments. In this extend the system is excited by a noisy environment. The dual quantities pressures and velocities are measured at its interface. Finally, an inverse method allows the identification of the researched impedance matrix.

1.5 Dissertation contribution

In Chapter 1, the industrial problematic "*Description and quantification of the sound transmission from the exhaust outlet into the interior of a vehicle*" has been presented. Considering the proposed industrial constraints, the acoustical substructuring method Patch Transfer Functions is considered as one of the viable alternative to fulfill this problematic.

Chapter 2 addresses the framework of the Patch Transfer Function method. The principles and theoretical background of this substructuring approach are explained in details. The potential benefits of an *in situ* characterization of a complex vibro-acoustic subsystem in an industrial context is underlined. The scientific problematic "*Characterization of Patch Transfer Functions of a subsystem by means of measurement on a coupled system*" is formulated.

The development reported in each of the following chapter may encompass one or several extensions of the current state of the art:

Chapter 3 addresses the scientific problematic. An inverse method is developed to characterize surface patch impedance by means of acoustic measurements on a fully coupled system. A first example of application is analyzed.
Chapter 4 identifies the limits of the method. The variations of the previous numerical experimental setup, including the presence of simulated measurement uncertainties, turn into a severe instabilities. No *a priori* indicator such as the condition number of the matrix being inverted has been identified to detect this instability.
Chapter 5 proposes a statistical regularization method. This method differs greatly from the standard regularization methods. Instead of adapting the input data in order to stabilize the numerical inversion, the proposed method applies statistics on the results of several identifications. A statistical indicator allows extracting the underlying physical signification partially included in each identification. Tested on the same numerical experimental setup as encountered in the previous chapter, the instability turns into a statistical stability.
Chapter 6 proposes a validation of the statistical identification method on a real experimental setup constituted by a rectangular box open through one of its surface to a non-characterized room. Without any information about the coupled room nor about the subsystem to characterize (the box), the intrinsic uncoupled acoustic impedance of the box can be deduced on the coupling surface.

2 Coupling of vibro-acoustical subsystems

"I realize that this is in some measure an act of faith and vision. ..."

John Fitzgerald Kennedy (1917–1963) in "Address at Rice University in Houston on the Nation's Space Effort", 1962 [1].

Chapter contents:

2.1 Introduction **37**

2.2 Acoustical cavities **38**

2.2.1 Arbitrary uncoupled cavity 38

2.2.2 Arbitrary coupled cavity 41

2.2.3 Patch transfer functions method 43

2.3 Numerical simulation **47**

2.3.1 Reference solution 47

2.3.2 Patch transfer functions method formulation 48

2.3.3 Expression of impedances in Parallelepiped cavities 51

2.3.4 Simulation & Result 53

2.4 Formulation for a vehicle **55**

2.4.1 Black box vision 56

2.4.2 Vehicle 57

2.4.3 Opportunities and limitations 61

2.5 Summary **62**

2.1 Introduction

This chapter introduces, in more details, the framework of the Patch Transfer Functions (PTF) method. Three sections are proposed:

Sec. 2.2. Exposition and discussion around the mathematical background. The transition between the physical description by mean of integrals and the discretized version is gradually addressed.
Sec. 2.3. Presentation of the method for the coupling of two parallelepiped cavities. The approximations arising from the usage of the method are discussed.

Sec. 2.4. Application of the method to the industrial problematic "*Description and quantification of the sound transmission from the exhaust outlet into the interior of a vehicle*".

Many concepts and equations presented in this chapter are used along the entire document—highly cross-referenced.

2.2 Acoustical cavities

In this section, the theoretical background of the strong coupling between two acoustical cavities will be addressed. At first, the equations are presented on two uncoupled arbitrary shaped cavities. In the second time, the coupling will be discussed. Therefore, two methods will be addressed:

Integral formulation. Is the exact solution, addressed in Sec. 2.2.1 and in Sec. 2.2.2.
Discretized formulation. Is an approximated solution—i.e. Patch Transfer Functions method (Sec. 2.2.3).

This presentation intends to illustrate, on the particular case of closed cavities, the link between the exact solution and its approximation with the Patch Transfer Functions method.

2.2.1 Arbitrary uncoupled cavity

Stating of the problem

The calculation of the sound pressure $P(M,\omega)\colon(\mathbb{R}^3,\mathbb{R})\mapsto\mathbb{C}$ and the particle velocity $\vec{V}(M,\omega)\colon(\mathbb{R}^3,\mathbb{R})\mapsto\mathbb{C}^3$, at any point M of a cavity, are presented here on a general case (Figure 2.1). Then, the calculation of the impedances needed as an input for the Patch Transfer Functions method will be derived. In a purpose of notation simplification, the angular frequency ω will be omitted in the following development.

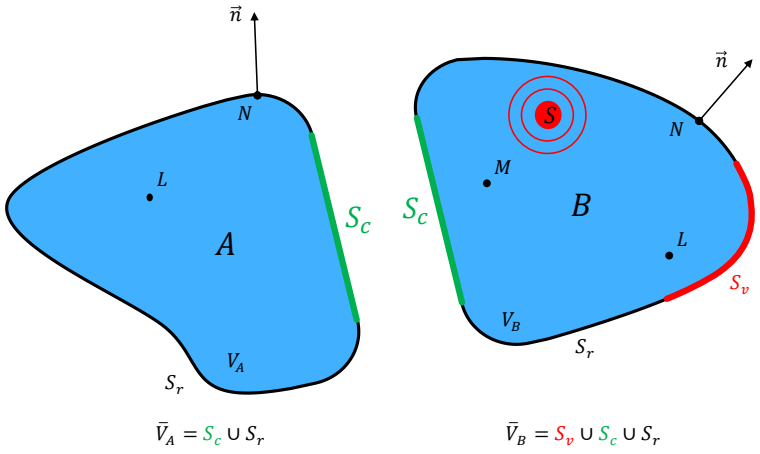

Figure 2.1: The general problem considered here is a cavity of volume V filled with air, bounded with rigid walls $\bar{V}$—outward unit vector normal $\vec{n}$. The enveloping rigid surface $\bar{V}$ is partitioned into a vibrating surface S_v (where a normal velocity $\vec{V}(N) = V_n(N).\vec{n}$ is prescribed) and a blocked surface S_r (where the normal velocity is zero). A point source S of strength $Q(\omega)\colon\mathbb{R}\to\mathbb{C}$, is placed at coordinates $M_S(M_{Sx}, M_{Sy}, M_{Sz})\in\mathbb{R}^3$. A listening point L is located at coordinates $M_L(M_{Lx}, M_{Ly}, M_{Lz})\in\mathbb{R}^3$. For the sake of notation simplicity, "S" and "L" are used indifferently to represent the nature of the point—source or listening point—and its position. M represents an arbitrary point in the cavity. N represents an arbitrary point on the surface.

Transcription of the physical problem into equations

At any point M of the volume—except on the source S—the homogeneous Helmholtz equation is valid. The presence of a point source results in a singularity described with a source density and a Dirac distribution such as $\iiint_V Q(\omega)\delta(M - M_S)dV = Q(\omega)$:

$$\nabla^2 P(M) + k^2 P(M) = Q(\omega)\delta(M - M_S), \forall M \in V \tag{2.1}$$

where ∇^2 is the Laplacian operator, k is the acoustic wavenumber ω/c and c is the celerity of the sound propagation in the acoustical fluid—i.e. air.

On the vibrating surface S_v, Euler equation yields:

$$\vec{\nabla} P(N).\vec{n} = -i\omega\rho_0 V_n(N), \forall N \in S_v \tag{2.2}$$

where $\vec{\nabla}$ is the gradient operator and ρ_0 is the density of air. On the non-vibrating surface S_r, Euler equation yields:

$$\vec{\nabla} P(N).\vec{n} = 0, \forall N \in S_r \tag{2.3}$$

The cavity has inherent pressure eigenmodes ϕ_k verifying—per definition—the homogeneous Helmholtz equation and the rigid boundary condition:

$$\begin{cases} \nabla^2\phi_k(M) + k_k^2\phi_k(M) = 0, \forall M \in V \\ \vec{\nabla}\phi_k(N).\vec{n} = 0 \qquad\qquad , \forall N \in S_r \cup S_v \end{cases} \tag{2.4}$$

where k_k is the acoustic wavenumber of mode k. The volume normalization of these modes is such as:

$$\iiint_V \phi_l(M)\phi_k(M)dv = \Lambda_l\delta_{lk}, \forall M \in V \tag{2.5}$$

where Λ_l is the norm of pressure eigenmode l. Physically, orthogonality means that each mode shape is unique and cannot be obtained through a linear combination of any other mode shapes. The pressure can be written on this orthogonal basis:

$$P(M) = \sum_{k=1}^{\infty} \xi_k(\omega)\phi_k(M), \forall M \in V \tag{2.6}$$

where $\xi_k(\omega)$ is the modal amplitude of mode k. The physical counter part of this mathematical property of orthogonal basis is that when the air in a cavity is vibrating, the pressure at any frequency in free or forced vibration is a combination of all its normal modes.

Equation 2.6 represents an equality if all modes are used. The number of modes of a system is equal to the number of degrees-of-freedom, and thus infinite for a continuous system. If the first m modes among all existing modes are used only, the computed pressure represents an approximation:

$$P(M) \approx \sum_{k=1}^{m} \xi_k(\omega)\phi_k(M), \forall M \in V \tag{2.7}$$

How many modes should be considered?

The convergence of a vibro-acoustic numerical simulation often depending on the number of modes that have been considered, the answer to this question is of prime importance.

Many advanced methods, such as the residual modes, have been developed in order to accelerate the convergence of the modal summation. It allows a good result within a limited computational effort [29].

In this dissertation, no such advanced methods will be used. Yet, the simulation of analytical equations allows considering an important number of modes. In addition, some convergence studies have been carried on.

Problem resolution

The Green's theorem states that:

$$\iiint_V (U\nabla^2 V - V\nabla^2 U)dv = \iint_{\bar{V}} (U\vec{\nabla}V - V\vec{\nabla}U)\vec{n}ds \tag{2.8}$$

where $\vec{\nabla}$ is the gradient operator, $\vec{n}$ is the outward unit normal to the surface $\bar{V}$ of the closed volume V. The field U and V can be arbitrary, as long as their partial is continuous and twice differentiable.

As the Helmholtz's equation is of a form compatible to this theorem, it has a fundamental consequence. The sound field in any closed volume without source is totally described with the knowledge of the pressure and the velocity on its surrounding surface.

This theorem represents the framework of the acoustical integral formulation. The numerical simulation, boundary element method—based on this framework—intends to estimate numerically the Green's function.

Some mathematical symbolic calculations lead to the expression of $P(M)$. Some noncritical calculation steps are omitted.

$\iiint_V (2.1)\phi_k(M) - (2.4)P(M)$ yields:

$$\iiint_V \phi_k(M)\nabla^2 P(M) - P(M)\nabla^2\phi_k(M)dV + \left(k^2 - k_k^2\right)\iiint_V \phi_k(M)P(M)dV = \phi_k(S)Q(\omega) \tag{2.9}$$

Green's theorem (Eq 2.82.8) allows to consider the volume-integral over V, as a surface-integral over $S_v \cup S_r$. In addition, the pressure $P(M)$ can be expressed using (2.6):

$$\iint_{S_v \cup S_r} \left(\phi_k(N)\vec{\nabla}P(N) - P(N)\vec{\nabla}\phi_k(N)\right)\vec{n}ds + \left(k^2 - k_k^2\right)\iiint_V \left(\phi_k(M)\sum_{l=0}^{\infty}\xi_l(\omega)\phi_l(M)\right)dV = \phi_k(S)Q(\omega) \tag{2.10}$$

The boundary conditions equations (2.2), (2.3), and (2.4) simplify the surface-integral. For the volume-integral, using the orthogonality property of mode (2.5)—and some mathematical re-writing—the summation on index l and the index l itself vanish. $\xi_l(\omega)$ becomes $\xi_k(\omega)$ and is expressed as:

$$\xi_k(\omega) = Q(\omega)\frac{\phi_k(S)}{(k^2 - k_k^2)\Lambda_k} + i\omega\rho_0\frac{1}{(k^2 - k_k^2)\Lambda_k}\iint_{S_v}\phi_k(N)V_n(N)ds \tag{2.11}$$

The expression of $P(M)$ at any point of the volume is obtained using Eq. (2.6):

$$P(M) = Q(\omega)\sum_{k=1}^{\infty}\frac{\phi_k(M)\phi_k(S)}{(k^2-k_k^2)\Lambda_k} + i\omega\rho_0\sum_{k=1}^{\infty}\left(\frac{\phi_k(M)}{(k^2-k_k^2)\Lambda_k}\iint_{S_v}\phi_k(N)V_n(N)ds\right) \tag{2.12}$$

The velocity $\vec{V}(M)$ at any point of the volume is obtained using Euler's equation (Eq. (2.13)):

$$\vec{V}(M) = \frac{i}{\omega\rho_0}\vec{\nabla}(P) \tag{2.13}$$

Air damping introduction

The mathematical representation of energy loss in a system is still an open question of physics [73]. Nevertheless, the introduction of a structural modal damping— i.e. η_k of mode k—is a simple convenient approach. The modal damping is introduced by changing the denominator "$\left(\omega^2-\omega_k^2\right)$" of any equation into "$\left(\omega^2-\omega_k^2-i\eta_k\omega_k\omega\right)$"—respectively "$(k^2-k_k^2)$" into "$\left(k^2-k_k^2-i\eta_k k_k k\right)$".

This method works only on acoustical or structural systems where the modal basis is appropriate. Among others, infinite systems do not have eigenmodes.

Green's function

The expression of $P(L)$ at any point of the volume Eq. (2.12) can be written according to Eq. (2.14) as the following form:

$$P(L) = \iiint_V G(L,M)q(\omega)dv + i\omega\rho_0\iint_{\bar{V}}G(L,N)V_n(N)ds \tag{2.14}$$

Note that the second term of the surface integral vanishes. Indeed, as the cavity is considered with rigid walls $\vec{\nabla}G(L,B)$ is equal to $\vec{0}$. It is a direct consequence of the initial hypothesis—Eq. (2.4). Considering Eq. (2.12), the Green's function $G(L,M)$ reads:

$$G(L,M) = \sum_{k=1}^{\infty}\frac{\phi_k(L)\phi_k(M)}{(k^2-k_k^2)\Lambda_k} \tag{2.15}$$

Eq. (2.14) underlines the fact that the sound field at a given position L is the superposition of the effect of many sources. Some of which are located in the volume (in our case only one) and the others on the surface. The sources on the surface are active through the surface vibration. The Green's function $G(L,M)$, respectively $G(L,N)$, describes the sound transmission between point M and L—respectively N and L. The distinction of the nature of the points M in the volume and N on the volume is a pure notation convention. The Green's function is unique, though the points where it is evaluated are changing.

2.2.2 Arbitrary coupled cavity

Stating of the problem

Let's consider that cavity C can be split in two coupled cavities A and B as shown in Figure 2.2. The coupling surface S_c is a virtual surface defined arbitrarily between cavities A and B.

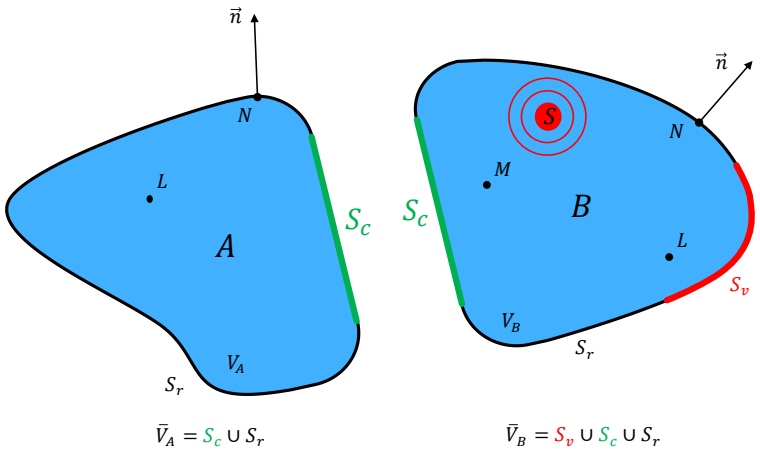

Figure 2.2: Cavity A has volume V_a and boundary surface $\bar{V}_a$; cavity B has volume V_b and boundary surface $\bar{V}_b$. The cavity C is the union of cavities joined by a surface S_c common to both surfaces $\bar{V}_a$ and $\bar{V}_b$.

Uncoupled cavities

Let's consider the two uncoupled cavities. The pressure in each point of the respective cavity is derived from Eq. (2.14). For cavity A it reads:

$$P_A(L) = i\omega\rho \iint_{S_c} G_A(L,N) V_{An}(N) ds \tag{2.16}$$

For the cavity B it reads:

$$P_B(L) = G_B(L,S) Q_B(\omega) + i\omega\rho \iint_{S_v} G_B(L,N) V_{Bn}(N) ds + i\omega\rho \iint_{S_c} G_B(L,N) V_{Bn}(N) ds \tag{2.17}$$

These two equations are always valid, whether the cavities are coupled or not.

Coupling the two cavities

Locally, at each point of this virtual surface, the pressure and the velocity must be identical, whether the point is considered being in one or the other system. In terms of equation, it reads:

$$\begin{cases} P_A(L) = P_B(L) = P_C(L) & ,\forall L \in S_c \\ -V_{An}(L) = V_{Bn}(L) = V_{Cn}(L), & \forall L \in S_c \end{cases} \tag{2.18}$$

The apparition of the minus for the velocity $V_{na}(L)$ is the result of an arbitrary convention. When the two systems are coupled, the outward normal $\vec{n}$ of surface S_r is not defined anymore. One must decide which normal of one of the two subsystems should be kept. Both choices are valid and do not impact the end result, but is solely the intermediate calculation. As an arbitrary choice, the normal considered is the original one of the system B.

The solution of this integral system of equations Eq. (2.16), Eq. (2.17) and Eq. (2.18), conduces to the coupled velocity $V_c(L)$ which satisfies the physical compromise between the drive of each subsystem. With the knowledge of this velocity, the pressure at any point of one of the cavities A or B could be computed using Eq. (2.16) or Eq. (2.17).

In many situations, even in some systems that might be considered as simple, the analytical solution might not be found without any mathematical approximation—e.g. variational calculation. The Patch Transfer Functions method is such a method.

2.2.3 Patch transfer functions method

Problem statement

The demonstration is based on the problem presented on Figure 2.3. The system C is considered as being the coupling of two subsystems A and B coupled by a virtual surface S_c. The continuous surface S_c is discretized in surfaces Γ_i. A point source of strength $Q_b(\omega)$ is placed at position S in the sub-cavity B and a listening point L is present in the sub-cavity A and B.

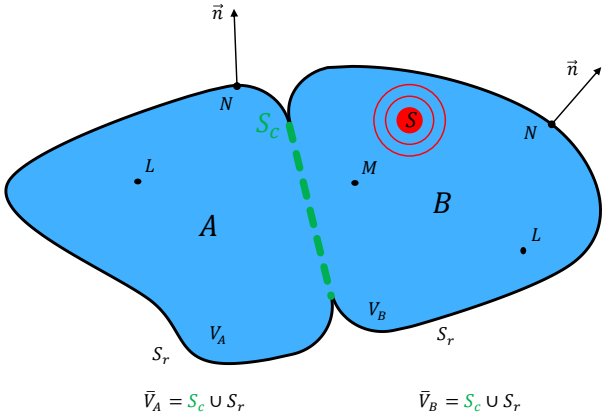

Figure 2.3: The system C is considered as being the coupling of two subsystems A and B coupled by a virtual surface S_c. The continuous surface S_c is discretized in surfaces Γ_i. A point source of strength $Q_b(\omega)$ is placed at position S in the sub-cavity B and a listening point L is present in the sub-cavity A and B. In this example, no vibrational input is present on the surface.

Continuous to discrete vision

When the two cavities are coupled by the surface S_c the Eq. (2.16), Eq. (2.17), and Eq. (2.18) are valid and written as the following form:

$$\begin{cases} P_A(L) = -i\omega\rho \iint_{S_c} G_A(L,N) V_c(N) ds & ,\forall L \in S_c \\ P_B(L) = G_B(L,S) Q_B(\omega) + i\omega\rho \iint_{S_c} G_B(L,N) V_c(N) ds & ,\forall L \in S_c \\ P_A(L) = P_B(L) & ,\forall L \in S_c \end{cases} \tag{2.19}$$

As this set of equations is valid at any point of the interface S_c, it is also valid at each point of each elementary surface Γ_i —i.e. $P_A(L) = P_B(L), \forall L \in \Gamma_i$. This local equilibrium is resulting in a more global equilibrium over each surface Γ_i:

$$P_A(L) = P_B(L), \forall L \in \Gamma_i \Rightarrow \frac{1}{\Gamma_i} \iint_{\Gamma_i} P_A(L) d\Gamma_i = \frac{1}{\Gamma_i} \iint_{\Gamma_i} P_B(L) d\Gamma_i \ , \forall \Gamma_i \tag{2.20}$$

Note that this implication is perfectly valid without any approximation. Nevertheless, this equation is a non-return statement. The inverse statement is generally false—i.e. a global equilibrium does not imply a local equilibrium. As Eq. (2.20) is actually a pressure spatial average, the following notation will be used:

$$\frac{1}{\Gamma_i} \iint_{\Gamma_i} P_A(L) d\Gamma_i = \langle P_A(L) \rangle_{L \in \Gamma_i} \tag{2.21}$$

Changing the terms of Eq. (2.20) by their expression yields:

$$\frac{1}{\Gamma_i}\iint_{\Gamma_i}\left(-i\omega\rho\iint_{S_c}G_A(L,N)V_c(N)ds\right)d\Gamma_i = \frac{1}{\Gamma_i}\iint_{\Gamma_i}\left(i\omega\rho\iint_{S_c}G_B(L,N)V_c(N)ds\right)d\Gamma_i + \langle G_B(L,S)\rangle_{L\in\Gamma_i}\,Q_B(\omega) \tag{2.22}$$

The two integrals over S_c can be computed as a sum of j integrals over each elementary surface Γ_j. For example, the first integral reads:

$$\iint_{S_c}G_A(L,N)V_c(N)ds = \sum_j\iint_{\Gamma_j}G_A(L,N)V_c(N)d\Gamma_j \tag{2.23}$$

At this point, the first approximation is introduced: if dimensions of the surface Γ_j are much smaller than the acoustic wavelength, the velocity $V_c(N)$ can be assumed as constant over the elementary surface Γ_j—i.e. $V_c(N) = V_j, \forall N \in \Gamma_j$. In this way the elementary surfaces can be illustrated by a virtual piston with no mass, moving toward the normal direction with the velocity V_j.

With this approximation, Eq. (2.23) reads:

$$\iint_{S_c}G_A(L,N)V_c(N)ds \approx \sum_j V_j\iint_{\Gamma_j}G_A(L,N)d\Gamma_j = \sum_j\Gamma_j V_j\langle G_A(L,N)\rangle_{N\in\Gamma_j} \tag{2.24}$$

Finally, for each elementary surface Γ_i, Eq. (2.22) yields:

$$\sum_j -i\omega\rho\Gamma_j V_j\langle G_A(L,N)\rangle_{L\in\Gamma_i,N\in\Gamma_j} = \sum_j i\omega\rho\Gamma_j V_j\langle G_B(L,N)\rangle_{L\in\Gamma_i,N\in\Gamma_j} + \langle G_B(L,S)\rangle_{L\in\Gamma_i}\,Q_B(\omega) \tag{2.25}$$

Eq. (2.25) is written for all the N_i surfaces. Therefore a compact matrix formulation can be used:

$$-i\omega\rho\left[\Gamma_j\langle G_A(L,N)\rangle_{L\in\Gamma_i,N\in\Gamma_j}\right]\{V_j\} = i\omega\rho\left[\langle G_B(L,N)\rangle_{L\in\Gamma_i,N\in\Gamma_j}\Gamma_j\right]\{V_j\} + \{\langle G_B(L,S)\rangle_{L\in\Gamma_i}\}\,Q_B(\omega) \tag{2.26}$$

This equation can be rewritten as a function of impedances [Pa/Input]:

$$-\left[Z^A_{i\leftarrow j}\right]\{V_j\} = \left[Z^B_{i\leftarrow j}\right]\{V_j\} + \{Z^B_{i\leftarrow s}\}Q_B(\omega) \tag{2.27}$$

The impedance $Z^A_{i\leftarrow j}$ of sub-domain A is defined as the ratio between the space averaged pressure $\langle P_A(L)\rangle_{\mathrm{L}\in\Gamma_i}$ on patch i and the velocity V_j of patch j. This kind of impedance is called "patch-to-patch" impedance. The mathematical expression of the impedances and their relation to the Green's function is provided below in the section "Acoustic impedance in a cavity".

Eq. (2.29) is a key point of the PTF method. In this equation, the impedance matrices $\left[Z^A_{i\leftarrow j}\right]$ and $\left[Z^B_{i\leftarrow j}\right]$ and the impedance vector $\left\{Z^B_{i\leftarrow s}\right\}$ constitute information on the uncoupled sub-domains A and B. Conversely, $\{V_j\}$ is a coupling velocity vector that represents the effect of the coupling between the two sub-domains. Therefore, the coupling velocity vector $\{V_j\}$ can be expressed as a function of information on the uncoupled sub-domains:

$$\{V_j\} = -\left[\left[Z^A_{i\leftarrow j}\right] + \left[Z^B_{i\leftarrow j}\right]\right]^{-1}\{Z^B_{i\leftarrow s}\}Q_B(\omega) \tag{2.28}$$

This solution is an approximation of the exact solution, found in the previous section, as long as the coupling surface is discretized into elementary surfaces (patches) on which the coupling velocity is supposed to be constant. As demonstrated in [25], this approximation is valid if the dimensions of the patches are smaller than the half-wavelength in the acoustic medium.

Solving the system of equations 2.30 allows computing the coupling velocities V_j of each patches of the coupling surface. Therefore, the pressure at any point inside the sub-domains can be deduced from Eq. (2.21). According to the discretization of the coupling surface, Eq. (2.21) is rewritten as:

$$\begin{cases} P_A(L) \approx P'_A(L) = -i\omega\rho \sum_j \Gamma_j V_j \langle G_A(L,N)\rangle_{N\in\Gamma_j} & ,\forall L \in A \\ P_B(L) \approx P'_B(L) = +i\omega\rho \sum_j \Gamma_j V_j \langle G_B(L,N)\rangle_{N\in\Gamma_j} + G_B(L,S)Q_B(\omega), & \forall L \in B \end{cases} \tag{2.29}$$

Stated with impedances' matrices Eq. (2.29) yields:

$$\begin{cases} P'_A(L) = -\left[Z^A_{L\leftarrow j}\right]\{V_j\} & ,\forall L \in A \\ P'_B(L) = \left[Z^B_{L\leftarrow j}\right]\{V_j\} + Z^B_{L\leftarrow S}Q_B(\omega), & \forall L \in B \end{cases} \tag{2.30}$$

where $Z^A_{L\leftarrow j}$ stands for the ratio between the pressure at point L in the sub-domain A and the velocity V_j of the patch j. This kind of impedance is often called "patch-to-point" impedance. As the hypothesis of patches involves a loss of information, the exact solution $P(L)$ cannot be retrieved. Nevertheless, the exact pressure is estimated (Eq. (2.30)) by the pressure $P'(L)$ within the consideration of discretization's effect. When the size of the patches tends to zero, the estimation tends to the exact solution—i.e. $\lim_{\Gamma\to 0} P'(L) = P(L)$.

In addition, the convergence of the method for light fluid is extremely prompt [25]. Indeed, large patches up to a size of $\lambda/4$ or even $\lambda/2$ are sufficient to insure the convergence of the Patch Transfer Functions method. More information are found in "On the sampling criterion for structural radiation in fluid" [74].

Acoustic impedance in a cavity

In Eq. (2.27) and Eq. (2.30), the impedance notation has been introduced. The formulation of these terms is solely, implicitly presented. This section intends to present these terms explicitly and with some physical interpretations. The physical interpretation of these terms is quite easy as soon as the interface S_r between the two cavities A and B are considered as independent pistons Γ moving along their normal. For clarification purpose, the patches of each subsystem are indexed with a dual notation:

Patches Γ *of subsystem* A. Indexed indifferently with i and j—i.e. Γ_i and Γ_j.
Patches Γ *of subsystem* B. Indexed indifferently with i and j—i.e. Γ_i and Γ_j.

The impedance calculations are presented without any precision whether working in subsystem A or B. One must obviously consider the parameters associated to the subsystem being characterized—i.e. $Z^A_{L\leftarrow S}$ is computed using $G_A(L,S)$.

Point to point impedance

Mathematical definition. Eq. (2.30), Eq. (2.29), and Eq. (2.15) leads to:

$$Z_{L\leftarrow S} = G(L,S) = \sum_{k=1}^{\infty} \frac{\phi_k(L)\phi_k(S)}{(k^2 - k_k^2)\Lambda_k} = \frac{P(L)}{Q(\omega)} \tag{2.31}$$

Physical interpretation. Ratio between the sound pressure at the listening point $P(L)$—caused by a point source placed at position S—and the source strength $Q(\omega)$. All surfaces in the system are blocked.

Patch to patch impedance

Mathematical definition. Eq. (2.26), Eq. (2.27), and Eq. (2.15) lead to:

$$Z_{i\leftarrow j} = i\omega\rho\Gamma_j\langle G(L,N)\rangle_{L\in\Gamma_i, N\in\Gamma_j} = i\omega\rho\sum_{k=1}^{\infty} \frac{\langle\phi_k(L)\rangle_{L\in\Gamma_i}\langle\phi_k(N)\rangle_{N\in\Gamma_j}\Gamma_j}{(k^2 - k_k^2)\Lambda_k} = \frac{\langle P(L)\rangle_{L\in\Gamma_i}}{V_j} \tag{2.32}$$

Physical interpretation. Ratio between the space average pressure on the surface Γ_i of patch i and the normal velocity of patch j—surface Γ_j. The patch j is vibrating in a translation motion along its normal—$V_n(N) = V_j, \forall N \in \Gamma_j$. All other surfaces in the system are blocked and the point source is inactive.

Point to patch impedance

Mathematical definition: Eq. (2.26), Eq. (2.27), and Eq. (2.15) lead to:

$$Z_{i\leftarrow S} = \langle G(L,S)\rangle_{N\in\Gamma_i} = \sum_{k=1}^{\infty} \frac{\langle\phi_k(L)\rangle_{L\in\Gamma_i}\phi_k(S)}{(k^2 - k_k^2)\Lambda_k} = \frac{\langle P(L)\rangle_{L\in\Gamma_i}}{Q(\omega)} \tag{2.33}$$

Physical interpretation. Ratio between the space average pressure on the surface Γ_i of patch i caused by a point source placed at positon S and the source strength $Q(\omega)$. All surfaces in the system are blocked.

Patch to point impedance

Mathematical definition. Eq. (2.30), Eq (2.29), and Eq. (2.15) lead to:

$$Z_{L\leftarrow j} = i\omega\rho\Gamma_j\langle G(L,N)\rangle_{N\in\Gamma_j} = \sum_{k=1}^{\infty} \frac{\phi_k(L)\langle\phi_k(N)\rangle_{N\in\Gamma_j}\Gamma_j}{(k^2 - k_k^2)\Lambda_k} = \frac{P(L)}{V_j} \tag{2.34}$$

Physical interpretation. Ratio between the sound pressure at listening position L and the normal velocity of patch j—surface Γ_j. The patch j is vibrating in a translation motion upon its normal—$V_n(N) = V_j, \forall N \in \Gamma_j$. All other surfaces are blocked and the point source is not active.

Alternative method for the estimation of space averaged value

The computation of the *patch to patch impedance* Eq. (2.32) and the *point to patch impedance* Eq. (2.33) relies on the computation of the space average pressure on the surface Γ_i of patch i caused respectively by either the patch j or the point source. From the perspective of experimental characterization of a subsystem, the measurement of spatial averaged quantities is often not straightforward—e.g. standard measurement facilities in the field of NVH are generally designed to measure local quantities using microphones or accelerometers.

Nevertheless, if the patch i is small enough, the space average pressure on the surface Γ_i might be estimated with the value of the pressure at its center. When this estimation is done, for the calculation of the Patch Transfer Functions method and the resulting assembly, the word "center" will be used—e.g. PTF Coupling (Center). To avoid any confusion, the word "spatial average" will be used to describe the standard Patch Transfer Functions method—e.g. PTF Coupling (Spatial average). Table 2.1 presents an overview.

Table 2.1: Overview of the computation of the patch to patch impedance and the point to patch impedance. The indicator "Spatial average" corresponds to the standard definition of the Patch Transfer Functions method, while the indicator "Center" corresponds to an estimation. The associated mathematical equations are indicated.

Impedance	PTF (Spatial average)	PTF (Center)
Patch to patch	Patch to patch Eq. (2.32)	Patch to point Eq. (2.34)
Point to patch	Point to patch Eq. (2.33)	Point to point Eq. (2.31)

Note that many different points might be considered to evaluate the so-called "PTF (Center)". The arbitrary choice made here is to retain the center of the associated patch.

2.3 Numerical simulation

For sake of illustration of the previous theory, the simple test case of a monopole acting in a rectangular box will be used. First, a reference solution is presented. Then, this cavity will be split into two smaller rectangular cavities coupled through a rectangular surface. This problem will be solved by the PTF approach and compared to the reference solution.

2.3.1 Reference solution

The considered problem is a cavity C of volume V filled with air, bounded by rigid walls S_r. The walls form a parallelepiped volume of size L_x, L_y, L_z. A point source S of strength $Q(\omega)\colon \mathbb{R} \to \mathbb{C}$, is placed at coordinates $M_S(M_{Sx}, M_{Sy}, M_{Sz}) \in \mathbb{R}^3$. The listening point L is placed at coordinates $M_L(M_{Lx}, M_{Ly}, M_{Lz}) \in \mathbb{R}^3$. For the sake of notation simplicity, "S" and "L" are used indifferently to represent the nature of a point—source or listening point—and its position.

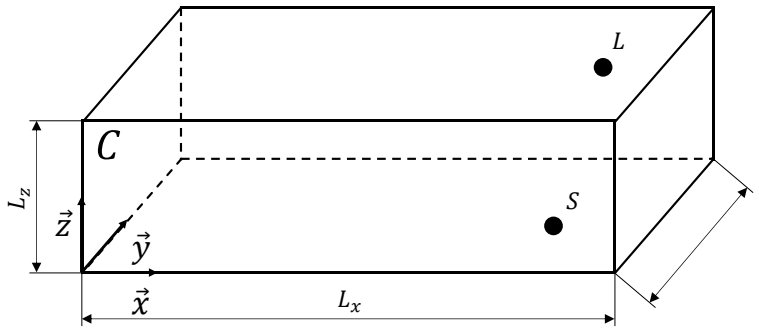

Figure 2.4: Geometry of the system C. A source S is positioned on point M_S. A listening point L is placed on point M_L.

The objective is to compute the sound pressure at the listening point L caused by the source S and all the reflections in the cavity $P(L, S, \omega)\colon (\mathbb{R}^3, \mathbb{R}^3, \mathbb{R}) \mapsto \mathbb{C}$. The reference solution Eq. (2.12) for any shaped cavity with introduction of a modal damping yields:

$$P(L,S,\omega) = Q(\omega)c^2 \sum_{k=1}^{\infty} \frac{\phi_k(L)\phi_k(S)}{(\omega^2 - \omega_k^2 - i\eta_k\omega_k\omega)\Lambda_k} \tag{2.35}$$

where $\phi_k(M)$ is the pressure mode shape k at the point M, $Q(\omega)$ represents the source strength, Λ_k, ω_k and η_k are respectively the norm, the angular frequency, and the modal damping of mode k.

2.3.2 Patch transfer functions method formulation

Step 1. Subdomain definition

The purpose here is to demonstrate the ability of the Patch Transfer Functions method to handle a strong coupling between two acoustical subsystems. Therefore, we consider that the system C is an assembly of the subsystem A and subsystem B (Figure 2.5):

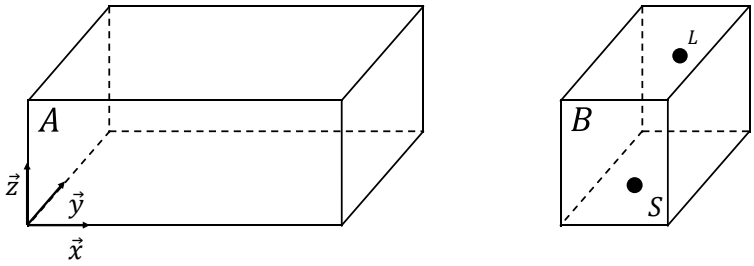

Figure 2.5: The coupled system—box C—is considered as being the coupling of two subsystems—boxes A and B.

Step 2. Coupling surface and division in patches

The subsystems A and B are coupled by a coupling surface. This coupling surface is divided into N elementary surfaces called patches (Figure 2.5 and Figure 2.6). It represents an approximation and the patches' sizes influence the accuracy of the results. However, in light fluid, the results converges with a $\lambda/4$ criterion where λ is the smallest wavelength at the maximum frequency of interest [25].

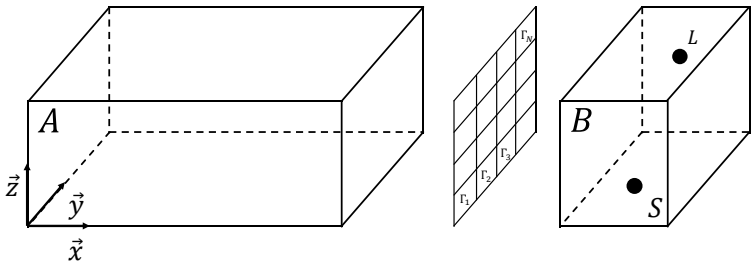

Figure 2.6: The coupling surface between the two subsystems A and B is discretized into N patches Γ.

Step 3. Behavior of uncoupled subdomain A

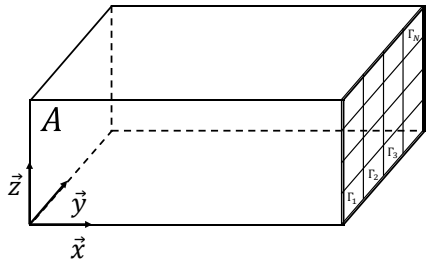

Figure 2.7: The subsystem A consists of a closed cavity where the opened coupling surface to subsystem B is replaced with N patches Γ indexed i and j.

As there is no source in the subsystem A, the space average pressure on the patch Γ_i is linked exclusively to the velocity of all patches Γ_j—acting as sources—and all acoustical reflections on the rigid wall cavity. This relatively complex physical phenomenon can be written down with a compact matrix form:

$$\left\{\langle P_A(L)\rangle_{L\in\Gamma_i}\right\} = \left[Z^A_{i\leftarrow j}\right]\left\{V^A_j\right\} \tag{2.36}$$

Eq. (2.36) stipulates that the pressures on all patches $\{\langle P_A(L)_{L\in\Gamma}\rangle\}\,(N,1)$ and their velocities $\{V^A_{Patch}\}\,(N,1)$ are linked by an inherent property of the subsystem A. This inherent property is mathematically represented with a square matrix $\left[Z^A_{i\leftarrow j}\right]\ (N,N)$ filled with patch to patch impedances $Z^A_{i\leftarrow j}$. The mathematical formulation of the calculation of the patch to patch impedance is presented in Eq. (2.32).

Step 3′. Pressure on patches on uncoupled subdomain B

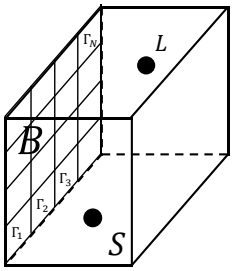

Figure 2.8: The subsystem B consists of a closed cavity where the opened coupling surface to the system A is replaced with N patches indexed i and j. The subsystem B contains the source S and the listening point L.

Similarly, the averaged pressure on patch Γ_i is due to the velocity of all patches j—acting as sources—and all acoustical reflections on the rigid wall cavity. In addition, the source creates a space average pressure on each blocked patch. The effect of the source includes also the acoustical reflections on the rigid wall cavity:

$$\left\{\langle P_B(L)\rangle_{L\in\Gamma_i}\right\} = \left[Z^B_{i\leftarrow j}\right]\left\{V^B_j\right\} + \left\{Z^B_{i\leftarrow S}\right\}Q_B(\omega) \tag{2.37}$$

Equation 2.37 represents a condensation of the behavior of the subsystem B on its interface—which is discretized into N patches. This relation stipulates that the pressure on all patches $\left\{\langle P_B(L)\rangle_{L\in\Gamma_i}\right\}(N,1)$ and their velocities $\left\{V^B_j\right\}\,(N,1)$ are linked by an inherent property of the subsystem B. This inherent property is mathematically represented with a square matrix $\left[Z^B_{i\leftarrow j}\right](N,N)$ filled with patch to patch impedances Eq. (2.32). In addition, the effect of the source is taken into consideration with the source strength $Q_B(\omega)$ and an impedance from source to patch $\{Z^B_{i\leftarrow S}\}$ Eq. (2.33).

Step 4. Coupling condition and resolution

If the two systems A and B happen to be in interaction, the inherent properties of each subsystem have to remain true. Mathematically, it means that Eq. (2.36) describing the behavior of subsystem A at its interface must still be valid—as well as Eq. (2.37) for the subsystem B.

If we consider the interaction between the two subsystems as being a full coupling, there should be some *physical compromise* between the drive of each subsystem. The full coupling can be seen as a no-mass rigid connection between each pair of coincident patch i of both subsystems A and B (Figure 2.9).

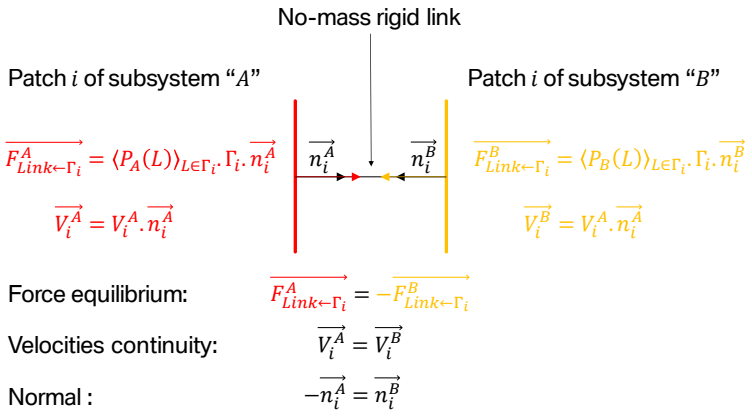

Figure 2.9: The full coupling of the subsystem A and B can be imagined as a no-mass rigid connection between each pair of coincident patch Γ_i of the two subsystems. The continuity of velocities and the dynamic equilibrium lead to equal velocities and opposed forces.

Considering the convention[7] of outward patch's normal vector as being the one of system B, the full coupling between each pair of coincident patch Γ_i of subsystem A and B yields:

$$\begin{cases} \{\langle P_A(L)\rangle_{L\in\Gamma_i}\} = \{\langle P_B(L)\rangle_{L\in\Gamma_i}\} = \{P_C\} \\ -\{V_j^A\} = \{V_j^B\} = \{V_j^C\} \end{cases} \tag{2.38}$$

When the two subsystems A and B are coupled, the response to an arbitrary external stimulation Eq. (2.36) and Eq. (2.37) is not *arbitrary* anymore and corresponds to the behavior of the coupled system. In this sense, the two equations read:

$$\begin{cases} \{P_C\} = -[Z^A_{i\leftarrow j}]\{V_j^C\} \\ \{P_C\} = +[Z^B_{i\leftarrow j}]\{V_j^C\} + \{Z^B_{i\leftarrow s}\}Q_B(\omega) \end{cases} \tag{2.39}$$

The solution of this matrix system of equations reads:

$$\{V_j^C\} = -\left[[Z^A_{i\leftarrow j}] + [Z^B_{i\leftarrow j}]\right]^{-1}\{Z^B_{i\leftarrow s}\}Q_B(\omega) \tag{2.40}$$

The coupled velocity $\{V_j^C\}$ represents the physical compromise between the drive of the two systems when they are forced to "work" together.

[7] The convention choice is arbitrary and still has no influence over the physical result. However, the consistency with chosen convention is important.

Step 5. Pressure at the listening point

Finally, the pressure at the listening point can be computed with:

$$P'_B(L) = \left[Z^B_{L\leftarrow j}\right]\{V_j\} + Z^B_{L\leftarrow S} Q_B(\omega) \tag{2.41}$$

where $Z^B_{L\leftarrow S}$ (1,1) represents the source to point impedance Eq. (2.31) and $\left[Z^B_{L\leftarrow j}\right]$ $(1, N)$ is the patch to point impedance Eq. (2.34).

2.3.3 Expression of impedances in Parallelepiped cavities

The simplicity of the parallelepiped cavity allows expressing the Green's function and therefore the diverse impedance matrices analytically. The required quantities $\phi_k(M)$, $\langle\phi_k(M)\rangle_{M\in\Gamma}$, k_k, and Λ_k are presented in this section. In the case of a more complex geometry, these parameters might be computed with a simulation method—e.g. Finite Element Method.

Pressure eigenmode

An eigenmode is described by three parameters:

Eigen shape. Or mode shape ϕ_k: $\mathbb{R}^3 \rightarrow \mathbb{R}$.
Eigen frequency. Or natural or resonance or modal angular frequency ω_k.
Modal damping. η_k.

The modal damping corresponds to the energy dissipation in the system. This value is generally acquired with experimental measures. In a rectangular shaped cavity the mathematical expression of ϕ_k and the associated ω_k yields:

$$\begin{cases} \phi_k(M) = \phi_{lmn}(M) = \cos\left(\dfrac{l\pi x}{L_x}\right)\cos\left(\dfrac{m\pi y}{L_y}\right)\cos\left(\dfrac{n\pi z}{L_z}\right) \\ \omega_k = \omega_{lmn} = \pi c\sqrt{\left(\dfrac{l}{L_x}\right)^2 + \left(\dfrac{m}{L_y}\right)^2 + \left(\dfrac{n}{L_z}\right)^2} \end{cases} \tag{2.42}$$

The subscript k matchs each combination of the three subscripts l, m, n representing the mode order in each direction[8] $(\vec{x}, \vec{y}, \vec{z})$. Physically, each Eigenmode, for each corresponding Eigen frequency, represents the shape of the pressure in the cavity without source—cf. per se solution of Eq. (2.4).

The normalization of the pressure mode shape is such as:

$$\iiint_V \phi_k^2(M)dv = \iiint_V \phi_{lmn}^2(M)dv = \Lambda_k = \frac{L_x L_y L_z}{2} 2^\alpha \tag{2.43}$$

where the coefficient α is the number of indices l, m, n equal to zero.

Pressure Eigen mode spatial average $\langle\phi_k(M)\rangle_\Gamma$

The calculation of the spatial average of the pressure mode shape is per se:

[8] This equation is valid only if the box edges are oriented in conformity to the directions $(\vec{x}, \vec{y}, \vec{z})$.

$$\langle \phi_k(M) \rangle_{M\in\Gamma} = \langle \phi_{lmn}(M) \rangle_{M\in\Gamma} = \iint_{\Gamma} \phi_{lmn}(M) d\Gamma \tag{2.44}$$

For the analytical calculation presented here, some hypotheses on the surface Γ are made. The surface is considered as a planar surface—cf. surface of a patch—where the normal is oriented along the direction $\vec{x}$. In addition, the shape of the patch is supposed to be rectangular with the edges oriented according to the directions $\vec{y}$ and $\vec{z}$. With these two hypotheses, the coordinates of any point M on the patch is given by:

$$M(x,y,z) \begin{cases} x = x_0 \\ y \in [y_1, y_2] \\ z \in [z_1, z_2] \end{cases} \tag{2.45}$$

Eq. (2.44) yield:

$$\langle \phi_k(M) \rangle_{M\in\Gamma} = \langle \phi_{lmn}(M) \rangle_{M\in\Gamma} = \frac{1}{\Gamma} \int_{y1}^{y_2} \int_{z_1}^{z_2} \phi_{lmn}(M) dydz \tag{2.46}$$

Using the expression of ϕ_{lmn} Eq. (2.42) and transforming a product of cosines in a sum:

$$\begin{aligned} \langle \phi_k(M) \rangle_{M\in\Gamma} = \frac{\cos\left(\frac{l\pi x_0}{L_x}\right)}{2(y_2-y_1)(z_2-z_1)} \int_{y_1}^{y_2} \int_{z_1}^{z_2} \cos\left(\frac{m\pi y}{L_y} + \frac{n\pi z}{L_z}\right) \\ + \cos\left(\frac{m\pi y}{L_y} - \frac{n\pi z}{L_z}\right) dydz \end{aligned} \tag{2.47}$$

Case 1. $m \neq 0; n \neq 0$

$$\langle \phi_k(M) \rangle_{M\in\Gamma} = o \int_{y_1}^{y_2} (a - b + c - d) dy$$

$$\begin{cases} o = \frac{L_z}{n\pi} \frac{\cos\left(\frac{l\pi x_0}{L_x}\right)}{2(y_2-y_1)(z_2-z_1)} \\ a = \sin\left(\frac{m\pi y}{L_y} + \frac{n\pi z_2}{L_z}\right) \\ b = \sin\left(\frac{m\pi y}{L_y} + \frac{n\pi z_1}{L_z}\right) \\ c = \sin\left(\frac{m\pi y}{L_y} - \frac{n\pi z_1}{L_z}\right) \\ d = \sin\left(\frac{m\pi y}{L_y} - \frac{n\pi z_2}{L_z}\right) \end{cases} \tag{2.48}$$

$$\langle \phi_{lmn}(M) \rangle_{M\in\Gamma} = o \left(\int_{y_1}^{y_2} a dy - \int_{y_1}^{y_2} b dy + \int_{y_1}^{y_2} c dy - \int_{y_1}^{y_2} d dy \right)$$

The final solution yields:

$$\langle \phi_{lmn}(M) \rangle_{M\in\Gamma} = \frac{\cos\left(\frac{l\pi x_0}{L_x}\right)}{2(y_2-y_1)(z_2-z_1)} \frac{L_y L_z}{n\pi^2 m} \left(\cos\left(\frac{m\pi y_1}{Ly} + \frac{n\pi z_2}{L_z}\right) - \cos\left(\frac{m\pi y_2}{L_y} + \frac{n\pi z_2}{L_z}\right) \cos\left(\frac{m\pi y_2}{Ly} + \frac{n\pi z_1}{L_z}\right) - \cos\left(\frac{m\pi y_1}{L_y} + \frac{n\pi z_1}{L_z}\right) \cos\left(\frac{m\pi y_1}{Ly} - \frac{n\pi z_1}{L_z}\right) - \cos\left(\frac{m\pi y_2}{L_y} - \frac{n\pi z_1}{L_z}\right) \cos\left(\frac{m\pi y_2}{Ly} - \frac{n\pi z_2}{L_z}\right) - \cos\left(\frac{m\pi y_1}{L_y} - \frac{n\pi z_2}{L_z}\right)\right) \tag{2.49}$$

Case 2. $m = 0; n = 0$

$$\langle \phi_k(M) \rangle_{M\in\Gamma} = \frac{\cos\left(\frac{l\pi x_0}{L_x}\right)}{(y_2-y_1)(z_2-z_1)} \int_{y_1}^{y_2}\int_{z_1}^{z_2} 1 dydz = \cos\left(\frac{l\pi x_0}{L_x}\right) \tag{2.50}$$

Case 3. $m \neq 0; n = 0$

$$\langle \phi_k(M) \rangle_{M\in\Gamma} = \frac{\cos\left(\frac{l\pi x_0}{L_x}\right)}{2(y_2-y_1)(z_2-z_1)} \int_{y_1}^{y_2}\int_{z_1}^{z_2} 2\cos\left(\frac{m\pi y}{L_y}\right) dydz$$
$$\langle \phi_k(M) \rangle_{M\in\Gamma} = \frac{\cos\left(\frac{l\pi x_0}{L_x}\right)}{(y_2-y_1)} \frac{L_y}{m\pi}\left(\sin\left(\frac{m\pi y_2}{L_y}\right) - \sin\left(\frac{m\pi y_1}{L_y}\right)\right) \tag{2.51}$$

Case.4. $m = 0; n \neq 0$

$$\langle \phi_k(M) \rangle_{M\in\Gamma} = \frac{\cos\left(\frac{l\pi x_0}{L_x}\right)}{2(y_2-y_1)(z_2-z_1)} \int_{y_1}^{y_2}\int_{z_1}^{z_2} 2\cos\left(\frac{n\pi z}{L_y}\right) dydz$$
$$\langle \phi_k(M) \rangle_{M\in\Gamma} = \frac{\cos\left(\frac{l\pi x_0}{L_x}\right)}{(z_2-z_1)} \frac{L_z}{n\pi}\left(\sin\left(\frac{n\pi z_2}{L_z}\right) - \sin\left(\frac{n\pi z_1}{L_z}\right)\right) \tag{2.52}$$

At this point, all the theoretical background needed for the numerical simulation has been presented.

2.3.4 Simulation & Result

The cavity *C* considered here is the coupling of two small cavities *A* and *B* coupled with solely two patches (Figure 2.10).

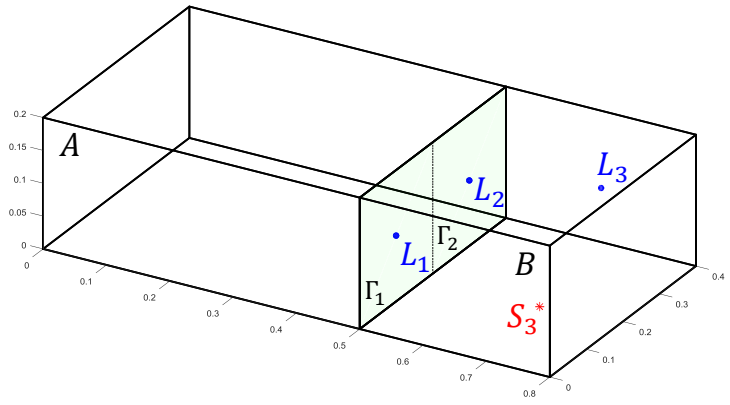

Figure 2.10: The box C is composed of the two sub boxes A and B coupled with an interface discretized in two patches Γ_1 and Γ_2. A listening point—L_1 and L_2—are placed at the center of each patch; a third listening point L_3 is placed in the subsystem B. A source S_3 is placed in the subsystem B.

The properties of all systems are listed in Table 2.2:

Table 2.2: Geometrical and physical properties of all the subsystems A and B and the resulting coupled system C. The lengths are indicated in meters $[m]$.

	Box A	Box B	Box C
$(L_x; L_y; L_z)$	$(0.50; 0.40; 0.20)$	$(0.30; 0.40; 0.20)$	$(0.80; 0.40; 0.20)$
S_3	—	$(0.25; 0.06; 0.07)$	$(0.75; 0.06; 0.07)$
L_1	$(0.50; 0.10; 0.10)$	$(0.00; 0.10; 0.10)$	$(0.50; 0.10; 0.10)$
L_2	$(0.50; 0.30; 0.10)$	$(0.00; 0.30; 0.10)$	$(0.50; 0.30; 0.10)$
L_3	—	$(0.22; 0.28; 0.15)$	$(0.72; 0.28; 0.15)$
ρ	$1.29\ [\mathrm{kg.m^{-3}}]$		
c	$340\ [\mathrm{m.s^{-1}}]$		
η	0.01		
Patches	2 Patches of size $(0.20; 0.20)$		—

The pressure at position L_3 caused by source S_3 is presented in Figure 2.11.

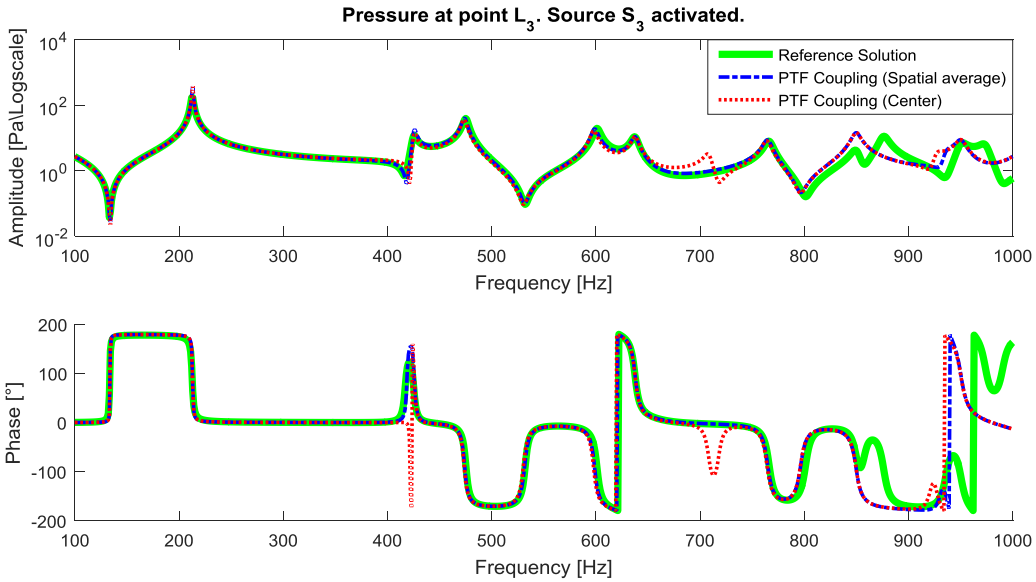

Figure 2.11: Pressure (amplitude and phase) at position L_3 in the cavity C caused by source S_3. Green solid line—"Reference Solution": Represents the reference solution in the box C. The pressure is computed according to Eq. (2.35); Blue dash-dotted line—"PTF Coupling (Spatial average)": Result of the computational coupling of the box A and B with the Patch Transfer Functions method; Red dotted line—"PTF Coupling (Center)": is similar to the "PTF Coupling (Spatial average)" where the patch to patch impedance is estimated with a patch to point impedance and the point to patch impedance is estimated with a point to point impedance—cf. Table 2.1.

The analysis of the results of the "PTF Coupling (Spatial average)" are conformed to the present state of the art of the Patch Transfer Functions method. M. Ouisse *et al.* have shown in [25] that the convergence of this sub-structuring method applied to a strong coupling of lightweight is occurring with a $\lambda/2$ criterion. For the 0.2 meter sized patches of this experiment, it corresponds to a frequency limit of 850 Hz. In Figure 2.11, it can be seen that this criterion is respected as well. Indeed, from a frequency of 850 Hz, the pressure at the listening point L_3 when the source S_3 is active differs from the exact solution.

The application of the "PTF Coupling (Center)" results in a coupling artifact in the frequency range 650–750 Hz. For the other frequencies, the results are in the same quality order than the conventional Patch Transfer Functions method "PTF Coupling (Spatial average)".

2.4 Formulation for a vehicle

In the last two sections, the theoretical background of the Patch Transfer Functions method has been addressed and illustrated with a numerical simulation on two parallelepiped cavities coupled with solely two patches. This section intends to present how such a substructuring method would be extended to a more complicated system like for a *full trimmed vehicle*[9].

[9] A full trimmed vehicle is a complete vehicle without any simplification—i.e. as delivered to the customers. In opposition a Trimmed Body (TMB), is a simplified vehicle, used for development and testing purposes, in which all component and subsystem which are not rigidly connected to the structure are removed—i.e. engine, gearbox, transmission, axels, radiator ... The definition of a TMB is not a standard and might slightly vary.

A fundamental aspect of any substructuring method is to consider a complex system as an assembly of smaller—generally simpler—subsystems coupled at theirs interfaces. It allows understanding and describing a complex system knowing only information about its subsystems. The complexity of any part of the subsystem is condensed solely at its interface with other systems. Once this condensation has been done—whether by means of testing, simulation, or even analytically—the substructuring method should allow describing the full system according to a specific purpose.

The method is independent of the physical complexity of the subcomponents being assembled. Once the subsystems are correctly described, the assembly is representative of the whole coupled system. Yet, the correct description of the subsystem, in a way compatible with the substructuring method, is generally the most challenging and difficult operation that must be undertaken (Chap. 3).

2.4.1 Black box vision

The Patch Transfer Functions method can be seen as a framework allowing to assemble black boxes (Figure 2.12). Some of which might be acoustical, some of which might be structural or even vibro-acoustical subcomponents. In addition, any method can be used to characterize these black boxes. Each uncoupled black box can, for example, be characterized by numerical methods (finite element method, infinite element method, wave-based method, etc.) or experimental methods. For this reason, a structural component such as a *fully trimmed vehicle* might be considered as a vibro-acoustical subsystem.

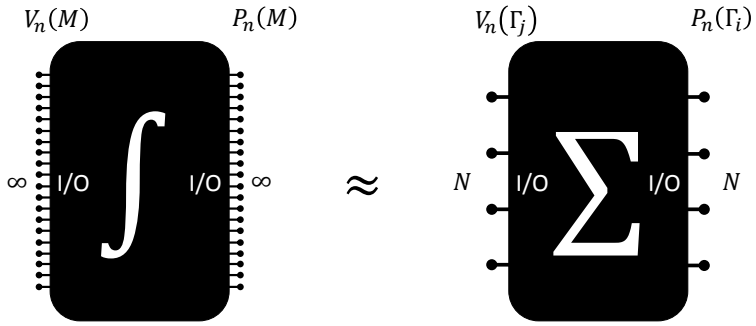

Figure 2.12: Schematic vision of a vibro-acoustical subsystem described at its interface with dual value pressure and normal velocity.

In Figure 2.12. the information about a subsystem is condensed at its interface represented here with pins. While the integral vision—Green's function—requires an infinity of input/output pins, the discretized vision allows considering a finite number of input/output pins. In almost any case, the conversion from the continuous vision to the discrete vision results in an acceptable, yet irreversible, loss of information.

On the one hand, with the integral vision (Sec. 2.2.2), the infinite number of input/output pins are related together with a Green's function—i.e. a transfer function. While on the other hand, for the discrete version (Sec. 2.2.3) the reduced number of input/output pins are related together with impedance or an admittance matrix.

What about the in-plane displacements?

A vibrating structure, might has in-plane and out-of-plane vibrations. Yet, in the framework of non-viscous linear acoustics, in-plane vibrations do not radiate any acoustical energy in the fluid. On the opposite, if the fluid is vibrating with an in-plane movement—in regards to the direction of the surface of the structure—no energy will be

transmitted to the structure. Therefore, at the interface of two acoustical subsystems or vibro-acoustical subsystems, the in-plane movement do not need to be taken into consideration.

In short, the dual physical quantities retained for the Patch Transfer Functions method are solely the out-of-plane movements and the pressure. This, by no means, implies that in-plane movements are not existing nor impacted by out-of-plane movements, but they are unnecessary for our purpose.

2.4.2 Vehicle

This section is focused on a closed vehicle, which corresponds to the most encountered situation. A closed vehicle is a vehicle without any openings[10] to the exterior. In this case, there is no direct acoustical sound transmission from the exterior to the interior. In this situation the sound transmission corresponds to the one depicted in Figure 1.6 without the two arrows (b) and (b'). For a sake of clarity, this situation is depicted on a simple two dimensional representation (Figure 2.13).

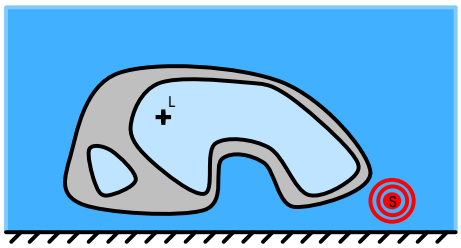

Figure 2.13: Schematic two-dimensional representation of the sound transmission from the exhaust to the interior of a vehicle. The abstract vehicle is depicted in gray. The point source S represents the exhaust outlet while the point L is an arbitrary point in the interior of the vehicle—e.g. passenger's ear. The full system is placed in a semi-free field environment. The structure is surrounded by air at the exterior and in the interior.

The Patch Transfer Functions method is also able to couple any vibro-acoustical subsystem. Considering an opened vehicle—vehicle with an open sun roof, window, or even a ventilation orifice—does not represent any theoretical difficulty. Such systems have already been treated successfully in the literature [26] and later in [33].

Step 1. Subdomain definition

Many subdomain definitions are possible, nevertheless, a decomposition in three subsystems is appropriate. The initial and complex sound transmission problem is subdivided into three subsystems. Each subsystem is bounded by a rigid surface depicted with the color black as shown in Figure 2.14.

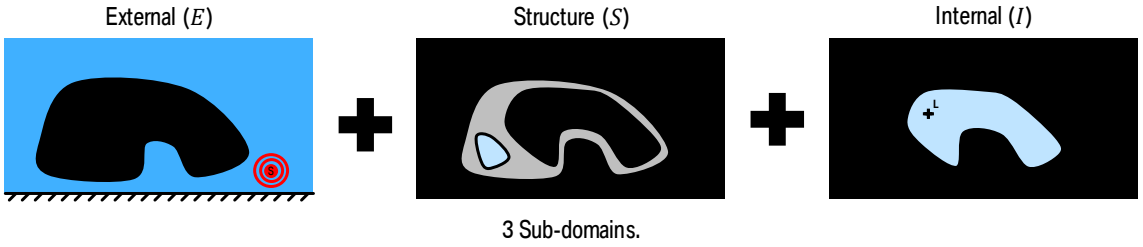

Figure 2.14: The initial and complex sound transmission problem is subdivided into three subsystems. Each subsystem is bounded by a rigid surface depicted with the color black. (E): Semi-free field with the point source S. The external skin of the vehicle is considered as a totally rigid surface; (S): The structure is

[10] In the strict sense no vehicle is totally closed. Some ventilation orifices are necessarily presents.

considered as a vibro-acoustical subsystem with blocked boundaries. The gray surface does not necessarily represent a structural part. Some of the gray surface, and even at the interface, might be composed of air. Yet in this scenario, one considers that there is no direct path between the exterior and the interior of the vehicle; (I): Air is in the interior of the habitable and has a listening point L.

Step 2. Coupling surfaces, division in patches and condensation

Two surfaces are coupling the structure to the internal and to the external domain:

> *Outer skin*. Coupling the structural domain to the external domain. Discretized in N_k patches, indexed indifferently with k or l—i.e. Γ_k or Γ_l.
> *Inner skin*. Coupling the structural domain to the internal domain. Discretized in N_i patches, indexed indifferently with i or j—i.e. Γ_i or Γ_j.

The dual notation is nothing else than a mathematical notation commodity—one letter is describing an exited patch while the other is referring to the receiving path. The complexity of each subsystem is condensed on coupling surfaces divided into patches (Figure 2.15).

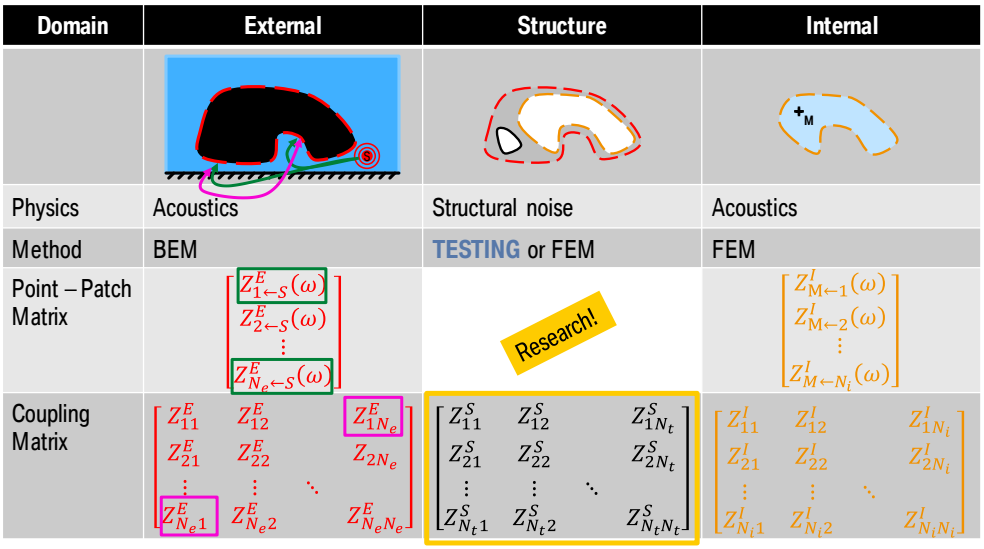

Figure 2.15: The dynamic properties of each uncoupled subsystem is described with a database of frequency transfer functions stored in impedance matrices. Any method can be used. In this case, the proposition is based on a hybrid approach using results from simulation and testing. BEM is a simulation method standing for Boundary Element Method. FEM is another simulation method standing for Finite Element Method.

Step 3. Response of uncoupled subdomains

The Patch Transfer Functions method is defined with spatial average of pressure and velocity over the surface of the patches. For a sake of simplicity, in this section the notation $\langle P(N)\rangle_{N\in\Gamma_k}$ is considered as implicit and simplified as P_k. The normal to each subsystem either structural, acoustical, or vibro-acoustical is the outward normal.

Internal subsystem (I):

Governing equation:

$$\{P_i^I\} = [Z_{i\leftarrow j}^I]\{V_j^I\} \tag{2.53}$$

Physical description. Since there is no source in the interior of the vehicle, the sound pressure on each internal patch Γ_i is linked to the velocity of all internal patches $\{V_j^I\}$ acting as a "loudspeaker". The impedance matrix $[Z_{i\leftarrow j}^I]$ takes into account all the acoustical

effects in the interior—i.e. sound scattering, high damping due to a high acoustical absorption etc. In the end, we are interested in the pressure at position L Eq.(2.54):

$$P(L) = \left[Z^I_{L\leftarrow j}\right]\{V^I_j\} \tag{2.54}$$

Physical interpretation. The pressure at the listening point is the summation of the effect of all internal patches considered as "loudspeakers". Obviously, this summation is made with complex algebra and some cancelation effects might appear.

Structural or vibro-acoustical subsystem (S):

Governing equation:

$$\begin{cases}\{P^S_i\} = \left[Z^S_{i\leftarrow j}\right]\{V^S_j\} + \left[Z^S_{i\leftarrow l}\right]\{V^S_l\} \\ \{P^S_k\} = \left[Z^S_{k\leftarrow j}\right]\{V^S_j\} + \left[Z^S_{k\leftarrow l}\right]\{V^S_l\}\end{cases} \tag{2.55}$$

Physical description. If all the patches of the structure are exited with a forced velocity, the resulting pressures are linked with condensed impedance. This description is not as intuitive as the description with an admittance. Yet, both versions are equally suitable and describe *in fine* an equivalent property. Actually, the condensed impedance matrix tends[11] to be equal to the inverse of the admittance matrix and *vice versa*.

External subsystem (E):

Governing equation:

$$\{P^E_k\} = \left[Z^E_{k\leftarrow l}\right]\{V^E_l\} + \{Z^E_{k\leftarrow S}\}Q_S(\omega) \tag{2.56}$$

Physical description. The acoustical sound pressure at each patch of the interface of the external system Γ_k is linked to the velocity of all external patches $\{V^E_l\}$, acting as a loudspeaker. The pressure caused by the source $Q_S(\omega)$ is also considered. The respective impedance matrices—$\left[Z^E_{k\leftarrow l}\right]$ and $\{Z^E_{k\leftarrow S}\}$—take into account all the acoustical effects in the external domain—i.e. sound scattering, reflections, pseudo resonances between the structure and the ground.

Step 4. Coupling conditions and resolution

When the three subsystems are coupled, the fundamental law of Newton yields:

$$\begin{cases}\{P^S_i\} = \{P^I_i\} = \{P^C_i\} \\ \{P^S_k\} = \{P^E_k\} = \{P^C_k\}\end{cases} \tag{2.57}$$

As the patches are physically at the same position, their velocity must be equal:

$$\begin{cases}\{V^S_j\} = -\{V^I_j\} = \{V^C_j\} \\ \{V^S_l\} = -\{V^E_l\} = \{V^C_l\}\end{cases} \tag{2.58}$$

Eq. (2.56), Eq. (2.55), Eq. (2.53), Eq. (2.57), and Eq. (2.58) can be rewritten as the following compact form:

[11] For many reasons—not only numerical ones—the admittance and the condensed impedance matrices are not necessarily rigorously the inverse of each other. This question is far beyond the scope of this dissertation and will not be addressed. For a deeper insight is the difference between admittance and impedance in the framework of dynamic substructuring, the reader is advised to read the publication of D. J. Rixen "Vibration source description in substructuring: A theoretical depiction" [108].

$$\begin{cases} \left([Z^S_{i\leftarrow j}] + [Z^I_{i\leftarrow j}]\right)\{V^C_j\} + & [Z^S_{i\leftarrow l}]\{V^C_l\} = \{0\} \\ [Z^S_{k\leftarrow j}]\{V^C_j\} + \left([Z^S_{k\leftarrow l}] + [Z^E_{k\leftarrow l}]\right)\{V^C_l\} & = \{Z^E_{k\leftarrow S}\}Q_S(\omega) \end{cases} \tag{2.59}$$

As a compact matrix form, Eq. (2.59) reads:

$$\begin{bmatrix} [Z^S_{i\leftarrow j}] + [Z^I_{i\leftarrow j}] & \vdots & [Z^S_{i\leftarrow l}] \\ \cdots & & \cdots \\ [Z^S_{k\leftarrow j}] & \vdots & [Z^S_{k\leftarrow l}] + [Z^E_{k\leftarrow l}] \end{bmatrix} \begin{Bmatrix} \{V^C_j\} \\ \cdots \\ \{V^C_l\} \end{Bmatrix} = \begin{Bmatrix} \{0\} \\ \cdots \\ \{Z^E_{k\leftarrow S}\}Q_S(\omega) \end{Bmatrix} \tag{2.60}$$

From Eq. (2.60), the coupled velocity is derived:

$$\begin{Bmatrix} \{V^C_j\} \\ \cdots \\ \{V^C_l\} \end{Bmatrix} = \begin{bmatrix} [Z^S_{i\leftarrow j}] + [Z^I_{i\leftarrow j}] & \vdots & [Z^S_{i\leftarrow l}] \\ \cdots & & \cdots \\ [Z^S_{k\leftarrow j}] & \vdots & [Z^S_{k\leftarrow l}] + [Z^E_{k\leftarrow l}] \end{bmatrix}^{-1} \begin{Bmatrix} \{0\} \\ \cdots \\ \{Z^E_{k\leftarrow S}\}Q_S(\omega) \end{Bmatrix} \tag{2.61}$$

The coupling velocity Eq. (2.61) corresponds to the physical compromise found by all subsystems forced to work together.

Step 5. Pressure at the listening point

Eq. (2.54) allows computing the pressure at the point of interest.

$$P(L) = -[Z^I_{L\leftarrow j}]\{V^C_j\} \tag{2.62}$$

Note that the minus sign is the consequence of the choice of the outward normal for the expression of the coupled velocity—cf. Eq. (2.58).

Description with black boxes

All these equations can be represented in form of interconnected black boxes (Figure 2.16). For a sake of clarity, only seven patches are depicted: four external patches indexed k and l and three internal patches indexed i and j. The upper-left box, and the upper-middle box are the pendant of Eq. (2.56). The central box symbolizes Eq. (2.55). The lower-middle box represents Eq. (2.53) and the lower-right box stands for Eq. (2.54). The coupling between the input/output of the different boxes is represented with interconnected wires. The wires are imposing some constraint to the interacting boxes, forced to work together—i.e. Eq. (2.57) and Eq. (2.58). The physical compromise happens in form of a coupled velocity found with Eq. (2.61). The coupled velocities of the internal patches applied to the lower-right box result according to Eq. (2.62) in the pressure at the listening point L.

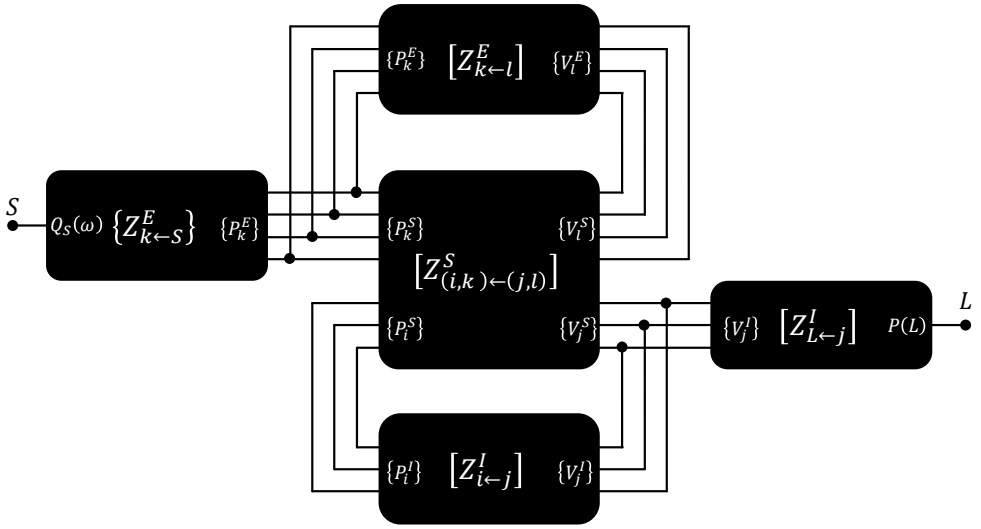

Figure 2.16: Symbolic representation of the sound transmission from the exhaust S, to L in the interior of a vehicle with interconnected black boxes.

Symbolic representation.

The provided representation is symbolic in the sense that it does not include all the details of the rigorous equations presented above. For example the normal convention resulting in a minus sign in Eq. (2.58) is not depicted. Nevertheless, this representation should support a comprehensive interpretation of the mathematical equations.

In a certain measure, this representation supports a simple conceptual interpretation of the complex phenomenon involved in the coupling of several subsystems. Actually the complexity arises from the interdependency of all subsystems. Each value—pressure or velocity—crossing any wire is influenced by all subsystems. This interdependency is visible in Eq. (2.61). Indeed the calculation of the coupled velocities, requires the properties of all subsystems (described in terms of impedance matrices) and the external solicitation $Q_S(\omega)$.

2.4.3 Opportunities and limitations

The application of the Patch Transfer Functions method to a full vehicle would present an industrial breakthrough. Indeed, the method, if applied, surpasses the industrial functional specifications. It enable the *description and quantification of the sound transmission from the exhaust outlet into the interior of a vehicle* within respect of all the four constraints defined in Sec. 1.3.3. In addition, due to the subsystem based writing, the Patch Transfer Functions method results in the following extra benefits:

Sound transmission understanding. Main paths, panel's contribution, lessons learned.
Target setting. The understanding would allow creating a structural target for the future vehicle.
Optimization. Best structural changes within given constraints to eliminate an exhaust inferred booming noise.

However, this method relies on the prior knowledge of the inherent properties of the subsystems—cf. in the form of an impedance or admittance matrix. This inherent property is often computed by numerical methods. Nevertheless, the "trimmed structure" of a full vehicle is so complex that the numerical method commonly delivers unsatisfactory results. In this case, the properties of the fully trimmed vehicle might be obtained using

experimental characterization. Unfortunately, for evident practical reasons, the structure of the fully trimmed vehicle cannot be characterized independently and mandatorily remains coupled with the fluid.

Due to this complication, the method cannot be applied directly to a full scale vehicle within an acceptable compromise. The scientific problematic "*Characterization of Patch Transfer Functions of a subsystem by means of measurement on a coupled system*" should be addressed first.

A vehicle is always filled with air. Why is it a problem?

Chap. 3 answers this question with technical details. Yet a descriptive answer here might be appropriate. With the Patch Transfer Functions methods, one could consider a subsystem as being the vehicle filled with air. In this way, a reconstruction of the sound pressure at the listening position would be possible. Unfortunately, this vision would decrease the industrial benefit. Indeed, the structure is generally the only acceptable optimization parameter. As a structural modification modifies, per se, only the structure and not the property of the air, a clear and independent knowledge of the structure property—cf. in terms of an impedance of admittance matrix—is preferable.

A conventional experimental measure of Patch Transfer Functions would, in the presence of air, mix the properties of the structure with the properties of the air inside and outside. It is still a consequence of the necessity to consider a 2-way $fluid \leftrightarrow structure$ coupling (Sec. 1.3.2). This coupling has been seen as a major complication for the description of the sound transmission. This consideration also increases drastically the complexity for the characterization of the subsystem *structure of the fully trimmed vehicle*.

2.5 Summary

In this chapter, the theoretical background of the vibro-acoutical substructuring method Patch Transfer Functions method has been addressed. The application of this method, to a full vehicle would be an industrial breakthrough. Indeed the Patch Transfer Functions method is not only capable of describing the sound transmission into a system, but would be also able to predict the effect of system changes upon the sound transmission property—which turn into an opportunity for system optimization.

This approach, however, depends on acquaintance of the inherent vibro-acoustical impedance of each uncoupled subsystem. Numerical method can help to determine this inherent property. This technique, nevertheless, does not always work on complex systems and can produce unsatisfactory results for many industrial applications—e.g. full trimmed vehicle. In these cases, the vibro-acoustical impedance should be obtained using experimental characterization. Even with this approach, the industries still find it hard and sometimes impossible to characterize a stand-alone subsystem, since measurements can only be carried out on a full scale system. Therefore, some subsystem still has to be characterized while remaining coupled with others.

In this extend, the industrial problematic has turn into the scientific problematic: "*Characterization of Patch Transfer Functions of a subsystem by means of measurement on a coupled system*".

3 Decoupling & Experimental characterization

"We set sail on this new sea because there is new knowledge to be gained. ..."

John Fitzgerald Kennedy (1917–1963) in "Address at Rice University in Houston on the Nation's Space Effort", 1962 [1].

Chapter contents:

3.1 Introduction 63

3.2 Theoretical background 65

3.2.1 Black box vision 65

3.2.2 Inverse matrix formulation 65

3.2.3 Creation of the set of experiments 67

3.3 Numerical experiment 68

3.3.1 Concept 69

3.3.2 Problem statement 70

3.4 Results of the numerical experiment 72

3.4.1 Measure in the coupled system 72

3.4.2 Result of the characterization 76

3.4.3 Coupling of the subsystems 77

3.5 Summary 80

3.1 Introduction

This chapter addresses the problem, *"Characterization of Patch Transfer Functions of a subsystem by means of measurement on a coupled system"*. It is an original contribution corresponding to a new method for measuring patch transfer function that is of major interest to apply the PTF method for systems where the calculation of PTF is impossible due in particular to bad knowledge of systems. For car application trim is a typical case of interest of the proposed method. In this chapter only the basic idea is presented and tested on an elementary theoretical case.

The method is in some measures, the *inverse* problem in comparison to the *direct* problem tackled in Chap. 2. In the present work, the *direct* problem refers to the description of an assembly based on the knowledge of its subsystems—i.e. coupling. On the opposite, the *inverse* problem intends to characterize a subsystem based on the knowledge of the

coupled system. The difference between the *direct* and the *inverse* problem is illustrated in Figure 3.1 and Figure 3.2.

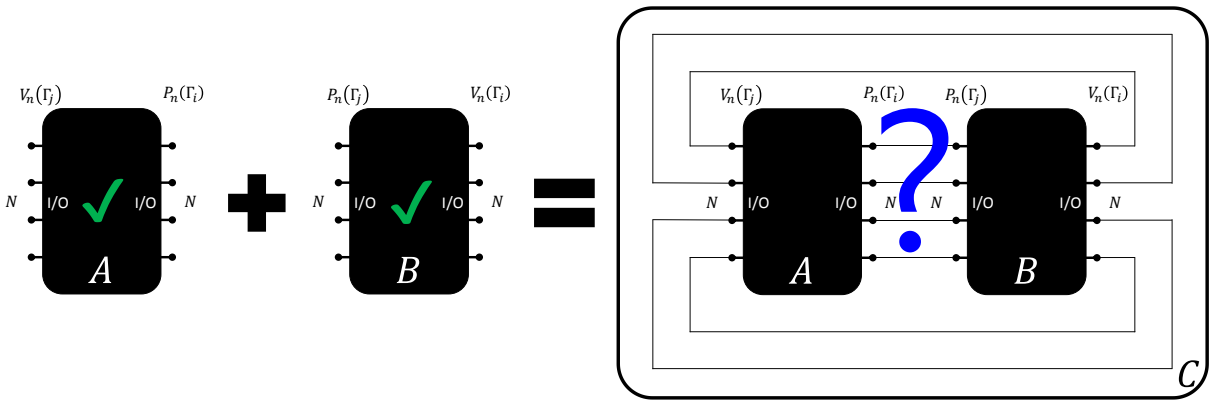

Figure 3.1: Coupling scheme of the direct Patch Transfer Functions method. The knowledge of the subsystem A and B allows to predict the behavior of the coupled system C. The system C consists in a complex interaction—strong coupling—between the subsystems A and B. The strong coupling is depicted with wires mapping the input/output of the black box associated to each subsystem. Each subsystem A or B might contain several internal subsystems.

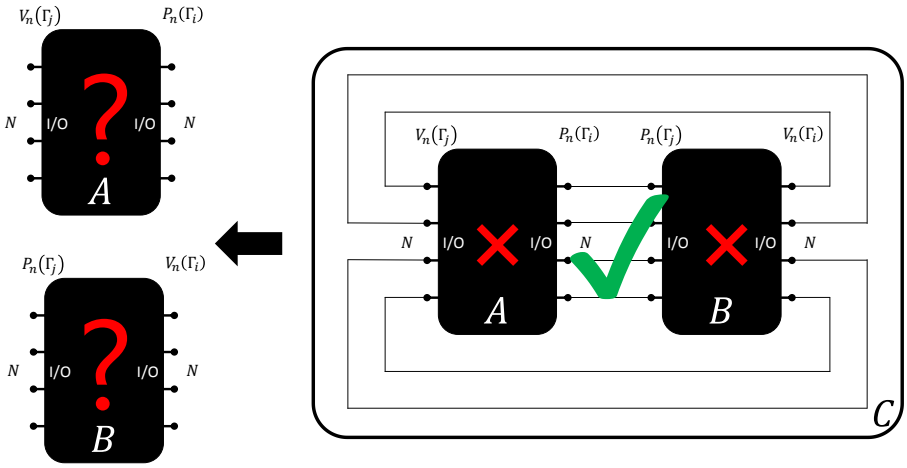

Figure 3.2: Decoupling scheme of the inverse Patch Transfer Functions method. The knowledge of the coupled system C allows to characterize the inherent property $[Z^A_{i\leftarrow j}]$ and $[Z^B_{i\leftarrow j}]$ of the uncoupled subsystem A and B. The information can be gained only on the fully coupled system C. No prior knowledge either of its subsystem A or subsystem B is necessary. Each subsystem A or B might contain several internal subsystems.

The formulation of the *inverse* problem on the form "$[Z] = [P][V]^{-1}$" found in the literature (see Sec. 1.4.2) should address the problem. This formulation is found and applied successfully in the PhD dissertation of G. Veronesi: "A novel PTF-based experimental characterisation for poro-elastic liners: Method and sampling criterion" [71]. As the poro-elastic liners presents some special properties—high damping resulting in a strong diagonal of the impedance matrix—this method should also be verified for a system with a low damping—resulting in high cross terms in the impedance matrix.

This chapter is composed in the following of three main sections. First, the theoretical background of the formulation "$[Z] = [P][V]^{-1}$" is addressed, the underlying experimental setup and the formulation of the matrices are explained. In the second section, a numerical experiment and its link with the industrial characterization problem is proposed. Finally, the first numerical experiment is carried out on a step-by-step way and the results are discussed.

3.2 Theoretical background

3.2.1 Black box vision

The description of a subsystem in the framework of the Patch Transfer Functions method relies on the more general concept of condensed transfer functions—or condensed impedance. The internal degrees of freedom that are not excited directly are "removed" or condensed on the coupling surface. The coupling interface is discretized in patches. As a result, such a subsystem can be illustrated with a black box as depicted in Figure 3.3. The N input/output pins of the black box are mapping to the dual physical quantities pressure and velocity on the N patches. The condensed impedance describes the system completely such as it is possible to write the relation $\{P_i^A\} = [Z_{i\leftarrow j}^A]\{V_j^A\}$ between the input/output pins.

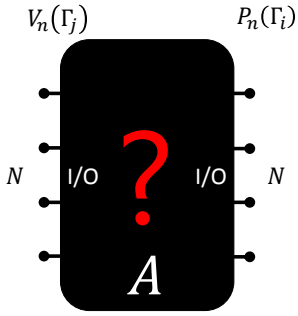

Figure 3.3: Symbolic representation of an uncoupled unknown passive vibro-acoustical subsystem A by means of a black box. The N input/output pins represent the velocity and the pressure on the N coupling patches. On this schematic representation, the fact that the system is uncoupled is illustrated by unconnected input/output pins. The fact that the condensed impedance matrix $[Z_{i\leftarrow j}^A]$ is unknown is depicted with the red question mark.

Mathematically, the concept of condensed impedance implies that Eq. (3.1) is always valid, whether the system is uncoupled or not. The subscript n stresses that the pressure "$\{P_i^A\}_n$" results from the velocity "$\{V_j^A\}_n$". The condensed impedance $[Z_{i\leftarrow j}^A]$ is a square matrix of size $(N;N)$, resulting in N^2 impedances to characterize. The impedance matrix—i.e. each impedance $Z_{i\leftarrow j}^A$—is frequency dependent[12]. If the angular frequency ω is varying according to a discrete basis—spectral lines—there is one impedance matrix per spectral line.

$$\{P_i^A\}_n = [Z_{i\leftarrow j}^A]\{V_j^A\}_n \tag{3.1}$$

The following section presents in detail the inverse methods "$[Z] = [P][V]^{-1}$" that intends to characterize the unknown condensed impedance matrix $[Z_{i\leftarrow j}^A]$ of the subsystem A.

3.2.2 Inverse matrix formulation

Uncoupled system

The inherent properties of an uncoupled system are not depending on the external solicitation. Mathematically, it means that Eq. (3.1) is valid for any excitation configuration here so called *experiment*. In the case of an uncoupled system shown in Figure 3.3, the *experiment* represents the knowledge of the resulting output pressures when input

[12] The frequency dependency is not mathematically depicted by any notation—although always present.

velocities are applied. In the following, it will be considered that these two quantities are accessible by measurements.

If N independent *experiments* n are done, Eq. (3.1) can be written N times:

$$\begin{cases} \{P_i^A\}_1 = [Z_{i\leftarrow j}^A]\{V_j^A\}_1 \\ \{P_i^A\}_2 = [Z_{i\leftarrow j}^A]\{V_j^A\}_2 \\ \quad\vdots \\ \{P_i^A\}_n = [Z_{i\leftarrow j}^A]\{V_j^A\}_n \\ \quad\vdots \\ \{P_i^A\}_N = [Z_{i\leftarrow j}^A]\{V_j^A\}_N \end{cases} \tag{3.2}$$

It is important to underline here that, for each equation in the set of equations (3.2), the impedance matrix $[Z_{i\leftarrow j}^A]$ is always the same. As already said: the inherent property of the subsystem are not depending on the external solicitation. This *set of experiments* results in N^2 equations that can be written in a compact form:

$$[P] = [Z_{i\leftarrow j}^A][V] \tag{3.3}$$

where $[P](N;N)$ is built according to relation:

$$[P] = \left[\{P_i^A\}_1, \{P_i^A\}_2, \dots, \{P_i^A\}_n, \dots, \{P_i^A\}_N\right] \tag{3.4}$$

and where $[V](N;N)$ is constituted according to relation:

$$[V] = \left[\{V_i^A\}_1, \{V_i^A\}_2, \dots, \{V_i^A\}_n, \dots, \{V_i^A\}_N\right] \tag{3.5}$$

Finally, the inherent property $[Z_{i\leftarrow j}^A]$ of the subsystem A—is found with Eq. (3.6):

$$[Z_{i\leftarrow j}^{A\,Id}] = [P][V]^{-1} \tag{3.6}$$

In order to avoid any confusion between the *real* and the *identified* condensed impedance matrix, the indicator "Id" will be used:

Real condensed patch to patch impedance: $[Z_{i\leftarrow j}^A]$ or $[Z_{i\leftarrow j}^{A\,Ref}]$.
Identified condensed patch to patch impedance: $[Z_{i\leftarrow j}^{A\,Id}]$.

As it is frequently the case with inverse problems, the *identified* quantities are generally not perfectly equal to the *physical* one—i.e. $[Z_{i\leftarrow j}^A] \neq [Z_{i\leftarrow j}^{A\,Id}]$. This difference might be caused by many phenomena. Such phenomenon will be addressed in Chap. 4 and some advanced strategies to get rid of it will be addressed in Chap. 5.

Particular case of the direct characterization method.

Note that the *direct* characterization method exposed in the state of the art (Sec. 1.4.2) might be considered as a particular case of the inverse method. Indeed, it corresponds to create a particular *set of experiments* resulting in a diagonal matrix of velocities $[V]$. If the matrix $[V]$ is the identity matrix, the trivial inversion means that the measured pressure matrix $[P]$ is *directly* equal to the researched condensed impedance matrix $[Z_{i\leftarrow j}^A]$. This method allows to identify one column of the impedance matrix per *experiment*. However, it implies being able to move each patch with a unit velocity maintaining other neighboring patches blocked. It is the strategy chosen by Du [70].

Coupled subsystem

Consider now that subsystem A is coupled with another subsystem B as presented in Figure 3.2. Its inherent properties are unchanged and the equation Eq. (3.1) is still valid. The only difference is that the velocity $\{V_j^A\}_n$ and the pressure $\{P_i^A\}_n$ are not arbitrary anymore, but partially influenced by the presence of subsystem B through the so-called coupled velocity $\{V_j^C\}_n$ and coupled pressure $\{P_i^C\}_n$ representing the coupling between both subsystems on the coupling surface. For each experiment n, it mathematically reads:

$$\begin{cases} \{P_i^A\}_n = \{P_i^B\}_n = \{P_i^C\}_n \\ \{V_j^A\}_n = -\{V_j^B\}_n = \{V_j^C\}_n \end{cases} \tag{3.7}$$

Normal convention.

Eq. (3.7) relies on an arbitrary choice for the direction of the outward normal. If the outward normal of subsystem A is not in the same direction as the coordinate system of system C a minus sign appears. The illustration provided on Figure 2.9 tackles this aspect with more details. In one word, when the systems are coupled, the pressure and the velocity of each subsystem are equal. Depending on some arbitrary choice, a minus sign is mathematically necessary.

In this extent, it means that the Eq. (3.1) can also be written with the coupled velocities and coupled pressures as presented in Eq. (3.8):

$$\{P_i^C\}_n = [Z_{i\leftarrow j}^A]\{V_j^C\}_n \tag{3.8}$$

Finally, the demonstration proposed in the previous section "Uncoupled system" is still valid. Indeed starting with Eq. (3.8) instead of Eq. (3.1) and replacing $\{P_i^A\}_n$ by $\{P_i^C\}_n$ and $\{V_i^A\}_n$ by $\{V_i^C\}_n$ in Eq. (3.2) up to Eq. (3.5), Eq. (3.6) allows to find the unknown condensed impedance matrix $[Z_{i\leftarrow j}^A]$ measuring the coupling pressures and velocities on the coupled system composed by subsystem A and B.

In other words, if there is a solution to create a convenient *set of experiments*—i.e. N independent *experiments* on the coupled system—the inverse method "$[Z] = [P][V]^{-1}$" applies. As the condensed impedance matrix is the information we were looking for, it means that the application of this inverse method allows the *"Characterization of Patch Transfer Functions of a subsystem by means of measurement on a coupled system"*.

3.2.3 Creation of the set of experiments

The method developed in the present work aims at characterizing some acoustic or vibro-acoustic subsystems with complex geometries as depicted in Figure 3.4. In this figure, the vibro-acoustic subsystem under investigation is the schematic structure. This subsystem is coupled to an inner volume and an outer semi-infinite domain through coupling surface discretized in N patches (N_i patches in the inner volume and N_o patches in the outer domain, $N = N_i + N_o$). As shown previously, the impedance matrix of the "schematic structure" can be retrieved if N independent experiments are performed.

The coupled subdomains (inner and outer subdomains) can be excited indirectly with a roving acoustical source placed in the air (Figure 3.4). For each source position, the structure is loaded with a different acoustical load resulting in different coupled velocities $\{V_i^C\}_n$ and coupled pressures $\{P_i^C\}_n$. The coupled pressures and velocities can be measured

directly with a PU Probe. Finally, the inverse method proposed in Sec. 3.2.2 allows to find the researched condensed impedance.

Important note about internal source

No source used in the *set of experiments* shall be internal to the subsystem under characterization. Indeed, if a source was present in the subsystem under characterization, Eq. (3.1) would not describe the system completely anymore—some information about the internal transfer would be missing. As a consequence, the inverse method proposed here does not apply.

For more insight about this explication, the reader might refer to Eq. (2.37) which takes into consideration the effect of an acoustical source in a subsystem.

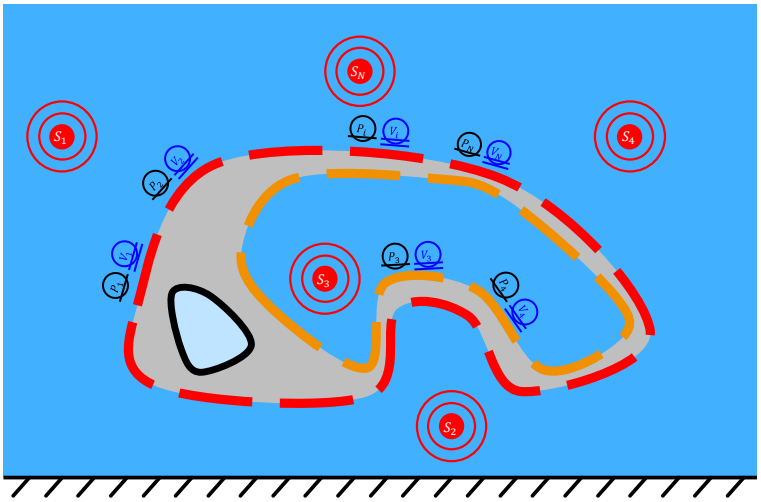

Figure 3.4: Schematic representation of an experimental setup, with instrumentation. A set of N experiments n necessary to determine the inherent condensed impedance matrix of a vibro-acoustical subsystem placed and filled with a fluid medium. The subsystem is composed of N patches. A roving acoustical source is placed sequentially at N different positions in the fluid. For each position of the source, the pressure and velocity of each patches (N in total) of the vibro-acoustical subsystem is measured—e.g. by means of microphones and accelerometers or PU Probes. The measure of the pressure is depicted with the black circle with one bar. The measure of the velocity is depicted with the blue circle with two bars. Based on this N experiments, the N^2 elements of the impedance matrix are recovered according to the procedure depicted in Sec. 3.2.2. The sources shall not be in the subsystem under characterization.

Before any application of the method on a real system, the validity of the theory of the inverse method should be verified. In this section, the theory presented in the previous section will be illustrated with a numerical experiment.

3.3 Numerical experiment

The framework of the Patch Transfer Functions method allows to consider any system as an assembly of black boxes. In this extend, the physical shape of a subsystem is not of primary importance. As a consequence, a complex subsystem such as a full vehicle can be illustrated with a *potato shaped* sketch—Sec. 2.4.2. In this section the validity of the method is illustrated on coupled *parallelepiped* acoustical cavities.

A major advantage working with such cavities is that the reference solution is perfectly known. Secondly, this problem is severe for at least two reasons: (i) the subsystems *A* and *B* are totally coupled and (ii) the geometrical symmetries in the system, combined with a

reactive[13] system, might lead to numerical difficulties. Therefore, the first validation test of the inverse method will be carried out on a coupled acoustical cavities with a numerical experiment.

3.3.1 Concept

The inverse characterization is first presented on the same geometry as the one encountered in the second chapter. The application of the vibro-acoustical substructuring Patch Transfer Functions method has been presented on a parallelepiped cavity C, considered as being the coupling of two known sub cavities A and B (Figure 2.5). The properties of the cavities and the sub cavities have been presented in Figure 2.10 and Table 2.2. Finally the results have been presented in Figure 2.11. In summary the scheme of the direct Patch Transfer Functions method is depicted in Figure 3.5:

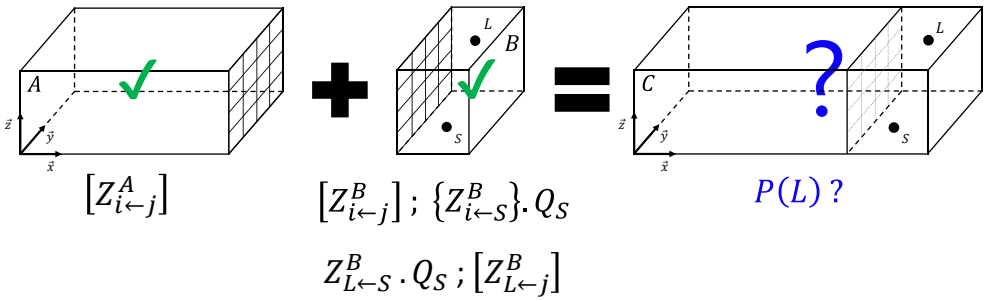

Figure 3.5: Scheme of the direct Patch Transfer Functions method. The knowledge of the inherent property of the sub cavities A and B—in the form of condensed impedance matrices—allows to compute the pressure at the listening point L caused by the point source S once the two sub cavities are virtually coupled forming a cavity C.

The subsystem A and B and the resulting coupled system C can be considered as being the illustration of more complex system such as the one presented on Figure 2.15:

> *Subsystem* A is the abstract version of the structural subsystem (S)—i.e. full vehicle.
> *Subsystem B* represents the abstract version of the internal subsystem (I) and the external subsystem (E)—i.e. air in and outside the vehicle.

In opposition to the direct method, the purpose of the inverse method is to determine the property of the subsystem A while measurement are possible only on the coupled system C. This intention is depicted in Figure 3.6.

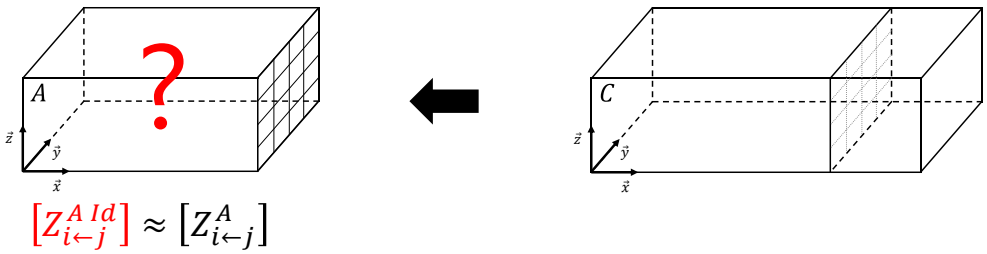

Figure 3.6: Schematic representation of the inverse problem. Here it is assumed that the subsystem A "full vehicle" cannot be physically uncoupled from the subsystem B "air inside and outside the vehicle". The

[13] As the system is totally closed with a low damping, there are almost no propagation effects.

purpose of the experimental inverse characterization is to characterize the inherent condensed impedance of subsystem A—i.e. $[Z^{A}_{i\leftarrow j}]$—while still strongly coupled with the subsystem B.

In this extend, the experimental inverse characterization proposed in Sec. 3.2 is applied to the coupled cavity C. As the subsystem A presents N patches, the *set of experiments* contains N experiments (Figure 3.7).

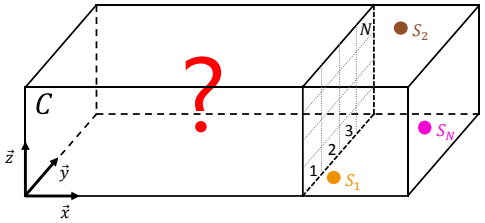

Figure 3.7: In the fully coupled system C, the source is placed sequentially at position $S_1, S_2, \ldots, S_N$. Each source position is associated to one experiment where the pressure and the velocity is measured at the center of the supposed patches. The collection of N experiments is called set of experiments. The source shall not be in the subsystem being characterized.

For each experiment—source at a given position—the pressure and the velocity is measured at the center of the *supposed patches*[14]. The collection of the N experiments is called *set of experiments*. The results of the *set of experiments* are stored in the matrices $[P]$ and $[V]$ according to Eq. (3.4) and Eq. (3.5). Finally, Eq. (3.6) allows to retrieve the inherent condensed impedance of subsystem $[Z^{A\,Id}_{i\leftarrow j}]$. For this inverse characterization, no *a priori* information about neither subsystem A nor subsystem B is necessary. The simulated measure is carried on only on the coupled system C.

3.3.2 Problem statement

For the numerical experiment the two patches cavity C presented in Sec. 2.3 is used. The *set of experiments* necessary for the characterization of the subsystem A is composed of two experiments:

Source S_1 is used for the first experiment.
Source S_2 is used for the second experiment.

The characterization of the sub cavity A with a numerical *set of experiments* in the coupled cavity C, including the position of the sources S_1 and S_2, is depicted in Figure 3.8:

[14] The expression "supposed patches" emphasizes that in the coupled configuration—e.g. system C—there is no physical patch at the interface of the subsystems—e.g. subsystems A and B.

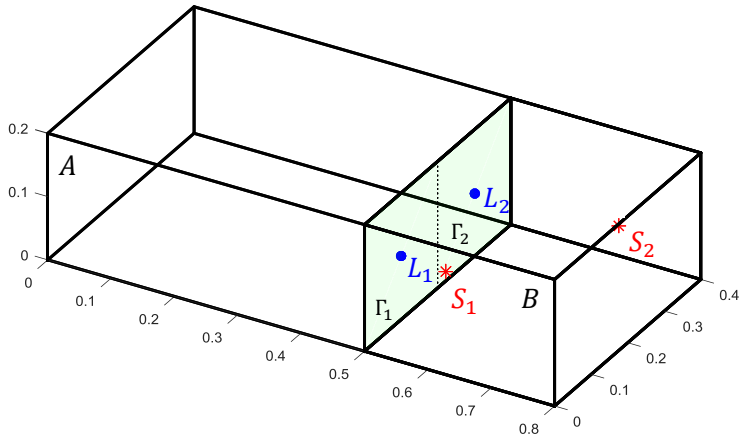

Figure 3.8: Description of the set of experiments necessary to characterize the impedance of the subsystem A. The set of experiments contains two positions of sources S_1 and S_2 in the system C to create two experiments for the characterization of the subsystem A—i.e. identification of the condensed impedance matrix $[Z^{A\,Id}_{i\leftarrow j}]$. The pressure and velocity is measured at the position L_1 and L_2 considered as being in the center of the two "supposed patches" Γ_1 and Γ_2. The patches are depicted only to illustrate where is the virtual limit between the two systems A and B.

The exact position of the sources and the properties of the boxes are listed in Table 3.1:

Table 3.1: Geometrical and physical properties of the systems C and the subsystems A and B. The positions of the two sources S_1 and S_2 and the two listening points L_1 and L_2 placed at the center of the "supposed patches" are provided. The length are in meter.

	Box A	Box B	Box C
$(L_x; L_y; L_z)$	$(0.50; 0.40; 0.20)$	$(0.30; 0.40; 0.20)$	$(0.80; 0.40; 0.20)$
S_1	—	$(0.10; 0.05; 0.13)$	$(0.60; 0.05; 0.13)$
S_2	—	$(0.20; 0.35; 0.08)$	$(0.70; 0.35; 0.08)$
L_1	$(0.50; 0.10; 0.10)$	$(0.00; 0.10; 0.10)$	$(0.50; 0.10; 0.10)$
L_2	$(0.50; 0.30; 0.10)$	$(0.00; 0.30; 0.10)$	$(0.50; 0.30; 0.10)$
ρ	$1.29\ [\mathrm{kg.m^{-3}}]$		
c	$340\ [\mathrm{m.s^{-1}}]$		
η	0.01		
Patches	2 patches of size $(0.20; 0.20)$		

For the first application, the inverse characterization method will be described step by step wise and the intermediate matrix $[P]$ and $[V]$ will be presented. The identified condensed impedance $[Z^{A\,Id}_{i\leftarrow j}]$ of the subsystem A will be graphically compared to the reference one $[Z^{A}_{i\leftarrow j}]$. Finally this impedance will be used to couple the subsystem A and B again—Sec. 3.4.3.

3.4 Results of the numerical experiment

3.4.1 Measure in the coupled system

The impedance matrix to identify is of size $(N; N)$ with $N = 2$. According to the procedure described in Sec. 3.2, as the inverse characterization requires one *set of experiments* containing N experiments, in this situation, two experiments are necessary.

Experiment 1

The source S_1 is acting in the cavity C. The pressure is numerically computed at listening position L_1 and L_2—center of each patch—using Eq. (2.31). The results are presented in the form of a vector—i.e. matrix of size $(2; 1)$. The velocity is numerically computed based on the pressure calculation and the Euler's Eq. (2.13). The results are also presented on a vector form. Both pressure and velocity vectors are graphically depicted on Figure 3.9.

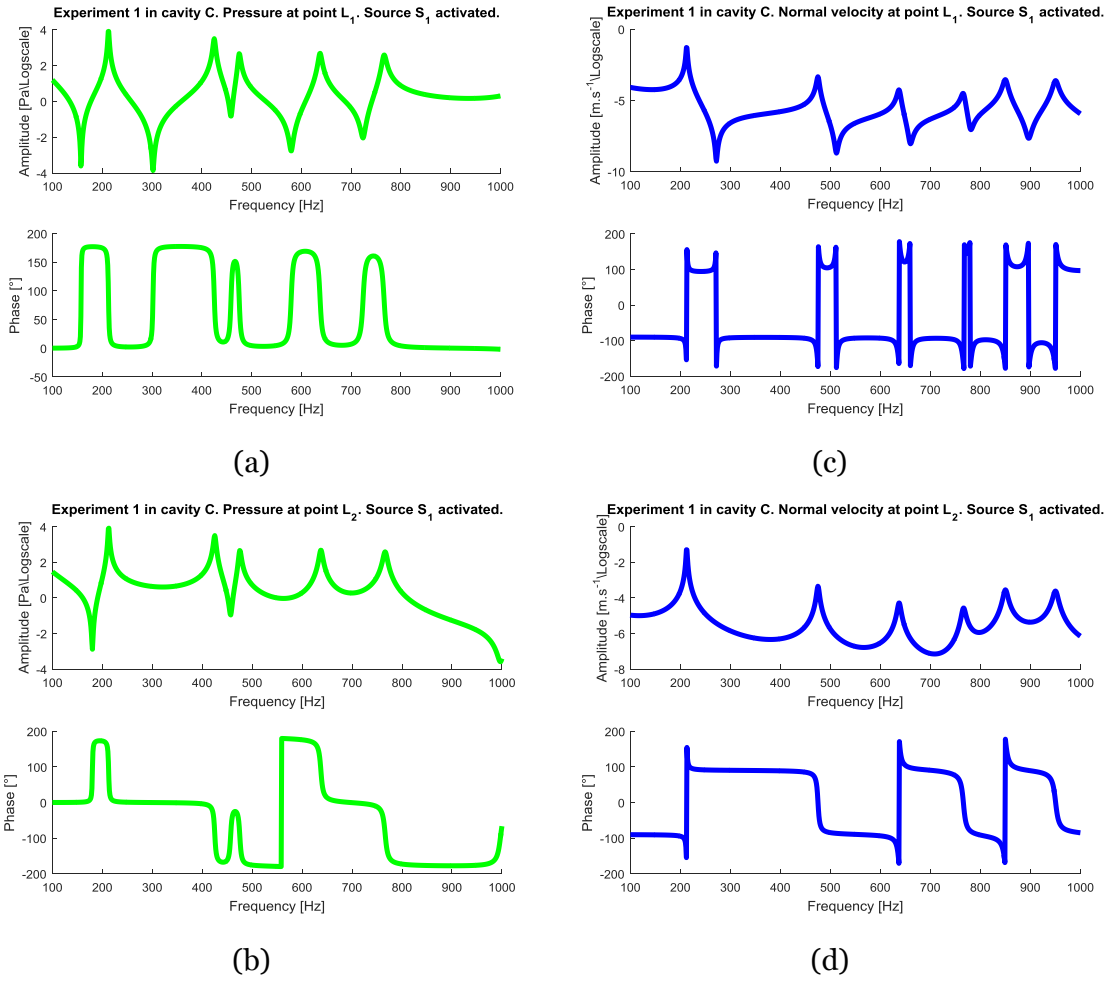

Figure 3.9: Results of the first experiment in the coupled cavity C. (a) and (b) are representing the pressure vector $\{P_i^C\}_1$; (c) and (d) are representing the velocity vector $\{V_i^C\}_1$.

Experiment 2

The source S_2 is acting in the cavity C. The pressure is numerically computed at listening position L_1 and L_2—center of the supposed patches—using Eq. (2.31). The results are presented in the form of a vector—i.e. matrix of size $(2;1)$. The velocity is numerically computed based on the pressure calculation and the Euler's equation Eq. (2.13). The results are also presented on a vector form. Both pressure and velocity vectors are graphically depicted on Figure 3.10.

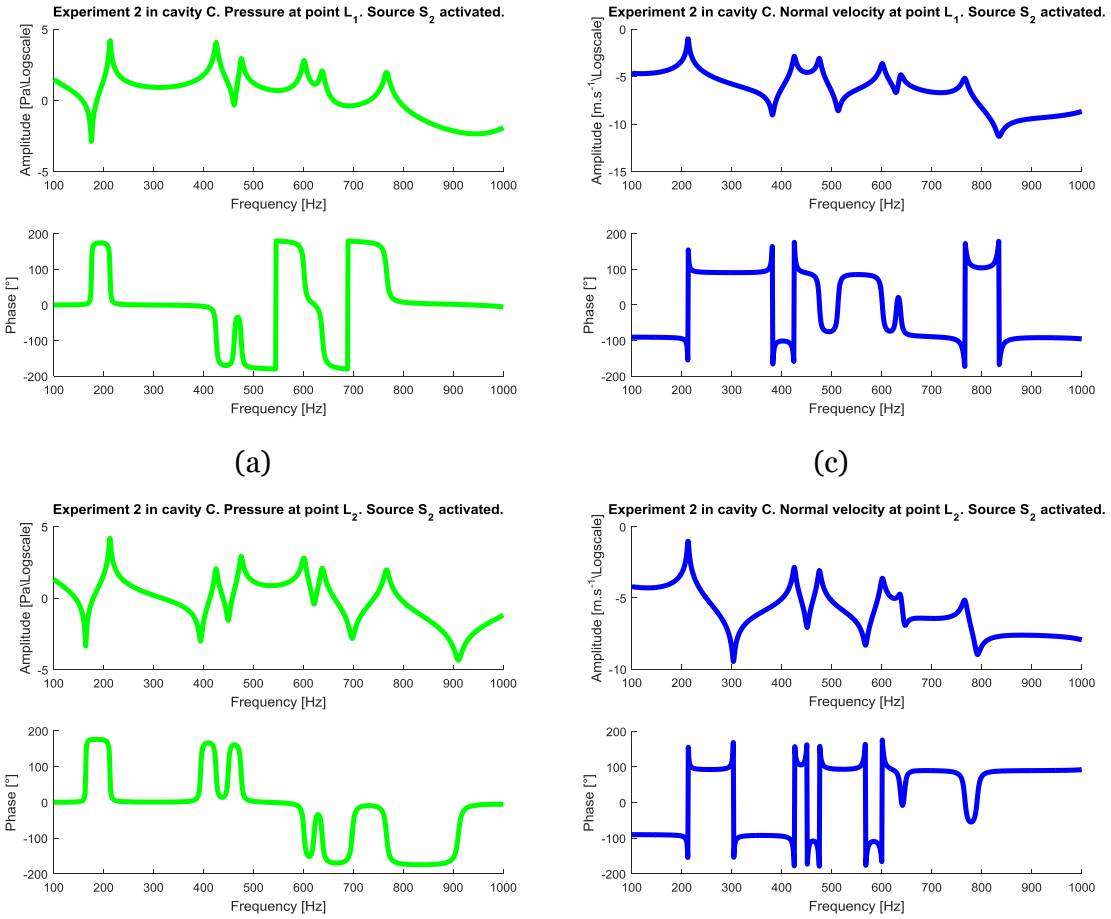

Figure 3.10: Results of the second experiment in the coupled cavity C. (a) and (b) are representing the pressure vector $\{P_i^C\}_2$; (c) and (d) are representing the velocity vector $\{V_i^C\}_2$.

Construction of the matrices $[P]$

The pressure results of the *set of experiments* are stored in a common matrix $[P]$. The matrix is constructed according to the procedure detailed in Sec. 3.2. It results in a matrix of size $(N; N)$ with N equal to 2 in the present *set of experiments*. Each term of the matrix $[P]$ are depicted in Figure 3.11.

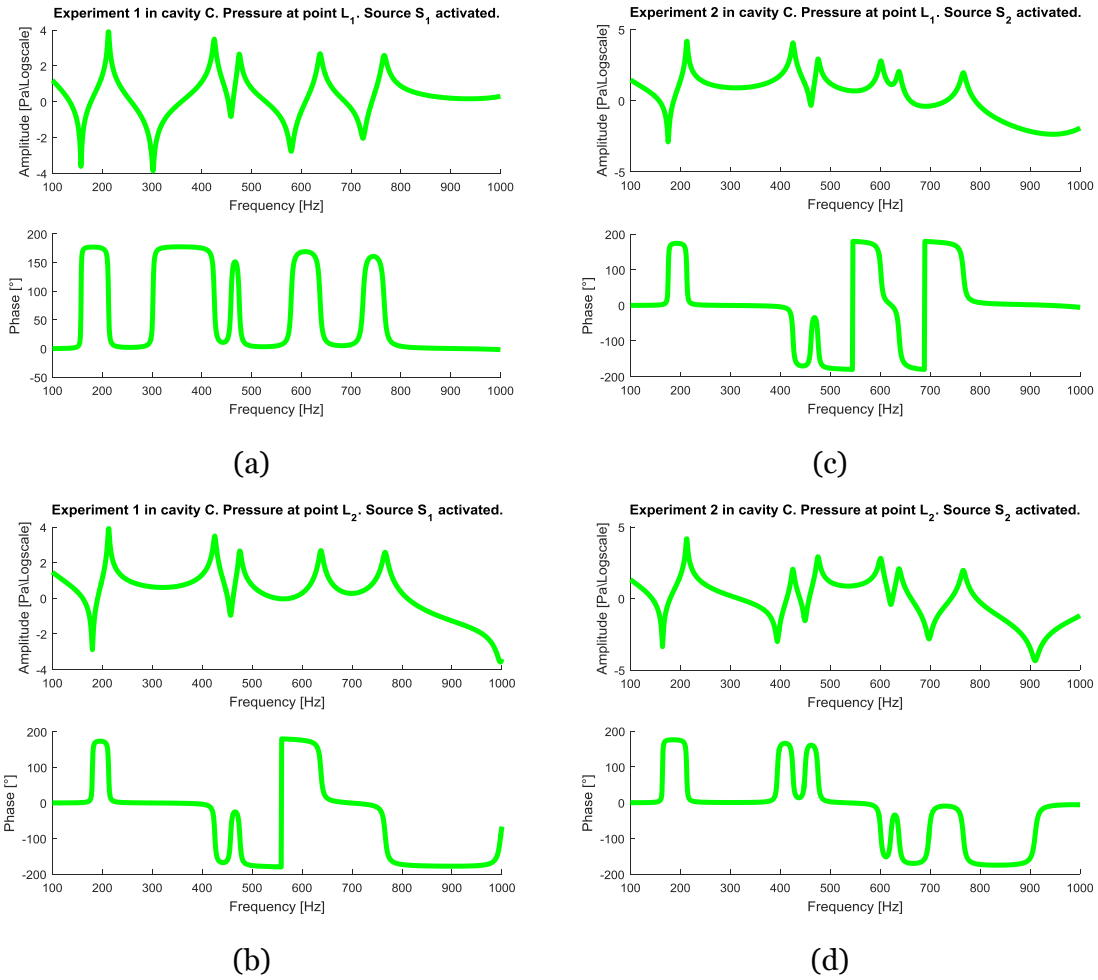

Figure 3.11: Presentation of the content of the matrix $[P]$ *of size* $(2; 2)$. *(a):* P_{11}*; (b):* P_{21}*; (c):* P_{12}*; (d):* P_{22}.

Construction of the matrices $[V]$

The velocity results of the *set of experiments*—i.e. first and the second experiment—are stored in a common matrix $[V]$. The matrix is constructed according to the procedure detailed in Sec. 3.2. It results in a matrix of size $(N; N)$ with N equal to 2 in the present *set of experiments*. Each term of the matrix $[V]$ is depicted in Figure 3.12

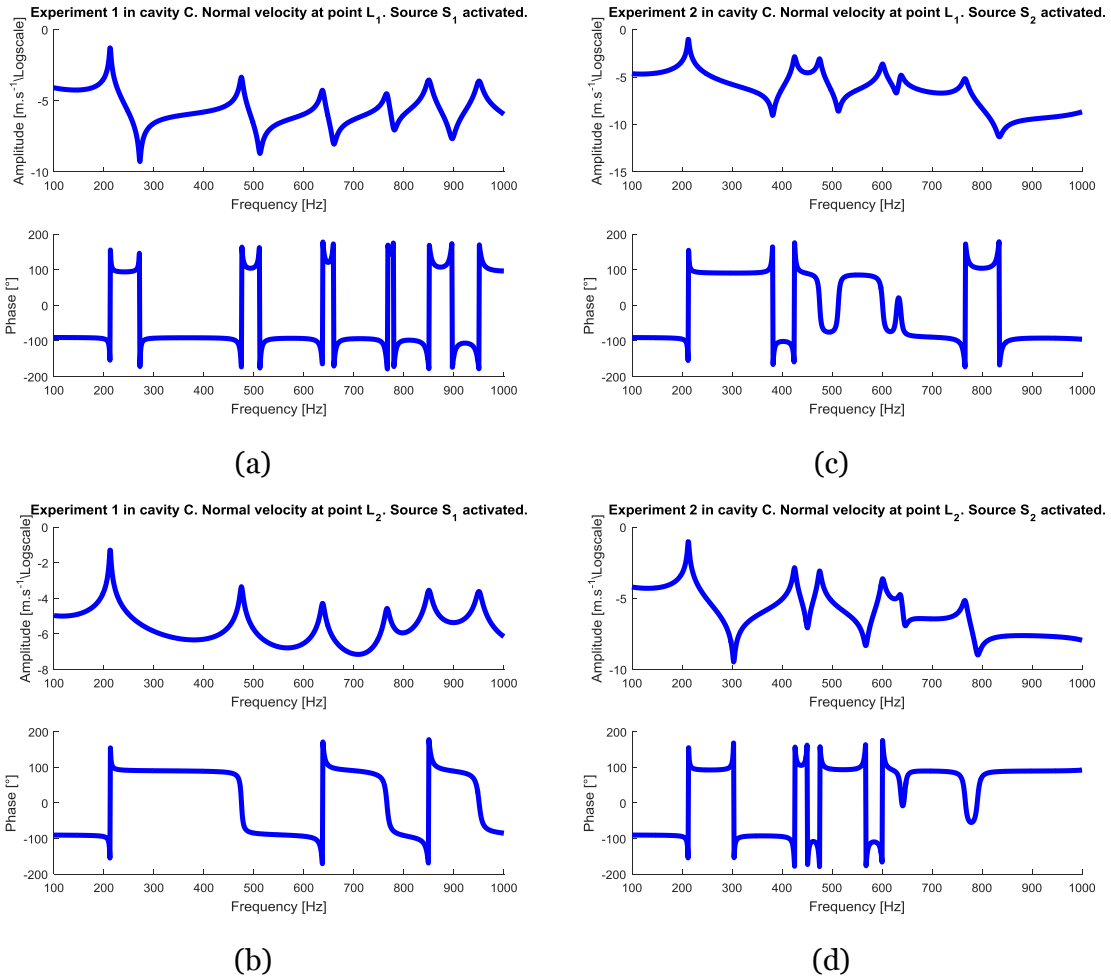

Figure 3.12: Presentation of the content of the matrix $[V]$ *of size* $(2; 2)$. *(a):* V_{11}*; (b):* V_{21}*; (c):* V_{12}*; (d):* V_{22}.

3.4.2 Result of the characterization

The matrices $[P]$ and $[V]$ presented in the last section allow—according to the principle "$[Z] = [P][V]^{-1}$"—to identify the condensed patch to patch matrix $\left[Z_{i\leftarrow j}^{A\ Id}\right]$ of the subsystem A. The results are presented in Figure 3.13.

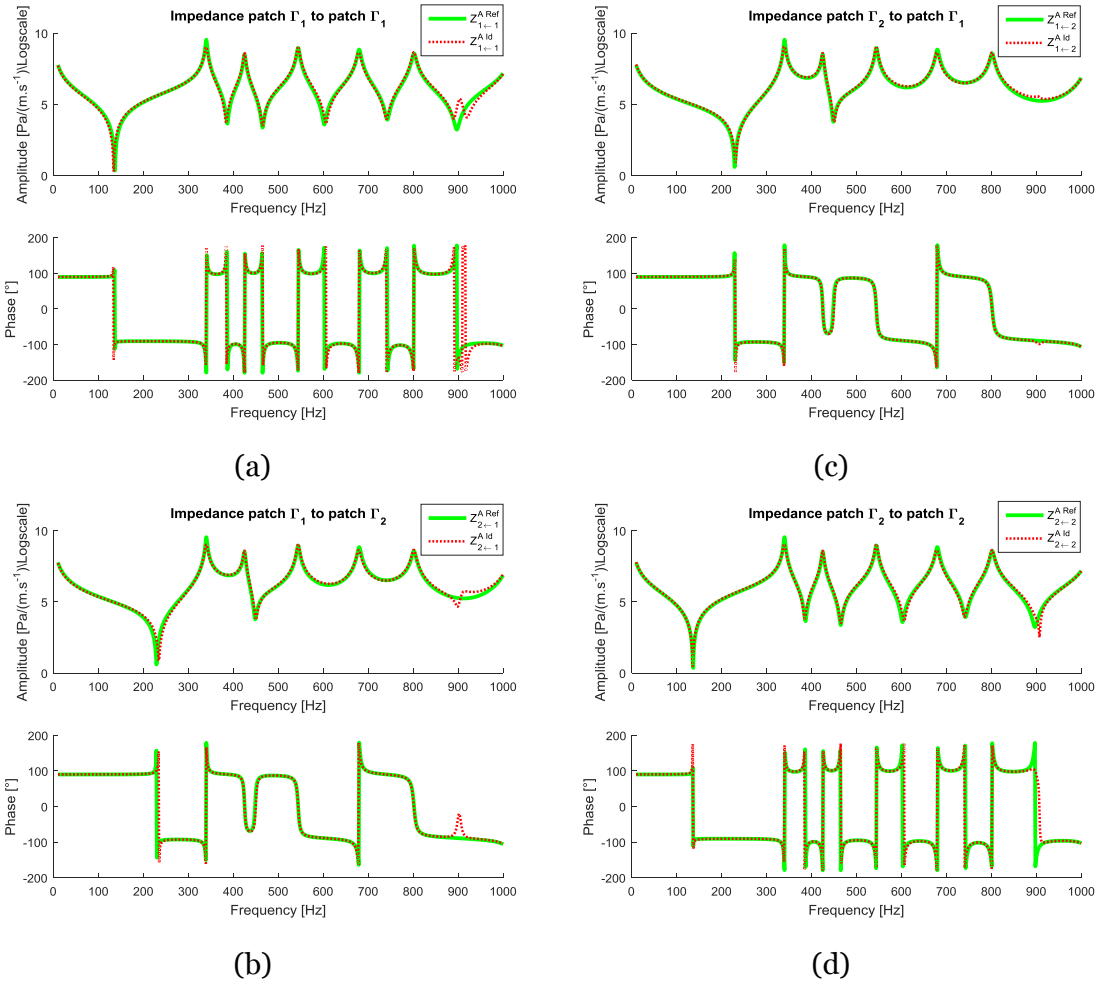

Figure 3.13: Graphical representation of the result of the identified condensed impedance matrix $\left[Z_{i\leftarrow j}^{A\,Id}\right]$ *(dotted red line) in comparison to the reference condensed impedance* $\left[Z_{i\leftarrow j}^{A\,Ref}\right]$ *(green solid line). The graphical position of the curves matches the standard representation of a matrix—i.e. (a):* $Z_{1\leftarrow 1}^{A}$*; (b):* $Z_{2\leftarrow 1}^{A}$*; (c):* $Z_{1\leftarrow 2}^{A}$*; (d):* $Z_{2\leftarrow 2}^{A}$*.*

Up to a frequency of about 900 Hz, the identified condensed impedance matrix $\left[Z_{i\leftarrow j}^{A\,Id}\right]$ of the subsystem A is extremely close to the reference condensed patch to patch impedance $\left[Z_{i\leftarrow j}^{A\,Ref}\right]$. Considering that no regularization method has been used, this result is really convenient. Therefore the inverse characterization method presented in Sec. 3.2—based on a roving source, the measure of the pressure and velocity at the virtual interface, and a problem of the form "$[Z] = [P][V]^{-1}$"—has up to this point demonstrates its validity.

3.4.3 Coupling of the subsystems

Concept

In the previous section, the unknown subsystem A has been characterized with a condensed impedance matrix $\left[Z_{i\leftarrow j}^{A\,Id}\right]$, with measurement on the coupled system C. In Chap. 2 it has been seen that based on such a condensed impedance, it is possible to couple subsystem with consideration of all resulting coupling effects. Therefore, the intention in this section it to show that the information gained on the subsystem A—while strongly coupled to another subsystem B—can be used to couple this system to another one.

Numerical experiment

The numerical experiment is carried out on the two patches cavity, presented in Sec. 2.3.4—cf. illustration in Figure 2.10 and properties in Table 2.2. The only yet major difference, is that the subsystem A is not supposed known *a priory* with the matrix $\left[Z_{i\leftarrow j}^{A}\right]$. On the opposite, the matrix $\left[Z_{i\leftarrow j}^{A}\right]$ will be replaced by the identified impedance matrix $\left[Z_{i\leftarrow j}^{A\,Id}\right]$ presented in Figure 3.13.

In order to avoid any numerical artefact—wrong intermediate result leading artificially to a good final result—the source S_3 used for the verification test has not been used for the characterization process. On the opposite the source S_1 and S_2 used for the characterization have been chosen deliberately distant from the source S_3 used for the verification. The position of each source is given numerically in Table 2.2 and Table 3.1.

As it has been showed in Figure 2.11 the choice of the definition of the Patch Transfer Functions method either "PTF Coupling (Spatial average)" or "PTF Coupling (Center)" has a small influence on the result. However, the following analysis will be done for both cases to verify if it has an influence on the reconstructed results.

Result

The results using the approach "PTF Coupling (Spatial average)" are presented in Figure 3.14. As in Chap. 2, up to 850 Hz, the difference with the reference solution computed in the cavity C is marginal.

In addition, it can be observed that using the method "PTF Coupling (Spatial average)" based on the knowledge of subsystem A obtained by the inverse characterization method, no additional error is created. The curve "PTF Coupling (Spatial average) using inverse characterization" is almost superposed to the curve "PTF Coupling (Spatial average)". This observation is a second example about the validity of the inverse characterization method proposed in this chapter.

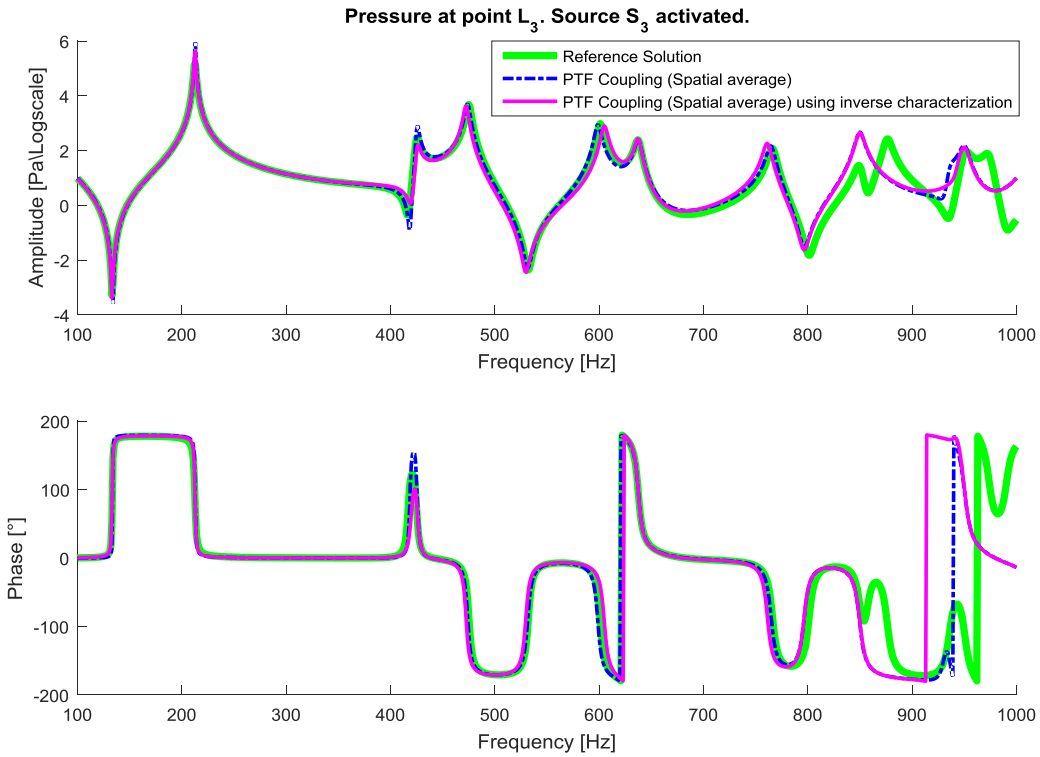

Figure 3.14: Pressure (amplitude and phase) at position L_3 in the cavity C caused by source S_3 Green solid line—"Reference Solution": Represents the reference solution in the box C. No substructuring method is used. The pressure is computed according to Eq. (2.35); Blue dash-dotted line—"PTF Coupling (Spatial average)": Result of the computational coupling of the known box A and B with the Patch Transfer Functions method; Magenta solid line—"PTF Coupling (Spatial average) using inverse characterization": is similar to the "PTF Coupling (Spatial average)" where the impedance $[Z^{A}_{i\leftarrow j}]$ of subsystem A has been considered as unknown and identified with the inverse characterization method—$[Z^{A\,Id}_{i\leftarrow j}]$.

The results using the approach "PTF Coupling (Center)" are presented in Figure 3.15. In Chap. 2, it has already been that the method "PTF Coupling (Center)" was able to couple the two sub cavities A and B. Indeed up to 850 Hz, the difference with the reference solution computed in the cavity C is marginal. Except for an already observed artefact in the frequency range 650–750 Hz. For the other frequencies, the results are in the same quality order than the conventional Patch Transfer Functions method "PTF Coupling (Spatial average)".

This result in repeated here. In addition, it can be observed that using in the method "PTF Coupling (Center)" based on the knowledge of subsystem A obtained by the inverse characterization method, no additional error is created. The curve "PTF Coupling (Spatial average) using inverse characterization" is almost superposed to the curve "PTF Coupling (Center)". This observation is another example about the validity of the inverse characterization method proposed in this chapter.

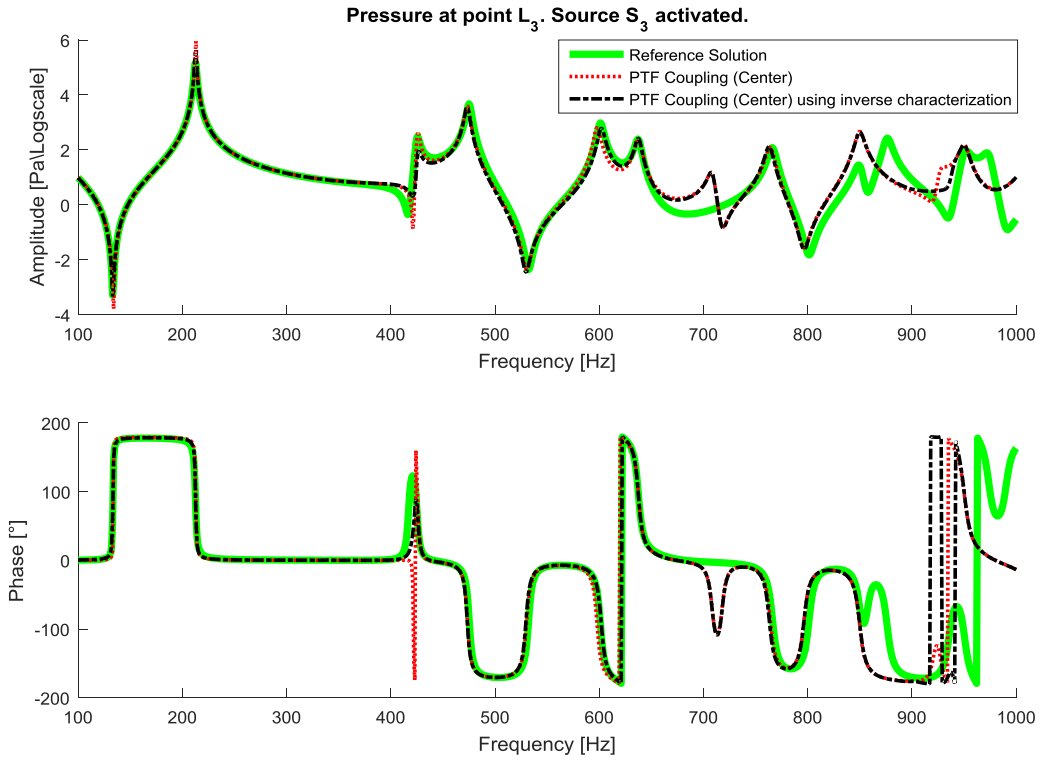

Figure 3.15: Pressure (amplitude and phase) at position L_3 in the cavity C caused by source S_3—cf. geometry of the box is depicted in Figure 2.10. Green solid line—"Reference Solution": Represents the reference solution in the box C. No substructuring method is used. The pressure is computed according to Eq. (2.35); Red dotted line—"PTF Coupling (Center)": Result of the computational coupling of the known box A and B with the Patch Transfer Functions method; Black dash-dotted line—"PTF Coupling (Center) using inverse characterization": is similar to the "PTF Coupling (Center)" where the impedance $[Z^{A}_{i\leftarrow j}]$ of subsystem A has been considered as unknown and identified with the inverse characterization method—$[Z^{A\,Id}_{i\leftarrow j}]$.

3.5 Summary

The inverse method presented in this chapter proposes an experimental method, allowing characterization of a particular subsystem—while coupled with another unknown subsystem. The experimental procedure counts on the knowledge of the pressures and the particle velocities at the subsystem interface, while exited by a roving acoustical source. On the one hand, no *a priori* information about any system—system under characterization or the full system—is necessary to employ the method. On the other hand, as long as the vibro-acoustic subsystem to be characterized has a linear behavior, the method is—from a theoretical point of view—applicable whatever the complexity of the system. For example: presence of unknown trim, presence of unknown vibro-acoustic components ...

The first results—obtained with a numerical experiment—show that the method is able to handle the characterization of a strongly coupled subsystem with an almost perfect identification. Secondly it has been seen that the system characterized with the inverse method, can be coupled again to another system and predict the response of the coupled system. In this extend, the validity of the theory presented in this chapter is up to this point validated. Nevertheless, the robustness of the method concerning the measuring condition has not been proven yet. The limitation of this method should be analyzed and overcome.

4 Limits of the method

"We have had our failures, but so have others, even if they do not admit them. And they may be less public.
To be sure, we are behind, and will be behind for some time in manned flight. But we do not intend to stay behind, and in this decade we shall make up and move ahead."

John Fitzgerald Kennedy (1917–1963) in "Address at Rice University in Houston on the Nation's Space Effort", 1962 [1].

Chapter contents:

4.1 Introduction 81

4.2 Metrics for results quality 82

4.2.1 Condition number 82

4.2.2 Mean quadratic error 83

4.3 Reference analysis in depth 83

4.3.1 Problem geometry 83

4.3.2 Modal summation convergence 84

4.3.3 Analysis of identification accidents 85

4.4 Instability due to the choice of set of experiments 89

4.4.1 Influence of choice of set of experiments 90

4.4.2 Best sets of experiments 91

4.4.3 Summary 95

4.5 Instability to measurement noise 95

4.5.1 Introduction of noise on the input data 96

4.5.2 Effect on the input data 97

4.5.3 Effect on the output data 97

4.6 Summary 101

4.1 Introduction

The inverse method proposed in Chap. 3—i.e. *set of experiments* with a roving acoustical source and formulation of the problem on the form "$[Z] = [P][V]^{-1}$"—has addressed the problematic *"Characterization of Patch Transfer Functions of a subsystem by means of measurement on a coupled system"*. The theoretical background of the proposed method has been applied on a simple numerical experiment as a validation of the principle. This

first characterization was good enough to predict the pressure at a given listening point once the system has been coupled again to another system.

Chap. 4 investigates the limits of the method, such as the nature of the *set of experiments* used for the characterization and the presence of noise in the measurement. Along these lines, some objective metrics describing the results quality are necessary. This objective description allows carrying on parametric analyses. The metrics will be first defined and illustrated on the results presented graphically in the previous chapter.

4.2 Metrics for results quality

Two metrics are introduced: the condition number and the mean quadratic error. These two indicators are delivering different meaningful information:

Condition number. Applies to the matrix $[V]$. It Indicates whether the numerical inversion process should be trusted or not. Value within the interval $[1, +\infty[$. Best value is near to one.

Mean quadratic error. Applies to the matrices $\left[Z_{i\leftarrow j}^{A\,Id}\right]$ and $\left[Z_{i\leftarrow j}^{A\,Ref}\right]$. It evaluates the discrepancies between the two matrices. Value within the interval $[0, +\infty[$. Best value is near to zero.

The condition number should be considered as an intermediate indication of the quality of the result while the mean quadratic error truly compares the final result to the reference. This section presents in more details how these indicators are computed. In addition, some small variations of these metrics will be used in this chapter and will be introduced directly in the concerned section.

4.2.1 Condition number

The method proposed in the third chapter relies on the inversion of a quadratic complex matrix (N, N) of coupled velocities noted $[V]$. The matrix $[V]$ is evaluated at each spectral line, corresponding to a given angular frequency ω. Whether this velocity is estimated as a mean value over the surface of the virtual patch or estimated at the center of the virtual patch, the inversion might be problematic when the matrix has a bad condition number.

The condition number measures how much the result of the inversion is affected by a small changes in the matrix to be inverted. When the condition number of a matrix is high—ill-conditioned matrix—a small difference in the matrix before the inversion might result in large difference after the inversion. As with any numerical simulation, the precision is intrinsically not infinite, a small truncation error appears. If the matrix is sufficiently ill-conditioned, it might result in an inverse matrix with an extremely large amplification of this insignificant truncation approximation.

Several definitions of the condition number of a matrix could be considered. The definition considered in this dissertation is the second-norm condition number—i.e. ratio of the largest singular value to the smallest one. A value of the condition number near one indicates a well-conditioned matrix.

The condition number will be found in this dissertation in two forms:

Per spectral line. Computed at each spectral line—i.e. at a specific frequency.
Frequency range. Mean value over a given frequency range.

The condition number gives an indication about the stability of the inversion process itself, nevertheless it does not help to decide whether the quality of the identification is good or not.

4.2.2 Mean quadratic error

In this chapter the reference solution is known, therefore many indicators should be able to compare the identified matrix $\left[Z_{i\leftarrow j}^{A\,Id}\right]$ to the reference matrix $\left[Z_{i\leftarrow j}^{A\,Ref}\right]$. The mean quadratic error represents such an indicator.

The identified matrix $\left[Z_{i\leftarrow j}^{A\,Id}\right]$ is computed for each frequency. For each spectral line, this matrix can be compared with the reference matrix. The mean quadratic error for a specific frequency is computed according to Eq. (4.1).

$$M_{qe} = \frac{1}{N^2}\sum_{i=1}^{N}\sum_{j=1}^{N}\left(\left|Z_{i\leftarrow j}^{A\,Id} - Z_{i\leftarrow j}^{A\,Ref}\right|^2\right) \tag{4.1}$$

The mean quadratic error M_{qe} is a real scalar value that measures the average error (averaged on all patches) observed between the identified impedance matrix and the reference. The mean quadratic error will be found in this dissertation in two forms:

Per spectral line. Computed at each spectral line—Eq. (4.1).
Frequency range. Mean value of the result of Eq. (4.1) for each spectral line.

The mean quadratic error is not normalized by the norm of the reference. Its value depends thus on the mean value of the impedance terms. This particularity is suitable for the comparison of an identified impedance. Indeed once a system is coupled to another one, the system with the strongest impedance tends to impose its drive. Therefore, the large impedance should be well estimated, while small impedance shall be poorly estimated.

Before using the metrics intensively on parametric analysis, the metrics will be used on the results already presented in the previous chapter.

4.3 Reference analysis in depth

4.3.1 Problem geometry

The geometry used in the so called reference analysis used in Chap. 2 as well as in Chap. 3 is depicted in Figure 3.8 and the corresponding properties are listed in Table 3.1. Cavity C is *virtually* split in sub cavities A and B. The description of a system with its eigenmodes normally provides a solid basis to physical interpretations. In this extend, the first modes of each cavity are listed in Table 4.1.

Table 4.1: Eigen mode in the sub-cavities A , B and C with blocked boundary conditions. The eigen-frequencies are computed for the frequency range 0–1,000 Hz. The corresponding mode indices l, m and n corresponding to each frequency are provided.

Box *A*				Box *B*				Box *C*			
f (Hz)	l	m	n	f (Hz)	l	m	n	f (Hz)	l	m	n
0	0	0	0	0	0	0	0	0	0	0	0
340	1	0	0	425	0	1	0	213	1	0	0
425	0	1	0	567	1	0	0	425	0	1	0
544	1	1	0	708	1	1	0	425	2	0	0
680	2	0	0	850	0	0	1	475	1	1	0
802	2	1	0	850	0	2	0	601	2	1	0
850	0	0	1	950	0	1	1	638	3	0	0
850	0	2	0					766	3	1	0
915	1	0	1					850	0	0	1
915	1	2	0					850	0	2	0
950	0	1	1					850	4	0	0
								876	1	0	1
								876	1	2	0
								950	0	1	1
								950	2	0	1
								950	2	2	0
								950	4	1	0
								974	1	1	1

The simple geometry of the cavities, exhibiting many symmetries, results in a rather particular phenomenon. Indeed, the resonance frequencies computed according to Eq. (2.42) are exhibiting following phenomenon: some Eigen modes with different mode shapes have exactly the same frequency. For example in the cavity C, four different modes have an eigen-frequency equal to 950 Hz, three with an eigen-frequency equal to 850 Hz … This phenomenon is one reason why *simple* geometry might result in *specific* phenomena. In a more complex systems the probability of such an event is rather limited.

4.3.2 Modal summation convergence

In the numerical experiment, the matrices $[P]$ and $[V]$ are computed using a modal summation using Eq. (2.31). The exact solution would demand to compute the summation up to an infinite number of modes. For the needs of numerical computation, the summation is necessarily truncated. It means that a given number of modes is conserved while still an infinity high order modes are rejected. Due to the form of the equation—"$\left(k^2 - k_k^2\right)$" at the denominator—the impact of any mode which frequency is much higher than the considered frequency does not contribute a lot. Nevertheless, since an infinity of modes is rejected, the convergence of the modal summation is not self-evident.

In order to verify the convergence of the modal summation, the two metrics presented in Sec 4.2 are plotted with a growing number of modes used for the computation. The

convergence of the condition number of the matrix $[V]$ averaged over the frequency band is illustrated on Figure 4.1. Similarly the convergence of the mean quadratic error is provided on Figure 4.2. For both curves, the number on the x-axis is not the number of modes, but the maximal mode order "$MaxModalOrder$" in each direction—i.e. maximal value of each subscript l, m and n found in Eq. (2.42). The number of modes is actually equal to $(MaxModalOrder + 1)^3$.

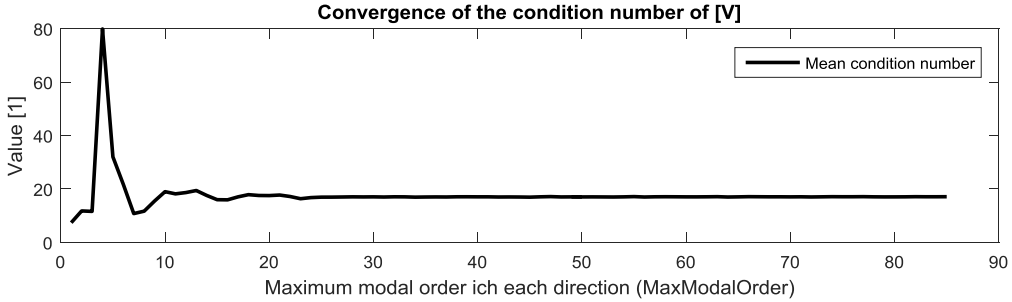

Figure 4.1: Convergence plot of the condition number of $[V]$ as a function of the modal truncation. X-axis: Presents the modal order limit for a mode in each direction—i.e. "$MaxModalOrder$"; Y-Axis: Displays the mean condition number of the matrix $[V]$ over the full frequency range 10–1,000 Hz.

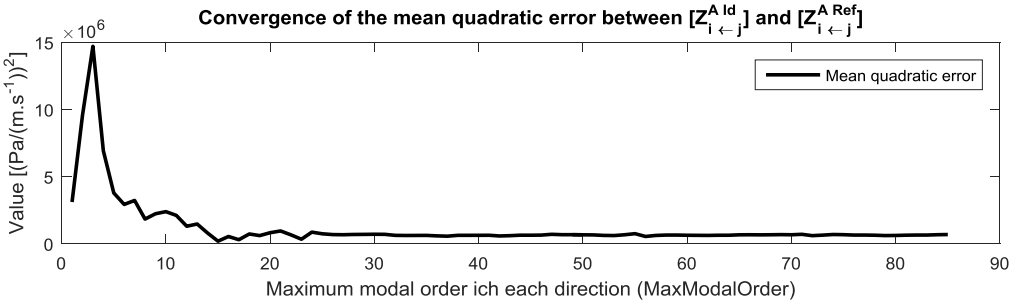

Figure 4.2: Convergence plot of the mean quadratic error as a function of the modal truncation. X-axis: Presents the modal order limit for a mode in each direction—i.e. "$MaxModalOrder$"; Y-Axis: Displays the mean quadratic error of matrix $\left[Z_{i\leftarrow j}^{A\ Id}\right]$ versus $\left[Z_{i\leftarrow j}^{A\ Ref}\right]$ over the full frequency range 10–1,000 Hz. The reference matrix has been computed according to Eq. (2.32) with a "$MaxModalOrder$" equal to 100.

Considering the simplicity of the considered model, solely two patches, the number of modes to consider in order to reach the convergence of the solution before (condition number of $[V]$) and after the inversion (mean quadratic error between $\left[Z_{i\leftarrow j}^{A\ Id}\right]$ and $\left[Z_{i\leftarrow j}^{A\ Ref}\right]$) is exorbitant. Indeed the convergence is definitively reached for indices l, m and n up to 20, meaning that 9261 modes have been considered. The first excluded mode has a frequency of 4,462 Hz and corresponding subscripts (l, m, n) equal to (21,0,0).

For the further analysis on this example, the modal basis will be truncated at a "$MaxModalOrder$" larger than 20.

4.3.3 Analysis of identification accidents

Considering $MaxModalOrder = 85$, Figure 4.3 presents the evolution of the condition number and the mean quadratic error as a function of frequency. Eigen-frequencies of sub-cavities A and B (considering that all the walls of the sub-cavities are rigid, see Table 4.1) as well as the one of cavity C are represented by symbols.

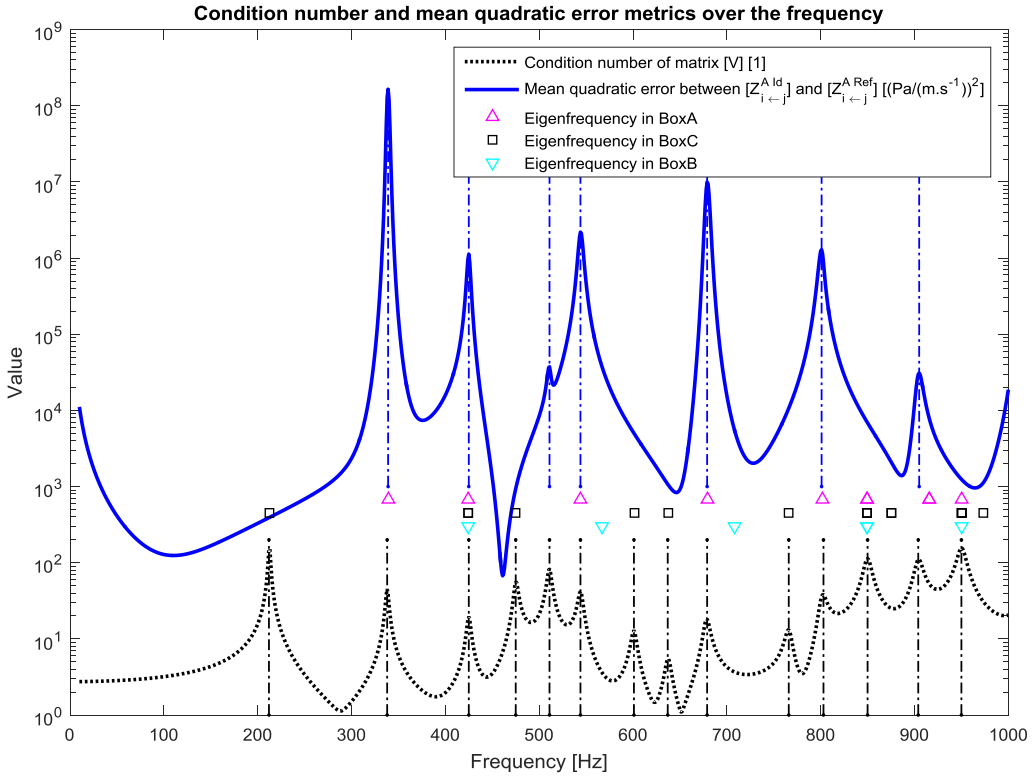

Figure 4.3: The value of the two indicators condition number of matrix $[V]$ (black dotted line) and the mean quadratic error between $\left[Z_{i\leftarrow j}^{A\ Id}\right]$ and $\left[Z_{i\leftarrow j}^{A\ Ref}\right]$ (blue solid line) are represented on the same plot over the frequency range 10-1,000 Hz. The condition number (black dotted line) comprises 14 local maxima at the frequencies: 212; 338; 425; 475; 511; 544; 601; 637; 679; 766; 803; 850; 904; 950 Hz represented by vertical black dash-dot lines. The mean quadratic error (blue solid line) contains 7 local maxima at the frequencies: 339; 425; 511; 544; 679; 801; 905 Hz represented by vertical blue dash-dot lines. The Eigen frequencies of cavities A, B and C with rigid boundary condition provided in Table 4.1 are marked respectively with: magenta upward-pointing triangle, cyan downward-pointing triangle, black square. The vertical position over the y-axes of these markers does not have any physical signification.

As Figure 4.3 has a high information density, it will be analyzed all along this section. In order to reduce the quantity of information, this figure will be analyzed in terms of *events*. Indeed, the figure can be interpreted as a series of *events*, each one happening at a given discrete frequency. For the further analysis, 9 type of *events* have are retained. Table 4.2 presents a description of each *event*.

Table 4.2: Description and graphical representation of 9 type of events encountered on Figure 4.3.

Event	Description	Occurrences
$MaxCond$	Local maximum of condition number (Vertical black dash-dot lines)	14
$MaxMQE$	Local maximum of Mean Quadratic Error (Vertical blue dash-dot lines)	7
$EigenfrequencyAnyBox$	Eigenfrequency in one or more subsystem (Magenta upward-pointing triangle OR Cyan downward-pointing triangle OR Black square)	17
$Eigenfrequency\ Box\ A$	Eigenfrequency in Box A (Magenta upward-pointing triangle)	8
$Eigenfrequency\ exclusively\ Box\ A$	Eigenfrequency in Box A only (Magenta upward-pointing triangle only)	5
$Eigenfrequency\ Box\ B$	Eigenfrequency in Box B (Cyan downward-pointing triangle)	5
$Eigenfrequency\ exclusively\ Box\ B$	Eigenfrequency in Box B only (Cyan downward-pointing triangle only)	2
$Eigenfrequency\ Box\ C$	Eigenfrequency in Box C (Black square)	10
$Eigenfrequency\ exclusively\ Box\ C$	Eigenfrequency in Box C only (Black square only)	7

The analysis of Figure 4.3 in terms of the *events* presented in Table 4.2 will be carried out up to the end of this section. The governing motivation is to find in which measure these *events* are related. This analysis will be done with a statistical analysis. This method is *per se* in no mean a demonstration, yet the information gained might be valuable.

Link between condition number and mean quadratic error

Observing the *events* local maxima of the two curves, some similarities as well as some difference are observed. In Table 4.3, a statistical analysis investigate if these two quantities are somehow related and in which extend.

Table 4.3: Statistical occurrence and non-occurrence of two implications between the event local maxima of the condition number ($MaxCond$) and the event local maxima of the mean quadratic error ($MaxMQE$).

Question	True		False		Validity
$MaxCond \rightarrow MaxMQE$	7/14	50%	7/14	50%	No
$MaxMQE \rightarrow MaxCond$	7/7	100%	0/7	0%	Yes

Based on the observed data, the conclusion might be formulated as following:

> *A Bad condition number* does not necessarily imply a bad identification.
> *A Bad identification* is always due to a bad condition number.

This observation stresses the particularity of the formulation of the problem on the form "$[Z] = [P][V]^{-1}$". Each poor identification of the impedance might be caused by an ill-conditioned velocity matrix, but an ill-conditioned matrix does not result automatically in a bad identification. The further analysis aims to provide a better insight in the cause of this observation.

Link between modes in the cavity and mean quadratic error

The position of many local maxima of the two curves seems to match the Eigen frequencies of some of the subsystem A, B or C. Some coincidences, as well as some differences are observed. The results of the statistical analysis are presented in Table 4.4.

Table 4.4: Statistical occurrence and non-occurrence of four implications. First two implications: Frequency matching of the local maxima of the mean quadratic error ($MaxMQE$) and one or many Eigenfrequencies of any of the box A, B, or C ($EigenfrequencyAnyBox$); Last two implications: Frequency matching of the local maxima of the condition number ($MaxCond$) and one or many Eigenfrequencies of any of the box A, B, or C ($EigenfrequencyAnyBox$).

Question	True		False		Validity
$EigenfrequencyAnyBox \rightarrow MaxMQE$	5/17	29%	12/17	71%	No
$MaxMQE \rightarrow EigenfrequencyAnyBox$	5/7	71%	2/7	29%	Trend
$EigenfrequencyAnyBox \rightarrow MaxCond$	12/17	71%	5/17	29%	Trend
$MaxCond \rightarrow EigenfrequencyAnyBox$	12/14	86%	2/14	14%	Strong

No perfect implication is observed, but one rule has been infirmed, three tendencies are observed one of which is a strong one. This analysis might be not enough discriminating. The following analysis will focus on which subsystem A, B or C does interfere most with the identification quality.

Influence of the Eigenfrequencies of each subsystem

Many of the Eigenfrequencies of box A are deteriorating the impedance estimation. Four implications concerning their potential influence are presented in Table 4.5.

Table 4.5: Statistical occurrence and non-occurrence of four implications. First two implications: Frequency matching of the local maxima of the mean quadratic error ($MaxMQE$) and one or many Eigenfrequencies of box A ($Eigenfrequency\ Box\ A$); Last two implications: Frequency matching of the local maxima of the condition number ($MaxCond$) and one or many Eigenfrequencies of box A ($Eigenfrequency\ Box\ A$).

Question	True		False		Validity
$Eigenfrequency\ Box\ A \rightarrow MaxMQE$	5/8	63%	3/8	38%	Trend
$MaxMQE \rightarrow Eigenfrequency\ Box\ A$	5/7	71%	2/7	29%	Trend
$Eigenfrequency\ exclusively\ Box\ A \rightarrow MaxMQE$	4/5	80%	1/5	20%	Strong
$MaxMQE \rightarrow Eigenfrequency\ exclusively\ Box\ A$	4/7	57%	3/7	43%	No

The resonances of the system B does not impact the identification. The results are furnished in Table 4.6.

Table 4.6: Statistical occurrence and non-occurrence of four implications. First two implications: Frequency matching of the local maxima of the mean quadratic error ($MaxMQE$) and one or many Eigenfrequencies of

box B (Eigenfrequency Box B); Last two implications: Frequency matching of the local maxima of the condition number (MaxCond) and one or many Eigenfrequencies of box B (Eigenfrequency Box B).

Question	True		False		Validity
$Eigenfrequency\ Box\ B \rightarrow MaxMQE$	1/5	20%	4/5	80%	No
$MQE \rightarrow Eigenfrequency\ Box\ B$	1/7	14%	6/7	86%	No
$Eigenfrequency\ exclusively\ Box\ B \rightarrow MaxMQE$	0/2	0%	2/2	100%	No
$MaxMQE \rightarrow Eigenfrequency\ exclusively\ Box\ B$	0/7	0%	7/7	100%	No

The resonances of the full system—box C—also does not impact the identification. See results in Table 4.7.

Table 4.7: Statistical occurrence and non-occurrence of four implications. First two implications: Frequency matching of the local maxima of the mean quadratic error (MaxMQE) and one or many Eigenfrequencies of box C (Eigenfrequency Box C); Last two implications: Frequency matching of the local maxima of the condition number (MaxCond) and one or many Eigenfrequencies of box C (Eigenfrequency Box C).

Question	True		False		Validity
$Eigenfrequency\ Box\ C \rightarrow MaxMQE$	1/10	10%	9/10	90%	No
$MaxMQE \rightarrow Eigenfrequency\ Box\ C$	1/7	14%	6/7	86%	No
$Eigenfrequency\ exclusively\ Box\ C \rightarrow MaxMQE$	0/7	0%	7/7	100%	No
$MaxMQE \rightarrow Eigenfrequency\ exclusively\ Box\ C$	0/7	0%	7/7	100%	No

Summary

Based on the observed data, the conclusion might be formulated as following:

> *A Bad condition number* does not necessarily imply a bad identification.
> *A Bad identification* is always due to a bad condition number.
> *Influence of subsystems*. The subsystem under identification—box A—has a preponderant influence on its identification. The resonances of the other subsystems B and C does not penalize the identification.

Many other parameters might impact the quality of the identification. The two following sections address the influence of the set of experiments and the presence of noise in the measurement.

4.4 Instability due to the choice of set of experiments

Up to this point, the characterization of the condensed impedance matrix of subsystem A has been carried out with solely one *set of experiments*—i.e. only one position of sources S_1 and S_2 has been tested. This analysis has resulted in a good identification as presented in Sec. 3.4, and in Sec. 4.3.

The choice of the *set of experiments* might have an effect on the quality of the identification. This section intends to analyze such an effect with two questions in the foreground:

- Are some *sets of experiments* more appropriate than others are?
- Is it possible to derive a rule to create an appropriate *set of experiments*?

4.4.1 Influence of choice of set of experiments

In this section, the characterization of the subsystem A is achieved thanks to three different *set of experiments*. One of which is the *set of experiments* used up to this point—arbitrarily called "Set of experiments 1 (Reference)". The two others *set of experiments* (2 and 3) are first introduced in this section as presented in Table 4.8.

Table 4.8: Illustration of the three sets of experiments used for the characterization of the box A. For each set of experiments, the numerical position of the two necessary sources S_1 and S_2 (red point) is provided. The center of the two virtual patches L_1 and L_2 is represented with a blue point. All unchanged properties are found in Table 3.1.

Set of experiments 1 (Reference)	Set of experiments 2	Set of experiments 3
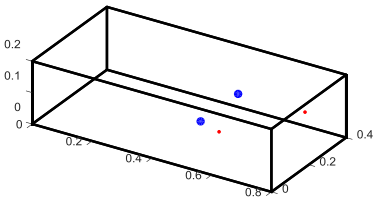	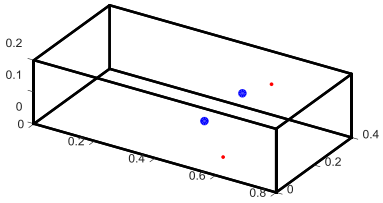	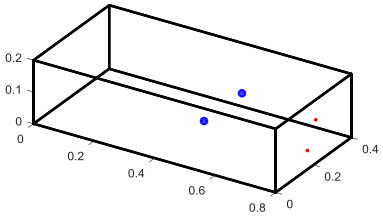
S_1: (0.60; 0.05; 0.13)	S_1: (0.56; 0.36; 0.12)	S_1: (0.72; 0.34; 0.06)
S_2: (0.70; 0.35; 0.08)	S_2: (0.60; 0.04; 0.04)	S_2: (0.78; 0.20; 0.04)

Each *set of experiments* allows to identify the condensed impedance matrix $\left[Z_{i\leftarrow j}^{A\,Id}\right]$ of the subsystem A. The condition number of the matrix $[V]$ and the mean quadratic error between the matrices $\left[Z_{i\leftarrow j}^{A\,Id}\right]$ and $\left[Z_{i\leftarrow j}^{A\,Ref}\right]$ are presented in Table 4.9. in each case.

Table 4.9: Metrics of the quality result for each set of experiments. Both indicators are computed according to the mean value over the full frequency range 10–1,000 Hz.

Name	Set of experiments 1 (Reference)	Set of experiments 2	Set of experiments 3
Condition number	17.10	10.37	12.54
Mean quadratic error	$6.45e+05$	3.85e + 06	4.60e + 04

This analysis supports the evidence that the identification process and its result are influenced by the *set of experiments*. Indeed, the condition number and the mean quadratic error vary according to the chosen *set of experiments*. Once again, no direct link is observed between the condition number (intermediate indicator) and the mean quadratic error (final indicator). Among the three *sets of experiments* the following observations can be done:

> *Set of experiments 2*. Smallest condition number, but results in the worst identification.
> *Set of experiments 3*. Intermediate condition number, but results in the best identification.

In order to get more insight in the details of the indicators, Figure 4.4 proposes their values over the frequency. The *set of experiments* 3 results in many occurrence in a much better

identification than the two others sets, although the condition number is not the smallest one among the experiments.

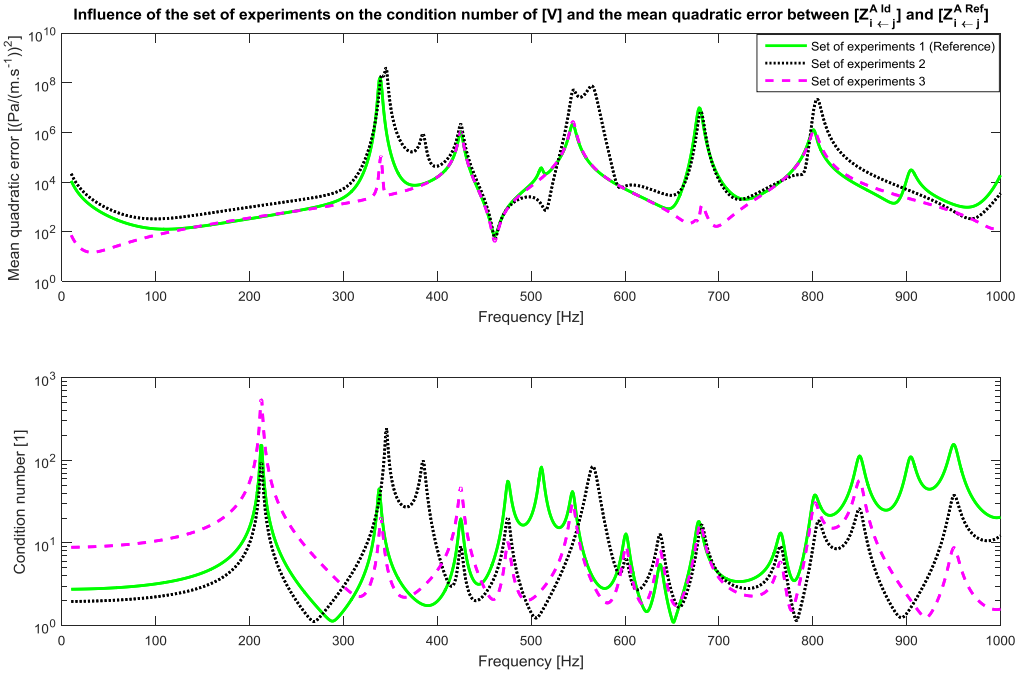

Figure 4.4: Condition number of matrix $[V]$ (bottom) and mean quadratic error between $[Z_{i\leftarrow j}^{A\ Id}]$ and $[Z_{i\leftarrow j}^{A\ Ref}]$ (top) in the frequency range 10-1,000 Hz. Green solid line: "set of experiments 1 (Reference); black dotted line: Set of experiments 2; magenta dashed line: Set of experiments 3.

This analysis points out that some *sets of experiments* are more appropriate than others for the identification of the subsystem A. The two following sections explore this question with more insight.

4.4.2 Best sets of experiments

Presentation of the method

The *set of experiments* has an influence on the quality of the characterization. In this section a large number of *sets of experiments* are computed and evaluated through the two metrics—condition number and mean quadratic error.

The characterization of the subsystem A requires the knowledge of the coupled pressure and velocity measured at the points L_1 and L_2 for two independent experiments. In total 2,394 source positions have been computed. The number of possible *sets of experiments* represents the number of combinations of 2 sources in a set of 2,394 sources. According to Eq. 4.2—applied with $Ns = 2{,}394$ and $N = 2$ —it represents 2,864,421 *sets of experiments*.

$$\binom{Ns}{N} = \frac{Ns!}{N!\,(Ns-N)!} \tag{4.2}$$

The 2,864,421 *sets of experiments* are represented in (Figure 4.5).

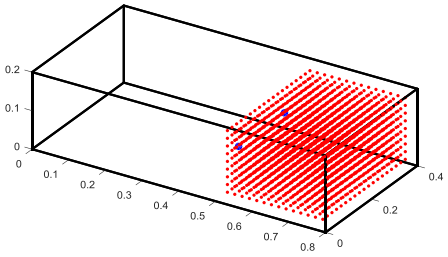

Figure 4.5: Representation of the computed sets of experiments. The center of the virtual patches of the subsystem A—L_1 and L_2—are depicted with the blue points. The red points are representing the 2,394 admissible positions of each source S_1 and S_2. The source S_1 has to be selected among one of the 2,394 positions depicted in red. The source S_2 has to be at a different position than the source S_1 leading to 2,393 possibilities. This choice represents one set of experiments. In total, the resulting number of sets of experiments reaches 2,864,421—i.e. mathematical combinations of 2 elements in a set of 2,394 elements.

All the 2,864,421 *sets of experiments* are evaluated according to the two metrics. This procedure allows finding out the best *set of experiments*, the ten best *sets of experiments* and so on. Actually, the analysis pattern is the same as the one encountered in Sec. 4.4.1, with the evaluation of 2,864,421 *sets of experiments* instead of 3. Three cases are discussed: The best *set of experiments*, the ten best *sets of experiments* and the hundred best *sets of experiments*.

Best set of experiments

The best *set of experiments* according to the best condition number of matrix [V] and the set of experiments leading to the best identification $\left[Z_{i\leftarrow j}^{A\,Id}\right]$ according to the criterion of mean quadratic error are depicted in Figure 4.6.

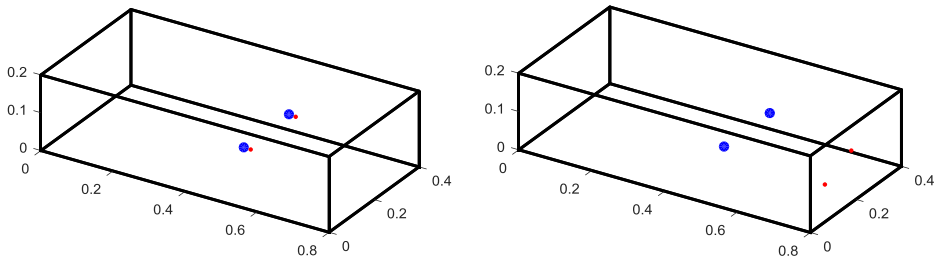

(a) (b)

Figure 4.6: (a): Set of experiments with to the best condition number of matrix $[V]$; (b): Set of experiments leading to the best identification $\left[Z_{i\leftarrow j}^{A\,Id}\right]$ according to the criterion of mean quadratic error. The corresponding sources position—S_1 and S_2—are depicted by red points, the centers of the patches of subsystem A are depicted by blue points.

The numerical details concerning these two best *sets of experiments* are provided in Table 4.10.

Table 4.10: Numerical properties of the best set of experiments according to the criterion of condition number or mean quadratic error. Both criteria are evaluated independently from each other on the frequency range 10–1,000 Hz.

Best set of experiments according to:	Condition number	Mean quadratic error
S_1	$(0.52; 0.10; 0.10)$	$(0.74; 0.16; 0.04)$
S_2	$(0.52; 0.30; 0.10)$	$(0.70; 0.34; 0.04)$
Condition number	1.05	11.16
Mean quadratic error	$2.45e+06$	$4.53e+04$

The *set of experiments* resulting in the best condition number differs from the one leading to the best identification:

> *Best condition number*. The sources S_1 and S_2 are extremely close to the measuring points L_1 and L_2—i.e. center of the patches.
> *Best identification*. The sources S_1 and S_2 are far away from the measuring points L_1 and L_2.

In both cases, the sources are facing, or almost facing, the center of the patches.

First ten best sets of experiments

The 10 best *sets of experiments* are depicted in Figure 4.7 according to the two criteria.

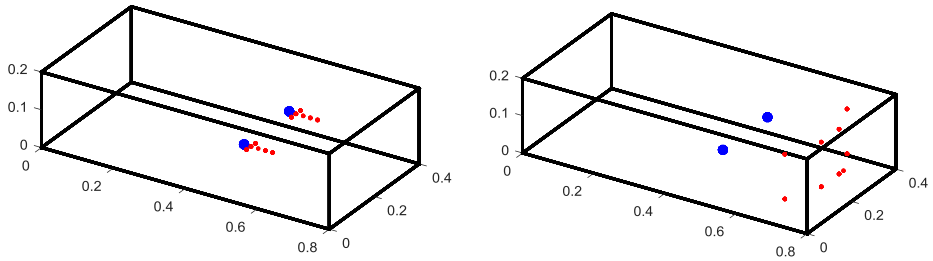

Figure 4.7: (a): 10 sets of experiments with the best condition number of matrix $[V]$; (b): 10 sets of experiments leading to the best identification $\left[Z_{i\leftarrow j}^{A\,Id}\right]$ according to the criterion of mean quadratic error. The corresponding sources position—S_1 and S_2—are depicted in red, the center of the patches of subsystem A are depicted in blue.

The numerical details concerning the best 10 *sets of experiments* are provided in Table 4.11.

Table 4.11: Numerical properties of the 10 best sets of experiments according to the criterion condition number or mean quadratic error. Both criteria are evaluated independently from each other on the frequency range 10–1,000 Hz.

10 best sets of experiments according to:	Condition number	Mean quadratic error
Condition number (Range)	[1.05; 1.44]	[11.16; 11.30]
Mean quadratic error (Range)	[2.42e + 06; 2.51e + 06]	[4.53e + 04; 4.53e + 04]

The 10 *sets of experiments* resulting in the best condition number differ from the ones leading to the best identification:

> *Best condition number*. The sources S_1 and S_2 are extremely close to the measuring points L_1 and L_2. The sources are facing or almost facing the points L_1 and L_2. The sources tend to be concentrate at a specific position.
> *Best identification*. The sources S_1 and S_2 are far away from the measuring points L_1 and L_2. The sources are not facing the points L_1 and L_2, but tend to move away from the planes positioned at $y = 0.10$ and $y = 0.20$ meters. The sources tend to occupy the back of cavity C.

The last test with the hundred best *sets of experiments* confirms this observation.

First hundred best sets of experiments

The 100 best *sets of experiments* are depicted in Figure 4.8.

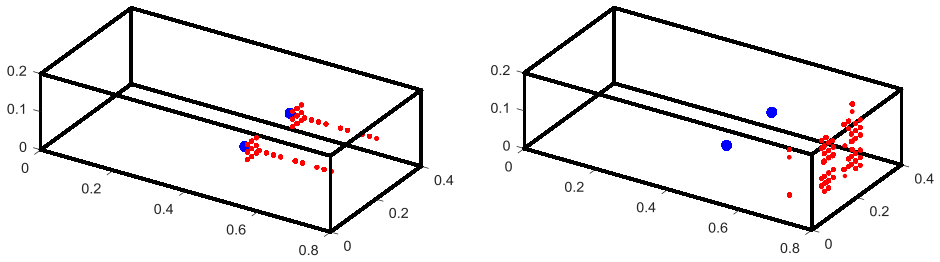

Figure 4.8: (a): 100 sets of experiments with the best condition number of matrix $[V]$; (b): 100 sets of experiments leading to the best identification $[Z_{i\leftarrow j}^{A\,Id}]$ according to the criterion of mean quadratic error. The corresponding sources position—S_1 and S_2—are depicted in red, the center of the patches of subsystem A are depicted in blue.

The numerical details concerning the best 100 *sets of experiments* are provided in Table 4.12.

Table 4.12: Numerical properties of the 100 best sets of experiments according to the criterion condition number or mean quadratic error. Both criteria are evaluated independently from each other on the frequency range 10–1,000 Hz.

100 best sets of experiments according to:	Condition number	Mean quadratic error
Condition number (Range)	[1.05; 2.07]	[10.14; 13.44]
Mean quadratic error (Range)	[2.41e + 06; 2.65e + 06]	[4.53e + 04; 4.55e + 04]

The observation confirms the tendency identified with the 10 best *sets of experiments*.

4.4.3 Summary

The two questions proposed in the introduction of Sec. 4.4 have been addressed. Some *sets of experiments* are more appropriate than others for the identification of the subsystem A and it is possible to derive a rule to create an appropriate *set of experiments*. The sources used in the *set of experiments* should be positioned respecting two criteria:

Criterion 1. The sources should be far away from the patches.
Criterion 2. Each source should be far away from any other sources.

The first criterion is the most important one. If not respected, the velocity on the surface of the patches might have a strong dynamic (near field of the source). As the model, which intends to be identified, assumes that the velocity is approached by a constant velocity over the surface of the patches (cf. Eq. 2.24), a mismatch appears between the input data and the data the model is able to describe. The direct problem becomes a mathematical surjection and is therefore not invertible. Criterion 1 makes sure that the problem is a mathematical bijection resulting in a unique inversion.

The second criterion intends to improve the condition number of the matrix $[V]$. When the sources are distant from each other, each experiment of the *set of experiments* tends to be independent from the others. Nevertheless, this independency is limited when the system is dominated by Eigen modes (high reactive system). At each resonance frequency, the condition number is necessarily degraded. A solution would be to place the sources close to the patches. Even if the system is dominated by eigenmode, due to the nearfield effect, each experiment would be different. Nevertheless, this solution would break the criterion 1 and should not be practiced.

4.5 Instability to measurement noise

The inverse identification method exposed in Chap. 3 has been applied on a numerical experiment. The required input data—matrices $[P]$ and $[V]$ —have been *virtually measured* and thus with a very low uncertainty level. As a result, the unknown condensed impedance matrix has been very close to the reference. Yet in practice, the input data intend to be obtained by means of experiments. Due to many unwanted complex physical phenomena in the measurement setup, a measured physical quantity does not perfectly match the real physical quantity. In the field of signal processing, the result of most of the undesired disturbances is called noise.

Modern equipment—i.e. laboratory, sensors, frontend etc.—are designed to minimize the presence of noise in the measurement. Therefore, a measured quantity should be really close to the physical one. Nevertheless, as many inverse problem are *per se* highly sensitive

to small variations in the input data, the presence of noise might result in many complications. It is the reason why the influence of noise is discussed here.

In the practice, the level of this noise is compared to the level of the measured signal. If both are expressed in decibels, the level difference is the so-called Signal-to-Noise Ratio (SNR). The signal-to-noise ratio should be as high as possible. In order to improve the SNR, the background noise level should be reduced or the measured signal should be increased. Better equipment allows to improve the SNR by both means. In the current state of the art [75], the SNR value might be subjectively appreciated as following: less than 9 dB poor; 10–19 dB fair; 20–29 dB good; 30–39 dB excellent.

As the noise in a measurement system is dependent from the acquisition system, no universal solution exists in order to introduce a representative virtual noise into perfect simulations. Therefore, the details of the introduction of noise will be addressed first. The effect of noise is first discussed from the side of the input data—effect on matrices $[P]$ and $[V]$. Secondly, the effect on the output data—condensed impedance matrix $[Z]$—is addressed.

4.5.1 Introduction of noise on the input data

In this section, two kinds of noises are virtually introduced into the noise-free simulated measurement:

Additive noise. Result of external factors such as a non-perfectly silent measurement laboratory or due to internal factor such as electrical noise in the measurement system itself. This noise is independent from the level of the measured signal.
Multiplicative noise. It represents a calibration uncertainty. In this case, the error depends on the measured value. Indeed the absolute error is higher for a large signal as than for a low signal.

Technically, the noise is introduced to the noise-free matrices $[P]$ and $[V]$ resulting in $[\tilde{P}]$ and $[\tilde{V}]$. As each column of the matrices $[P]$ and $[V]$ represents the result of a different experiment n (vector $\{P_i^C\}_n$ and $\{V_j^C\}_n$), the noise is introduced separately on these vectors and for each *experiment*. The noise is introduced to each vector in a way similar to the one encountered in the paper of Q. Leclère [75]. The noisy vectors $\{\tilde{P}_i^C\}_n$ is computed using additive and multiplicative noises. The expression of the ith value is given by Eq. 4.3.

$$\tilde{P}_i^C{}_n = P_i^C{}_n + 10^{-\frac{SNR}{20}} \left(\alpha e^{i\theta} P_i^C{}_n + \beta e^{i\phi} . Median\left(\sqrt{\left\| \{P_i^C\}_n \right\|} \right) \right) \tag{4.3}$$

α and β are two zero-mean Gaussian random variables with a unit variance, θ and ϕ are two random variables uniformly distributed between 0 and 2π. The noisy velocity vector $\left\{ \widetilde{(V_j^C)} \right\}_n$ is computed using Eq. 4.4.

$$\tilde{V}_j^C{}_n = V_j^C{}_n + 10^{-\frac{SNR'}{20}} \left(\alpha' e^{i\theta'} V_i^C{}_n + \beta' e^{i\phi'} . Median\left(\sqrt{\left\| \{V_j^C\}_n \right\|} \right) \right) \tag{4.4}$$

Eq. 4.3 and Eq. 4.4 are mathematically the same. Nevertheless, they are repeated here to highlight their independency. Indeed, each random parameter α, β, θ, and ϕ is uncorrelated in comparison to α', β', θ', and ϕ'.

4.5.2 Effect on the input data

The effect of the noise is first presented from the side of the input data. A graphical representation of noise, with a SNR of 20 dB is presented in Figure 4.9. This figure matches Figure 3.9 of the reference analysis presented in Sec. 3.3.2. A noise is added to the perfect noise-free simulated data according to the previous procedure. To differentiate the effect of the additive and the multiplicative noise, each compound is presented separately.

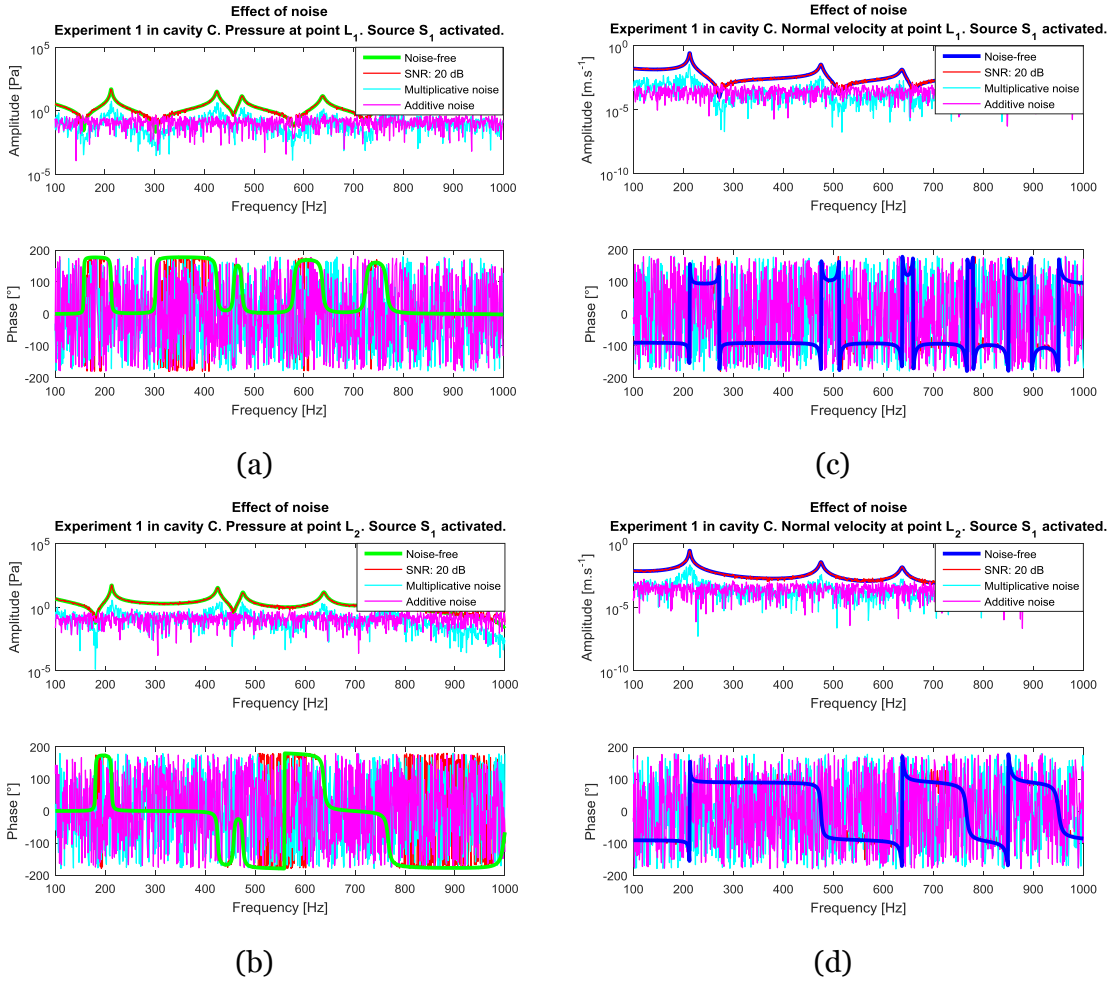

Figure 4.9: Effect of a noise of SNR 20 dB on the noise-free simulated data of the first experiment in the coupled cavity C—cf. Figure 3.9. (a) and (b) are representing the noise-free pressure vector $\{P_i^C\}_1$ (green) and the noisy vector $\{\tilde{P}_i^C\}_1$ (red). (c) and (d) are representing the noise-free velocity vector $\{V_j^C\}_1$ (blue) and the noisy vector $\{\tilde{V}_j^C\}_1$ (red). For each component of both vectors, both component of the noise is represented: additive noise (magenta), multiplicative noise (cyan).

4.5.3 Effect on the output data

In this section, the effect of an increasing noise—i.e. decreasing SNR—is addressed. The analysis is carried out according to the following pattern:

- Noise of a given SNR is added to the noise-free matrices $[P]$ and $[V]$ resulting in two noisy-matrices $[\tilde{P}]$ and $[\tilde{V}]$.
- The matrix $[\tilde{V}]$ is analyzed with the condition number metrics.
- Inversion using the formulation $\left[\tilde{Z}_{i\leftarrow j}^{A\ Id}\right] = [\tilde{P}][\tilde{V}]^{-1}$.

- The identified matrix $\left[\tilde{Z}_{i\leftarrow j}^{A\,Id}\right]$ is compared to the reference $\left[Z_{i\leftarrow j}^{A\,Ref}\right]$ by means of the quadratic error metrics.

The two metrics introduced in Sec. 4.2 are used in both formulations: "*frequency range*" and "*per spectral line*". The first one is a global indicator whereas the second provides more insight. Note that due to the inherent random aspect of a noise, the matrices$[\tilde{P}]$, $[\tilde{V}]$ and the resulting matrix $\left[\tilde{Z}_{i\leftarrow j}^{A\,Id}\right]$ are, for each simulation, slightly different. Therefore, the following analysis is treating the general tendency rather than small details—that might changes from one to the other simulation.

Condition number metrics

The introduction of noise in the velocity matrix $[V]$ as an influence on the condition number of $[\tilde{V}]$ as shown in Figure 4.10. When the noise decreases—SNR value grows—the condition number converges, as expected, on the value 17.10 (Table 4.8). When the noise increases—SNR value drops—the condition number decreases. This observation is at a first glance counter intuitive, and the "*frequency range*" version of the condition number metrics does not provide any further explanation.

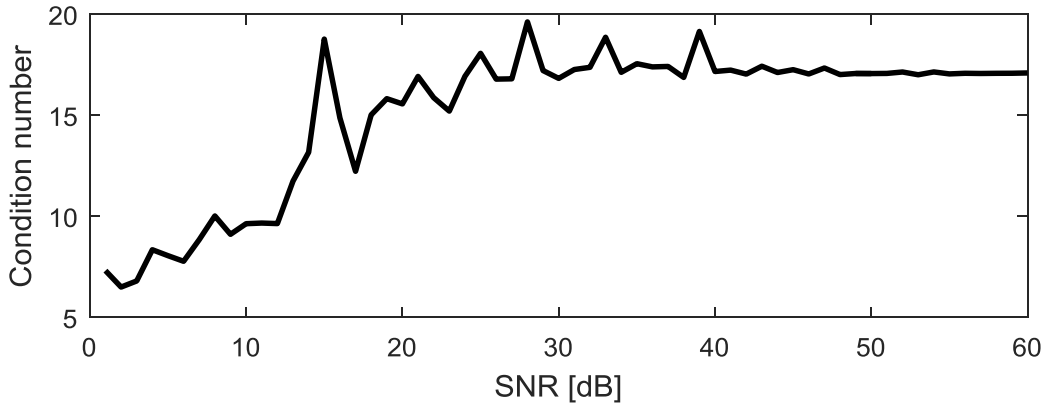

Figure 4.10: Effect of noise of a growing SNR on the condition number of matrix $[\tilde{V}]$.

The results of the "*per spectral line*" version of the condition number metrics of $[\tilde{V}]$are presented in Figure 4.11. For a low level of noise—e.g. SNR equal to 60 dB—the variation of the color along the x-axis matches the variation of the black dotted line in Figure 4.3. The pendant of the 14 local maxima is the presence of 14 stripes centered at the same frequencies. For a growing value of noise, the stripes are becoming blurred and thus the global indicator presented in Figure 4.10 is decreasing.

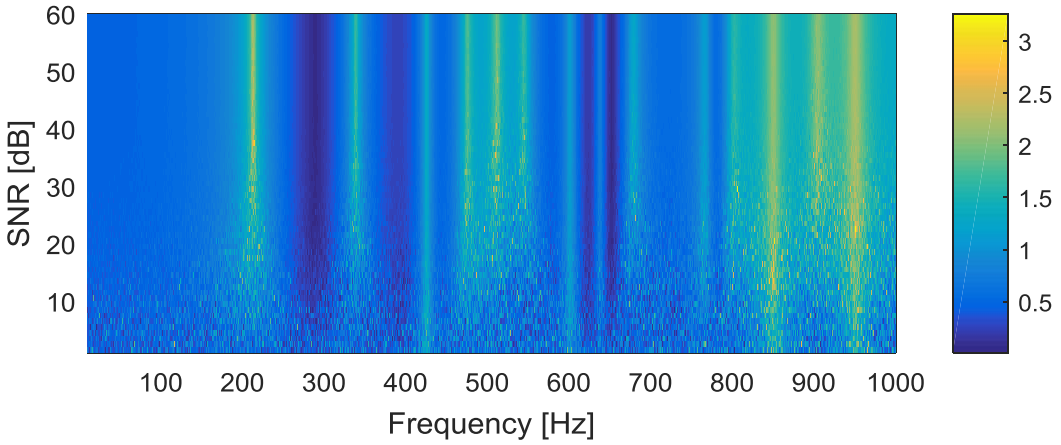

Figure 4.11: Color representation of the value of the condition number of the matrix $[\tilde{V}]$ for a given frequency (x-axis) and a given SNR (y-axis). The value are depicted with a log-scale. 14 stripes are observed centered on the frequencies: 212; 338; 425; 475; 511; 544; 601; 637; 679; 766; 803; 850; 904; 950 Hz. The stripes are sharp for low level of noise—i.e. high value of SNR—and become blurred for the higher level of noise.

In Sec. 4.3.3 a correlation has been observed between the 14 maxima of the condition number and the resonance of one of the subsystem A, B or C. The phenomenon might be interpreted as following: at the resonance frequency of any of the subsystem the velocity measured with the first experiment $\{V_j^C\}_1$ and the second experiment $\{V_j^C\}_2$ is dominated by the concerned eigenmode, and are thus, not independent from each other. It introduces an interdependency between both lines of the matrix $[V]$. As the noise increases, a virtual degree of independency is added between both vectors $\{\tilde{V}_j^C\}_1$ and $\{\tilde{V}_j^C\}_2$. As a result the condition number of $[\tilde{V}]$ decreases—i.e. each stripe becomes blurred.

Mean quadratic error metrics

The introduction of noise on both matrices $[P]$ and $[V]$ has an impact on the identified impedance matrix noted $\left[\tilde{Z}_{i\leftarrow j}^{A\,Id}\right]$. Figure 4.12 points out the degradation of the results when the noise level is increasing. In other words, the improvement of the condition of $[\tilde{V}]$ in the presence of an increasing noise does not end with a better identification of the impedance matrix.

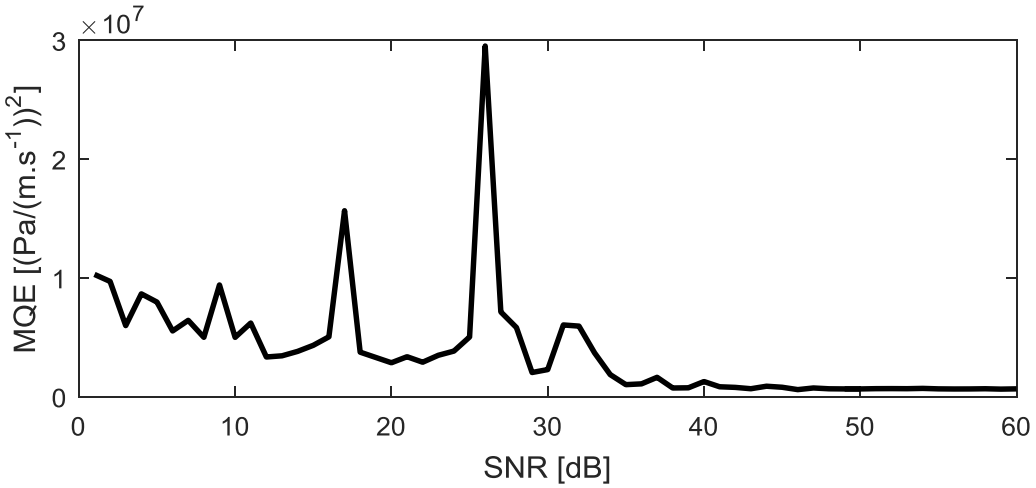

Figure 4.12: Effect of a noise of growing SNR on the identification of the impedance matrix $[\tilde{Z}_{i\leftarrow j}^{A\,Id}]$. *The indicator mean quadratic error (MQE) between* $[\tilde{Z}_{i\leftarrow j}^{A\,Id}]$ *and* $\left[Z_{i\leftarrow j}^{A\,Ref}\right]$ *is computed over the full frequency range 10–1,000 Hz—"frequency range" version.*

This curve shows a high sensitivity of the method to the presence of noise. First, the high dynamic for the *SNR* going from 0 up to 40 dB reveals that for comparable level of noise, depending on the inherent random aspect of the noise, the identification might be dramatically impacted. Second, the final convergence on the value 6.45e + 05 is reached for *SNR* value higher than 40 dB which is almost impossible to achieve with an experimental setup.

Figure 4.13 displays the "*per spectral line*" form of the mean quadratic error between $[\tilde{Z}_{i\leftarrow j}^{A\,Id}]$ and $\left[Z_{i\leftarrow j}^{A\,Ref}\right]$. For a low level of noise—e.g. *SNR* equal to 60 dB—the changes of color along the x-axis counterpart the evolution of the blue solid line of Figure 4.3. The pendant of the 7 local maxima occurs in 7 strips centered at the same frequencies. The growing value of noise, does not blur the stripes—as it was the case for the condition number of $[\tilde{V}]$—worse, the presence of noise has the tendency to increase the width of each stripe. Finally, it introduces new identification error where the identification was almost perfect without noise.

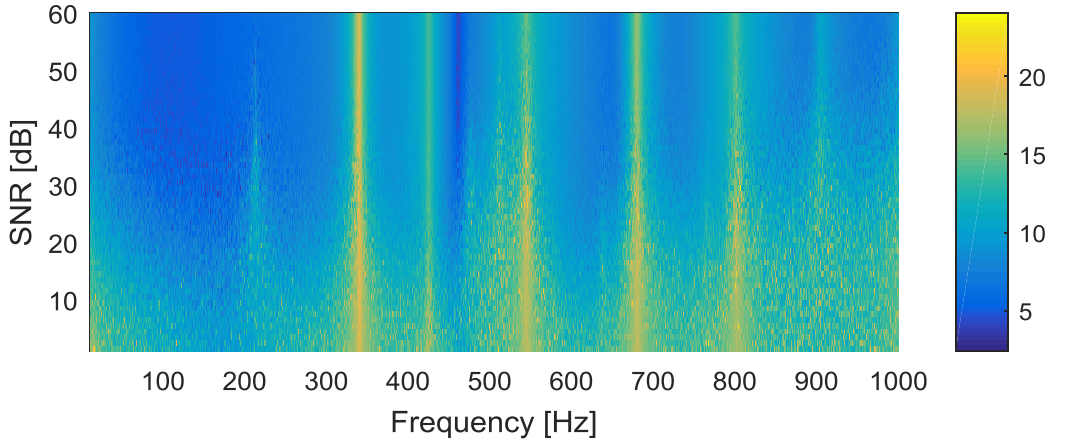

Figure 4.13: Color representation of the value of the mean quadratic error between the matrices $[\tilde{Z}_{i\leftarrow j}^{A\,Id}]$ *and* $\left[Z_{i\leftarrow j}^{A\,Ref}\right]$ *for a given frequency (x-axis) and a given SNR (y-axis). The values are shown on a log scale. 7 stripes are observed at the frequencies: 339; 425; 511; 544; 679; 801; 905 Hz. The stripes are getting wider with the noise increases.*

This analysis provides another example of the low correlation between the two metrics. The addition of noise in the noise-free velocity matrix improves its condition number. Nevertheless, the identification of the impedance matrix is degraded. At this stage of development, the method would not succeed in the identification of the impedance matrix of a subsystem by means of experiments. Indeed its sensitivity to noise is too significant in comparison with the state of the art of measuring equipments.

4.6 Summary

The original method, presented in the third chapter, has been validated from a theoretical point of view. Some numerical experiments have proven that it also works in practice within ideal conditions. Indeed the method has been able to characterize the impedance of a fully coupled system. The characterization was good enough to predict the pressure at a given listening point once the system has been coupled again to another system.

The fourth chapter has intended to find the limit of this method. Some metrics has been exposed in order to quantify the quality of the results. Thanks to these metrics, it has been possible to observe how unstable the method is. Indeed, as soon as the experimental conditions—i.e. numerically simulated—have been slightly degraded the results quality has been drastically affected. Changing the position of the source necessary to the characterization, as well as the introduction of simulated noise, has resulted in numerical instabilities.

The instability to the position of the sources used in the experimental setup should be overcome if two rules are respected. Nevertheless, as no *a priori* indicator—generally the condition number—which would detect a poor experimental setup has been identified, this method may fail using real experiments. Some solutions might be found to overcome this problem.

5 Advanced strategies

"What was once the furthest outpost on the old frontier of the West will be the furthest outpost on the new frontier of science and space."

John Fitzgerald Kennedy (1917–1963) in "Address at Rice University in Houston on the Nation's Space Effort", 1962 [1].

Chapter contents:

5.1 Introduction 103

5.2 Statistical identification 104

5.2.1 Concept 104

5.2.2 Statistical indicator mean and median 105

5.3 Statistical stability: set of experiments 107

5.3.1 Problem statement 107

5.3.2 Result analysis without statistical post-processing 109

5.3.3 Statistical identification 112

5.3.4 Extended analysis of statistical stability 116

5.4 Statistical stability: addition of noise 118

5.4.1 Regularization by means of noise 118

5.4.2 Statistical stability: Noisy sets of experiments 121

5.5 Summary 123

5.1 Introduction

Chap. 4 has pointed out restrictions of the original inverse experimental method presented in Chap. 3. The method, allowing characterization of a strongly coupled subsystem, relies on a single *set of experiments* composed of N experiments and a formulation of the form "$[Z] = [P][V]^{-1}$"—where both matrices are of size $(N;N)$. Unfortunately, the method is sensitive to the nature of the *set of experiments*: position of the N required sources or presence of noise in the measurement. The first drawback is partially solved observing two rules for the constitution of a correct *set of experiments*. Yet the second weakness—noise in the measurement resulting in $[\tilde{P}]$ and $[\tilde{V}]$—remains. As a consequence, without advanced strategy, the result of this method should not be trusted.

These phenomena are well-known weaknesses of inverse methods, therefore many advanced methods have already been developed [76]. The Tikhonov method and the truncated singular value decomposition are the most common regularization method [77] [78]. Both methods are relying on the correct estimation of a regularization parameter. The most popular method for the determination of the value of the regularization

parameter are: the ordinary cross validation; the generalized cross validation and the L-curve. Depending on the problem one of these methods might be more appropriated to find an optimal regularization parameter [79] [80].

Yet in this dissertation, a very different approach is proposed. No regularization method will be used. This choice includes pros and cons, but it definitively supports the scientific originality of this dissertation. The concept of a statistical method is presented first. Secondly, the statistical method is used to overcome both instabilities presented in Sec. 4.4 and Sec. 4.5, which may turn into a statistical stability.

5.2 Statistical identification

5.2.1 Concept

The method proposed in this chapter relies in some measure in the use of partial information contained in the results provided by a *set of experiments*. A different *set of experiments*—sources positions or presence of noise—results in a different identification of $[Z^{Id}]$ (better or worse), but still contains a partial physical signification. If a total $TSoe$ of *sets of experiments* are created, each one containing a partial physical reality, the reality might be recovered with statistical indicators (Table 5.1). The set containing the $TSoe$ *sets of experiments* is called: "*Set of sets of experiments*".

Table 5.1: Concept of the statistical method. A set of sets of experiments is used as an input. It contains itself, TSoe sets of experiments numerated Soe from 1 to TSoe. Each set of experiments allows, with the proposed inverse method, to identify the researched impedance matrix $[Z^{Id}]_{Soe}$. Unfortunately, each identified matrix slightly differs than the physical one—i.e. $[Z^{Id}]_{Soe} \neq [Z^{Ref}]$. Nevertheless, each identification should contain at least a partial physical signification. With a statistical treatment, based on these TSoe identifications, a single matrix $[Z^{Id}]^{Stat}$ is computed. If the procedure is working properly, the identified impedance matrix should have a physical signification—i.e. $[Z^{Id}]^{Stat} \approx [Z^{Ref}]$.

	Set of *sets of experiments*					
Set of experiments	1	2	...	Soe	...	$TSoe$
Measurement	$[P]_1; [V]_1$	$[P]_2; [V]_2$	...	$[P]_{Soe}; [V]_{Soe}$	...	$[P]_{TSoe}; [V]_{TSoe}$
Inversion	$[Z^{Id}]_1$	$[Z^{Id}]_2$	...	$[Z^{Id}]_{Soe}$	...	$[Z^{Id}]_{TSoe}$
Statistics	$[Z^{Id}]^{Stat}$					

Two possibilities will be investigated to create several *sets of experiments* called *set of sets of experiments*:

> *Roving source.* One, some, or all the N sources positions necessary for a single *set of experiments*, move to another positions. It result in a partially or complete new *set of experiments* (See. Sec 5.3).
> *Addition of noise.* A virtual noise is added on top of the physical measurements—which may already contain a noise. The matrices $[P]$ and $[V]$ are transformed into matrices $[\tilde{P}]$ and $[\tilde{V}]$. As a noise has an inherent random characteristic the operation might be repeated several times (See. Sec. 5.4.1).

Another solution is to combine both principles (Sec. 5.4.2). Along this chapter, two basic statistical indicators—*mean* and *median*—and their utilization are presented. After that, they are tested on both instabilities encountered in Chap. 4.

“Experimental setup”; “Experiment”; “Set of experiments”; “Set of sets of experiments”.

The words “*experiment*” and “*set*” appear in many word combinations along this dissertation. In Chap. 5 the complex constellation “*set of sets of experiments”* has been introduced. This note intends to remind the definitions of all these combinations:

Experimental setup. Coupled system, including the subsystem under characterization with the instrumentation—sources, PU-Probe or microphone and accelerometer. If the system under characterization has N paches, N measuring points are necessary, and a minimum of N source is necessary (See. Figure 3.4). Yet the words “*Experimental setup*” is independent of the number of sources—number of sources is Ns.

Experiment. The source is acting at a given position, the coupled pressure and velocity on the N patches is stored in two vectors $\{P_i^C\}_e$ and $\{V_j^C\}_e$ —the index e stands for “experiment”.

Set of experiments. The method proposed in Chap. 3 requires N *experiments*—index e from 1 to N. The result of such a *set of experiments* are stored in two matrices $[P]_{Soe}$ and $[V]_{Soe}$ of size $(N;N)$—the index Soe stands for “*Set of experiments*”. Mathematically the *set of experiments* of index Soe reads $\left\{\left\{\{P_i^C\}_1;\{V_j^C\}_1\right\},\left\{\{P_i^C\}_2;\{V_j^C\}_2\right\},\dots,\left\{\{P_i^C\}_e;\{V_j^C\}_e\right\},\dots,\left\{\{P_i^C\}_N;\{V_j^C\}_N\right\}\right\}_{Soe}$ where all information are organized in two matrices $[P]_{Soe}$ and $[V]_{Soe}$. One *set of experiments* allows one and only one identification of matrix $[Z^{Id}]_{Soe}$—indexed by Soe.

Set of sets of experiments. If a total number of *sets of experiments* $TSoe$ is available, each *set of experiments* indexed Soe is stored in one set called “*Set of sets of experiments*”. Mathematically this *set of sets of experiments* reads $\{\{[P]_1;[V]_1\},\{[P]_2;[V]_2\},\dots,\{[P]_{Soe};[V]_{Soe}\},\dots,\{[P]_{TSoe};[V]_{TSoe}\}\}$ it results in a set of identified impedance matrices $\{[Z^{Id}]_1,[Z^{Id}]_2,\dots,[Z^{Id}]_{Soe},\dots,[Z^{Id}]_{TSoe}\}$. Applied on this set, the statistical method calculates one and only one impedance matrix $[Z^{Id}]_{SoSoe}^{Stat}$ —it is considered that the statistical method uses all the members of the set.

Any *set of experiments* presented in this dissertation is composed of exactly N *experiments*. As N is the number of patches, the matrices $[P]$ and $[V]$ are always square—size $(N;N)$.

5.2.2 Statistical indicator mean and median

In this section, it is assumed that a set of impedance matrices $\{[Z^{Id}]_1,[Z^{Id}]_2,\dots,[Z^{Id}]_{Soe},\dots,[Z^{Id}]_{TSoe}\}$ has been computed. Using an appropriate statistical indicator, the underlying physical signification should be acquired. The impedance matrix identified with the proposed statistical method is denoted $[Z^{Id}]^{Stat}$. This section exposes two indicators, the *mean* and the *median*.

For both indicators, the identification of matrix $[Z^{Id}]^{Stat}$ at a given frequency is made using the set of impedance matrices $\{[Z^{Id}]_1,[Z^{Id}]_2,\dots,[Z^{Id}]_{Soe},\dots,[Z^{Id}]_{TSoe}\}$. Actually, there is one matrix per spectral line. As it is the case for all matrices and vectors in this dissertation, the frequency dependency ω is not repeated with a dedicated mathematical notation.

Mean

Each complex element $\left(Z_{i\leftarrow j}^{Id}\right)^{Mean}$—line i and column j of matrix $[Z^{Id}]^{Mean}$—is computed according to Eq. 5.1:

$$\left(Z_{i\leftarrow j}^{Id}\right)^{Mean} = \frac{\left(Z_{i\leftarrow j}^{Id}\right)_1 + \left(Z_{i\leftarrow j}^{Id}\right)_2 + \cdots + \left(Z_{i\leftarrow j}^{Id}\right)_{Soe} + \cdots + \left(Z_{i\leftarrow j}^{Id}\right)_{TSoe}}{TSoe} \tag{5.1}$$

In this case, the subscript "$Stat$" is replaced by "$Mean$". This notation emphasis that in this case, the chosen statistical indicator is a conventional complex mean—$Mean$: $\mathbb{C}^{TSoe} \mapsto \mathbb{C}$.

Median

The median may be seen as the mathematical pendant of the German proverb *"Die Wahrheit liegt in der Mitte"—"The truth lies in the middle"*. Indeed, for a sorted set of real numbers, the median is the value separating the higher half of the data from the lower half. Depending on the cardinality[15]—even or odd—the median is computed differently:

> *Odd cardinality*. The median returns the central value of the sorted set—e.g. $Median(\{-1.3, 1.6, 2.4\}) = 1.6$.
> *Even cardinality*. The median returns the mean of the two central values of the sorted set—e.g. $Median(\{-1.3, 1.6,\ 2.4, 3.1\}) = Mean(\{1.6, 2.4\}) = 2.0$.

As the median is defined only for a set of real numbers, two steps are necessary to apply it to a set of complex numbers. Many definitions would be admissible, yet in this dissertation, the median of a set of complex numbers is defined according to Eq. (5.2), Eq. (5.3) and Eq. (5.5).

The complex element $\left(Z_{i\leftarrow j}^{Id}\right)^{Median}$ —line i and column j of matrix $[Z^{Id}]^{Median}$ —is computed in two independent steps: calculation of the modulus and calculation of the phase. The modulus is computed using Eq. (5.2):

$$\left(\left\|Z_{i\leftarrow j}^{Id}\right\|\right)^{Median} = Median\left\{\left(\left\|Z_{i\leftarrow j}^{Id}\right\|\right)_1, \left(\left\|Z_{i\leftarrow j}^{Id}\right\|\right)_2, \dots, \left(\left\|Z_{i\leftarrow j}^{Id}\right\|\right)_{Soe}, \dots, \left(\left\|Z_{i\leftarrow j}^{Id}\right\|\right)_{TSoe}\right\} \tag{5.2}$$

The phase is obtained separately using Eq. (5.3):

$$\begin{aligned}&\left(\phi\left(Z_{i\leftarrow j}^{Id}\right)\right)^{Median}\\ &= Median\left\{\phi\left(\left(Z_{i\leftarrow j}^{Id}\right)_1\right), \phi\left(\left(Z_{i\leftarrow j}^{Id}\right)_2\right), \dots, \phi\left(\left(Z_{i\leftarrow j}^{Id}\right)_{Soe}\right), \dots, \phi\left(\left(Z_{i\leftarrow j}^{Id}\right)_{TSoe}\right)\right\}\end{aligned} \tag{5.3}$$

where the phase $\phi\left(\left(Z_{i\leftarrow j}^{Id}\right)_{Soe}\right)$ is computed with Eq. (5.4):

$$\phi\left(\left(Z_{i\leftarrow j}^{Id}\right)_{Soe}\right) = \operatorname{atan}\left(\frac{\Im\left(Z_{i\leftarrow j}^{Id}\right)_{Soe}}{\Re\left(Z_{i\leftarrow j}^{Id}\right)_{Soe}}\right) \tag{5.4}$$

Finally, each complex element $\left(Z_{i\leftarrow j}^{Id}\right)^{Median}$ is computed using Eq. (5.5):

[15] Cardinality stands for "number of elements in the set".

$$\left(Z_{i\leftarrow j}^{Id}\right)^{Median} = \left(\left\|Z_{i\leftarrow j}^{Id}\right\|\right)^{Median} \cdot \left(\cos\left(\phi\left(Z_{i\leftarrow j}^{Id}\right)\right)^{Median} + i\sin\left(\phi\left(Z_{i\leftarrow j}^{Id}\right)\right)^{Median}\right) \quad (5.5)$$

In this case, the subscript "$Stat$" becomes "$Median$". This notation emphasis that in this case, the chosen statistical indicator is the median[16] with $Median: \mathbb{C}^{TSoe} \mapsto \mathbb{C}$.

Mean vs Median

The statistical indicator *mean* and *median* are much more different than they appear. The mean of a set of elements is affected by each element of the set. As a result, if the set contains an outsider value (very large or very small in comparison to the others) the result might be drastically affected. On the opposite, the median of a set of elements is generally not impacted by an outsider value.

5.3 Statistical stability: set of experiments

In this section, the principle of using a roving source to create several *sets of experiments* called *set of sets of experiments* is investigated. The initially proposed characterization method requires exactly N experiments—i.e. N source positions corresponding to the number of patches. If instead Ns source positions are used with $Ns \geq N$, many *sets of experiments* can be created (Eq. (4.2)). This section is the pendant of Sec. 4.4 where the instability to the set of experiments turn into a statistical stability.

5.3.1 Problem statement

The theory exposed in this chapter is directly applied to the two patches cavity C presented in Sec. 3.3.2. For the needs of the statistical identification of the impedance matrix $\left[Z_{i\leftarrow j}^{A}\right]$, Ns sources are required. As an arbitrary choice, 6 sources are used. Each source is placed at random position on the right side of cavity C. Two sets of 6 sources are analyzed Figure 5.1 and will be used in the following two *set of sets of experiments* to illustrate the difference between *mean* and *median*.

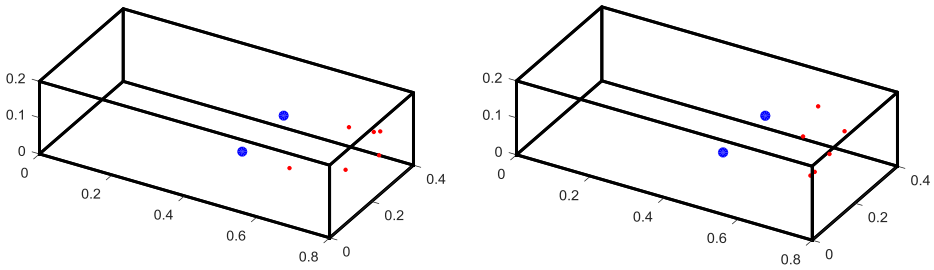

Figure 5.1: Illustration of two chosen experimental setups for the identification of the impedance matrix $\left[Z_{i\leftarrow j}^{A}\right]$ of the sub-cavity A—left side of the coupled cavity C—by means of a statistical inverse method. The number of patches N is 2 and the number of sources Ns has been arbitrarily chosen as being 6. The position of the sources (red points), in the right side of cavity C has been defined by a random process. (a): Experimental setup 1 with the sources used to create the set of sets of experiments 1; (b): Experimental setup 2 with the sources used to create the set of sets of experiments 2.

The position of each source is provided in Table 5.2.

[16] The median is not defined for a set of complex number. The word *median* in this dissertation systematically refers to the definition presented here. Other definitions might be acceptable yet not reported in this dissertation.

Table 5.2: Coordinate of the 6 sources of the experimental setup 1 and 2, expressed in the global axis of box C. The other properties are unchanged and presented in Table 3.1.

	Source	Coordinate		Source	Coordinate
Experimental setup 1	S_1	(0.76; 0.28; 0.14)	Experimental setup 2	S_1	(0.62; 0.34; 0.14)
	S_2	(0.74; 0.34; 0.04)		S_2	(0.68; 0.36; 0.08)
	S_3	(0.72; 0.38; 0.08)		S_3	(0.72; 0.22; 0.10)
	S_4	(0.74; 0.18; 0.08)		S_4	(0.68; 0.20; 0.04)
	S_5	(0.62; 0.12; 0.08)		S_5	(0.66; 0.20; 0.14)
	S_6	(0.68; 0.30; 0.12)		S_6	(0.68; 0.22; 0.04)

Each proposed simulated experimental setup allows to construct several sets of experiments—stored in a single "*set of sets of experiments*". In this case, the number of combinations of 2 sources in a set of 6 sources, is 15 Eq. (4.2). The constitution of both sets of sets of experiments is provided in Table 5.3.

Table 5.3: Constitution of the two sets of sets of experiments.

	Set of experiments	Used Sources		Set of experiments	Used Sources
Set of sets of experiments 1	01	$(S_1; S_2)$	Set of sets of experiments 2	01	$(S_1; S_2)$
	02	$(S_1; S_3)$		02	$(S_1; S_3)$
	03	$(S_1; S_4)$		03	$(S_1; S_4)$
	04	$(S_1; S_5)$		04	$(S_1; S_5)$
	05	$(S_1; S_6)$		05	$(S_1; S_6)$
	06	$(S_2; S_3)$		06	$(S_2; S_3)$
	07	$(S_2; S_4)$		07	$(S_2; S_4)$
	08	$(S_2; S_5)$		08	$(S_2; S_5)$
	09	$(S_2; S_6)$		09	$(S_2; S_6)$
	10	$(S_3; S_4)$		10	$(S_3; S_4)$
	11	$(S_3; S_5)$		11	$(S_3; S_5)$
	12	$(S_3; S_6)$		12	$(S_3; S_6)$
	13	$(S_4; S_5)$		13	$(S_4; S_5)$
	14	$(S_4; S_6)$		14	$(S_4; S_6)$
	15	$(S_5; S_6)$		15	$(S_5; S_6)$

The result of each set of experiments is addressed first, secondly the statistical post-processing is applied and finally the stability of the statistical indicator is addressed.

5.3.2 Result analysis without statistical post-processing

Set of sets of experiments 1

Each set of experiments *Soe*, allows one identification of matrix $\left[Z_{i\leftarrow j}^{A\,Id}\right]$ noted $\left[Z_{i\leftarrow j}^{A\,Id}\right]_{Soe}$, which is compared to the physical researched impedance matrix $\left[Z_{i\leftarrow j}^{A\,Ref}\right]$, by means of the quadratic error metric. The results are presented in Table 5.4.

Table 5.4: Nature and result of each set of experiments forming the set of sets of experiments 1. The sets of experiments are sorted according to the mean quadratic error—descending quality.

	Set of experiments	Results $[P]_{Soe}; [V]_{Soe}$	Identification $\left[Z_{i\leftarrow j}^{A\,Id}\right]_{Soe}$	Mean quadratic error $\left[Z_{i\leftarrow j}^{A\,Id}\right]_{Soe}$ vs $\left[Z_{i\leftarrow j}^{A\,Ref}\right]$
Set of sets of experiments 1	10	$[P]_{10}; [V]_{10}$	$\left[Z_{i\leftarrow j}^{A\,Id}\right]_{10}$	$4.72e+04$
	07	$[P]_{07}; [V]_{07}$	$\left[Z_{i\leftarrow j}^{A\,Id}\right]_{07}$	$4.77e+04$
	03	$[P]_{03}; [V]_{03}$	$\left[Z_{i\leftarrow j}^{A\,Id}\right]_{03}$	$6.19e+04$
	01	$[P]_{01}; [V]_{01}$	$\left[Z_{i\leftarrow j}^{A\,Id}\right]_{01}$	$6.44e+04$
	02	$[P]_{02}; [V]_{02}$	$\left[Z_{i\leftarrow j}^{A\,Id}\right]_{02}$	$8.95e+04$
	06	$[P]_{06}; [V]_{06}$	$\left[Z_{i\leftarrow j}^{A\,Id}\right]_{06}$	$1.37e+05$
	14	$[P]_{14}; [V]_{14}$	$\left[Z_{i\leftarrow j}^{A\,Id}\right]_{14}$	$4.53e+05$
	04	$[P]_{04}; [V]_{04}$	$\left[Z_{i\leftarrow j}^{A\,Id}\right]_{04}$	$1.76e+06$
	05	$[P]_{05}; [V]_{05}$	$\left[Z_{i\leftarrow j}^{A\,Id}\right]_{05}$	$2.11e+06$
	13	$[P]_{13}; [V]_{13}$	$\left[Z_{i\leftarrow j}^{A\,Id}\right]_{13}$	$2.12e+06$
	08	$[P]_{08}; [V]_{08}$	$\left[Z_{i\leftarrow j}^{A\,Id}\right]_{08}$	$2.15e+06$
	11	$[P]_{11}; [V]_{11}$	$\left[Z_{i\leftarrow j}^{A\,Id}\right]_{11}$	$2.33e+06$
	15	$[P]_{15}; [V]_{15}$	$\left[Z_{i\leftarrow j}^{A\,Id}\right]_{15}$	$2.76e+06$
	09	$[P]_{09}; [V]_{09}$	$\left[Z_{i\leftarrow j}^{A\,Id}\right]_{09}$	$3.36e+06$
	12	$[P]_{12}; [V]_{12}$	$\left[Z_{i\leftarrow j}^{A\,Id}\right]_{12}$	$4.81e+08$

The analysis of the results confirms the observations presented in Sec. 4.4. The nature of the set of experiments impacts the identification and without statistical post-processing, each set of experiments *Soe* results in a different identification of matrix $\left[Z_{i\leftarrow j}^{A\,Id}\right]_{Soe}$. The set of experiments 10 leads to the best identification and the number 12 causes the worst identification.

For a better subjective appreciation of the results' quality—non-quality—without statistical post-processing, the best and the worst identification of matrix $\left[Z_{i\leftarrow j}^{A\,Id}\right]$—i.e. set of experiments 10 and 12—are presented in Figure 5.2. The worst identification differs from the reference, while the best identification appears to match the reference almost perfectly.

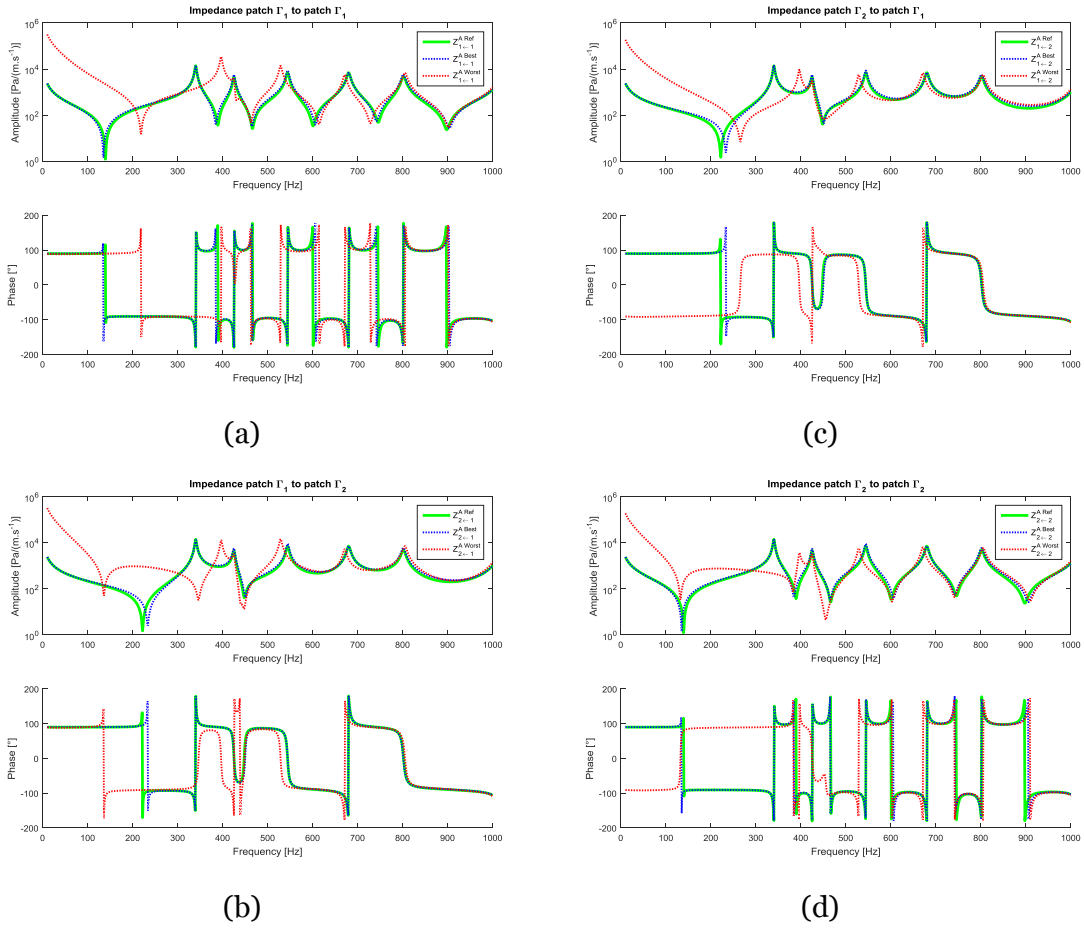

Figure 5.2: Graphical representation of the result of the best and the worst identification of $\left[Z_{i\leftarrow j}^{A\ Id}\right]$ *among the 15 sets of experiments included in the set of sets of experiments 1, compared to the reference* $\left[Z_{i\leftarrow j}^{A\ Ref}\right]$ *(Green solid line). The 10st set of experiments results in the best identification (blue dotted line); the 12th set of experiments caused the worst identification (red dotted line). The graphical position of the curves matches the standard representation of a matrix—i.e. (a):* $Z_{1\leftarrow 1}^{A}$*; (b):* $Z_{2\leftarrow 1}^{A}$*; (c):* $Z_{1\leftarrow 2}^{A}$*; (d):* $Z_{2\leftarrow 2}^{A}$*.*

Set of sets of experiments 2

During an experimental procedure, things might go totally wrong, either for physical or manipulation error. The *set of sets of experiments 2* (Table 5.5) has been retained because it contains such a situation. Indeed the position of the sources S_4 and S_5 involved in the 13th set of experiments violates the second criterion exposed in Sec. 4.4.3: "Each source should be far away from any other sources". As a result, the identification of $\left[Z_{i\leftarrow j}^{A\ Id}\right]_{13}$ is extremely poor. On the opposite, the 6th set of experiments results in the best identification.

Table 5.5: Nature and result of each set of experiments forming the set of set of experiments 2. The sets of experiments are sorted according to the mean quadratic error—descending quality. The mean quadratic error of the 13th tends to infinity.

	Set of experiments	Results $[P]_{Soe}; [V]_{Soe}$	Identification $\left[Z_{i\leftarrow j}^{A\,Id}\right]_{Soe}$	Mean quadratic error $\left[Z_{i\leftarrow j}^{A\,Id}\right]_{Soe}$ vs $\left[Z_{i\leftarrow j}^{A\,Ref}\right]$
Set of sets of experiments 2	06	$[P]_{06}; [V]_{06}$	$\left[Z_{i\leftarrow j}^{A\,Id}\right]_{06}$	$8.53e+04$
	05	$[P]_{05}; [V]_{05}$	$\left[Z_{i\leftarrow j}^{A\,Id}\right]_{05}$	$3.71e+05$
	04	$[P]_{04}; [V]_{04}$	$\left[Z_{i\leftarrow j}^{A\,Id}\right]_{04}$	$4.31e+05$
	02	$[P]_{02}; [V]_{02}$	$\left[Z_{i\leftarrow j}^{A\,Id}\right]_{02}$	$4.56e+05$
	03	$[P]_{03}; [V]_{03}$	$\left[Z_{i\leftarrow j}^{A\,Id}\right]_{03}$	$5.35e+05$
	08	$[P]_{08}; [V]_{08}$	$\left[Z_{i\leftarrow j}^{A\,Id}\right]_{08}$	$5.47e+05$
	07	$[P]_{07}; [V]_{07}$	$\left[Z_{i\leftarrow j}^{A\,Id}\right]_{07}$	$6.63e+05$
	11	$[P]_{11}; [V]_{11}$	$\left[Z_{i\leftarrow j}^{A\,Id}\right]_{11}$	$7.94e+05$
	15	$[P]_{15}; [V]_{15}$	$\left[Z_{i\leftarrow j}^{A\,Id}\right]_{15}$	$8.24e+05$
	09	$[P]_{09}; [V]_{09}$	$\left[Z_{i\leftarrow j}^{A\,Id}\right]_{09}$	$8.82e+05$
	14	$[P]_{14}; [V]_{14}$	$\left[Z_{i\leftarrow j}^{A\,Id}\right]_{14}$	$9.29e+05$
	10	$[P]_{10}; [V]_{10}$	$\left[Z_{i\leftarrow j}^{A\,Id}\right]_{10}$	$9.67e+05$
	01	$[P]_{01}; [V]_{01}$	$\left[Z_{i\leftarrow j}^{A\,Id}\right]_{01}$	$1.16e+06$
	12	$[P]_{12}; [V]_{12}$	$\left[Z_{i\leftarrow j}^{A\,Id}\right]_{12}$	$2.51e+06$
	13	$[P]_{13}; [V]_{13}$	$\left[Z_{i\leftarrow j}^{A\,Id}\right]_{13}$	∞

An attentive comparison of both sets of sets of experiments (1 and 2) highlights that up to a certain limit they are of similar quality. Indeed if the worst set of experiments of both sets—i.e. 12th for the first and 13th for the second—are not considered, the identification of each included set of experiments is comparable:

> *Set of sets of experiments 1*. Without its worst set of experiments 12, the mean quadratic error resulting of its 14 others sets of experiments is in the range $[4.72e+04; 3.36e+06]$.
> *Set of sets of experiments 2*. Without its worst set of experiments 13, the mean quadratic error resulting of its 14 others sets of experiments is in the range $[8.53e+04; 2.51e+06]$.

For a better subjective appreciation of the identification of $\left[Z_{i\leftarrow j}^{A\,Id}\right]_6$ and $\left[Z_{i\leftarrow j}^{A\,Id}\right]_{13}$ both matrix are presented in Figure 5.3. This representation is equivalent to Figure 5.2 applied to the set of sets of experiments 2. The non-quality of the identification resulting from set of experiments 13 is clearly visible. The values seem to follow a random process and are extremely large in comparison to the reality.

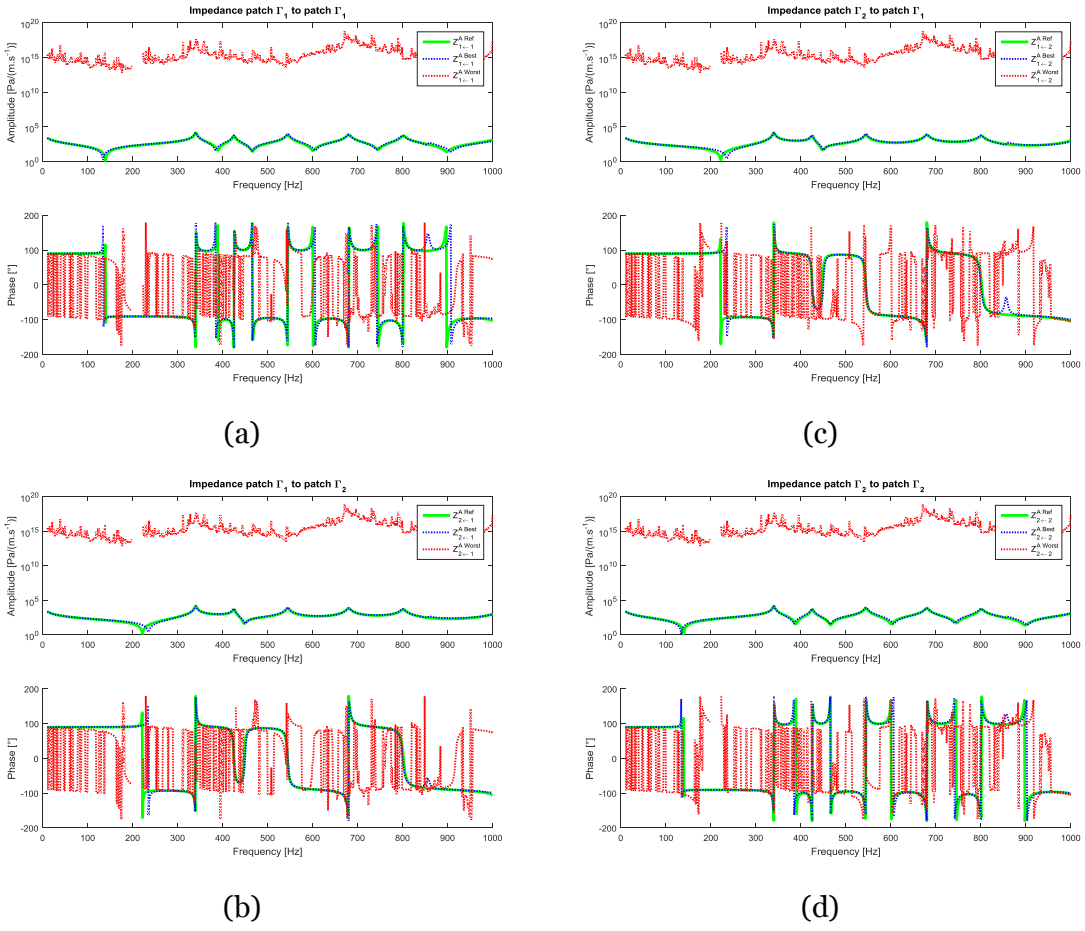

Figure 5.3: Graphical representation of the result of the best and the worst identification of $\left[Z_{i\leftarrow j}^{A\ Id}\right]$ *among the 15 sets of experiments included in the set of sets of experiments 2. Compared to the reference* $\left[Z_{i\leftarrow j}^{A\ Ref}\right]$ *(Green solid line), The 6st set of experiments results in the best identification (blue dotted line); the set of experiments 13th causes the worst identification (red dotted line). The disruption in the curve are due to a numerical limitation in the numerical calculation system—i.e. values are higher than the chosen numerical limit. The graphical position of the curves matches the standard representation of a matrix—i.e. (a):* $Z_{1\leftarrow 1}^{A}$*; (b):* $Z_{2\leftarrow 1}^{A}$*; (c):* $Z_{1\leftarrow 2}^{A}$*; (d):* $Z_{2\leftarrow 2}^{A}$*.*

In this section, two sets of sets of experiments have been created based on two experimental setups with 6 randomly positioned sources. As each set of experiments has been created with random source positions, it does not necessarily respects both criteria proposed in Sec. 4.4.3. As a result, the identification of each set of experiments varies greatly, from an almost perfect identification to a catastrophic identification. Nevertheless, a partial physical reality should be present in each identification.

5.3.3 Statistical identification

This section proposes the application of both statistical indicators—*mean* and *median*—on set of sets of experiments 1 and set of sets of experiments 2 proposed in the previous section. It results in 4 identifications of matrix $[Z^{Id}]_{SoSoe}^{Stat}$—i.e. one per set of sets of experiments *SoSoe* and one per statistical indicator. The focus is to identify which indicator is better appropriate to find the underlying physical reality in a set of sets of experiments.

Set of sets of experiments 1

The quality of the identified matrix $[Z^{A\,Id}]_1^{Mean}$ and $[Z^{A\,Id}]_1^{Median}$ is first analyzed with the global metrics mean quadratic error (Table 5.6). Both statistical estimation are better than the worst identification of the input set, but not as good as the best one. In this example, the median provides a better identification than the mean.

Table 5.6: Mean quadratic error resulting from both statistical identifications—mean and median—applied to the set of sets of experiments 1. The result of the best and worst set of experiments—10th and 12th—provided in Table 5.4 are repeated.

	Mean quadratic error of			
	Input		Output	
	Best set of experiments	Worst set of experiments	Mean	Median
Matrix	$[Z_{i\leftarrow j}^{A\,Id}]_{10}$	$[Z_{i\leftarrow j}^{A\,Id}]_{12}$	$[Z^{A\,Id}]_1^{Mean}$	$[Z^{A\,Id}]_1^{Median}$
Mean quadratic error	$4.72e+04$	$4.81e+08$	$2.45e+06$	$5.66e+05$

For a better subjective appreciation of the results, both matrices $[Z^{A\,Id}]_1^{Mean}$ and $[Z^{A\,Id}]_1^{Median}$ are presented in Figure 5.4. The visual comparison turns into a clear advantage of the estimation by means of the median instead of the mean.

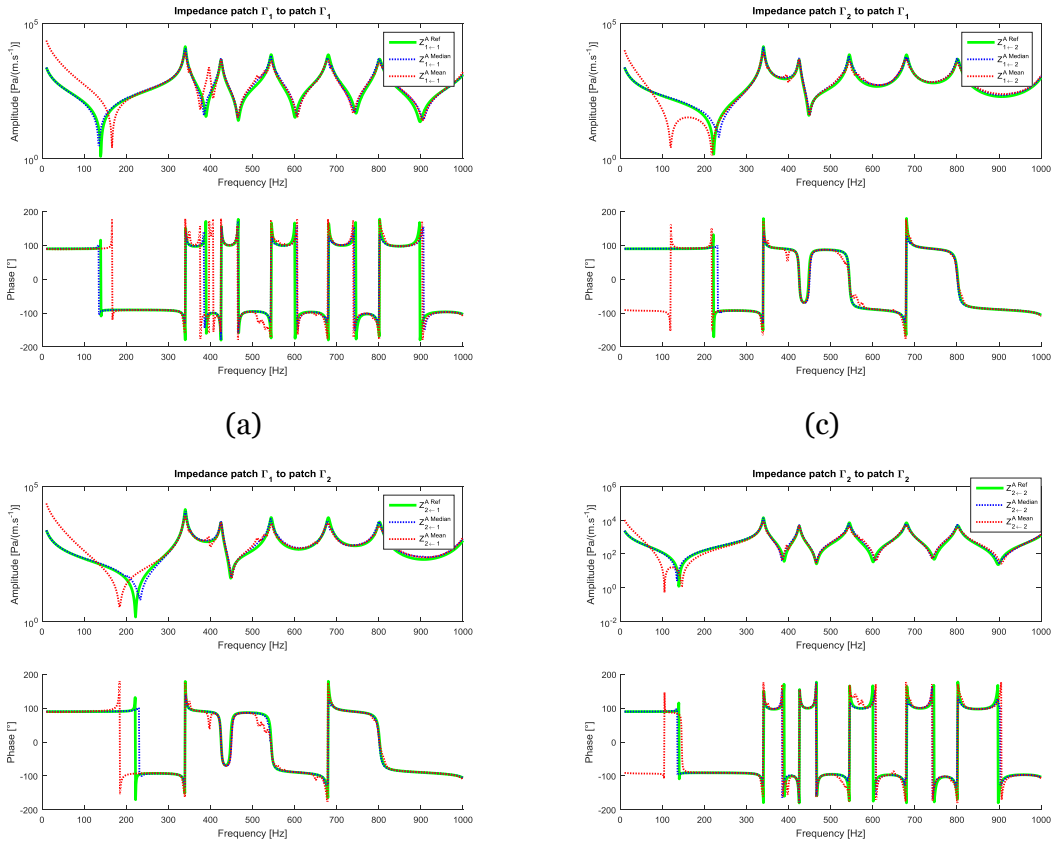

Figure 5.4: Result of the statistical identification using the set of sets of experiments 1: Reference impedance matrix $[Z^{A\,Ref}]$ (Green solid line); Identification by means of the median $[Z^{A\,Id}]_1^{Median}$ (blue dotted line); Identification by means of the mean $[Z^{A\,Id}]_1^{Mean}$ (red dotted line). The graphical position of the curves matches the standard representation of a matrix—i.e. (a): $Z_{1\leftarrow 1}^{A}$; (b): $Z_{2\leftarrow 1}^{A}$; (c): $Z_{1\leftarrow 2}^{A}$; (d): $Z_{2\leftarrow 2}^{A}$.

Set of sets of experiments 2

The quality of the identified matrix $[Z^{A\,Id}]_2^{Mean}$ and $[Z^{A\,Id}]_2^{Median}$ is first analyzed with the global metrics mean quadratic error (Table 5.7). The identification by means of the statistical indicator *mean* does not provide a good identification. On the other hand, the *median* provides a good identification—actually slightly better than the one resulting of set of sets of experiments 1. The identification using the median is also in this case not as good as the best set of experiments—i.e. 6th set of experiments.

Table 5.7: Mean quadratic error resulting from both statistical identifications—mean and median—applied to the set of sets of experiments 2. The result of the best and the worst set of experiments—6th and 13th—provided in Table 5.5 are repeated.

	Mean quadratic error of			
	Input		Output	
	Best set of experiments	Worst set of experiments	Mean	Median
Matrix	$\left[Z_{i\leftarrow j}^{A\,Id}\right]_6$	$\left[Z_{i\leftarrow j}^{A\,Id}\right]_{13}$	$[Z^{A\,Id}]_1^{Mean}$	$[Z^{A\,Id}]_1^{Median}$
Mean quadratic error	8.53e + 04	∞	∞	3.94e + 05

For a better subjective appreciation of the results, both matrices $[Z^{A\,Id}]_2^{Mean}$ and $[Z^{A\,Id}]_2^{Median}$ are presented in Figure 5.5.

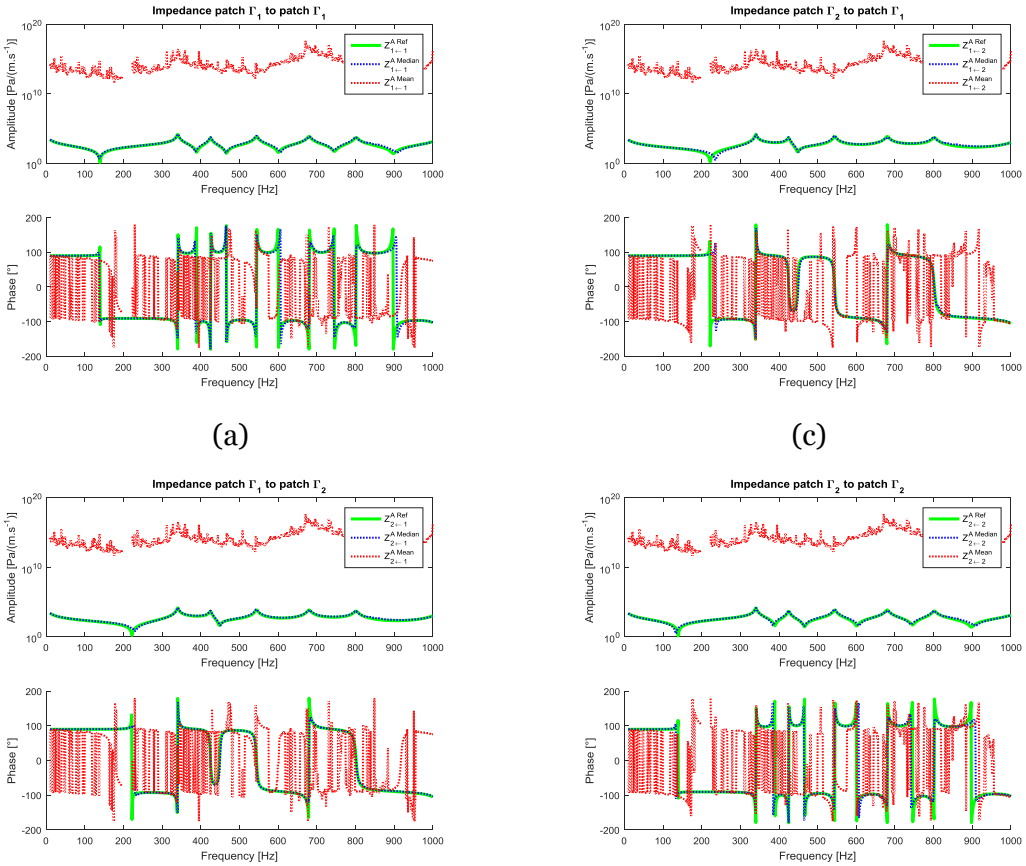

Figure 5.5: Result of the statistical identification using the set of sets of experiments 1: Reference $[Z^{A\,Ref}]$ *(Green solid line); Identification by means of the median* $[Z^{A\,Id}]_2^{Median}$ *(blue dotted line); Identification by means of the mean* $[Z^{A\,Id}]_2^{Mean}$ *(red dotted line). The graphical position of the curves matches the standard representation of a matrix—i.e. (a):* $Z^A_{1\leftarrow1}$*; (b):* $Z^A_{2\leftarrow1}$*; (c):* $Z^A_{1\leftarrow2}$*; (d):* $Z^A_{2\leftarrow2}$*.*

The statistical estimation by means of the statistical indicator *mean* is completely corrupted by the *ill* set of experiments—13th—included in the input. Indeed, the matrix $[Z^{A\,Id}]_2^{Mean}$ is actually really similar to $[Z^{A\,Id}]_{13}$ presented on Figure 5.3. The *mean* is completely driven by the presence of the large values included in set of experiments 13.

On the opposite, the estimation with the *median* does not suffer the presence of the *ill* set of experiments 13. This observation is an occurrence of the observation presented in the note of Sec. 5.2.2. The *median* is *generally* robust faced to outsider values in a set (very large of very small in comparison to the others) while the *mean* is not.

In this section, the statistical identification proposed in Sec. 5.2 has been tested on two sets of sets of experiments. Both sets have been created using all the combination of 6 randomly chosen sources. Yet the set of sets of experiments 2 has been retained for its poor quality—containing a single *ill* set of experiments. The results of both statistical indicators are summarized has following:

> *Mean*. Applied to a wholesome set of sets of experiments, this indicator provides a correct identification. Nonetheless, the presence of an *ill* set of experiments in the input data turns into a catastrophic identification.
> *Median*. The *median* provides a good identification in both cases. The presence of an *ill* set of experiments in the input data does not impact the identification quality.

Up to this point, the statistical identification using the *median* has a clear advantage in terms of quality and robustness in comparison to the *mean*. To confirm these observations, much more sets of sets of experiments should be investigated.

5.3.4 Extended analysis of statistical stability

This section reflects the same analysis as the one carried out previously from Sec. 5.3.1 up to Sec. 5.3.3. The difference is that instead of analyzing 2 sets of sets of experiments in depth, 150,000 sets of sets of experiments are considered. The pattern of the analysis for each set of sets of experiments indexed "$SoSoe$" is the following:

Step 1. 6 sources are randomly positioned in the right side of cavity C. The result is an experimental setup. (Pendant of Figure 5.1 and Table 5.2).
Step 2. The six experiments indexed e are carried out—one source active. For each experiment, the coupled pressure $\{P_i^C\}_e$ and velocity $\{V_j^C\}_e$ is stored.
Step 3. The set of sets of experiments $SoSoe$ is constituted. It contains the 15 sets of experiments Soe resulting of the combination of 2 experiments in a set of 6 experiments. (Pendant of Table 5.3).
Step 4. The set of sets of experiments $SoSoe$ is analyzed. Each set of experiments Soe—of the set of sets of experiments $SoSoe$—results in a single identification of the matrix $\left[Z_{i\leftarrow j}^{A\,Id}\right]_{Soe}$, which is compared to the reference $\left[Z_{i\leftarrow j}^{A\,Ref}\right]$. The mean quadratic error of both best and worst sets of experiments is identified. It represents a quality indicator of the set of sets of experiments $SoSoe$ (Pendant of Table 5.4 and Table 5.5).
Step 5. The set of sets of experiments $SoSoe$ is passed to the statistical indicators *mean* and *median*. It results in the output matrix $[Z^{A\,Id}]_{SoSoe}^{Mean}$ and $[Z^{A\,Id}]_{SoSoe}^{Median}$ (Pendant of Figure 5.4 and Figure 5.5).
Step 6. Both output matrices $[Z^{A\,Id}]_{SoSoe}^{Mean}$ and $[Z^{A\,Id}]_{SoSoe}^{Median}$ are compared to the reference $\left[Z^{A\,Ref}\right]$ with the metric mean quadratic error (Pendant of Table 5.6 and Table 5.7).

Finally the results are stored in form of Table 5.8. Due to its considerable size—total number of tested sets of sets of experiments $TSoSoe$ equals 150,000—the table is presented on a generic form without any value. The results are rather graphically presented on Figure 5.6.

Table 5.8: Generic synthesis table, containing the evaluation of a number TSoSoe "Total Sets of Sets of experiments" of sets of sets of experiments. The retained dada allow to gain an insight between the quality of the input data—best and worst set of experiments of the set of sets of experiments—passed to the statistical

value, and the resulting quality of the output. The quality is measured in both cases with the metric mean quadratic error.

	Mean quadratic error of			
	Input		Output	
Set of sets of experiments	Best set of experiments	Worst set of experiments	Mean	Median
01	$[Z_{i\leftarrow j}^{A\,Id}]_{??}$	$[Z_{i\leftarrow j}^{A\,Id}]_{??}$	$[Z^{A\,Id}]_{01}^{Mean}$	$[Z^{A\,Id}]_{01}^{Median}$
02	$[Z_{i\leftarrow j}^{A\,Id}]_{??}$	$[Z_{i\leftarrow j}^{A\,Id}]_{??}$	$[Z^{A\,Id}]_{02}^{Mean}$	$[Z^{A\,Id}]_{02}^{Median}$
⋮	⋮	⋮	⋮	⋮
$SoSoe$	$[Z_{i\leftarrow j}^{A\,Id}]_{??}$	$[Z_{i\leftarrow j}^{A\,Id}]_{??}$	$[Z^{A\,Id}]_{SoSoe}^{Mean}$	$[Z^{A\,Id}]_{SoSoe}^{Median}$
⋮	⋮	⋮	⋮	⋮
$TSoSoe$	$[Z_{i\leftarrow j}^{A\,Id}]_{??}$	$[Z_{i\leftarrow j}^{A\,Id}]_{??}$	$[Z^{A\,Id}]T_{SoSoe}^{Mean}$	$[Z^{A\,Id}]_{TSoSoe}^{Median}$

This analysis attributes a clear and decisive advantage of the statistical indicator *median* compared to the *mean*. The mean might provide a wrong identification of the researched impedance matrix—instability to the set of sets of experiments. On the opposite, the *median* is robust faced to the quality variation of the set of sets of experiments.

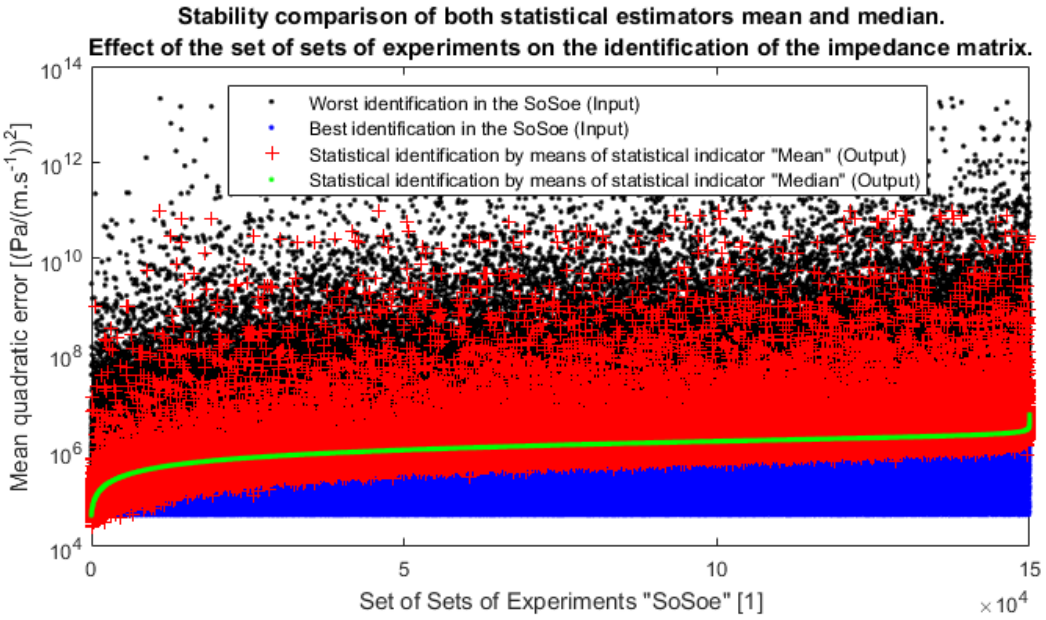

Figure 5.6: Graphical representation of the 150,000 sets of sets of experiments present in Table 5.8. For each set of sets of experiments represented on the x-axis, the mean quadratic error of its worst (Black dot) and its best (Blue dot) set of experiments is positioned on the y-axis. In addition the mean quadratic error of both statistical indicator is represented: Mean (Red plus sign); Median (Green marker). For a better visualization, the sets of sets of experiments have been named a posteriori, according to the criterion mean quadratic error of the statistical estimation by means of the median.

This representation validates all the observations made up to this point. Based on the observation of "150,000+2" sets of sets of experiments, the difference between both indicators *mean* and *median* is clear:

Mean. Applied to the wholesome set of sets of experiments, this indicator provides a decent identification. Nonetheless, the presence of an *ill* set of experiments in the input data, turns into a catastrophic identification.
Median. The median provides a good and stable identification in all encountered cases—i.e. even in the presence of some *ill* sets of experiments.

The *median* solves the problem pointed out in Sec. 4.4: "Instability due to the choice of set of experiments". The instability could be eventually avoided if both criteria presented in Sec. 4.4.3, were respected. Yet a manipulation error might happen in practice, and at the moment no *a priori* indicator which would detect it has been found yet. For example the condition number of a matrix to be inverted is generally such an *a priori* criterion, but as it has been seen in Chap. 4 it is not the case for this method. As soon as not one but many sets of experiments are considered—each one containing a partial physical signification—the statistical identification by means of the *median* allows finding the researched impedance matrix with a good precision. A decisive advantage of the *median* is its stability to some *ill* sets of experiments.

5.4 Statistical stability: addition of noise

The proposed statistical method relies on the information contained in several *sets of experiments* stored in a *set of sets of experiments*. Sec. 5.2.1 has proposed two methods to create such a *set of sets of experiments*: the first one—*roving source*—has been addressed in the previous section; the second one—*addition of noise*—is addressed here in Sec. 5.4.1. Finally, Sec. 5.4.2 proposes the—*roving source*—as encountered in Sec. 5.3, with the presence of an unwanted measurement noise.

5.4.1 Regularization by means of noise

Analysis pattern

This section is founded on the results of the three sets of experiments presented in Sec. 4.4.1 and the noise addition pattern presented in Sec. 4.5.3:

Step 1. A numerical noise of signal-to-noise ratio SNR_m[17] is added on top of the noise-free simulated measurement. It simulates physical uncertainties in the measurement process. The noise-free matrices $[P]$ and $[V]$ are transformed into matrices $[\tilde{P}]$ and $[\tilde{V}]$.
Step 2. Inversion using the formulation $\left[\tilde{Z}_{i\leftarrow j}^{A\,Id}\right] = [\tilde{P}][\tilde{V}]^{-1}$.
Step 3. The identified matrix $\left[\tilde{Z}_{i\leftarrow j}^{A\,Id}\right]$ is compared to the reference $\left[Z_{i\leftarrow j}^{A\,Ref}\right]$ by means of the mean quadratic error.

Starting at this point, a virtual *set of experiments* indexed Soe is created with addition of a numerical noise:

Step 4. Addition of a noise of signal-to-noise ratio of SNR_r[18] on top of the noisy measurements. Matrices $[\tilde{P}]$ and $[\tilde{V}]$ are becoming $[\widetilde{P}]_{Soe}$ and $[\widetilde{V}]_{Soe}$.

[17] The subscript "m" of "SNR_m" stands for "measurement". This noise is unwanted but inherent to any physical measurement.
[18] This noise is voluntarily added on top of the noisy measurements. As the intention is to regularize the inversion, the "r" of "SNR_r" stands for "regularization".

Step 5. The result of the identification—$\left[\widetilde{Z_{i\leftarrow j}^{A\,Id}}\right]_{Soe} = [\widetilde{P}]_{Soe}\ [\widetilde{V}]_{Soe}^{-1}$—is added to the *set of sets of experiments*.

The process—*Step 4* and *Step 5*—is repeated $TSoe$ times resulting in a *set of sets of experiments* of cardinality $TSoe$. It contains the input data—$TSoe$ variations of the identified matrix $\left[\widetilde{Z_{i\leftarrow j}^{A\,Id}}\right]_{Soe}$—required for the use of the statistical identification:

Step 6. Each statistical indicators *mean* and *median* is computed resulting in $[Z^{A\,Id}]^{Mean}$ and $[Z^{A\,Id}]^{Median}$.

Step 7. Each identified matrix $[Z^{A\,Id}]^{Mean}$ and $[Z^{A\,Id}]^{Median}$ is compared to the reference $\left[Z_{i\leftarrow j}^{A\,Ref}\right]$ by means of the mean quadratic error metrics.

Set of experiments 1

The simulation pattern presented above is conducted on the set of experiments 1 presented in Sec. 4.4.1. The simulated *unwanted* experimental noise has a signal-to-noise ratio of SNR_m equal to 20 dB. It intends to represent a good measurement. The signal-to-noise ratio of the regularization noise SNR_r added on top of the noisy measure is growing from 100 up to 0 dB. For each level of regularization noise, the total number of created *sets of experiments* $TSoe$ is equal to 21. The results are presented in Figure 5.7.

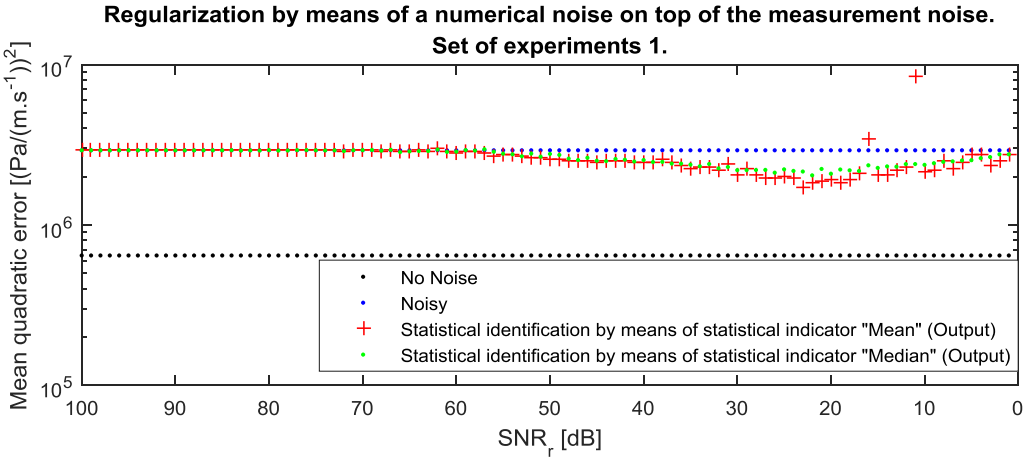

Figure 5.7: Results of the regularization by means of noise on the results of the set of experiments 1. Y-axis: represents the mean quadratic error of all identified impedance matrices in comparison to the reference. X-axis: signal-to-noise ratio SNR_r of the noise used for the regularization. In addition to the results of the statistical indicator mean (red crosses) and median (green points), the results without noise (black dots) and without regularization (blue dots) are presented.

Without noise (black dots) the mean quadratic error is equal to $6.45e+05$ as found in Table 4.9. The addition of the simulated noise of SNR_m equal to 20 dB deteriorates the identification. Indeed the mean quadratic error reaches $3.63e+06$. The proposed regularization, by means of noise, slightly ameliorates the quality of the identification. The level of the regularization noise results in a minor variation of the identification's quality. In this case, both statistical indicators, *mean* and *median* are delivering comparable results. Nevertheless, the variations of the quality of the result using the indicator *mean* is larger than the one encountered with the indicator *median*.

The same analysis is carried out on the set of experiments 2 and 3.

Set of experiments 2

The results of the method applied on the set of experiments 2 are presented in Figure 5.8.

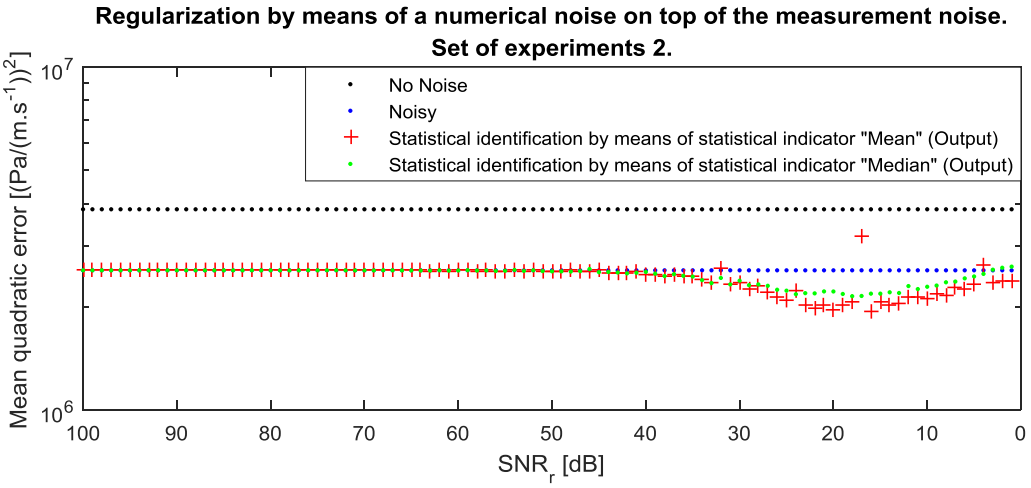

Figure 5.8: Results of the regularization by means of noise on the results of the set of experiments 2. See. Figure 5.7 for the legend's details.

The results display a new phenomenon. Indeed, the results obtained after the introduction of the *unwanted* noise are even better than without noise—mean quadratic error decreases from $5.39e+06$ to $3.85e+06$.

This observation should be rather considered as a particular phenomenon. The system under characterization and the coupled system itself is a totally reactive system which is *per se* a negative point for an inverse method. Indeed on the resonance frequencies, the system is strongly dominated by the concerned eigenmode and thus almost independent from the excitation. In this case, the addition of noise might help the inversion adding an *artificial* independency between the measurements.

In addition of this particular phenomenon, the regularization method by means of noise, improves the results even more. In this case, a regularization noise with a level of 20 dB provides the best results.

Set of experiments 3

The results of the regularization method by mean of numerical noise on the set of experiments 3 are presented on Figure 5.9.

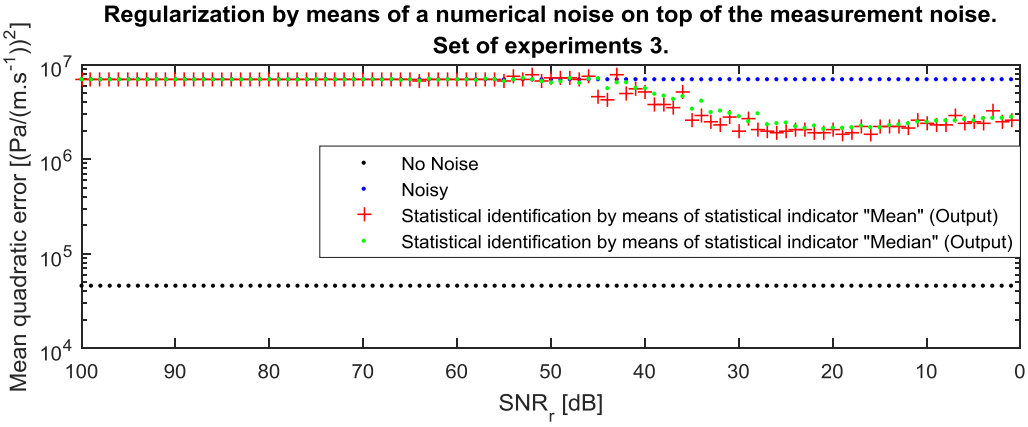

Figure 5.9: Results of the regularization by means of noise on the results of the set of experiments 3. See. Figure 5.7 for the legend's details.

On the set of experiments 3 the addition of the measurement noise, deteriorates the results of the identification from $4.60e+04$ to $3.68e+06$. The rest of the analysis is totally identical to the one proposed for the set of experiment 1, and thus not repeated here.

Summary

In Sec. 4.5, the original method has been found instable to the presence of noise in the measurement. The proposed regularization method, based on the addition of a simulated noise, and the use of one of the statistical indicator *mean* or *median* improves the stability of the method. In this case, the statistical indicator *median* has a small advantage in comparison to the statistical indicator *mean*. Yet both provide good results.

5.4.2 Statistical stability: Noisy sets of experiments

This section proposes the same analysis as the one encountered in Sec. 5.3, with consideration of an *unwanted* noise in the measurements. A noise of a varying signal-to-noise ratio is added on top of the noise-free measurements.

Set of sets of experiments 1

The constitution of the *set of sets of experiments 1* is unchanged and thus not repeated here (See Sec. 5.3.1). The difference appears in the constitution of Table 5.4. An *unwanted* simulated noise of signal-to-noise ratio SNR_m is added to each noise-free *set of experiments*. The noise-free matrices, $[P]_{Soe}$ and $[V]_{Soe}$, of set of experiments Soe are becoming $[\tilde{P}]_{Soe}$ and $[\tilde{V}]_{Soe}$. The resulting identification is noted $\left[\tilde{Z}_{i\leftarrow j}^{A\ Id}\right]_{Soe}$.

Once the identification by means of the statistical indicators *mean* and *median* have been done, the results—best set of experiments; worst set of experiments; *mean* and *median*—are stored in a table similar to Table 5.6. This representation intends to provide an insight in the quality of the output data in comparison to the quality of the input data.

This pattern is carried out several times with different level of *unwanted* noise—i.e. SNR_m. The results are presented on Figure 5.10.

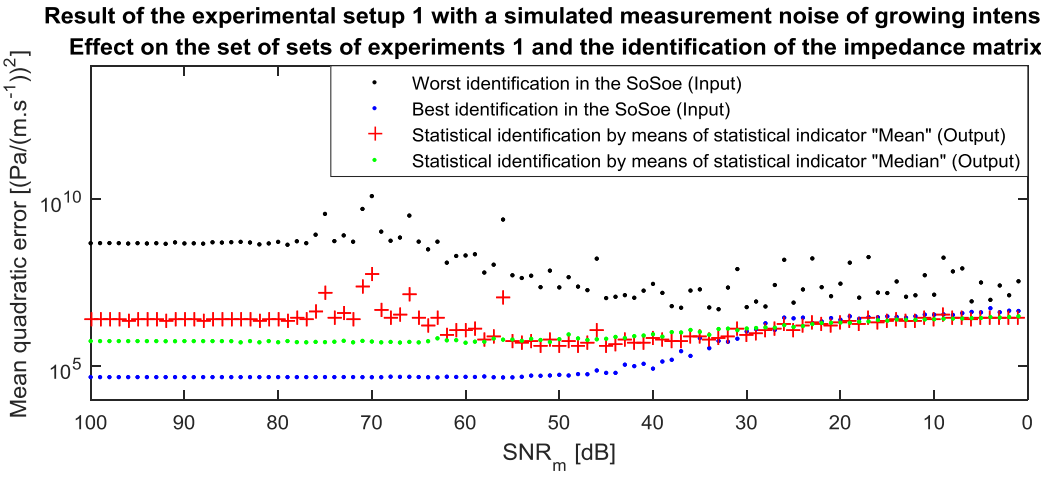

Figure 5.10: Graphical representation of the influence of noise on the set of sets of experiments 1. Both perspectives—input and output—are considered. Y-axis: Mean quadratic error of the diverse identifications in comparison to the reference. X-axis: Signal-to-noise ratio of the unwanted noise added into the noise-free measurement.

The growing level of *unwanted* noise in the measurement—i.e. decreasing SNR_m value—has an impact on both the input and the output of the statistical identification method. The results from the side of the input are considered first.

On the one hand, the quality of the best set of experiments[19] in the set of sets of experiments decreases. On the other hand, the quality of the worst set of experiments[20] tends to increase. This counter intuitive observation has been already observed and addressed on Figure 5.8 and its analysis.

From the perspective of the output, both indicators *mean* and *median* are resulting in a stable identification. This is particularly true for the *median*. Indeed, the *mean* tends to be impacted by the presence of *ill* set of experiments in the input set of sets of experiments. On the proposed figure, the presence of a really bad set of experiments (large mean quadratic error) result is a bad identification. On the opposite the identification using the *median* is not affected by the presence of an outsider in the input set of sets of experiments 1. The increase of noise in the measurement, results in a moderate degradation of the identification.

Set of sets of experiments 2

The same analysis is carried out on the set of sets of experiments 2. The result are provided on Figure 5.11.

[19] Without noise, the best set of experiments among the 15 sets of experiments is the 10th. With the presence of the *unwanted* noise, it does not necessarily remains the 10th.
[20] Without noise, the worst set of experiments among the 15 sets of experiments is the 12th. As encountered for the best set of experiments it might also change depending on each realization of the added noise.

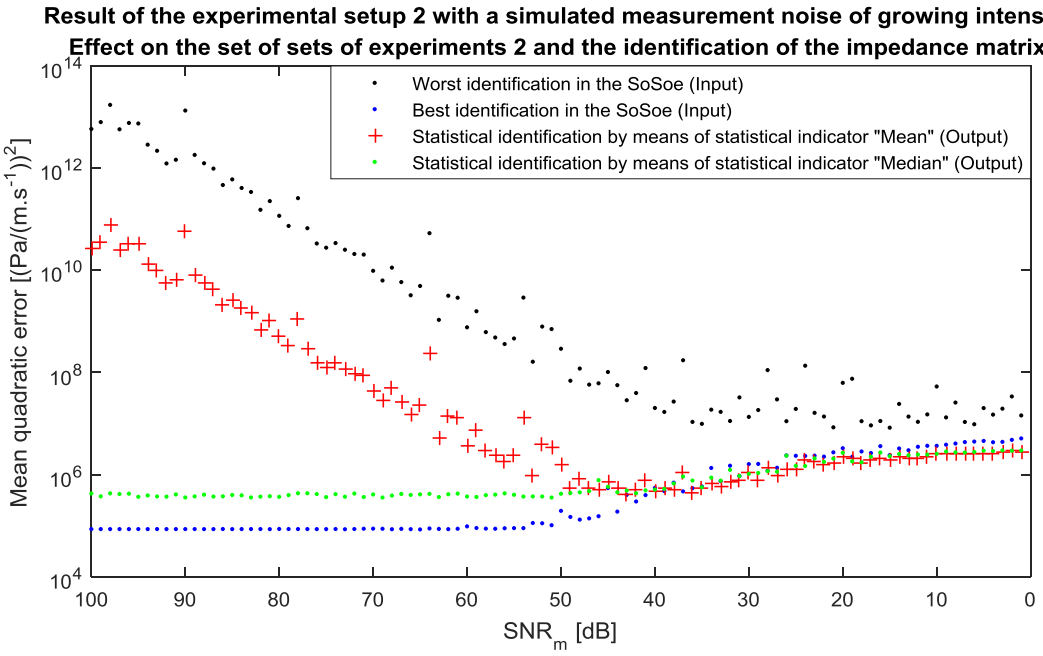

Figure 5.11: Graphical representation of the influence of noise on the set of sets of experiments 2. More details are provided on the caption of Figure 5.10.

The results and their interpretations are identical as the one encountered with the set of sets of experiments 1. An interesting observation however, is that for high level of noise, both statistical identifications—*mean* and *median*—tend to be better than the best set of experiments included in the input set of sets of experiments. This *positive* effect is a result of the mathematical formulation of these indictors—Eq. (5.1) up to Eq. (5.5). The evaluation of both indicators is computed independently for each spectral line and for each term of the impedance matrix. As a result this method might provide an identification at a local scale—spectral line and term of the impedance matrix—which is better than the best set of experiments (considered so at a global scale). This phenomenon is also observed in Figure 5.10.

Summary

The instability of the method in the presence of noise in the measurement pointed out in Sec. 4.5 turns into a statistical stability. The indicators *mean* and *median* are able to recover the physical meaning partially included in each imperfect set of experiments. The statistical indicator *median*, due to its insensibility face to some outsider values, is preferable in comparison to the statistical indicator *mean*.

5.5 Summary

Chap. 3 has addressed the problem, *"Characterization of Patch Transfer Functions of a subsystem by means of measurement on a coupled system"*. The first results—obtained with a numerical experimental setup—have shown that the method is able to handle the characterization of a strongly coupled system. Nevertheless, it has been seen in Chap. 4 that this can turn into a critical instability method when faced to minor changes in the experimental setup—position of the sources; presence of noise in the measurement. Indeed, a small variation of the experimental setup, and therefore in the resulting *set of experiments,* had resulted in a different identification of the subsystem under characterization.

A different *set of experiments*—sources positions or presence of noise—might result in a different identification (better or worse), but still contains a partial physical signification. If several *sets of experiments* are created, each one containing a partial physical meaning, the reality might be recovered with an adapted statistical indicator.

Two statistical indicators *mean* and *median* have been proposed. Both are overcoming the two instabilities discovered in Chap. 4. Yet, the *mean* suffers the presence of one or several *ill* sets of experiments, whereas the *median* is not affected by outsiders. For this reason, the statistical method by mean of the *median* is retained for further validation tests on a *physical* experimental setup.

6 Experimental validation

"I'm the one who is doing all the work, so we just want you to stay cool for a minute. [Laughter]
However, I think we're going to do it, and I think that we must pay what needs to be paid. I don't think we ought to waste any money, but I think we ought to do the job. And this will be done in the decade of the sixties. It may be done while some of you are still here at school at this college and university. It will be done during the terms of office of some of the people who sit here on this platform. But it will be done. And it will be done before the end of this decade."

John Fitzgerald Kennedy (1917–1963) in "Address at Rice University in Houston on the Nation's Space Effort", 1962 [1].

Chapter contents:

6.1 Introduction **125**

6.2 Problem statement **126**

6.3 Experimental setup **127**

6.4 Statistical identification **129**

6.5 Summary **131**

6.1 Introduction

The scientific problem "*Characterization of Patch Transfer Functions of a subsystem by means of measurement on a coupled system*" has been addressed with an inverse method, combined with a statistical identification. The method has been validated on numerical experiments, including the presence of uncertainties. In this final chapter, the method is tested on a *physical* experiment.

The physical experiment carried out in this chapter, differs from the previous numerical experiments for three main reasons:

Natural presence of uncertainties. Uncertainties—e.g. noise in the measurements—are not simulated anymore, but inherently exist.
More patches. The number of patches is increased.
Addition of an infinite system. The system under characterization, is strongly coupled with an *unknown* semi-free field.

This chapter is structured in three sections. The problem statement is addressed first. Secondly, the nature and the instrumentation of the experiment setup is addressed. Finally, the results are exposed and discussed.

6.2 Problem statement

The model intended to be characterized—Figure 6.1 (a)—is a cavity M, of volume V, filled with air, bounded by rigid walls S_r. The walls form a parallelepiped volume of size $(0.820; 0.608; 0.530)$ m. The surface at $z = 0.530$ m is divided into 20 patches of size $(0.164; 0.152)$ m.

The identified impedances will be compared to the reference solution, computed using Eq. 2.32. Indeed, the system M can be described with a patch to patch impedance matrix $[Z^M_{i\leftarrow j}]$, describing the system in form of a blocked pressure. The estimation of row j row of matrix $[Z^M_{i\leftarrow j}]$ consists in computing the blocked pressure on all patches i, while patch j is vibrating in a translation motion along its normal. All other patches in the system are blocked. Contrary to the theoretical model M, the system E is coupled a unknown semi-free field. From a practical point of view, the pressure and particle velocities have been measured at center of patches as depicted in Figure 6.1.

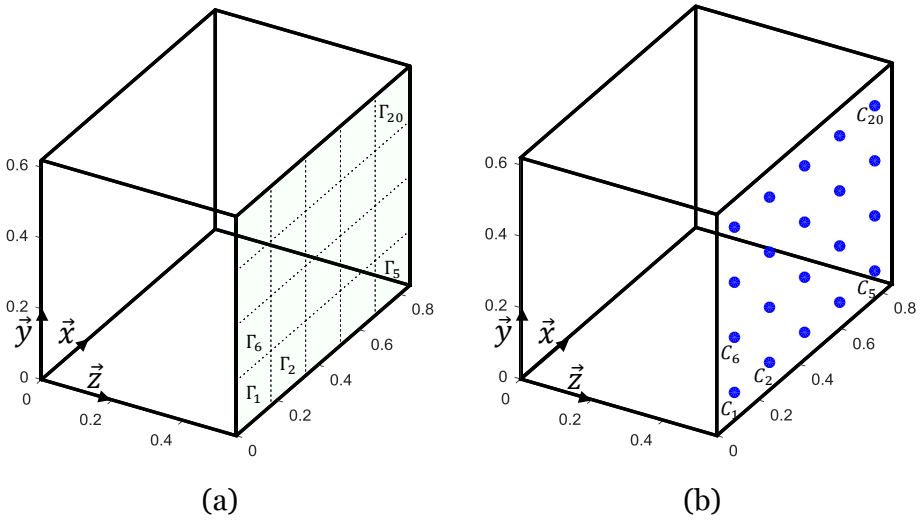

Figure 6.1: (a): Schematic representation of the model M, which intends to be characterized. The internal dimensions are $(0.820; 0.608; 0.530)m$. The surface, located at $z = 0{,}530m$ is divided into 20 patches of size $(0.164; 0.152)m$—5 patches along direction $\vec{x}$; 4 patches along direction $\vec{y}$. Each patch is indexed by a number. The numbers are sorted according to direction $\vec{x}$ and secondly according to direction $\vec{y}$. (b): Representation of the experimental system E available for the measurement. System E differs from system M by the nature of the surface positioned at $z = 0{,}530$. The surface is neither rigid nor discretized in patches, but completely opened to the air in the surroundings. The center of each virtual patches Γ_i is marked with a blue dot indexed C_i.

Table 6.1 summarizes the properties of subsystems M and E.

Table 6.1: Geometrical and physical properties of subsystems M and E.

	Box M	Box E
Nature	Mathematical model	Experimental model
$(L_x; L_y; L_z)$	$(0.820; 0.608; 0.530)$	
Patches Γ	20 patches size $(0.164; 0.152)$	—
Center C	—	20 points
ρ	1.29 $[\mathrm{kg.m^{-3}}]$	Unknown
c	340 $[\mathrm{m.s^{-1}}]$	Unknown
η	0.01	Unknown

It is important to underline here that no information about the system under characterization nor about the coupled semi-free field are necessary. This point is particularly convenient for experimental application of the method on industrial systems. Neither the physical characteristics of the subdomains nor their geometry has to be known. This is surely one of the main advantages of the proposed method.

In this extend, the proposed characterization matches perfectly the problem "*Characterization of Patch Transfer Functions of a subsystem by means of measurement on a coupled system*".

6.3 Experimental setup

The experimental setup is built in order to use the statistical identification method proposed in Chap. 5. Several *sets of experiments* are created using the principle of the roving source detailed in Sec. 5.3. For the considered system M, the number of patches N is equal to 20. As a result the number of positions of the roving source Ns, must be at least equal to 20.

The total number of *sets of experiments* the roving source technique allows to create is given by Eq. 4.2. Figure 6.2 provides a numerical evaluation of this equation. If 20 source's positions are used, a single *set of experiments* can be created. In this case, the statistical methods proposed in Chap. 5 would be trivial—output equals the input. In fact, it would correspond to the method proposed in Chap. 3, disqualified in Chap. 4 for its instability. On the opposite, as soon as the number of the source's positions is greater than 20, the resulting number of *sets of experiments* grows, quickly. It allows taking advantage of the statistical method proposed in Chap. 5.

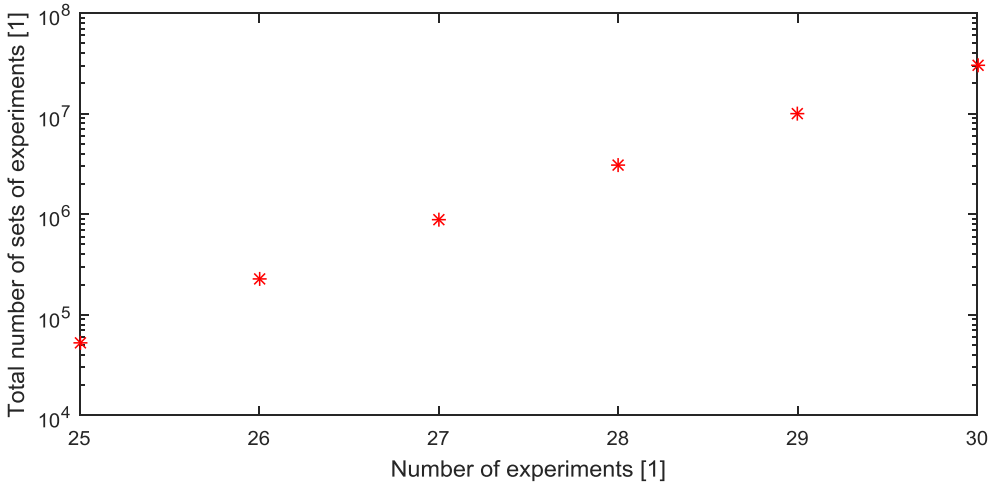

Figure 6.2: Total number of sets of experiments, depending on the number of experiments—i.e. source's positions. The plot is adapted to the system intended to be characterized—i.e. 20 patches. The curve is represented on a logarithmic scale.

Figure 6.3 proposes an experimental setup with 25 source's positions. The firsts 20 sources' positions are facing the center of the virtual patches within a distance of 0.250 meters along direction $\vec{z}$. 4 sources' positions are facing the corner of the box at a distance of 0.800 meters. The fifth source's position matches the barycenter of the last four sources' positions. Experiment n corresponds to the measure of the pressure and the velocity at the center of each of the 20 virtual patches, while the point source is acting at position S_n. The result of experiment n is stored in vector $\{P_i^C\}_n$ and in vector $\{V_i^C\}_n$. Since 25 source' positions are proposed, it results in 25 experiments. Finally, the total number of possible *sets of experiments* reaches 53,130—cf. Eq. 4.2.

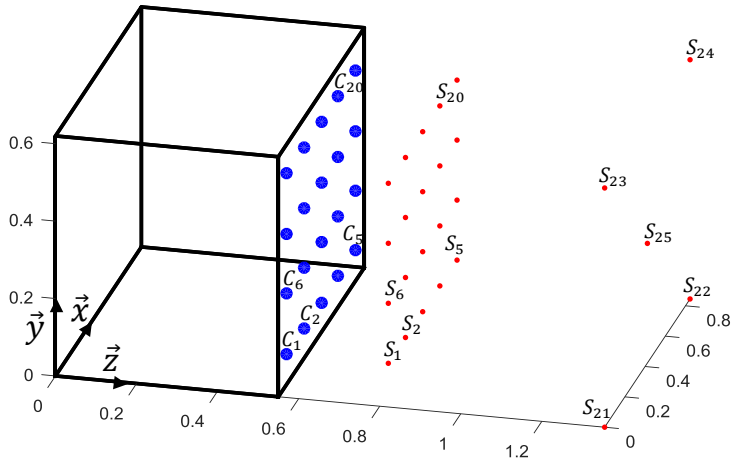

Figure 6.3: Experimental setup on the system E which intends characterization of the mathematical model M by means of measurements. The 20 measurement points—pressure and particle velocity—are located at the center of each virtual patch (blue points). Experiment n corresponds to the measure of the pressure and the velocity on the 20 measurement points, while the source is acting at position S_n. 25 source's positions are considered.

The physical realization of the experimental setup proposed on Figure 6.3 is illustrated on Figure 6.4. The axis $\vec{z}$ of the box E is pointing up. As no information about the external domain is necessary, the characterization is independent from the *unknown* system,

coupled to the system under characterization. In this experimental setup, the *unknown* external system happens to be a semi-free field environment.

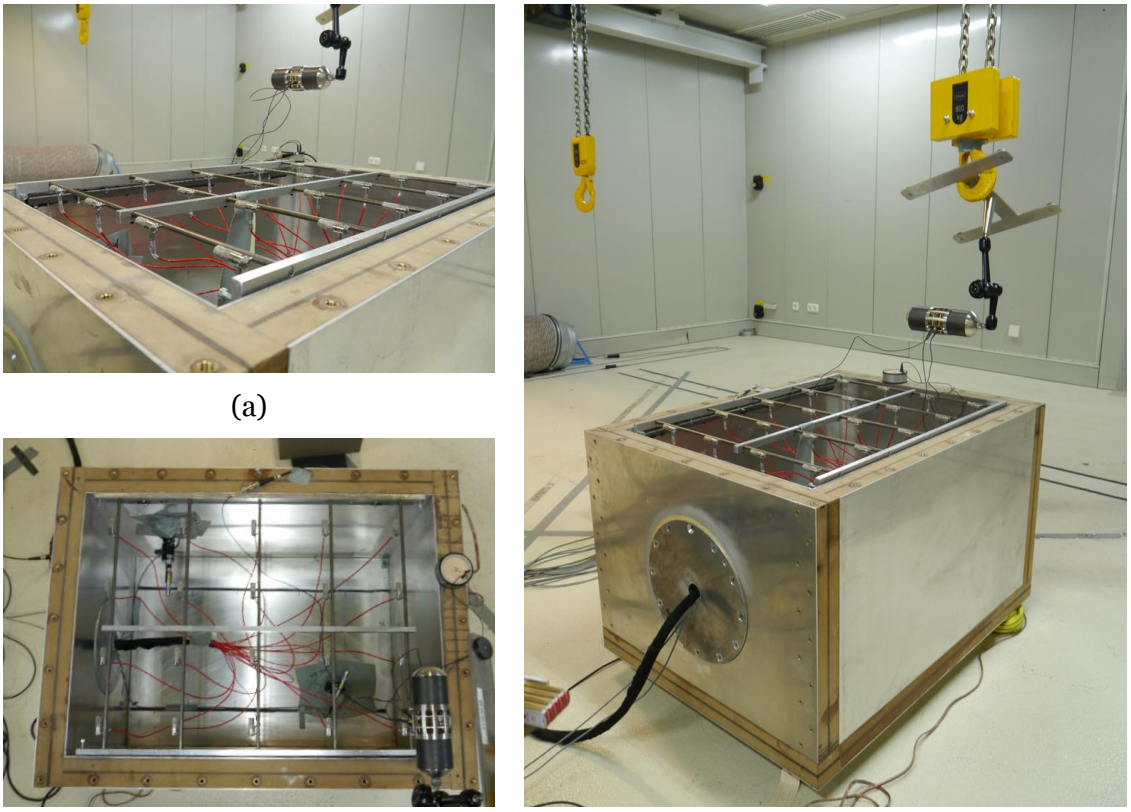

(a) (b) (c)

Figure 6.4: Physical realization of the experimental setup proposed on Figure 6.3. (a): Detail of the array of 20 PU-Probes. Each probe is measuring simultaneously the pressure and the particle velocity; (b): Top view of the array supporting the 20 PU-Probes; (c): Overview of the realization of one experiment—roving source at a given position. The point source hangs from a mobile hoist (yellow hook). Note that each view is representing a different experiment—i.e. point source at a different position.

PU-Probe; Microflown, µ-flown

A PU-Probe is a sensor able to measure simultaneously the sound pressure and the particle velocity. Microflown is the main manufacturer of PU-Probe. Microflown was invented at the university of Twente. The company Microflown has been created for the commercialization of this discovery. H.-E. de Bree has presented the technology in "The µ-flown: a novel device for measuring acoustic flows" [81]. "An Overview of Microflown Technologies" is found in [82]. This technology is briefly presented in the book of M. Möser covering the measurement equipment in the field of acoustics [83].

6.4 Statistical identification

The experimental setup allows the creation of 53,130 *sets of experiments*, stored in a *set of sets of experiments*. This *set of sets of experiments*, would result in a single statistical identification of the researched impedance matrix. Nevertheless, the method does not require the use of all *sets of experiments*.

In this section, the statistical identification is not applied to the complete *set of sets of experiments* of cardinality 53,130, but instead on a subset of cardinality 21. In other words, among the 53,130 possible *sets of experiments*, only 21 are retained. The number 21 has

been determined arbitrarily. The choice of the *sets of experiments* to hold is made according to a random process.

The statistical identification of the mathematical system M by means of experiments on a system E results in one impedance matrix $[Z^{M\,Id}]^{Stat}$ of size 20 by 20. Both statistical indicators *mean* and *median* are computed—i.e. matrices $[Z^{M\,Id}]^{Mean}$ and $[Z^{M\,Id}]^{Median}$. Two impedances curves—among 400—are presented.

Figure 6.5 presents the auto-impedance on patch Γ_1. Both statistical identifications *mean* and *median* are close to the reference in terms of amplitude. The phase differs from the reference. The *median* results in a much better identification, than the *mean*. The discrepancies visible in Figure 6.5 may also be explained by the differences between chosen parameters (sound speed, damping factor, density of air) that were not directly measured and chosen arbitrarily.

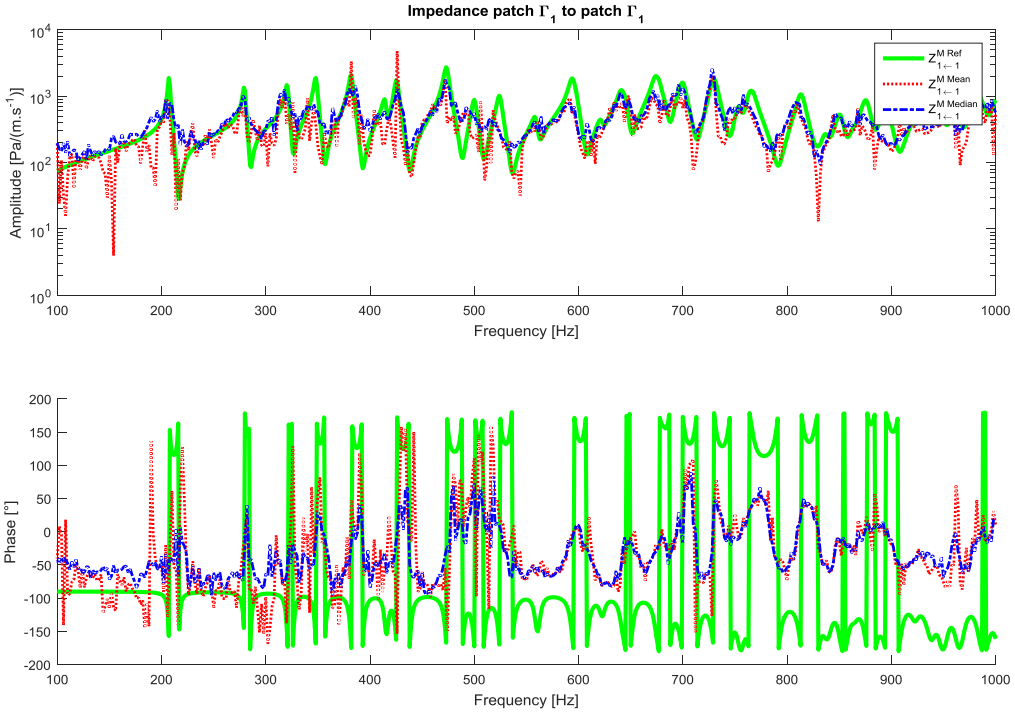

Figure 6.5: Result of the statistical identification of the auto-impedance on patch Γ_1. For the statistical identification, 21 sets of experiments are used among the 53,130 possible with the proposed experimental setup. Reference impedance $Z_{1\leftarrow1}^{M\,Ref}$ (Green solid line); Identification by means of the mean $\left(Z_{1\leftarrow1}^{M\,Id}\right)^{Mean}$ (red dotted line); Identification by means of the median $\left(Z_{1\leftarrow1}^{M\,Id}\right)^{Median}$ (blue dash dotted line).

Figure 6.6 contains the impedance from path Γ_{16} to patch Γ_3. Both statistical identifications are close to the reference in terms of amplitude and phase. On this case, the identification by means of the *median* is also better than the one provided by the *mean*.

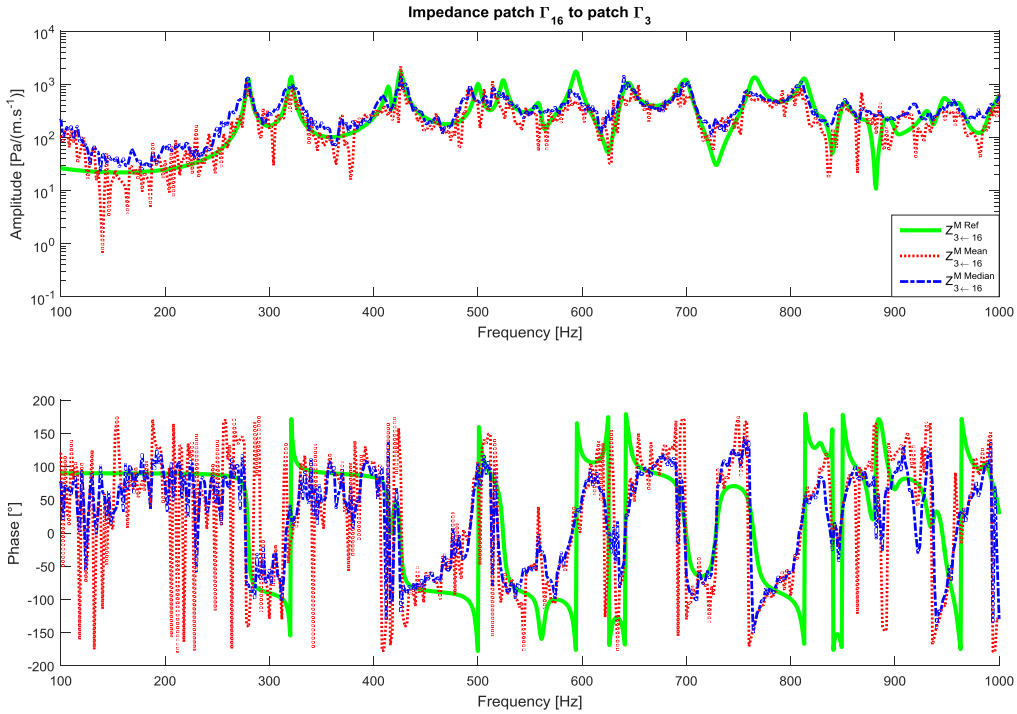

Figure 6.6: Result of the statistical identification of the impedance from patch Γ_{16} to patch Γ_3 Reference impedance $Z^{M\,Ref}_{3\leftarrow 16}$ (Green solid line); Identification by means of the mean $\left(Z^{M\,Id}_{3\leftarrow 16}\right)^{Mean}$ (red dotted line); Identification by means of the median $\left(Z^{M\,Id}_{3\leftarrow 16}\right)^{Median}$ (blue dash dotted line).

The results of the identification are considered as appropriate. As often encountered in many fields of science, the results of an experiment generally does not perfectly fit the reference. In this case, the reference has been calculated with Eq. 2.32.

The amplitude of the identification follows the reference within a small tracking error. On the other hand, the identification of the phase seems to be more challenging. The observed difference is probably the result of a phase with a "*too high*" dynamic. The high dynamic of the phase is a characteristic of reactive system with low damping. This drawback should not be present in the case of a system with a higher damping. Thankfully, the vast majorities of industrial systems have a higher damping than a rigid cavity of air.

6.5 Summary

In this chapter, the statistical identification method proposed in Chap. 5 has been tested on a physical experiment. The results presented in Chap. 5 had demonstrated the ability of the method to handle this problem. The stability of the method to uncertainties in the measurement had been tested with a numerical experiment. In opposition, in this chapter, the experiment has been realized physically.

The major challenge of an inverse method used with experimental data is its stability to measurement uncertainties. The primary source of uncertainties is most certainly the presence of disturbing noise and the calibration error of the measuring equipment. The experiment has been conducted with standard equipment, without any additional precaution as encountered for a standard measurement. In other word, the quality of the measurement—noise, calibration's error, etc.—should be representative of the test bench where the method could be applied. According to this result, the presence of representative

uncertainties in the measurements has not resulted in an instability. On the opposite, the method has provided a good identification.

In addition, two other challenges have been overcome:

> *More patches*. The number of patches has been increased to reach a number which is more representative of a real application.
> *Addition of an infinite system*. The system under characterization was strongly coupled with an *unknown* semi-free field.

7 Conclusions

"Many years ago the great British explorer George Mallory, who was to die on Month Everest, was asked why did he want to climb it. He said, "Because it is there."
Well, space is there, and we're going to climb it, and the moon and the planets are there, and new hopes for knowledge and peace are there. And, therefore, as we set sail we ask God's blessing on the most hazardous and dangerous and greatest adventure on which man has ever embarked."

John Fitzgerald Kennedy (1917–1963) in "Address at Rice University in Houston on the Nation's Space Effort", 1962 [1].

Chapter contents:

7.1 Summary **133**
7.1.1 Industrial context 133
7.1.2 Limits and advanced strategies 134
7.1.3 Experimental validation 135
7.2 Recommendation **135**
7.3 Résumé étendu en français **136**
7.3.1 Contexte industriel 136
7.3.2 Sous structuration vibro-acoustique 138
7.3.3 Caractérisation expérimentale 140
7.3.4 Limites et stratégies avancées 141
7.3.5 Validation expérimentale 142

7.1 Summary

7.1.1 Industrial context

During the development process of a vehicle, the area of expertise of noise vibration and harshness—known as NVH—appears in various contexts. The spectrum of activities starts from the confrontation of inconvenient noises up to the sound design of the vehicle acoustical character. Achieving some satisfactory NVH performances is still challenging work considering the decrease of the total weight of the vehicle.

Exhaust sound has a significant impact on the acoustic comfort and defines the acoustic signature profile of the car brand. The driver and passenger's perception of the exhaust sound can be optimized by means of two levers: the source strength and the vehicle isolation. The first lever consists in working on the side of the exhaust system itself. The

second consists in working on the structure, and the sound isolation package of the full vehicle.

As the source strength, at the exhaust outlet, has a leading contribution for the external noise—which is subject to strict regulation—much more effort has been done to simulate and control it. On the opposite, the transfer function is more a matter of comfort, and has not been yet subject to a comparable effort. The current study is focused on the physical comprehension and the optimization of the sound transmission from the exhaust outlet into the interior of a vehicle—i.e. second lever.

For physical and technical reasons, the low frequency (20–250 Hz) content of the exhaust sound in the interior of the vehicle, is particularly challenging. In some instance the low frequency acoustical phenomenon "booming noise" appears. The human perception of this phenomenon stands in the overlapping of hearing and feeling—e.g. loud music with a lot of "bass"; blast of air caused by a thunderclap. Whether this physical phenomenon is for good or ill depends on the vehicle's character and the occupants' expectations—e.g. comfortable ride; feedback of a powerful acceleration. But, still it is in most situation a non-desirable effect.

The principal function of the method to be developed is:

> *Description and quantification of the sound transmission from the exhaust outlet into the interior of a vehicle.*

The following constraint functions have to be considered:

> *Low frequency range*. Starting from the threshold of hearing 20 Hz and up to 250 Hz.
> *Strong coupling*. The lightweight vehicle structure is fully coupled with the air.
> *Opened system*. The vehicle might present leakage or openings.
> *Experimental data*. Some information might be acquired with experimental method only on available prototypes.

In the proposed state of the art, the acoustical substructuring method Patch Transfer Functions is considered as one of the viable alternative to fulfill this problematic. Yet the application of the method to a full vehicle requires to address the problem: "*Characterization of Patch Transfer Functions of a subsystem by means of measurement on a coupled system*".

This dissertation has presented a crucial part of the Patch Transfer Functions method: the measurement of Patch Transfer Functions of an uncoupled system from the response of a coupled subsystem. In industrial structure, this inverse *in-situ* characterization is generally the only available possibility. Yet, due to the ill posed nature of the problem, the inversion process is difficult.

7.1.2 Limits and advanced strategies

In order to identify the limits of the method, several *sets of experiments* have been tested. Two instability factor have been identified:

> *Position of the source*. Depending on the position of the source used for the characterization, resulting in a different *set of experiments*, the quality of the identification has been affected.
> *Presence of noise in the measurement*. The presence of noise in the measurement has turned into an instability.

The first drawback is partially solved observing two rules for the constitution of a correct *set of experiments*:

> *Criterion 1*. The sources should be far away from the patches.
> *Criterion 2*. Each source should be far away from any other sources.

Yet the second weakness—noise in the measurement resulting remains. As a consequence, more advanced strategies have been developed.

A different *set of experiments*—sources positions or presence of noise—results in a different identification (better or worse), but contains a partial physical signification. If a total $TSoe$ of *sets of experiments* are created, each one containing a partial physical reality, the reality might be recovered with statistical indicators. The set containing the $TSoe$ *sets of experiments* is called: "*Set of sets of experiments*".

Two principles are used to create several *sets of experiments* called *set of sets of experiments*:

> *Roving source*. One, some, or all the N sources positions necessary for a single *set of experiments*, move to another positions. It results in a partially or complete new *set of experiments*.
> *Addition of noise*. A virtual noise is added on top of the physical measurements—which may already contain a noise. As a noise has an inherent random characteristic the operation might be repeated several times.

Two basic statistical indicators—*mean* and *median*—and their utilization has been proposed. Both are overcoming the two previously encountered instabilities. Yet, the *mean* suffers the presence of one or several *ill* sets of experiments, whereas the *median* is not affected by outsiders. For this reason the statistical method by mean of the *median* has been retained for further validation tests on a *physical* experimental setup.

7.1.3 Experimental validation

The inverse identification method combined with a statistical identification has been tested on a physical experimental setup. In this extend the measurement uncertainties have not been simulated anymore, but intrinsically present in the measurements. In addition, in comparison to the previously tested numerical setup, two other challenges have been overcome:

> *More patches*. The number of patches has been increased.
> *Addition of an infinite system*. The system under characterization, was strongly coupled with an *unknown* semi-free field.

The statistical method tested on a physical experiment setup solves the problem intended to be solved. Up to this point no counter example has been found. In addition the author is not aware of any error or bias, which might be included in this study. For all these reasons, the method is—at this degree of knowledge—deemed to be appropriate to solve the problem "*Characterization of Patch Transfer Functions of a subsystem by means of measurement on a coupled system*".

7.2 Recommendation

The application of the Patch Transfer Functions method to a full vehicle would present an industrial breakthrough. Indeed, the method if applied, surpasses the industrial functional specifications (Sec. 1.3.3). It enable the *description and quantification of the sound*

transmission from the exhaust outlet into the interior of a vehicle within respect of all the four constraints. In addition, due to the subsystem based writing, the Patch Transfer Functions method results in the following extra benefits:

> *Sound transmission understanding*. Main paths, panel's contribution, lessons learned.
> *Target setting*. The understanding would allow creating a structural target for the future vehicle.
> *Optimization*. Best structural changes within given constraints to eliminate an exhaust inferred booming noise.

This method is part of the framework of dynamic substructuring. Dynamic substructuring promises, the full understanding of a complex system based on the knowledge on its subsystems. This approach has the following benefits:

> *Physical understanding*. Managing the growing complexity is most certainly a key success factor.
> *Organization*. Many teams can contribute to a model with the most appropriated tool.
> *Target setting*. The full understanding of the interaction between subsystems allows to set targets to achieve the performance of the full system.
> *Modification prediction*. As the dynamic is fully represented, the modification of a subsystem on the full system can be predicted with an extremely small calculation cost.
> *System optimization*. As the numerical cost of a modification is insignificant—in comparison with a non-condensed model—an optimization algorithm might find a global optimum.

For sure the industrial application of a new method promises hardship and high cost. Many technical and organizational difficulties will be encountered along the way. Walking the path does not guarantee success, but not walking any path most certainly guarantee failure. Whether the choice is to explore further the direction of dynamic substructuring or not, the author would like to conclude with the opinion of JFK concerning the engagement—*or not*—in the space race: "*If we are to go only half way, or reduce our sights in the face of difficulty, in my judgment it would be better not to go at all*".

7.3 Résumé étendu en français

7.3.1 Contexte industriel

Au cours du développement d'un véhicule, l'expertise dans le domaine de l'acoustique et des vibrations, apparait dans plusieurs contextes. Les activités vont de la résolution d'un problème particulier à la création d'une signature acoustique conforme au caractère du véhicule.

Le bruit de la ligne d'échappement à l'intérieur du véhicule a un fort impact sur le confort acoustique, ainsi que de la sonorité générale du véhicule. La perception du conducteur, et des passagers peut être optimisée par deux leviers : la puissance acoustique rayonnée par le système d'échappement et l'insonorisation du véhicule. Le premier levier consiste à travailler sur la ligne d'échappement. Le second consiste à optimiser la structure et l'habillage de l'habitacle.

Etant donné que la puissance acoustique rayonnée par la ligne d'échappement a une forte contribution sur le niveau de bruit extérieur des véhicules, soumis à des normes strictes,

ce levier est parfaitement maîtrisé et systématiquement utilisé. A l'inverse, le transfert du son de l'extérieur à l'intérieur du véhicule représente un levier affectant le confort acoustique intérieur uniquement (non soumis à une norme). De fait ce levier est bien moins maîtrisé. Aussi, l'étude ci-présente porte exclusivement sur ce dernier : Optimisation de la transmission du son de la ligne d'échappement de l'extérieur à l'intérieur du véhicule.

Pour des raisons physiques et techniques, le contenu en basses fréquences (20–250 Hz) de la ligne d'échappement se transmet facilement à l'intérieur du véhicule. Dans certains cas, un phénomène de bourdonnement en résulte. Le bourdonnement s'entend et se ressent par le corps entier (similarité à l'écoute à fort volume d'une musique avec un contenue signifiant en basses fréquences; tonnerre résultant d'un éclair). Si parfois, ce phénomène peut être souhaité, notamment pour augmenter l'émotion liée à une forte accélération, le bourdonnement à l'intérieur de l'habitacle est généralement indésirable.

La complexité de la transmission du son rend l'analyse du phénomène de bourdonnement complexe, et ainsi l'application d'une solution. La description de la transmission du son entre le système d'échappement et l'intérieur du véhicule est présentée sur la Figure 7.1.

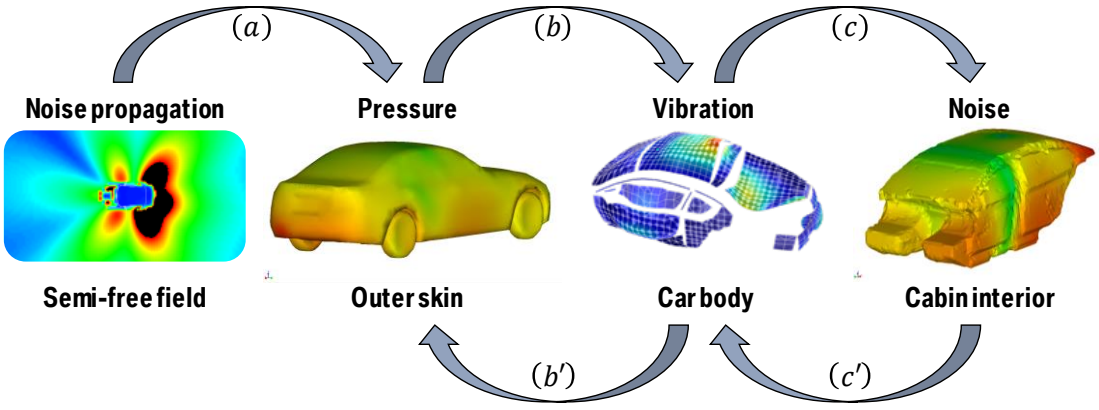

Figure 7.1: Description de la transmission du son entre la canule du système d'échappement et l'intérieur d'un véhicule. (a) : Les ondes sonores générées au niveau de la canule se propagent et interfèrent avec la surface du véhicule. Il en résulte un champ de pression. (b) : La structure du véhicule vibre sous l'application du chargement acoustique extérieur. (c) : La surface intérieure du véhicule rayonne à l'intérieur du véhicule. (c′) : Le champ acoustique à l'intérieur du véhicule interagit avec la structure et en change son état vibratoire. (b′) : Les vibrations de la structure rayonnent à l'extérieur du véhicule. Le champ extérieur devient la superposition de l'interférence du champ direct sur une structure rigide, et le son rayonné par la structure vibrante.

L'hypothèse de couplage faible est fréquemment utilisée dans le domaine de l'acoustique. Néanmoins elle n'est pas valable pour le phénomène de bourdonnement. L'expérience industrielle montre que le couplage fluide structure à l'intérieur du véhicule doit être considéré comme fort. La méthode à développer doit donc prendre en compte cette complication.

La fonction principale de la méthode à développer est la suivante :

> *Description et quantification de la transmission du son entre la bouche d'échappement et l'intérieur du véhicule.*

Les fonctions contraintes suivantes doivent être prises en compte :

> *Domaine des basses fréquences.* De la limite auditive 20 Hz à 250 Hz.

Couplage fort. La structure légère du véhicule est fortement couplée avec l'air de l'habitacle.
Système ouvert. Le véhicule peut présenter des orifices reliant l'intérieur et l'extérieur.
Données expérimentales. Certaines données pourraient être acquises de façon expérimentale uniquement.

Dans l'état de l'art proposé, la méthode de sous-structuration de domaine Patch Transfer Functions est considérée comme une alternative viable pour répondre à ce cahier des charges.

7.3.2 Sous structuration vibro-acoustique

Dans une mesure de clarté, le système étudié (véhicule complet) est représenté sur la Figure 7.2 par une géométrie simple à deux dimensions.

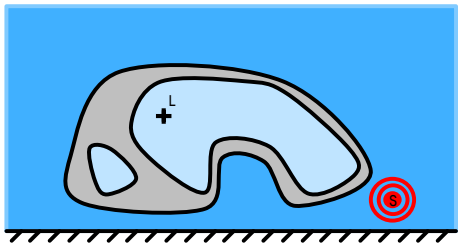

Figure 7.2: Représentation schématique en deux dimensions de la transmission du son entre la canule du système d'échappement et l'intérieur du véhicule. La structure du véhicule est symbolisée par la couleur grise. Le point S représente la canule du système d'échappement ; le point L représente un point à l'intérieur de l'habitable (ex. position des oreilles du conducteur). La cavité supplémentaire pourrait représenter le volume du coffre. Le système est placé dans un champ semi-infini.

Le système complexe est sous-structuré en trois sous-systèmes.

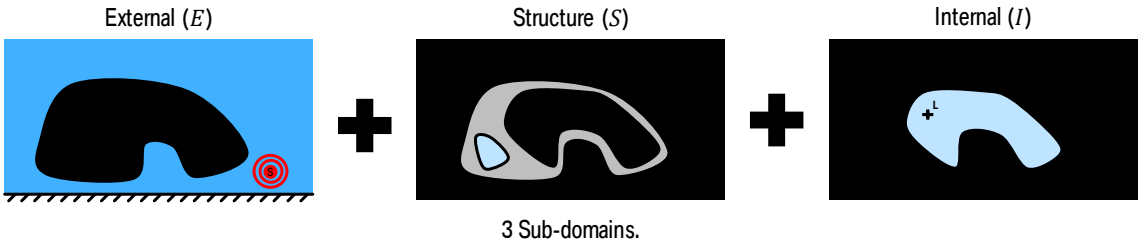

Figure 7.3: Le problème initial de transmission du son est divisé en trois sous-systèmes. Chaque sous-système à une condition limite de type bloquée, représentée par la couleur noire. (E) Champ-semi infini avec la présence de la source S. La surface extérieure du véhicule est considérée comme totalement bloquée. (S) : Structure avec une condition limite de type bloqué au niveau de chaque interface. (I) : Air à l'intérieur de l'habitacle contenant le point d'écoute L.

La complexité de chaque sous-système se trouve condensée au niveau de leurs interfaces discrétisées en patches. Chaque système est décrit mathématiquement avec une ou plusieurs matrices d'impédance. Comme suggéré dans la Figure 7.4, les informations contenues dans chaque matrice peuvent être obtenues par une méthode différente.

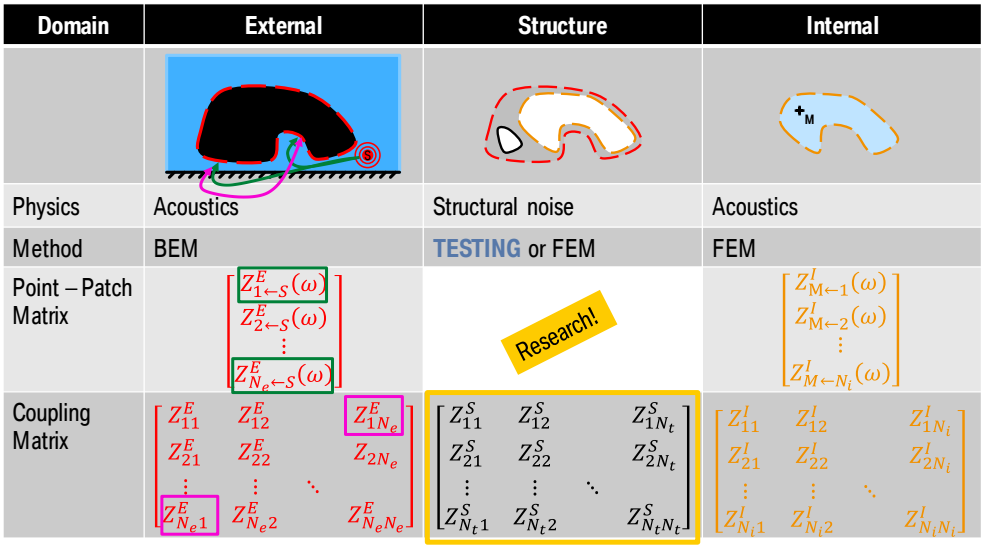

Figure 7.4: Les propriétés dynamiques de chaque sous-système sont décrites aux moyens de fonctions de transferts organisées sous forme de matrices. Le moyen d'acquisition d'une fonction de transfert peut être choisi indépendamment pour chaque sous-système. Dans le tableau suivant une approche hybride est proposée, combinant simulation et mesure expérimentale. La méthode des éléments finis de frontière (BEM) est appropriée pour la caractérisation du milieu extérieur. Pour la structure une méthode de test (objet de l'étude présente) est envisageable. Pour l'air à l'intérieur du véhicule, la méthode des éléments finis FEM est parfaitement adaptée.

Les systèmes découplés (décrits avec des matrices d'impédance condensées) peuvent être couplés mathématiquement par des opérations d'algèbre linéaire. En d'autres termes, la pression acoustique aux oreilles du conducteur peut être écrite mathématiquement sous la forme d'un opérateur mathématique.

L'application de la méthode Patch Transfer Functions à un véhicule complet représenterait une avancée significative. La méthode permet en effet de répondre à la problématique industrielle : *Description et quantification de la transmission du son entre la canule du système d'échappement et l'intérieur du véhicule*. Tout en respectant les fonctions contraintes exposées plus haut. De plus, la description du fonctionnement du système complet, sur la base de ses sous-systèmes, permet de répondre à des demandes supplémentaires :

> *Compréhension du phénomène.* Chemins principaux, analyse de contribution des surfaces.
> *Définition d'objectifs.* La vision en termes de sous-systèmes permet de compléter leur cahier des charges.
> *Optimisation.* Changement minimal au niveau de la structure conduisant à une réduction significative du phénomène de bourdonnement.

Néanmoins le fait que la méthode soit basée sur la connaissance préalable des sous-systèmes (sous forme de matrice d'impédance) a aussi des inconvénients. Dans la majorité des cas, des méthodes numériques sont utilisées pour le calcul des matrices d'impédance. Cependant, dans le cas de structure avec un habillage complexe, les simulations numériques délivrent fréquemment des résultats de qualité insuffisante. Les propriétés d'un tel système peuvent être acquises par une caractérisation expérimentale. Hélas cette caractérisation expérimentale est complexe, et non incluse dans l'état de l'art.

En raison de cette complication, la méthode Patch Transfert Fonctions ne peut pas être appliquée directement à un véhicule complet. La problématique scientifique

« *Caractérisation expérimentale d'un sous-système par des mesures sur un système couplé* » doit être résolue au préalable.

7.3.3 Caractérisation expérimentale

La difficulté à surmonter concerne la caractérisation expérimentale du sous-système S appelé structure. Ce sous-système comporte, en plus de la structure au sens propre, l'habillage intérieur. L'air à l'intérieur du véhicule ne pouvant pas être retiré, le système S demeure nécessairement couplé à l'air à l'intérieur du véhicule.

Une caractérisation expérimentale directe consisterait en une des deux méthodes suivantes :

> *Impédance* $[Z] \approx [Y]^{-1}$. L'interface entière du système S est bloquée. Chaque colonne de la matrice [Z] est mesurée en une opération : Elle correspond à la pression de réaction sur chacun des patchs lorsqu'un patch est animé d'une vitesse unitaire.
> *Admittance* $[Y] \approx [Z]^{-1}$. L'interface du système S est en condition libre. Chaque colonne de la matrice d'admittance [Y] est mesurée en une opération : Elle correspond à la vitesse libre de chacun des patchs lorsqu'un patch est excité par une pression unitaire.

La première méthode nécessiterait un banc d'essai extrêmement complexe. La seconde méthode nécessiterait un banc d'essais sous vide. Aucune de ces méthodes n'est acceptable dans la pratique. Ainsi une méthode de caractérisation indirecte doit être développée. Les différents types de conditions aux limites du système S sont illustrés sur la Figure 7.5.

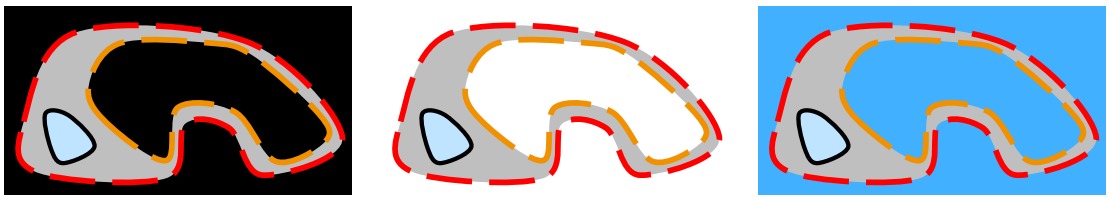

(a) (b) (c)

Figure 7.5: Sous-système S représenté dans différents types de conditions aux limites. (a) : Bloqué. (b) : Libre. (c) : Couplé avec l'air à l'intérieur et à l'extérieur du véhicule. Cette condition limite est l'unique condition limite disponible dans la pratique.

La méthode inverse proposée repose sur un *ensemble d'expériences* composé de N expériences. N correspond au nombre de patchs dans le système à caractériser. Pour chaque expérience, la structure est excitée par une source acoustique placée à une position donnée. Le schéma du montage expérimental est présenté sur la Figure 7.6.

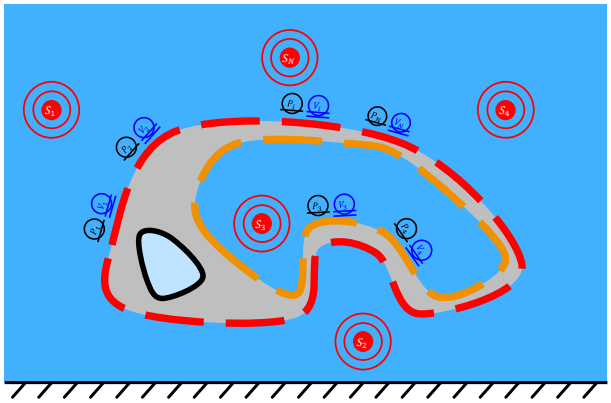

Figure 7.6: Représentation schématique du montage expérimental. Le sous-système à caractériser comporte N patchs. Un ensemble de N expériences est nécessaire pour l'application de la méthode. Une source acoustique est placée de façon séquentielle à N positions différentes dans l'air. Pour chaque position de la source, la pression et la vitesse normale au niveau de chaque patch (N au total) sont mesurées. La mesure peut être effectuée avec des microphones et des accéléromètres ou une sonde PU qui combine un microphone et un capteur de vitesse particulaire. La mesure de la pression est représentée avec le cercle noir avec une barre. La mesure de la vitesse est représentée par le cercle bleu avec deux barres.

Une fois les mesures réalisées, une méthode spécifique permet de calculer la matrice d'impédance recherchée. Avant d'appliquer la méthode à un véhicule complet, un test a été effectué sur une géométrie académique.

Les premiers résultats obtenus avec une expérience numérique ont permis de valider la méthode proposée. La méthode a en effet été capable de découpler deux systèmes fortement couplés. Ainsi la problématique « *Caractérisation expérimentale d'un sous-système par des mesures sur un système couplé* » a été résolue.

7.3.4 Limites et stratégies avancées

Une fois la méthode validée sur quelques *ensembles d'expériences* numériques, la recherche des limites de la méthode a été engagée. Durant cette phase, deux facteurs d'instabilité ont été découverts :

Position des sources. Selon la position des sources utilisées pour la caractérisation, la qualité de l'identification peut se dégrader.
Présence de bruit dans les mesures. La présence de bruit dans les mesures se traduit par une instabilité.

Le premier problème peut être résolu si deux règles sont respectées lors de la constitution de l'*ensemble d'expériences* :

Critère 1. Les sources doivent être loin des patchs.
Critère 2. Les sources doivent être éloignées les unes des autres.

Cependant la sensibilité de la méthode au bruit a nécessité le développement de stratégies avancées.

Si un *ensemble d'expériences*, position des sources utilisées, ou présence de bruit, produit une identification différente, il devrait néanmoins contenir une signification physique partielle. Si au total non pas un *ensemble d'expériences*, mais *TSoe* sont créés, chacun contenant une signification physique partielle, la réalité devrait pouvoir être retrouvée à l'aide d'indicateurs statistiques. L'*ensemble* contenant *TSoe ensembles d'expériences* est appelé « *ensemble d'ensembles d'expériences* ».

Deux principes sont utilisés pour créer plusieurs *ensembles d'expériences* :

Repositionnement des sources. Une, plusieurs ou toutes les *N* sources utilisées pour la création d'un *ensemble d'expériences* sont repositionnées. Il en résulte un *ensemble d'expériences* partiellement ou complètement nouveau.
Addition d'un bruit. Un bruit virtuel est numériquement ajouté aux mesures, il en résulte un nouvel *ensemble d'expériences*. Étant donné la nature aléatoire d'un bruit, cette opération peut être répétée plusieurs fois.

Deux indicateurs statistiques, *moyenne* et *médiane*, ont été proposés. Si l'indicateur *moyenne* améliore généralement les résultats, il reste impacté par la présentation d'un *ensemble d'expériences* très mal conditionné. A l'inverse, l'indicateur *médiane* est aucunement impacté par la présence d'un *ensemble d'expériences* très mal conditionné. Ainsi l'indicateur statistique *médiane* a été retenu pour la validation de la méthode sur un montage expérimental physique.

7.3.5 Validation expérimentale

La méthode d'identification inverse, combinée avec un indicateur statistique a été testé sur un montage expérimental physique. Deux difficultés supplémentaires ont été introduites en comparaison avec les expériences numériques précédentes :

Nombre de patchs. Forte augmentation du nombre de patchs.
Ajout d'un système semi-infini. Le système à caractériser est fortement couplé à un milieu semi-infini inconnu.

La méthode originale d'identification inverse, combinée à l'indicateur statistique *médiane* a répondu à la problématique proposée. A ce jour, aucun contre-exemple n'a été trouvé. L'auteur n'ayant pas connaissance d'une erreur ou d'un biais présent dans l'étude proposée, la méthode originale présentée est considérée comme appropriée pour répondre à la problématique proposée : « *Caractérisation expérimentale d'un sous-système par des mesures sur un système couplé* ».

References

[1] J. F. Kennedy, "Address at Rice University in Houston on the Nation's Space Effort," *Public Papers of the Presidents of the United States,* vol. 1, p. 669–670, 1962.

[2] P. Zeller, Handbuch Fahrzeugakustik. Grundlagen, Auslegung, Berechnung, Versuch, Springer, 2009.

[3] K. Genuit, Sound-Engineering im Automobilbereich, Berlin Heidelberg, Germany: Springer, 2010.

[4] H. Fastl and E. Zwicker, Psychoacoustics – Facts and Models, Berlin Heidelberg, Germany: Springer, 2007.

[5] P. M. Morse and K. Uno Ingard, Theoretical Acoustics, Princeton, NJ: Princeton University Press, 1986.

[6] H. W. Flannery, B. P. Teukolsky, S. A. and W. T. Vetterling, Numerical recipes, Cambridge, United Kingdom: Cambridge University Press, 1987.

[7] M. V. van der Seijs, "Experimental dynamic substructuring: Analysis and design strategies for vehicle development," PhD dissertation, Delft University of Technology, Delft, The Netherlands, 2016.

[8] D. de Klerk, D. J. Rixen and S. N. Voormeeren, "General Framework for Dynamic Substructuring: History, Review, and Classification of Techniques," *AIAA Journal,* vol. 46, no. 5, p. 1169–1181, 2008.

[9] O. Heaviside, "Electrical Papers," *London: Macmillan,* vol. 1–2, 1882–1884.

[10] P. Gardonio and M. J. Brennan, "On the origins and development of mobility and impedance methods in structural dynamics," *Journal of Sound and Vibration,* vol. 249, no. 3, p. 557–573, 2002.

[11] A. G. Webster, "Acoustical impedance and the theory of horns and of the phonograph," *Proceedings of the National Academy of Sciences,* vol. 5, no. 7, p. 275–282, 1919.

[12] F. A. Firestone, "A new analogy between mechanical and electronical systems," *The Journal of the Acoustical Society of America,* vol. 4, no. 3, p. 249–267, 1933.

[13] P. Le Corbeiller and Y.-W. Yeung, "Duality in Mechanics," *The Journal of the Acoustical Society of America,* vol. 24, no. 6, p. 643–648, 1952.

[14] G. J. O'Hara, "Mechanical Impedance and Mobility Concepts," *The Journal of the Acoustical Society of America,* vol. 41, no. 5, p. 1180–1184, 1967.

[15] S. Rubin, "Transmission matrices for vibration and their relation to admittance and impedance," *Journal of Manufacturing Science and Engineering,* no. 89.1, p. 9–21, 1964.

[16] S. Rubin, "Mechanical Immittance- and Transmission-Matrix Concepts," *Journal of the Acoustical Society of America,* no. 41.5, p. 1171–1179, 1967.

[17] C. Höller and B. M. Gibbs, "Indirect determination of the mobility of structure-borne sound sources," *Journal of Sound and Vibration,* vol. 334, no. 26, p. 38–58, 2015.

[18] V. Meyer, L. Maxit, J.-L. Guyader and T. Leissing, "Prediction of the vibroacoustic behavior of a submerged shell with non-axisymmetric internal substructures by a condensed transfer function method," *Journal of Sound and Vibration,* vol. 360, p. 260–276, 2016.

[19] S. M. Kim and M. J. Brennan, "A compact matrix formulation using the impedance and mobility approach for the analysis of structural-acoustics systems," *Journal of Sound and Vibration,* vol. 223, no. 1, p. 97–113, 1999.

[20] C. Cacciolati and J.-L. Guyader, "Acoustic mobility for vibroacoustic prediction," in *Proceedings of ICSV 7*, Garmisch-Partenkirchen, Germany, 2000.

[21] J.-D. Chazot and J.-L. Guyader, "Prediction of transmission loss of double panels with a patch-mobility method," *The Journal of the Acoustical Society of America,* vol. 121, no. 1, p. 267–278, 2006.

[22] J.-D. Chazot and J.-L. Guyader, "Transmission loss of double panels filled with porogranular materials," *The Journal of the Acoustical Society of America,* vol. 126, p. 3040–3048, 2009.

[23] J.-L. Guyader, C. Cacciolati and J. D. Chazot, "Transmission loss prediction of double panels filled with porous materials and mechanical stiffeners," in *Proceedings of ICA*, Sydney, Australia, 2010.

[24] L. Maxit, C. Cacciolati and J.-L. Guyader, "Airborne noise prediction using patch acoustic impedance," in *Proceedings of ICSV 9*, Orlando, USA, 2002.

[25] M. Ouisse, L. Maxit, C. Cacciolati and J.-L. Guyader, "Patch Transfer Functions as a Tool to Couple Linear Acoustic Problems," *Journal of Vibration and Acoustics,* vol. 127, no. 5, p. 458–466, 2004.

[26] J. Rejlek, G. Veronesi, C. Albert, E. Nijman and A. Bocquillet, "A Combined Computational-Experimental Approach for Modelling of Coupled Vibro-Acoustic Problems," *SAE International,* 2013.

[27] N. Totaro, B. Andro, C. Péteul and J.-L. Guyader, "Extension of the Patch Transfer Functions method (PTF method) to high frequency domain (sub-cavities decomposition)," in *proceedings of Inter-Noise 2007*, Istanbul, Turkey, 28–31 august 2007.

[28] M. Aucejo, "Vibro-acoustique des structures immergées sous écoulement turbulent," PhD dissertation, Institut National des Sciences Appliquées de Lyon, Villeurbanne, France, 2010.

[29] M. Aucejo, L. Maxit, N. Totaro and J.-L. Guyader, "Convergence acceleration using the residual shape technique when solving structure–acoustic coupling with the Patch Transfer Functions method," *Computers & Structures,* vol. 88, no. 11–12, p. 728–736, 2010.

[30] L. Maxit, M. Aucejo and J.-L. Guyader, "Improving the Patch Transfer Function Approach for Fluid-Structure Modelling in Heavy Fluid," *Journal of Vibration and Acoustics,* vol. 134, no. 5, 2012.

[31] L. Maxit, C. Yang, L. Cheng and J.-L. Guyader, "Modeling of micro-perforated panels in a complex vibro-acoustic environment using patch transfer function approach," *The Journal of the Acoustical Society of America,* vol. 131, no. 3, p. 2118–2130, 2012.

[32] G. Veronesi, C. Albert, E. Nijman, J. Rejlek and A. Bocquillet, "Patch Transfer Function Approach for Analysis of Coupled Vibro-Acoustic Problems Involving Porous Materials," *SAE International,* 2014.

[33] C. G. Albert, G. Veronesi, E. Nijman and J. Rejlek, "Prediction of the vibro-acoustic response of a structure-liner-fluid system based on a patch transfer function approach and direct experimental subsystem characterisation," *Applied Acoustics,* vol. 112, p. 14–24, 2016.

[34] N. Totaro and J.-L. Guyader, "Efficient positioning of absorbing material in complex systems by using the Patch Transfer Function method," *Journal of Sound and Vibration,* vol. 331, no. 13, p. 3130–3143, 2012.

[35] A. Le Bot, Foundation of Statistical Energy Analysis in Vibroacoustics, OUP Oxford, 2015.

[36] T. Lafont, N. Totaro and A. Le Bot, "Coupling strength assumption in statistical energy analysis," *Proceedings of the Royal Society of London A: Mathematical, Physical and Engineering Sciences,* vol. 473, no. 2200, 2017.

[37] J.-L. Guyader and N. Totaro, "Structural partitioning and power flow analysis. The Keys for vibroacoustic pre-design.," in *proceedings of Inter-Noise 2004*, Prague, Czech Republic, 22–25 august 2004.

[38] N. Totaro and J.-L. Guyader, "SEA substructuring using cluster analysis: The MIR index," *Journal of Sound and Vibration,* vol. 290, no. 1–2, p. 264–289, 2006.

[39] N. Totaro and J.-L. Guyader, "Automatic SEA partitioning of complex structures using cluster analysis," in *ISMA 2004, (pp. 1613–1628)*, Belgium, 2004.

[40] M. Kassem, C. Soize and L. Gagliardini, "Structural partitioning of complex structures in the medium-frequency range. An application to an automotive vehicle," *Journal of Sound and Vibration,* vol. 330, no. 5, p. 937–946, 2011.

[41] C. Díaz-Cereceda, J. Poblet-Puig and A. Rodríguez-Ferran, "Automatic subsystem identification in statistical energy analysis," *Mechanical Systems and Signal Processing,* vol. 54–55, p. 182–194, 2015.

[42] A. Bocquillet, "Méthodes énergétiques de caractérisations vibroacoustiques des réseaux complexes," PhD dissertation, Ecole centrale de Lyon, Écully, France, 2000.

[43] L. Maxit, "Extension et reformulation du modèle SEA par la prise en compte de la répartition des énergies modales," PhD dissertation, Institut National des Sciences Appliquées de Lyon, Villeurbanne, France, 2000.

[44] L. Maxit and J.-L. Guyader, "Estimation of SEA coupling loss factors using a dual formulation and FEM modal information, Part I: Theory," *Journal of Sound and Vibration,* vol. 239, no. 5, p. 907–930, 2001.

[45] L. Maxit and J.-L. Guyader, "Estimation of SEA coupling loss factors using a dual formulation and FEM modal information, Part II: Numerical applications," *Journal of Sound and Vibration,* vol. 239, no. 5, p. 931–948, 2001.

[46] L. Maxit and J.-L. Guyader, "Extension of SEA model to subsystems with non-uniform modal energy distribution," *Journal of Sound and Vibration,* vol. 265, no. 2, p. 337–358, 2003.

[47] N. Totaro, C. Dodard and J.-L. Guyader, "SEA Coupling Loss Factors of Complex Vibro-Acoustic Systems," *Journal of Vibration and Acoustics,* vol. 131, no. 4, pp. 041009–041009-8, 2009.

[48] H. D. Hwang, "Extension de la méthode SmEdA par la prise en compte des matériaux dissipatifs en moyennes fréquences," Ph.D. dissertation, Institut National des Sciences Appliquées de Lyon, Villeurbanne, France, 2015.

[49] H. D. Hwang, L. Maxit, K. Ege, Y. Georges and J.-L. Guyader, "SmEdA vibro-acoustic modelling in the mid-frequency range including the effect of dissipative treatments," *Journal of Sound and Vibration,* vol. 393, p. 187–215, 2017.

[50] M. Möser and W. Kropp, Körperschall, Berlin Heidelberg, Germany: Springer, 2010.

[51] M. Möser, Technische Akustik, Berlin Heidelberg, Germany: Springer, 2015.

[52] G. R. Sinambari and S. Sentpali, Ingenieurakustik, Wiesbaden, Germany: Springer, 2014.

[53] D. Clouteau, R. Cottereau and G. Lombaert, "Dynamics of structures coupled with elastic media—A review of numerical models and methods," *Journal of Sound and Vibration,* vol. 332, no. 10, p. 2415–2436, 2013.

[54] O. C. Zienkiewicz, R. L. Taylor and J. Z. Zhu, Finite Element Method - Its Basis and Fundamentals, Elsevier, 2005.

[55] R. Courant, "Variational methods for the solution of problems of equilibrium and vibrations," *Bulletin of the American Mathematical Society,* vol. 49, no. 1, p. 1–23, 1943.

[56] D. J. Ewins, Modal Testing: Theory, Practice and Application, 2nd. Baldock, Hertfordshire, England: Research Studies Press, 2000.

[57] P. Avitabile, "Experimental Modal Analysis (A Simple Non-Mathematical Presentation)," *Sound and Vibration,* vol. 35, no. 1, p. 20–31, 2001.

[58] M. S. Shephard, M. W. Beall, R. M. O'Bara and B. E. Webster, "Toward simulation-based design," *Finite Elements in Analysis and Design,* vol. 40, no. 12, p. 1575–1598, 2004.

[59] J.-L. Migeot, J.-P. Coyette and G. Lielens, Phénomènes fondamentaux de l'acoustique linéaire, Paris, France: Lavoisier, 2015.

[60] E. Deckers, O. Atak, L. Coox, R. D'Amico, H. Devriendt, S. Jonckheere, K. Koo, B. Pluymers, D. Vandepitte and W. Desmet, "The wave based method: An overview of 15 years of research," *Wave Motion,* vol. 51, no. 4, p. 550–565, 2014.

[61] M. Pflüger, F. Brandl, U. Bernhard and K. Feitzelmayer, Fahrzeugakustik, Vienna, Austria: Springer, 2010.

[62] R. L. Mayes and M. R. Ross, "Advancements in hybrid dynamic models combining experimental and finite element substructures," *Mechanical Systems and Signal Processing,* vol. 31, p. 56–66, 2012.

[63] M. V. van der Seijs, D. de Klerk and D. J. Rixen, "General Framework for Transfer Path Analysis: History, Theory and Classification of Techniques," *Mechanical Systems & Signal Processing,* no. 68–69, p. 217–244, 2016.

[64] A. T. Moorhouse and G. Seiffert, "Characterisation of an airborne sound source for use in a virtual acoustic prototype," *Journal of Sound and Vibration,* vol. 296, no. 1–2, p. 334–352, 2006.

[65] A. T. Moorhouse, A. S. Elliott and T. A. Evans, "In situ measurement of the blocked force of structure-borne sound sources," *Journal of Sound and Vibration,* vol. 325, no. 4–5, p. 679–685, 2009.

[66] M. W. F. Wernsen, M. V. van der Seijs and D. de Klerk, "An indicator sensor criterion for in-situ characterisation of source vibrations," in *IMAC-XXXIV: International Modal Analysis Conference*, Orlando, FL, January, 2016.

[67] G. Pavic, "Air-borne sound source characterization by patch impedance coupling approach," *Journal of Sound and Vibration,* vol. 329, no. 23, p. 4907–4921, 2010.

[68] M. Aucejo, N. Totaro and J.-L. Guayder, "Identification of source velocities on 3D structures in non-anechoic environments: Theoretical background and experimental validation of the inverse patch transfer functions method," *Journal of Sound and Vibration,* vol. 329, no. 18, p. 3691–3708, 2010.

[69] D. Vigoureux, "Déconfinement de sources acoustiques par utilisation d'une méthode holographique à double information," PhD dissertation, Institut National des Sciences Appliquées de Lyon, Villeurbanne, France, 2012.

[70] L. Du, "Characterisation of Air-borne Sound Sources using Surface Coupling Techniques," PhD dissertation, Institut National des Sciences Appliquées de Lyon, Villeurbanne, France, 2016.

[71] G. Veronesi, "A novel PTF-based experimental characterisation for poro-elastic liners: Method and sampling criterion," PhD dissertation, Università degli Studi di Ferrara, Ferrara, Italy, 2015.

[72] S. Rakotonarivo, W. Kuperman and E. Williams, "Prédiction de l'impédance mécanique d'un objet élastique à partir de la corrélation de bruit aléatoire," in *13ème Congrès Français d'Acoustique*, Le Mans, France, 2016.

[73] S. Adhikari, "Damping Models for Structural Vibration," PhD dissertation, Cambridge University, Cambridge, England, 2000.

[74] G. Veronesi and E. Nijman, "On the sampling criterion for structural radiation in fluid," *The Journal of the Acoustical Society of America,* vol. 139, no. 5, p. 2982–2991, 2016.

[75] Q. Leclère, "Acoustic imaging using under-determined inverse approaches: Frequency limitations and optimal regularization," *Journal of Sound and Vibration,* vol. 321, no. 3–5, p. 605–619, 2009.

[76] P. C. Hansen, Rank-deficient and discrete ill-posed problems: numerical aspects of linear inversion, Siam, 2005.

[77] Y. Kim and P. A. Nelson, "Spatial resolution limits for the reconstruction of acoustic source strength by inverse methods," *Journal of Sound and Vibration,* vol. 265, no. 3, pp. 583-608, 2003.

[78] P.-A. Gauthier, A. Gérard, C. Comier and A. Berry, "Acoustical inverse problems regularization: direct definition of filter factors using Signal-to-Noise Ratio," *Journal of Sound and Vibration,* vol. 333, no. 3, pp. 761-773, 2014.

[79] N. Totaro, D. Vigoureux, Q. Leclere, J. Lagneaux and J.-L. Guyader, "Sound fields separation and reconstruction of irregularly shaped sources," *Journal of sound and vibration,* vol. 336, pp. 62-81, 2015.

[80] H. G. Choi, A. N. Thite and D. J. Thompson, "Comparison of methods for parameter selection in Tikhonov regularization with application to inverse force determination," *Journal of Sound and Vibration,* vol. 304, no. 3-5, pp. 894-917, 2007.

[81] H.-E. de Bree, P. Leussink, T. Korthorst, H. Jansen, T. S. J. Lammerink and M. Elwenspoek, "The μ-flown: a novel device for measuring acoustic flows," *Sensors and Actuators A: Physical,* vol. 54, no. 1–3, p. 552–557, 1996.

[82] H.-E. de Bree, "An Overview of Microflown Technologies," *Acta Acustica united with Acustica,* vol. 89, no. 1, p. 163–172, 2003.

[83] M. Möser, Messtechnik der Akustik, Berlin Heidelberg, Germany: Springer, 2010.

[84] B. Jetmundsen, R. Bielawa and W. Flannelly, "Generalized Frequency Domain Substructure Synthesis," *Journal of the American Helicopter Society,* no. 33.1, p. 55–64, 1988.

[85] D.-H. Lee, W.-S. Hwang and C.-M. Kim, "Design sensitivity analysis and optimization of an engine mount system using an FRF-based substructuring method," *Journal of Sound and Vibration,* vol. 255, no. 2, p. 383–397, 2002.

[86] S. Donders, B. Pluymers, P. Ragnarsson, R. Hadjit and W. Desmet, "The wave-based substructuring approach for the efficient description of interface dynamics in substructuring," *Journal of Sound and Vibration,* vol. 329, no. 8, p. 1062–1080, 2010.

[87] R. Roy and J. Craig, "Coupling of Substructures for Dynamic Analyses: an Overview," in *Structures, Structural Dynamics and Material Conference*, Atlanta, GA, 41st AIAA/ASME/ASCE/AHS/ASC, April 3-6, 2000.

[88] M. S. Allen, H. M. Gindlin and R. L. Mayes, "Experimental modal substructuring to estimate fixed-base modes from tests on a flexible fixture," *Journal of Sound and Vibration,* vol. 330, no. 18–19, p. 4413–4428, 2011.

[89] S. Weng, Y. Xia, X.-Q. Zhou, Y.-L. Xu and H.-P. Zhu, "Inverse substructure method for model updating of structures," *Journal of Sound and Vibration,* vol. 331, no. 25, p. 5449–5468, 2012.

[90] R. H. MacNeal, "A Hybrid Method of Component Mode Synthesis," *Computers & Structures,* vol. 1, p. 581–601, 1971.

[91] N. Totaro, "Caractérisation de sources aérodynamiques et sous-structuration pour la méthode SEA," PhD dissertation, Institut National des Sciences Appliquées de Lyon, Villeurbanne, France, 2004.

[92] H. Riou, P. Ladevèze and L. Kovalevsky, "The Variational Theory of Complex Rays: An answer to the resolution of mid-frequency 3D engineering problems," *Journal of Sound and Vibration,* vol. 332, no. 8, p. 1947–1960, 2013.

[93] G. Pavic, C. Sandier and X. Carniel, "Characterisation of a small vibration source," in *Proc. of ISMA2014 including USD2014*, Leuven, Belgium, 2014.

[94] A. Pereira, J. Antoni and Q. Leclère, "Empirical Bayesian regularization of the inverse acoustic problem," *Applied Acoustics,* vol. 97, p. 11–29, 2015.

[95] S. N. Voormeeren and D. J. Rixen, "A family of substructure decoupling techniques based on a dual assembly approach," *Mechanical Systems and Signal Processing,* vol. 27, p. 379–396, 2012.

[96] F. J. Fahy, "Some applications of the reciprocity principle in experimental vibroacoustics," *Acoustical Physics,* vol. 49, no. 2, p. 217–229, 2003.

[97] M. S. Allen, R. L. Mayes and E. J. Bergman, "Experimental modal substructuring to couple and uncouple substructures with flexible fixtures and multi-point connections," *Journal of Sound and Vibration,* vol. 329, no. 23, p. 4891–4906, 2010.

[98] B. Besselink, U. Tabak, A. Lutowska, N. van de Wouw, H. Nijmeijer, D. J. Rixen, M. E. Hochstenbach and W. H. A. Schilders, "A comparison of model reduction techniques from structural dynamics, numerical mathematics and systems and control," *Journal of Sound and Vibration,* vol. 332, no. 19, p. 4403–4422, 2013.

[99] A. S. Elliott, A. T. Moorhouse, T. Huntley and S. Tate, "In-situ source path contribution analysis of structure borne road noise," *Journal of Sound and Vibration,* vol. 332, no. 24, p. 6276–6295, 2013.

[100] W. D'Ambrogio and A. Fregolent, "Inverse dynamic substructuring using the direct hybrid assembly in the frequency domain," *Mechanical Systems and Signal Processing,* vol. 45, no. 2, p. 360–377, 2014.

[101] T. S. Kuhn, The Structure of Scientific Revolutions (3rd ed.), Chicago, IL: University of Chicago Press, 1996.

[102] D. Menzel, H. Fastl, R. Graf and J. Hellbrück, "Influence of vehicle color on loudness judgments," *The Journal of the Acoustical Society of America,* vol. 123, no. 5, pp. 2477-2479, 2008.

[103] T. Lafont, N. Totaro and A. Le Bot, "Review of statistical energy analysis hypotheses in vibroacoustics," *Proceedings of the Royal Society of London A: Mathematical, Physical and Engineering Sciences,* vol. 470, no. 2162, 2013.

[104] W. D'Ambrogio and A. Fregolent, "Decoupling procedures in the general framework of Frequency Based Substructuring," in *Proceedings of the XXVII International Modal Analysis Conference (IMAC)*, Orlando, FL, 2009.

[105] F. A. Firestone, "Twixt Earth and Sky with Rod and Tube; the Mobility and Classical Impedance Analogies," *The Journal of the Acoustical Society of America,* vol. 28, no. 6, p. 1117–1153, 1956.

[106] D. Nicgorski and P. Avitabile, "Conditioning of FRF measurements for use with frequency based substructuring," *Mechanical Systems and Signal Processing,* vol. 24, no. 2, p. 340–351, 2010.

[107] Z.-W. Wang, J. Wang, Y.-B. Zhang, C.-Y. Hu and Y. Zhu, "Application of the Inverse Substructure Method in the Investigation of Dynamic Characteristics of Product

Transport System," *Packaging Technology and Science,* vol. 25, no. 6, p. 351–362, 2012.

[108] D. J. Rixen, A. Boogaard, M. V. van der Seijs, G. van Schothorst and T. van der Poel, "Vibration source description in substructuring: A theoretical depiction," *Mechanical Systems and Signal Processing,* vol. 60–61, p. 498–511, 2015.

[109] J. C. Snowdon, "Mechanical four-pole parameters and their application," *Journal of Sound and Vibration,* vol. 15, no. 3, p. 307–323, 1971.

[110] P. Sjövall and T. Abrahamsson, "Substructure system identification from coupled system test data," *Mechanical Systems and Signal Processing,* vol. 22, no. 1, p. 15–33, 2008.

[111] Y. Ren and C. F. Beards, "On substructure synthesis with FRF data," *Journal of Sound and Vibration,* vol. 185, no. 5, p. 845–866, 1995.

[112] D. J. Rixen, "A dual Craig–Bampton method for dynamic substructuring," *Journal of Computational and Applied Mathematics,* vol. 168, no. 1–2, p. 383–391, 2004.

[113] L. D. Flippen Jr, "Current dynamic substructuring methods as approximations to condensation model reduction," *Computers & Mathematics with Applications,* vol. 27, no. 12, p. 17–29, 1994.

[114] L. D. Flippen Jr, "A theory of condensation model reduction," *Computers & Mathematics with Applications,* vol. 27, no. 2, p. 9–40, 1994.

[115] J. Wang, Z.-W. Wang and L.-X. Lu, "Step-by-step decoupling method for inverse substructuring analysis of a three-component coupled packaging system," *Journal of Vibration and Control,* vol. 21, no. 4, p. 676–683, 2013.

[116] L. Keersmaekers, L. Mertens, R. Penne, P. Guillaume and G. Steenackers, "Decoupling of mechanical systems based on in-situ frequency response functions: The link-preserving, decoupling method," *Mechanical Systems and Signal Processing,* vol. 58–59, p. 340–354, 2015.

[117] A. T. Moorhouse, T. A. Evans and A. S. Elliott, "Some relationships for coupled structures and their application to measurement of structural dynamic properties in situ," *Mechanical Systems and Signal Processing,* vol. 25, no. 5, p. 1574–1584, 2011.

[118] D. Nicgorski and P. Avitabile, "Experimental issues related to frequency response function measurements for frequency-based substructuring," *Mechanical Systems and Signal Processing,* vol. 24, no. 5, p. 1324–1337, 2010.

FOLIO ADMINISTRATIF

THESE DE L'UNIVERSITE DE LYON OPEREE AU SEIN DE L'INSA LYON

NOM : Grialou DATE de SOUTENANCE : 04/12/2018

Prénoms : Matthieu, Patrick

TITRE : Vibro-acoustics Substructuring:
Combining simulations and experimental identification of subdomains for low frequency vehicle acoustics

NATURE : Doctorat Numéro d'ordre : 2018LYSEI109

Ecole doctorale : Mécanique – Energétique – Génie civil – Acoustique

Spécialité : Acoustique

RESUME : La sonorité de l'échappement joue un rôle significatif sur le confort acoustique des occupants, ainsi que sur le caractère du véhicule. L'étude proposée porte sur la problématique industrielle suivante : « Description et quantification de la transmission du son entre la bouche d'échappement et l'intérieur du véhicule ». Physiquement la transmission sonore entre l'échappement et l'intérieur du véhicule s'effectue en trois étapes : Propagation des ondes sonores de la canule à la surface extérieure du véhicule et conversion en énergie vibratoire (1) ; Le bruit structurel se propage de la peau extérieure du véhicule à l'habillage intérieur (2) ; La surface intérieure du véhicule rayonne de l'énergie dans l'air à l'intérieur (3).
Dans l'état de l'art proposé, la méthode de sous-structuration vibro-acoustique Patch Transfer Functions (PTF) est considérée comme une alternative viable à la problématique proposée. Cependant, avant d'appliquer la méthode sur un véhicule complet, la problématique suivante devait être résolue : « Caractérisation expérimentale d'un sous-système par des mesures sur un système couplé ». Ce manuscrit propose une méthode originale pour mesurer des fonctions de transfert d'un système découplé, sur la base de la réponse d'un système couplé. En raison de la nature mal posée du problème inverse, une méthode originale de régularisation a été proposée. La méthode a été validée par des essais numériques, puis par un test physique.

MOTS-CLÉS : Sous-Structuration, vibro-acoustique, méthode hybride, méthode inverse, échappement, bourdonnement.

Laboratoire (s) de recherche : LVA

Directeur de thèse : Guyader Jean-Louis, Professeurs des Universités, INSA Lyon

Président de jury : Thomas Jean-Hugh (Rapporteur)

Composition du jury : Leclaire Philippe (Rapporteur), Rakotonarivo Sandrine (Examinatrice), Guyader Jean-Louis (Directeur de thèse), Totaro Nicolas (co-Directeur de thèse), Bocquillet Arnaud (Invité)